JOURNAL OF THE Electrochemical Society

. 107, No. 9 September 1960

GLC ANODE CUSTOMERS NOW BENEFIT FROM THE RESULTS OF OUR RESEARCH

As suppliers to major chlor-alkali producers here and abroad, it is part of our responsibility to employ the most modern research and development techniques in the constant improvement of GLC anode quality.

Our customers are now reaping the rewards of past explorations in terms of economical performance markedly superior to the standards of yesteryear.

Electrolytic cell operators, from their own experience, are becoming increasingly aware of the superior performance of GLC custom made anodes—a superiority that becomes even more marked at high current densities.

Our special anode production and research facilities have as their goal still better quality and higher performance characteristics for the GLC anodes of the future. In this way we hope to merit an increasingly important role in our partnership in your progress.

PRODUCTS ELECTRODE GLC DIVISION YOU CAN TRUST®

GREAT LAKES CARBON CORPORATION

18 EAST 48TH STREET, NEW YORK 17, N. Y. OFFICES IN PRINCIPAL CITIES

Manuscripts submitted to the Journal should be sent, in triplicate, to the Editorial Office at 1860 Broadway, New York 23, N. Y. They should conform to the Instructions to Authors, published on pp. 229C-230C of this issue. Manuscripts so submitted become the property of The Electrochemical Society and may not be published elsewhere, in whole or in part, unless permission is requested of and granted by the Editor.

Inquiries re positive microfilm copies for volumes should be addressed to University Microfilms, Inc., 313 N. First St., Ann Arbor, Mich.

The Electrochemical Society does not maintain a supply of reprints of papers appearing in its Journal. A photoprint copy of any particular paper, however, may be obtained by corresponding directly with the Engineering Societies Library, 29 W. 39 St., New York 18, N. Y.

Journal of the Electrochemical Society

SEPTEMBER 1960 **VOL. 107 • NO. 9**

CONTENTS

Published monthly by The Electrochemical Society, Inc., from Manchester, N. H., **Executive Offices, Editorial Office** and **Circulation Dept.,** and **Advertising Office** at 1860 Broadway, New York 23, N. Y., combining the JOURNAL and TRANSACTIONS OF THE ELECTROCHEMICAL SOCIETY. Statements and opinions given in articles and papers in the JOURNAL OF THE ELECTROCHEMICAL SOCIETY are those of the contributors, and The Electrochemical Society assumes no responsibility for them. Nondeductible subscription to members $5.00; subscription to nonmembers $18.00. Single copies $1.25 to members, $1.75 to nonmembers. Copyright, 1960 by The Electrochemical Society, Inc. Entered as second-class matter at the Post Office at Manchester, N. H., under the act of August 24, 1912.

15 THOUSANDTHS OF A SECOND IS A VERY LONG TIME

It's much faster than you can wink an eye, yet time enough for Bell Laboratories' new high-speed switching terminal to transfer your voice to another channel while you are talking by telephone.

The new terminal—recently introduced on the transatlantic cable—uses the idle time in the conversations of talkers on a group of channels to provide paths for other talkers. This time-sharing technique, called Time Assignment Speech Interpolation, permits the sending of 72 simultaneous phone conversations over this deep-sea system where only 36 could be sent before.

TASI takes advantage of the fact that in a normal telephone conversation you actually talk less than half the time. You do not talk when you are listening, and even when you do talk there are pauses between sentences, words, and syllables. When there are more talkers than channels, TASI puts this idle time to use.

Scanning each circuit thousands of times a second, TASI instantly notices when you aren't talking, then quickly switches in someone who *is*. TASI also notices when you resume talking, immediately finds a channel not in use that moment and switches you to it. Your voice may be switched many times during a single conversation in a time too fast—about 15 milliseconds—for your ear to perceive.

The TASI switching terminal was rendered feasible by the transistor—an invention of Bell Telephone Laboratories. More than 16,000 transistors are employed to achieve the compact, dependable, high-speed circuitry required. TASI is another example of how Bell Laboratories works to keep your telephone service the world's finest.

BELL TELEPHONE LABORATORIES

WORLD CENTER OF COMMUNICATIONS RESEARCH AND DEVELOPMENT

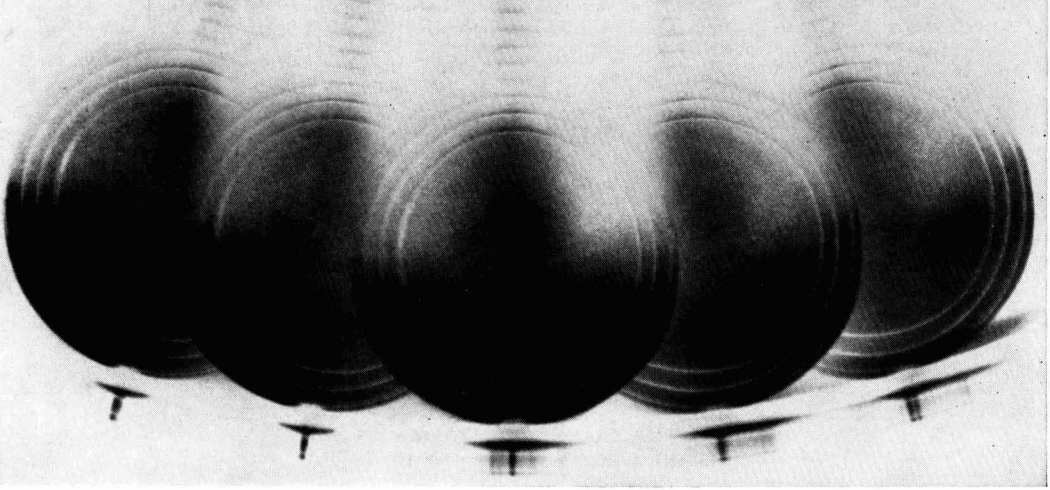

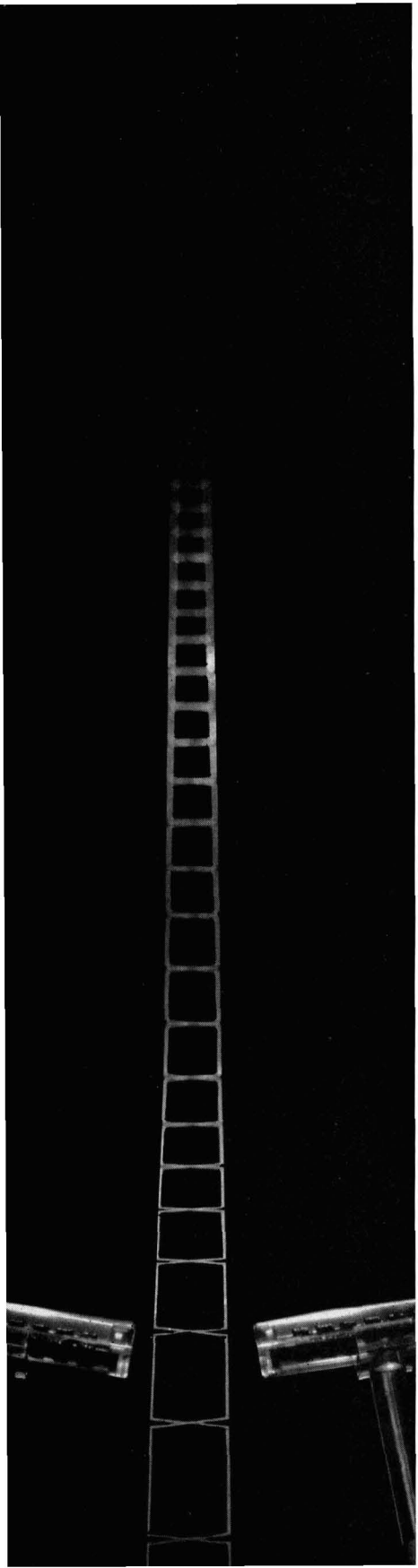

One of a series

The Case for the Terrestrial Traveler

Figure that every thirteen seconds American drivers motor 238,000 miles – the distance to the moon. Increasing the efficiency, comfort, ar safety of this incredible private transportation system (60 million cars!) is a top project goal of the General Motors Research Laboratorie From this sizable R & D program have already come a number of experimental controls and driver aids now being evaluated in the field.

New ways of supplying drivers with traffic and road information – electronic edge-of-road detectors; communication systems for giving drivers audible road and emergency information.

Simplified driver controls – Unicontrol, a servo system in which the driver steers, accelerates, and brakes his car with a single control stic

Tested methods of automatic vehicle control – refined computers ar electro-hydraulic servomechanisms that automatically guide cars and control their speed and spacing.

Underlying these developments are a continuing series of fundamental studies. In vehicle dynamics research: investigations of the effect of ti properties, suspension geometry, mass distribution, springs and dampers on the ride and handling characteristics of cars. In human factors research: experiments to determine the perception and response of drivers to various traffic situations using different car control systems.

At GM Research, we believe such fresh approaches will improve car-driver compatibility, providing additional convenience and enjoyment for tomorrow's terrestrial traveler.

General Motors Research Laboratories

Warren, Michigan

Car pickup coils and road wiring used for guidance and speed control in one experimental automatic highway system under study.

Editorial

Racial Discrimination and The ECS

NEGRO chemists are of course welcome at all meetings of The Electrochemical Society, both local and national. This applies to technical sessions, business meetings (if members of the Society), lunches, dinners, and all social functions. It is somewhat of a shock to realize that, while Negroes may attend any or all ECS functions in Houston, and may hire private dining rooms if they wish, they cannot obtain sleeping rooms in the headquarters hotel nor be served in its public dining rooms. In fact, the nearest hotel and restaurant accommodations will be in downtown Houston, some five miles away.

The Electrochemical Society has only a few Negro members, and not many nonmember Negro chemists come to the meetings. Attendance at the Houston sessions will not be impossible, even if somewhat inconvenient. Nevertheless, the Society will have to consider carefully whether, in the future, it is willing to accept this sort of nonsense. The American Chemical Society had a similar experience a few years ago (on a larger scale, since it has many more Negro members), when it held a National Meeting in Florida. The ACS probably will schedule no more meetings in the South because of the resulting embarrassment.

Racial discrimination is, of course, not unique to Southern States, as witnessed by the difficulties some delegations to the United Nations organizations have found in obtaining accommodations of their choice in New York City.

Skin color is not the determining factor for discrimination in Houston; theoretically, at least, colored people of other races than Negro are welcome in its hotels. Consequently, it has been suggested (humorously?) that Negroes who find it important to attend the meeting simply wear turbans or fezzes. We are sorry that we cannot recommend this subterfuge seriously. Mistakes have been made as when, a few years ago, a visiting Oriental dignitary and his entourage were led to a private dining room in a Houston hotel by a zealous hostess who mistook them for Negroes. As it happened, the group thought it was being honored with the private room at the time, shrugged off the insult when its significance was learned later.

Further consideration of the national problems of segregation-desegregation are definitely outside the scope of this editorial column. We only wish our readers to realize that racial discrimination can affect our Society too.

—CVK

FUTURE MEETINGS OF
The Electrochemical Society

Houston, Texas, October 9, 10, 11, 12, and 13, 1960

Headquarters at the Shamrock Hilton Hotel
Sessions will be scheduled on
Batteries, Corrosion, Electrodeposition,
Electrodeposition—Electrothermics & Metallurgy
Joint Symposium on Vapor Deposited Coatings,
Electronics (Semiconductors),
and Electrothermics and Metallurgy

★ ★ ★

Indianapolis, Ind., April 30, May 1, 2, 3, and 4, 1961

Headquarters at the Claypool Hotel
Sessions probably will be scheduled on
Electric Insulation, Electronics (including Luminescence and Semiconductors), Electrothermics and Metallurgy, Industrial Electrolytics, and Theoretical Electrochemistry

★ ★ ★

Detroit, Mich., October 1, 2, 3, 4, and 5, 1961

Headquarters at the Statler Hotel

★ ★ ★

Los Angeles, Calif., May 6, 7, 8, 9, and 10, 1962

Headquarters at the Statler Hilton Hotel

★ ★ ★

Boston, Mass., September 16, 17, 18, 19, and 20, 1962

Headquarters at the Statler Hilton Hotel

Papers are now being solicited for the meeting to be held in Indianapolis, Ind., April 30-May 4, 1961. Triplicate copies of each abstract *(not exceeding 75 words in length)* are due at Society Headquarters, 1860 Broadway, New York 23, N. Y., *not later than January 2, 1961* in order to be included in the program. *Please indicate on abstract for which Division's symposium the paper is to be scheduled, and underline the name of the author who will present the paper.* Complete manuscripts should be sent in triplicate to the Managing Editor of the JOURNAL at 1860 Broadway, New York 23, N. Y.

Presentation of a paper at a technical meeting of the Society does not guarantee publication in the JOURNAL. However, all papers so presented become the property of The Electrochemical Society, and may not be published elsewhere, either in whole or in part, unless permission for release is requested of and granted by the Editor. Papers already published elsewhere, or submitted for publication elsewhere, are not acceptable for oral presentation except on invitation by a Divisional program Chairman.

SOLID STATE ELECTRONICS

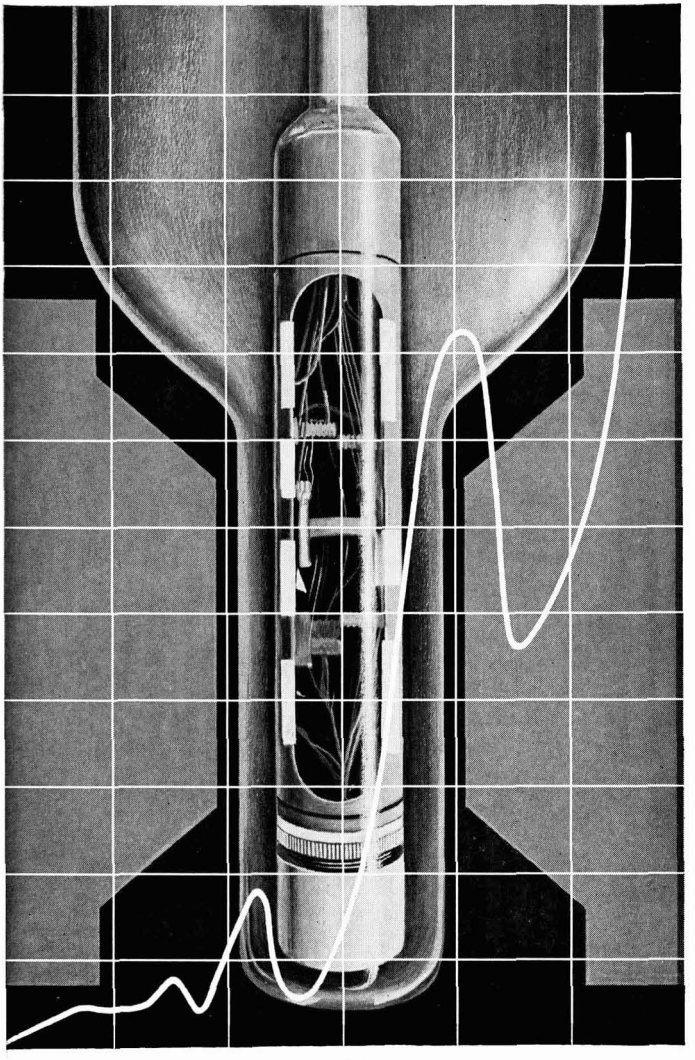

Observation of oscillatory behavior of magneto-resistance in semiconductors at low temperatures. This study of Landau levels in conduction or valence bands provides band structure information necessary to an understanding of transport properties.

At Lockheed Missiles and Space Division, solid state electronics encompasses a wide range of activities. Solid state physics concerns itself with theoretical and experimental work in the areas of paramagnetic resonance studies in solids; ferromagnetics and ferroelectrics; transport processes in solids; infrared spectroscopy; microwave properties of solids; radiation effects in semiconductors; crystal growth; and other related topics.

In solid state devices, the basic work applies to thermoelectric and radiant energy conversion; evaluation of environmental effects; and the study of new components based on ferrites, ferroelectrics, thin films, semiconductors, intermetallic compounds and other solid state materials.

Research in solid state circuits relates to circuit aspects of novel solid state components and systems, such as in microsystem electronics and in lumistor circuitry; and to unconventional uses of existing solid state devices.

Engineers and Scientists: Programs at Lockheed Missiles and Space Division reach far into the future and deal with unknown and challenging environments. If you are experienced in one of the above areas, or in related work, you are invited to join a company with an outstanding record of achievement and make an important individual contribution to your country's scientific progress. Write: Research and Development Staff, Dept. I-26, 962 W. El Camino Real, Sunnyvale, California. U.S. citizenship or existing Department of Defense industrial security clearance required.

Lockheed

MISSILES AND SPACE DIVISION

Systems Manager for the Navy POLARIS FBM; the Air Force AGENA Satellite in the DISCOVERER, MIDAS and SAMOS Programs; Air Force X-7; and Army KINGFISHER

SUNNYVALE, PALO ALTO, VAN NUYS, SANTA CRUZ, SANTA MARIA, CALIFORNIA · CAPE CANAVERAL, FLORIDA ALAMOGORDO, NEW MEXICO · HAWAII

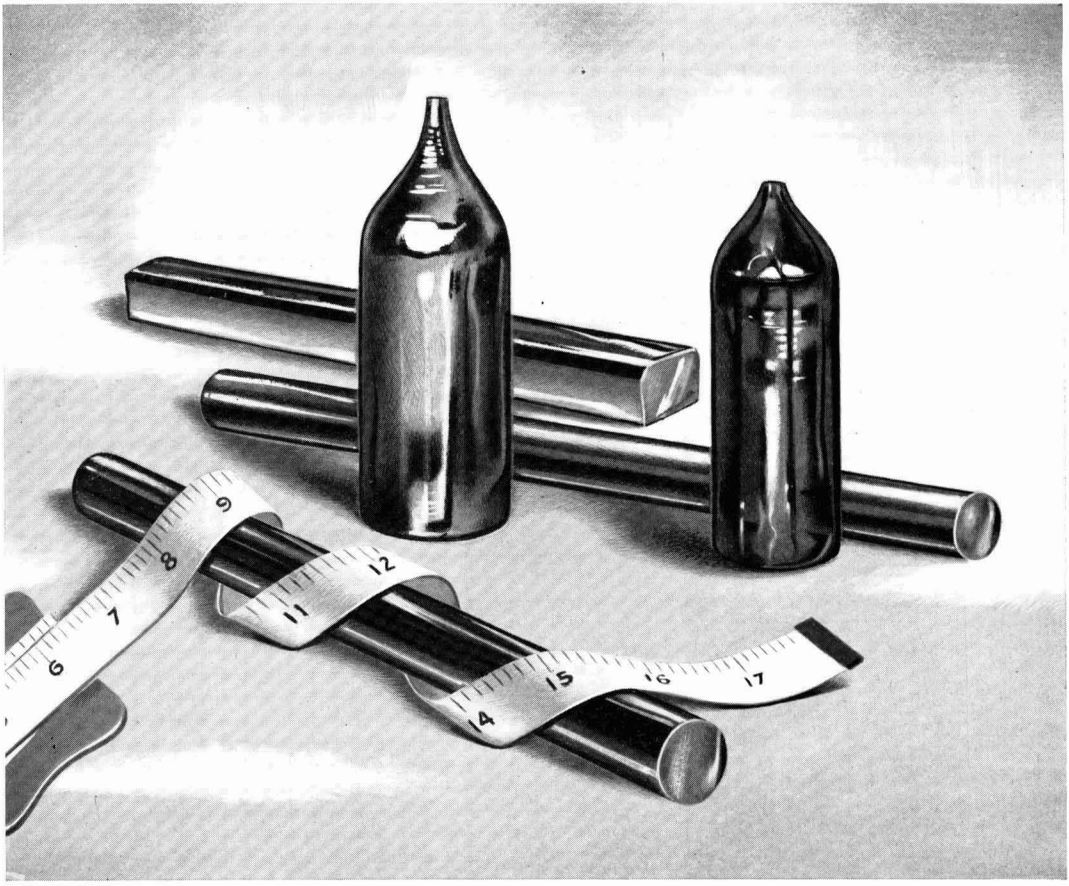

Now! Tailored to your budget!

Sylvania offers Germanium and Silicon Single Crystals in Production Quantities—at Attractive Prices

Now Sylvania offers to all device manufacturers the advantages of quantity production in the highly specialized field of germanium and silicon single crystals. These crystals are available at competitive prices and to desired specifications. Through the use of stringent quality-control techniques, you are assured of top-quality material—ready to use!

By specifying Sylvania crystals, you save the capital needed to invest in your own crystal-growing equipment. You save valuable space, time and technical manpower, too.

Another step in the Sylvania program to offer semiconductor materials and services to the device manufacturer is the completeness of product line. Sylvania now supplies germanium dioxide, intrinsic polycrystalline germanium, and doped germanium single crystals and slices. Polycrystalline silicon and doped silicon single crystals and slices are also available. To the germanium device manufacturer we can also offer our scrap-refining facilities.

For full details, a price on your quantity needs, plus your copy of a report on measuring and evaluating crystals for many specifications, write Chemical & Metallurgical Division, Sylvania Electric Products Inc., Towanda, Pennsylvania.

SYLVANIA

Subsidiary of **GENERAL TELEPHONE & ELECTRONICS**

Investigation of the Electrochemical Characteristics of Organic Compounds

V. Heterocyclic Nitro Compounds

R. Glicksman and C. K. Morehouse

Semiconductor and Materials Division, Radio Corporation of America, Somerville, New Jersey

ABSTRACT

A study of the electrochemical characteristics of nitropyridine and other heterocyclic nitro compounds shows that the cathode potential of these compounds during current flow is dependent on the aromaticity of the compound, as well as the type and position of substituent groups on the aromatic ring. The effect of these factors on the cathode potential is interpreted in terms of the electron density distribution in the molecule. Performance characteristics of magnesium dry cells containing 2,5-dinitrofuran and various nitropyridine compounds as cathodes are also presented.

Previous work by the authors (1, 2) has dealt with the effect of various types of groups and their position in the molecule on the cathode potential of aromatic nitro and nitroalkane compounds during current flow. As an extension of this work, a study of the electrochemical characteristics of heterocyclic nitro compounds and their use as cathodes in primary cells has been made and is presented in this paper.

Apparatus and Technique

A technique previously described by the authors (3) has been used to measure the operating potential during current flow and the coulombic capacity of the various heterocyclic nitro compounds. This technique consists in discharging at a constant current, in a large volume of electrolyte, a 0.5-g sample of the heterocyclic nitro cathode material mixed with 0.05 g of Shawinigan acetylene black. The change in cathode potential with time was measured with a L&N type-K potentiometer, using a saturated calomel reference electrode. Measured potentials were corrected for the *IR* drop associated with the apparatus and electrolyte by means of an oscillographic technique.

All half-cell potential data reported in this paper are referred to the normal hydrogen scale and include a liquid junction potential, which in most cases is small and can be neglected.

For most of the measurements an aqueous magnesium bromide electrolyte and a magnesium anode were used. For studying the effect of *p*H on potential, a zinc anode was employed with the acidic NH_4Cl-$ZnCl_2$-H_2O and basic NaOH-H_2O electrolytes.

Experimental Data and Discussion of Results

Nitropyridine and Nitroquinoline Compounds

A number of heterocyclic compounds possess the type of stability found in benzene. Among the more common heterocycles, pyridine is less easily substituted than benzene and, in general, surpasses it in aromatic character (4). On the other hand, the resonance energies of thiophene (31 kcal) and furan (23 kcal) indicated that these compounds are less stable than benzene (39 kcal) and pyridine (43 kcal) (5). The chemical reactivity of thiophene and furan, in general, is in good agreement with this fact.

Because substitution of aromatic compounds usually takes place through attack by electron seeking groups, positions that have the greatest electron density will be substituted most readily. However, a nitro group on a position of high electron density is more difficult to reduce than one on a position of low electron density (1, 2) and, therefore, one would expect the cathode potential of aromatic heterocyclic nitro compounds to be greater for those compounds which are less easily substituted, i.e., for the more highly aromatic systems such as pyridine.

The effect of aromaticity and group substitution on the electrode potential of heterocyclic nitro compounds was determined by half-cell potential studies of a number of nitropyridine and nitroquinoline compounds discharged continuously in 250 g/l $MgBr_2 \cdot 6H_2O$ electrolyte at a rate of 0.005 amp/g. The half-cell discharge curves are presented in Fig. 1-5, and theoretical capacity and electrode efficiency data for these compounds are given in Table

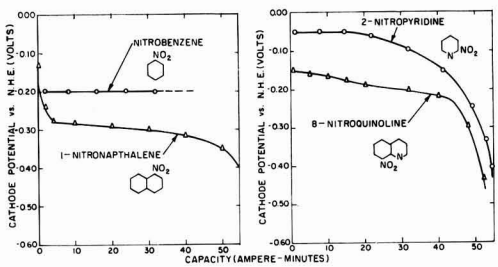

Fig. 1. Half-cell potential studies of various heterocyclic nitro compounds discharged in 250 g/l $MgBr_2 \cdot 6H_2O$ electrolyte at a rate of 0.005 amp/g.

Table I. Theoretical capacities and electrode efficiencies of various nitropyridine and nitroquinoline compounds

Compound	Theoretical capacity, amp-min/g	Experimental capacity,* amp-min/g	Electrode efficiencies, %
nitrobenzene	78.4	—	—
2-nitropyridine	77.7	51.5	66.3
4-hydroxy-2-nitropyridine	69.0	56.8	82.3
2-chloro-5-nitropyridine	60.9	46.9	77.0
2-hydroxy-5-nitropyridine	69.0	57.0	82.6
2-hydroxy-3-cyano-5-nitropyridine	58.5	50.6	86.5
2-amino-5-nitropyridine	69.3	60.6	87.6
2-amino-3-nitropyridine	69.3	57.8	83.4
4-amino-3-nitropyridine	69.3	65.5	94.5
4-nitropyridine	77.7	43.2	55.6
4-nitropyridine-N-oxide	69.0	32.8	47.5
m-dinitrobenzene	114.9	88.0	76.6
3, 5-dinitropyridine	114.0	71.1	62.4
2-hydroxy-3, 5-dinitropyridine	104.4	80.2	76.8
2-chloro-3, 5-dinitropyridine	94.6	50.4	53.3
1-nitronaphthalene	55.8	54.4	97.5
8-nitroquinoline	55.4	51.3	92.6
6-nitroquinoline	55.4	53.7	96.9
5-nitroquinoline	55.4	45.0	81.2
5-nitroisoquinoline	55.4	48.0	86.6
6, 8-dinitroquinoline	88.1	43.3	49.1

* Capacity calculated on the basis of a −0.40 v end potential.

I. The theoretical capacities were computed by means of Faraday's Law, assuming a 6-electron change per nitro group, and the electrode efficiencies were calculated from the data in Fig. 1-5, using a −0.40 v end potential to compute the capacities.

Figure 1 shows half-cell discharge data for nitrobenzene and 2-nitropyridine along with their corresponding bicyclic compounds, 1-nitronaphthalene and 8-nitroquinoline. The higher potential of 2-nitropyridine as compared with nitrobenzene is understandable in terms of resonance theory. In pyridine, the nitrogen atom has a greater attraction for electrons than has a carbon atom and decreases the availability of electrons. Thus, the effect of resonance in pyridine is to bring electrons from the α or 2 and γ or 4 positions to the nitrogen atom, which decreases the electron density at these positions relative to that at the β or 3 positions. The inductive effect is also operative, and because electrons are removed from the β positions of pyridine as well, this position too has a lower electron density than found in benzene. The nitropyridines then, because of the lower electron density in the vicinity of the reducible nitro group, should have a greater affinity for electrons and operate at higher cathode potentials than comparable nitrobenzene derivatives.

The effect induced by the nitrogen atom is similar to that found in nitrobenzene as evidenced by the fact that it is about as difficult to substitute on pyridine as on nitrobenzene. If this behavior is assumed to be caused by the similar ring electron densities of pyridine and nitrobenzene, it would be expected that the cathode potential of 2-nitropyridine would be comparable to that of o-dinitrobenzene. Half-cell discharge studies of o-dinitrobenzene under similar conditions of discharge confirm this reasoning.

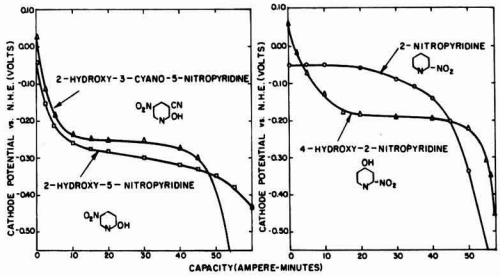

Fig. 2. Half-cell potential studies of various nitropyridine derivatives discharged in 250 g/l $MgBr_2 \cdot 6H_2O$ electrolyte at a rate of 0.005 amp/g.

Figure 1 also shows that the simple monocyclic nitro compounds, nitrobenzene and 2-nitropyridine, operate at higher potentials than their corresponding bicyclic compounds. These results are consistent with the stronger aromatic character of the monocycles as compared with the bicylic compounds. Because quinoline is related to naphthalene similarly to the way pyridine is related to benzene, the higher operating potential of 8-nitroquinoline as compared with 1-nitronaphthalene is to be expected.

In Fig. 2 are half-cell discharge data for various nitropyridine derivatives discharged at a rate of 0.005 amp/g in magnesium bromide electrolyte. These results indicate that the effect of substituent groups and their position in the molecule on the potential of nitropyridine compounds closely parallels their effect on the potential of nitrobenzene derivatives. For example, the presence of the electron-repelling hydroxyl group in 4-hydroxy-2-nitropyridine causes the cathode potential of this compound to be 0.15 v lower than the potential of 2-nitropyridine. The magnitude of this effect is comparable to that found for the corresponding nitrobenzene derivatives. Similarly the substitution of an electron attracting —CN group in the -3 position of 2-hydroxy-5-nitropyridine results in a compound, 2-hydroxy-3-cyano-5-nitropyridine, with a higher operating potential than the parent compound.

The half-cell potential-time discharge curves of these hydroxy nitropyridine compounds show a striking similarity to those of the hydroxy aromatic C-nitroso compounds (6). As is the case with the latter compounds, the high initial operating potentials of the hydroxy nitropyridines decrease rapidly during the first 10 amp-min of discharge and then assume a constant value for the remainder of the discharge.

This behavior can be explained in the following way: both the 2- and 4-hydroxy pyridines are tautomeric with the pyridones: e.g.,

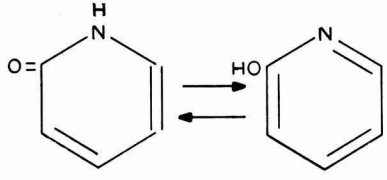

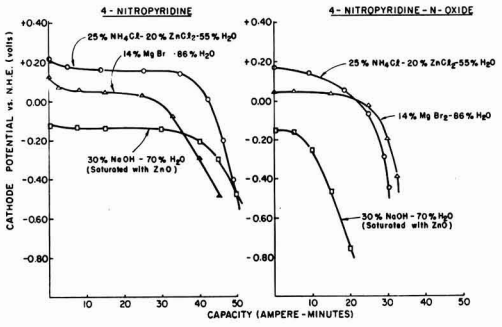

Fig. 3. Half-cell potential discharge curves of 4-nitropyridine and 4-nitropyridine-N-oxide discharged at a rate of 0.005 amp/g in various aqueous electrolytes.

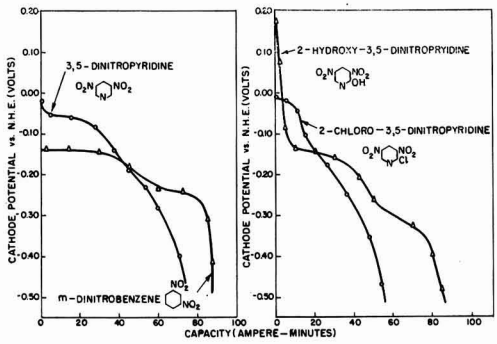

Fig. 4. Half-cell potential studies of various dinitropyridine compounds discharged in 250 g/l $MgBr_2 \cdot 6H_2O$ electrolyte at a rate of 0.005 amp/g.

and it is believed that the high initial potential of these compounds is a result of the pyridone structure. However, during the discharge, hydroxyl ion is formed as a consequence of the cathodic reduction reaction, and a neutralization reaction occurs with time between the hydroxypyridine form and the alkaline electrolyte with the formation of the strongly electron-repelling phenoxide ion. At this point, the cathode potential is due to that of the hydroxypyridine salt, and it remains constant at the lower potential throughout the remainder of the discharge.

The higher potential of 4-hydroxy-2-nitropyridine as compared with that of 2-hydroxy-5-nitropyridine is attributed to the fact that the nitro group in the former compound is on a position of lower electron density than the nitro group in 2-hydroxy-5-nitropyridine and is thus more readily reduced. This behavior is apparent when the possible resonance structures of pyridine are considered Thus, it would be expected that 2- and 4-nitropyridine compounds would operate at higher cathode potentials than comparable 3-nitropyridine compounds.

In Fig. 3 the high cathode potential of 4-nitropyridine compounds is demonstrated by the half-cell potential discharge curves of 4-nitropyridine and 4-nitropyridine-N-oxide obtained by discharging these compounds at a rate of 0.005 amp/g in aqueous $MgBr_2$, NaOH, and NH_4Cl-$ZnCl_2$ electrolytes. The curves show that both compounds operate at about the same potential, indicating the effect of the N-oxide group on the electrode potential to be very small. In general, the electrode potentials of these 4-nitropyridine compounds increase with decreasing electrolyte *p*H, a result similar to that found for the aromatic nitrobenzene compounds. However, unlike the aromatic nitrobenzene compounds which have poor electrode efficiencies in strongly basic electrolyte, 4-nitropyridine operates at an efficiency of 62.7% in this electrolyte.

Figure 4 gives half-cell potential discharge data for various 3,5-dinitropyridine compounds discharged continuously in a 250 g/l $MgBr_2 \cdot 6H_2O$ electrolyte at a rate of 0.005 amp/g. The data show that the dinitropyridine compounds operate at higher potentials than their corresponding mononitropyridine compounds. For example 2-hydroxy-3,5-dinitropyridine, for its first discharge step, operates at a potential approximately 0.14 v higher than that of 2-hydroxy-5-nitropyridine. In addition to their higher operating potentials, the dinitropyridine compounds have higher theoretical ampere-minute capacities than the mononitropyridine compounds and consequently show more promise for use as cathode materials in dry cells.

The data in Fig. 4 illustrate that the effect of substituted groups on the potential of 3,5-dinitropyridine is similar to that found for the aromatic dinitrobenzene and mononitropyridine compounds. The 0.08 v lower potential of m-dinitrobenzene as compared with 3,5-dinitropyridine also agrees with theory.

The half-cell potential discharge curves of various nitroquinoline compounds given in Fig. 5 show that the various isomeric mononitroquinoline compounds operate at comparable potentials of about −0.15 to −0.20 v for most of their discharge life. As expected, the cathode potential of 6,8-dinitroquinoline is 0.1 v higher than the potentials of 6- and 8-nitroquinoline.

The electrode efficiencies of the nitropyridine and nitroquinoline compounds are in general quite high as indicated by the data in Table I. For the 3-(or 5-) nitropyridine compounds efficiencies of 77-95% are obtained, while the nitroquinoline compounds operate at electrode efficiencies ranging from 81-97%.

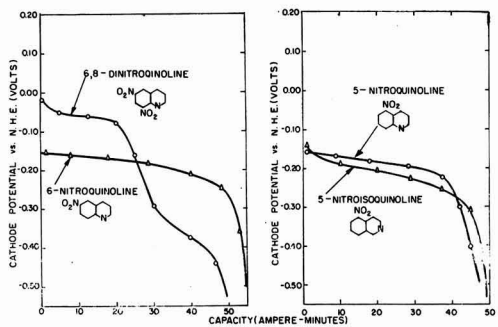

Fig. 5. Half-cell potential studies of various nitroquinoline compounds discharged in 250 g/l $MgBr_2 \cdot 6H_2O$ electrolyte at a rate of 0.005 amp/g.

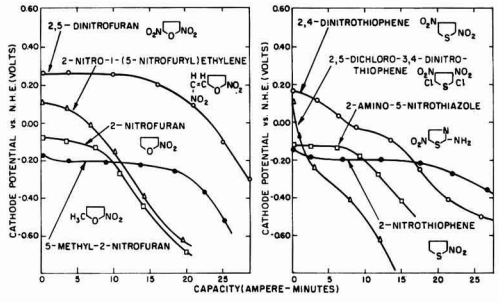

Fig. 6. Half-cell potential studies of various nitrofuran and nitrothiophene compounds discharged in 250 g/l $MgBr_2 \cdot 6H_2O$ electrolyte at a rate of 0.005 amp/g.

However, the more strongly oxidizing 2- and 4-nitropyridine and dinitropyridine compounds have lower efficiencies.

Nitrofuran, Nitrothiophene, and Other Five Membered Heterocyclic Nitro Compounds

In Fig. 6 are half-cell potential discharge curves of various nitrofuran and nitrothiophene compounds. Despite the weakly aromatic character of furan as compared with benzene and thiophene, 2-nitrofuran operates at a higher cathode potential than either nitrobenzene or 2-nitrothiophene under similar conditions of discharge. The apparent anomalous behavior of 2-nitrofuran may be explained by the fact that furan is not a true aromatic compound, and any generalization based on aromatic behavior would not be pertinent for this compound. For example, furan behaves like a typical diene in the Diels-Alder reaction, while ring cleavage by mineral acid shows its vinyl ether character. However, resonance energy considerations show that furan has some characteristics of a typical aromatic substance as well. It is thus apparent that the unsaturation of the furan nucleus will frequently manifest itself as a diene or vinyl ether, rather than as a true aromatic system typified by benzene.

The data in Fig. 6 also illustrate the effect of substituted groups on the potential of 2-nitrofuran. The cathode potentials of 2-nitrofuran derivatives increase as the 5-position is substituted with increasingly stronger electronegative groups, i.e., in the order $-CH_3$, —H, $-CH{=}CHNO_2$, $-NO_2$. As with the other nitro compounds studied, the effect of substituent groups on the cathode potential of 2-nitrofuran can be explained by their effect on the electron density in the vicinity of the reducible nitro group.

It is significant that the increase in potential caused by the addition of a $-NO_2$ group to the -5 position of 2-nitrofuran is 0.15-0.20 v greater than the increase found for the addition of a $-NO_2$ group to the ortho, para, or meta position of nitrobenzene. In this respect the nitrofurans behave more like the nitroalkanes than like the aromatic nitro compounds. Moreover, the nitrofurans, like the nitroalkanes, have exceedingly poor electrode efficiencies in the $MgBr_2$ electrolyte, giving values ranging from 16-31% for the four compounds studied.

Table II. Theoretical capacities and efficiencies of various five membered heterocyclic nitro compounds

Compound	Theoretical capacity, amp-min/g	Experimental capacity,* amp-min/g	Electrode efficiencies, %
nitrobenzene	78.4	—	—
2-nitrofuran	85.5	13.6	15.9
2, 5-dinitrofuran	122	30.7	25.2
2-nitro-1-(5-nitrofuryl) ethylene	52.4†	14.2	27.1
2-methyl-5-nitrofuran	75.8	23.2	30.6
2-nitrothiophene	74.8	31.6	42.2
2, 4-dinitrothiophene	111	20.9	18.8
2, 5-dichloro-3, 4-dinitro-thiophene	78.8	7.5	9.5
2-amino-5-nitrothiazole	67.0	14.5	21.6
1-nitronaphthalene	55.8	54.4	97.5
6-nitroindazole	59.1	51.9	87.8
6-nitrobenzimidazole	59.1	51.8	87.6
5-nitroindazole	59.1	16.5	27.9
5-nitrobenzotriazole	58.9	61.5	100
5-nitro-2-benzimidazol-ethiol	49.5	43.0	86.9

* Capacity calculated on the basis of a −0.40 v end potential.

† Theoretical capacity calculated on the basis of the reduction of furan nitro group only.

Figure 6 also gives half-cell potential discharge curves for various nitrothiophene derivatives and for 2-amino-5-nitrothiazole. Because thiophene undergoes the typical substitution reactions of aromatic compounds and is more reactive than benzene, its nitro derivative would be expected to operate at a lower cathode potential than nitrobenzene. However, the discharge curves in Fig. 1 and 6 show that both 2-nitrothiophene and nitrobenzene operate at comparable potentials of −0.20 v in the magnesium bromide electrolyte. The effect on the cathode potential of additional $-NO_2$ and —Cl groups on the thiophene nucleus is similar to that found with other nitro compounds as evidenced by the high cathode potentials of 2,4-dinitrothiophene and 2,5-dichloro-3,4-dinitrothiophene. However, the data in Table II show that these compounds operate at extremely poor electrode efficiencies.

The thiazoles, which are structurally similar to thiophene and to pyridine, show reactions similar to

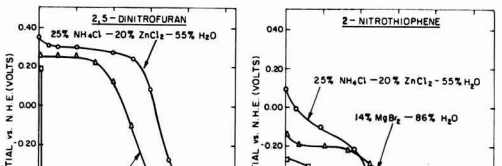

Fig. 7. Half-cell potential curves of 2,5-dinitrofuran and 2-nitrothiophene discharged at a rate of 0.005 amp/g in various aqueous electrolytes.

pyridine rather than those of thiophene. This behavior is particularly apparent in the resistance shown toward substitution reactions and is evidenced by the higher cathode potential of 2-amino-5-nitrothiazole as compared with nitrobenzene and 2-nitrothiophene.

Half-cell potential discharge studies were made on 2,5-dinitrofuran and 2-nitrothiophene to determine the effect of pH on the operating potential and capacity of these compounds. Figure 7 shows that the cathode capacity of 2,5-dinitrofuran increases only slightly with decreasing pH and is considerably less than the theoretical capacity (122 amp-min/g) of this compound. Similarly, 2-nitrothiophene shows no improvement in capacity with the more acidic NH_4Cl-$ZnCl_2$ electrolyte and actually shows a slight decrease. The poorer capacities obtained from these compounds in the strongly basic NaOH electrolyte are similar to those found for the aromatic nitro and nitroalkane compounds and can be attributed to the presence of side products which are formed by the condensation of the primary reduction products and to the poor stability of these compounds in this electrolyte.

In general the effect of decreasing electrolyte pH is to increase the cathode potential in agreement with theoretical considerations. It is interesting to note that the effect of pH on the cathode potential of 2,5-dinitrofuran is small, a relationship similar to that found for the nitroalkanes (2) but different from that found for the aromatic nitro compounds. The behavior of 2-nitrothiophene in this respect is closer to that of the aromatic nitrobenzene compounds.

In addition to the simple 5-membered heterocyclic compounds, each of the heterocyclic compounds can be fused to a benzene ring to give bicyclic systems which are comparable to naphthalene and quinoline. The half-cell potential discharge curves of various bicyclic heterocyclic nitro compounds are presented in Fig. 8. In general, these compounds, which contain two or three nitrogen atoms in the 5-membered ring, operate at potentials higher than that of 1-nitronaphthalene but lower than that of the nitroquinolines. As with the nitroquinoline compounds high electrode efficiencies are obtained with these bicyclic heterocyclic nitro compounds.

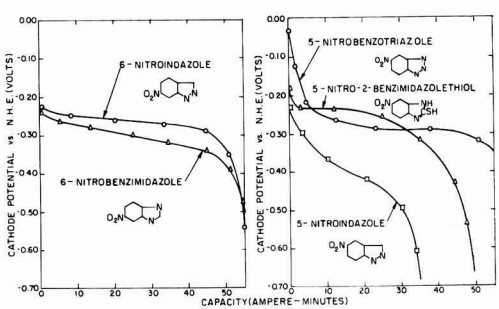

Fig. 8. Half-cell potential studies of various bicyclic heterocyclic nitro compounds discharged in 250 g/l $MgBr_2 \cdot 6H_2O$ electrolyte at a rate of 0.005 amp/g.

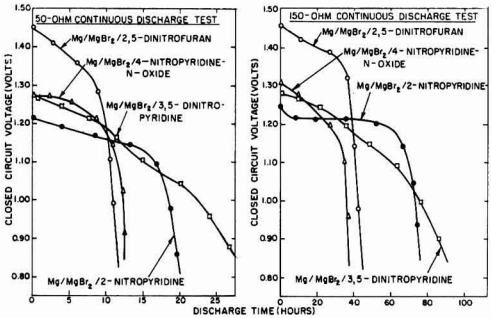

Fig. 9. AA-size magnesium dry cells containing various heterocyclic nitro compounds as cathodes discharged continuously through 50- and 150-ohm resistances.

Experimental Dry Cell Data

Experimental dry cells containing various heterocyclic nitro compounds as cathodes were assembled in the usual manner, using an AA-size can of impact-extruded magnesium AZ10A alloy and a magnesium bromide electrolyte. The cathode mix (weighing approximately 5 g) consisted of two parts by weight of Darco G-60 carbon black to one part by weight of the nitropyridine compounds. For cells containing 2,5-dinitrofuran as the cathode, two parts of the nitro compound was blended with one part by weight of Shawinigan acetylene black.

The performance characteristics of these Mg/$MgBr_2$/heterocyclic nitro AA-size cells on a 50- and 150-ohm continuous discharge test are shown in Fig. 9. The operating voltages of these cells closely parallel their half-cell potentials after corrections are made for the half-cell potential of the magnesium anode, which operates at a potential of about 1.3 v in this electrolyte. From the limited shelf-life data available, it appears that the cells containing the nitropyridine cathodes can be stored for extended periods of time without an appreciable decrease in cell performance, while the 2,5-dinitrofuran cells do not have an appreciable shelf life.

The use of heterocyclic nitro compounds as cathodes in dry cells appears to offer some advantages over the nitrobenzene compounds in that many of them operate at higher potentials at comparable electrode efficiencies. At present, these compounds are not as readily available as the nitrobenzene derivatives, being more difficult to synthesize; however, they offer a vast new source of potential cathode materials for future use. For example, considering only the pyridine compounds, almost every type of benzene compound has its analog in the pyridine series, and the number and types of pyridine derivatives are potentially as extensive as those in the benzene system.

Acknowledgment

The authors wish to acknowledge the support of this research by the Power Sources Division of the U. S. Army Signal Research and Development Laboratory under Contract No. DA-36-039-sc-78048. They also wish to express their appreciation to Dr. W. B. Hardy of American Cyanamid Company, and Dr. K. J. Hayes, of the Norwich Pharmacal Com-

pany, for supplying many of the compounds used in this investigation.

Manuscript received Feb. 12, 1960. This paper was prepared for delivery before the Columbus Meeting, Oct. 18-22, 1959.

Any discussion of this paper will appear in a Discussion Section to be published in the June 1961 JOURNAL.

REFERENCES

1. R. Glicksman and C. K. Morehouse, *This Journal*, **105**, 299 (1958).
2. R. Glicksman and C. K. Morehouse, *ibid.*, **106**, 288 (1959).
3. C. K. Morehouse and R. Glicksman, *ibid.*, **103**, 94 (1956).
4. L. F. Fieser and M. Fieser, "Organic Chemistry," p. 847, D. C. Heath and Co., Boston (1950).
5. L. Pauling, Gilman's "Organic Chemistry," Vol. II, pp. 1968-1969, John Wiley & Sons, Inc., New York (1947).
6. R. Glicksman and C. K. Morehouse, *This Journal*, **105**, 613 (1958).

Discharge of a Lead-Acid Cell through an R-L Circuit

J. J. Lander[1] **and E. E. Nelson**

Naval Research Laboratory, Washington, D. C.

ABSTRACT

Submarine cells of the lead-acid type were discharged through resistance-inductance circuits. The data are analyzed to show no contribution to voltage loss other than *IR* losses in the cell during the initial voltage transient; consequently, a method is provided for the determination of the internal resistance. Circuit geometry is an important factor determining the types of discharge curves which can be obtained.

It has been desirable for various reasons to determine the internal resistance and other electrical characteristics of lead-acid storage cells (1-5). Experimental determinations of the internal resistance have been more or less uncertain because of presumed effects contributed by polarization phenomena other than *IR* drop. In this work, measurements involving cell discharges through a resistance-inductance series circuit are shown which lead to a determination of the internal resistance of a fully charged cell.

Theory

When a constant voltage is discharged through a resistance-inductance circuit, current builds up with time and levels off to a constant value depending on the resistance and the inductance in the circuit, according to the equation

$$E = L\, dI/dt + RI \qquad [1]$$

If this relation is applied to the circuit shown in Fig. 1, it can be shown that the voltage change measured across V_T, after the switch is closed, will be given by the differential equation

$$dV_T/dt = -\left(\frac{R_o + R_I}{L}\right) V_T + \text{const.} \qquad [2]$$

At the instant the switch is closed, all the energy supplied by the voltage source is contained in the term $L\, dI/dt$, the value of I being zero. As time proceeds and I builds up, the voltage V_T will fall off logarithmically from its open-circuit value and approach a constant value as dI/dt approaches zero. If R_I is unknown, its value could be determined by measuring the voltage V_T and current with time. It would be given by dividing the current at any time into the difference between the open-circuit value of V_T and its value at the corresponding time. R_I might also be obtained from the slope of the dV_T/dt vs. V_T line if R_o and L were known.

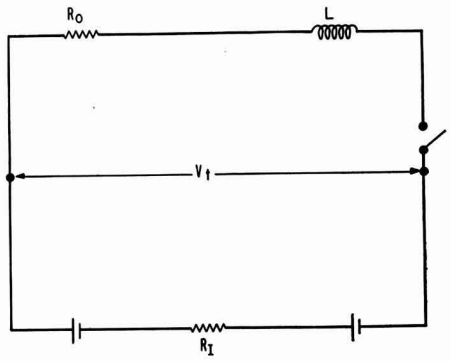

Fig. 1. An R-L series circuit

It might be assumed that a lead-acid cell discharging through an R-L circuit could be represented for some initial time interval by the circuit given in Fig. 1. The two potential sources would correspond to the positive and negative plates and V_T, the voltage measured across the cell terminals. It is not to be supposed that this circuit would represent the cell over a whole period of transient voltage, because other kinds of polarization besides *IR* drop are known. These would render the voltage source nonconstant, and Eq. [2] would not be adequate. If, however, the additional polarization should be slow to develop compared to the time necessary for the inductance field to be established, the proposed circuit would be a good representation of the initial voltage transient.

[1] Present address: Delco Remy Division, General Motors Corporation, Anderson, Indiana.

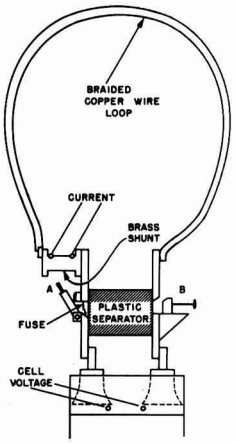

Fig. 2. Cell top and switch

Experimental Work

Experimental work consisted in discharging a fully charged submarine cell (~ 7000 amp-hr nominal capacity) through resistances of known values, while cell voltage and voltage drop across another small resistance in series were recorded as a function of time. The resistance consisted of ½ and 1 in. braided copper cables, or lengths of these in parallel, in series with a short, heavy brass tube of resistance 1.4×10^{-6} ohms. This tube was provided for measuring current. A switching device was mounted on the cell terminals as shown in Fig. 2. The cables were arranged in big loops, 4-5 ft in diameter to supply the inductance. It was attempted to keep the inductance loop relatively constant. Resistances were measured by running currents of about 100 amp through appropriate parts of the circuit and measuring voltage drops with a precision potentiometer.

In Fig. 2, A is a heavy six-bladed knife switch used to open the circuit; a fuse was placed in parallel to take the load when the switch was opened and then burn out to break the discharge circuit. The circuit was closed by driving the wedge switch B into its seat in the mounting. B was designed to make the circuit quickly and completely. All mechanically contacting parts were silver-plated to reduce contact resistance. Under best conditions the total resistance of the switch mounting could be reduced to $15\text{-}20 \times 10^{-6}$ ohms.

Procedure for making a run was as follows. The cell was charged to full gassing and then allowed to sit on open circuit overnight for the voltage to become steady. The shunt resistors were clamped into place with both switches open and their resistance values measured. Voltage connections were made to the recorder from the proper places in the discharge circuit; the knife switch was closed and the wedge switch slammed home. Current was allowed to run for the desired period; the circuit was broken and the cell charged for another run.

Cell voltages (V_p) were measured at the tops of the plates inside the cell, because preliminary data showed that measurements made across the cell terminals included enough inductance contribution

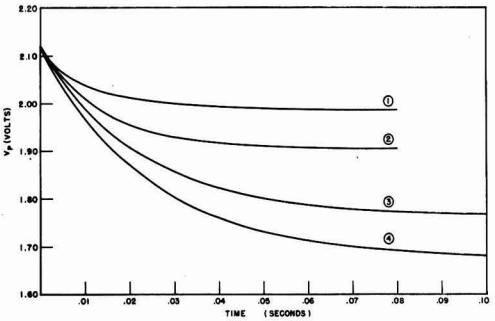

Fig. 3. Cell voltage vs. time

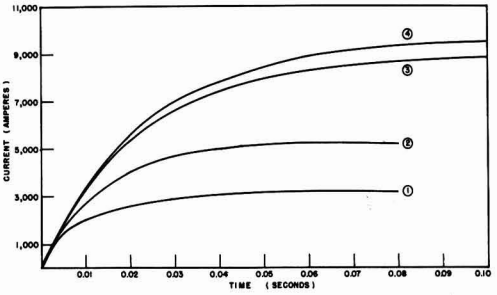

Fig. 4. Current vs. time

to render results very difficult to analyze quantitatively. Similarly, the short, heavy, brass tube was used so no appreciable inductance would be included in the current measurement.

A Brush recorder, type BL-202, was used to measure voltages. Time could be established to within 0.002 sec. This was considered to be of sufficient precision because the initial transients existed for times of 0.04-0.10 sec, depending on the L/R ratio, and because the measured voltages rose (from zero, in the case of current) and fell away (from OCV, in the case of cell voltage) very smoothly.

Data

Figures 3 and 4 show voltage decay and current rise curves over the first 0.1 sec or so, for the cell shorted through external shunts having resistances: 171, 193, 354, and 624×10^{-6} ohms. These data were all checked once and duplicate traces checked almost exactly when superimposed.

Discussion and Conclusion

The slopes of the voltage-time curves were measured and are shown plotted against the cell voltage in Fig. 5. The curves are linear; therefore Eq. [2] describes the discharges over these transient periods, i.e., these portions of the discharge data represent a constant potential driving current through an R-L circuit.

Presumably, the cell voltage might be constant over the ranges included in Fig. 5 and yet include some initial contribution, other than IR_l, to voltage decay. Therefore, the curves of Fig. 6 are shown where the voltage drop from open circuit is plotted against several values of current for each discharge.

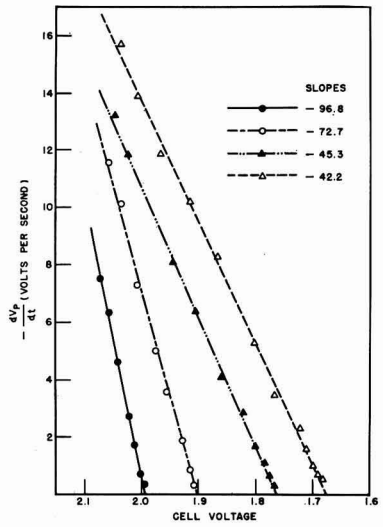

Fig. 5. $-dV_p/dt$ vs. cell voltage

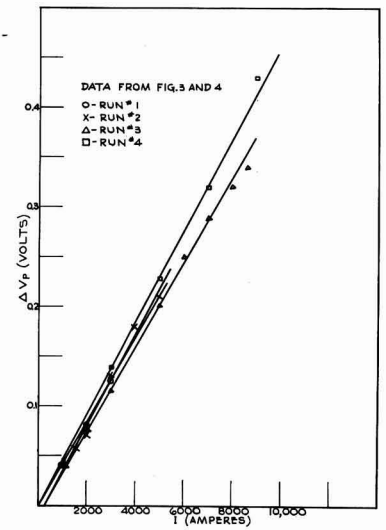

Fig. 6. Change in cell voltage vs. current, all runs

The curves are linear and nearly superimposable for each pair of runs and extrapolate through zero within 0.01 v.

It is concluded that there are no substantial (i.e., outside experimental error) contributions to voltage loss within the cell from sources other than IR loss over the discharge periods. The internal resistance obtained from the slopes of the curves of Fig. 6 has the value $43.7 \pm 3.8 \times 10^{-6}$ ohm. The resistance of the risers and lugs was measured during current flow and it contributes 10×10^{-6} ohm to the cell resistance measured at the tops of the lugs outside the cell, so total resistance of this cell in the fully charged condition was 53×10^{-6} ohm.

Values of inductance of the one-turn loop were estimated to be $5\text{-}8 \times 10^{-6}$ henry (6). Values calculated from the slopes of the curves of Fig. 5, knowing R_o and R_I, ranged between 5 and 7×10^{-6} henry.

One run was made in which time was extended out to 2 sec, during which cell voltage and single electrode potentials were measured. For this run, no polarization was evident at the negative plate after 0.1 sec, the total contribution from sources other than IR_I loss being located at the positive plate. With somewhat over 9000 amp flowing, positive plate polarization amounted to 0.05 v at 2 sec, and it was still increasing slowly when the run was stopped at about 5 sec.

Discharge Voltages Measured at the Cell Terminals

It has been mentioned that cell-voltage taps were located at the tops of the plates inside the cell to avoid contributions from the $L\ dI/dt$ term. One set of data will be presented to illustrate the effect of including such a contribution with the voltage taps at the cell terminals.

The circuit was rearranged to approach a short-circuit condition by removing the cables and swinging the short, heavy, current-measuring brass tube between the tops of the plates forming the switch mounting, so the external resistance consisted of the switch mounting and the brass tube in series. Reference to Fig. 2 will aid in getting the picture. The inductance loop was then bounded by the plates of the cell, the cell risers and lugs, the plates and switches comprising the switch mounting and the brass tube. The inductance of the loop was estimated to have a value of about 0.3×10^{-6} henry. For this run a different cell was used than was used for obtaining the previous data. It had a different number of plates but had the same nominal capacity.

The data for the run is given in Fig. 7. The shunt voltage curve (current) rose smoothly from zero to a value corresponding to 34,300 amperes.[2] The cell

[2] A word should be said about current density. The gross positive plate area is 64,000 cm² for this cell. Particle size measurements indicate the actual area of the active material could be as high as 3000 x the gross area, so current density can be in the range 0.5 to 1.7×10^{-4} amp/cm² depending on current distribution.

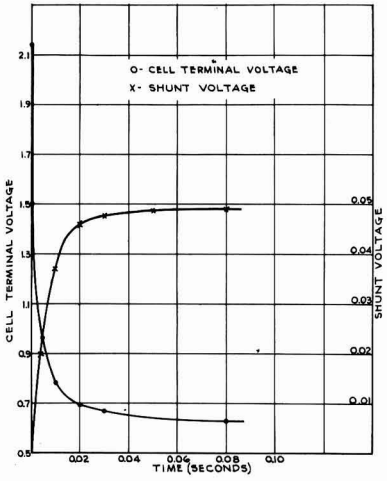

Fig. 7. Cell discharge data, voltage measured at cell terminals.

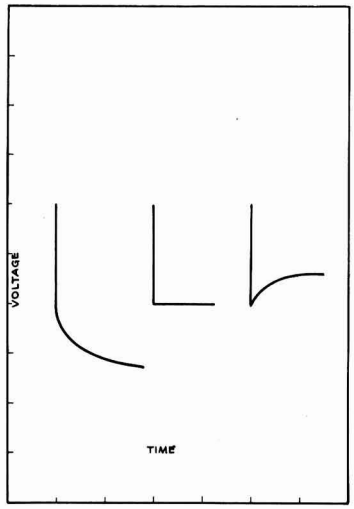

Fig. 8. Types of discharge curves possible in R-L circuits

voltage, however, fell immediately (i.e., within 0.002 sec) to a value of about 1.5 v, thereafter decaying smoothly to a value of 0.63 v.

Now, when the location of the cell voltage taps in relation to the geometry of the inductance loop is considered, it appears that the initial voltage drop could include 1/3-1/2 the initial $L\ dI/dt$ term. Furthermore, at zero time there can be no contribution from IR loss inside the cell because $I = 0$, or from electrochemical polarization because no current has passed. The conclusion that the initial voltage drop corresponds to an inductance contribution is inescapable.

The circuit inductance can be obtained from the time constant, i.e., t, when $I = 0.632\ I$ max. and total R in circuit from the equation: $L = tR$. t is 0.06 sec and R is approximated from the data assuming that when I levels off there is substantially no electrochemical contribution to polarization. If so, R_I is 43.7 x 10^{-6} ohm, R_o is 18.1 x 10^{-6} ohm, and L is 0.37 x 10^{-6} henry. Then, the initial voltage drop of 2.12-1.50 or 0.62 v is equal to $L_I\ dI/dt$, where L_I is the inductance contribution to the initial voltage drop measured at the terminals. dI/dt at zero time is 5.1 x 10^5 amp/sec from Fig. 7 and, therefore, L_I is 0.12 x 10^{-6} henry, i.e., within the estimated range of 1/3-1/2 of total L based on the circuit geometry.

One further point is to be made: by judicious selection of resistances in the latter circuit, polarization curves of the types illustrated in Fig. 8 could have been obtained, and this in a circuit containing R-L elements only. Of course, time constants would vary, depending on R, so the curves are illustrative only.

Manuscript received July 9, 1959. This paper was prepared for delivery before the Columbus Meeting, Oct. 18-22, 1959.

Any discussion of this paper will appear in a Discussion Section to be published in the June 1961 JOURNAL.

REFERENCES

1. E. Willihnganz, *Trans. Electrochem. Soc.*, **79**, 243, 253 (1941).
2. E. Willihnganz, "The Cold-Test Voltage of the Storage Battery," National Lead Co. Research Lab., Brooklyn, N. Y. (1944).
3. B. G. Bingham, Naval Research Lab. Report, No. 3707, June 30, 1950.
4. J. H. Kluck, Naval Research Lab. Report, No. 3839, July 27, 1951.
5. J. J. Lander and E. E. Nelson, Naval Research Lab. Report, No. 4347, May 10, 1954.
6. The Radio Amateur's Handbook, p. 460, American Radio Relay League, W. Hartford, Conn. (1945 ed.).

The Silver-Silver Oxide Electrode

B. D. Cahan, J. B. Ockerman, R. F. Amlie, and P. Rüetschi

Carl F. Norberg Research Center, The Electric Storage Battery Company, Yardley, Pennsylvania

ABSTRACT

An a-c square wave technique was used to study resistance and double-layer capacity during film formation on silver electrodes in KOH solutions. The peak in the voltage-time curve at constant current anodization is shown to coincide with complete surface coverage by Ag_2O and is not an ohmic resistance, but rather an overvoltage effect. Evidence for the existence of an unstable higher oxide than AgO (or additional oxygen) during oxygen evolution is presented. Microvolumetric gas measurements with large area electrodes on open-circuit decay also support this conclusion. The duration of the upper voltage plateau of the voltage-time curve during discharge of AgO electrodes is determined by contact phenomena among individual AgO particles, in particular by separation and passivation of the remaining AgO by insulating surface layers of Ag_2O.

Increased interest in the silver-silver oxide electrode has prompted a number of investigations about this system. However, the recent literature (1-15) shows a number of contradictions in the interpretation of the observed phenomena, in particular with regard to the presence of oxides higher than AgO on the electrode, and with regard to the shape of the voltage-time curves during constant current anodization and discharge of silver in KOH electrolyte.

It was decided, therefore to apply the a-c square-wave technique which was developed recently (16) to study films on lead electrodes. This technique in-

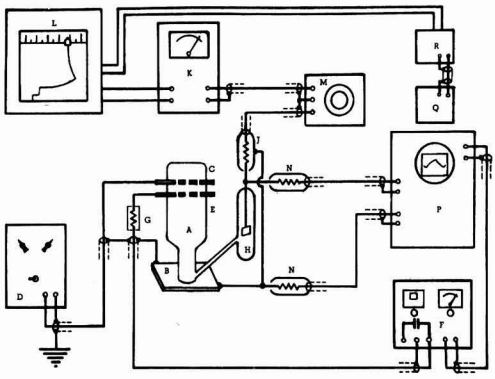

Fig. 1. Block diagram of electronic circuit: A, electrolytic cell; B, sample; C, upper platinum electrode; D, constant current supply; E, lower platinum electrode; F, square wave generator; G, noninductive resistor; H, reference electrode; J, 9 mΩ scope probe; K, electrometer; L, high speed recorder; M, bias box; N, 4 mΩ scope probes; P, oscilloscope; Q, camera; R, relay.

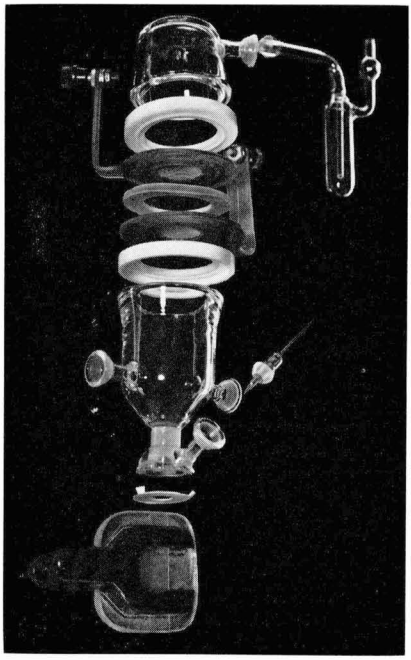

Fig. 2. Glass cell for the study of films at electrochemical interfaces.

volved the superposition of an a-c square wave current on the polarizing d-c constant current.

Experimental

The experimental set-up is illustrated schematically in Fig. 1. It shows the electrolytic cell, with separate auxiliary electrodes for the supply of a-c and d-c currents, and the recording equipment to follow the a-c and d-c response of the test electrode through a reference electrode. The instrumentation has been described in detail (16).

Figure 2 is a photograph of the cell. The test electrode, consisting of a sheet of silver, was clamped against the bottom of the cell with a thin Teflon gasket to prevent leakage. An area of 1 cm^2 was exposed to the electrolyte. A special micro reference-electrode was constructed in the following manner. A 28 gauge platinum wire was bent into a flat loop, 2 mm in length, and one end was pinch-sealed into a 3 mm Pyrex tube. The loop was heavily gold coated by placing gold chloride crystals on it and decomposing them by heating, and then fusing the gold into the surface of the platinum. Contact to the platinum wire in the tube was made by filling the tube with soft solder and by inserting a copper wire into the molten solder. The gold was then wetted with mercury such that it filled the loop. Mechanical cleaning of the gold-coated loop improved the wetting with mercury. This reference electrode was then placed into the KOH electrolyte to be used and anodized briefly. Microelectrodes prepared in this way gave potentials within 0.1 mv of a standard HgO reference electrode. The microelectrode was placed into the Luggin capillary, which intersected the side wall of the electrolytic cell within 0.3 mm of the electrode surface. This minimized the ohmic drop in the electrolyte during measurements of electrode potentials and provided for an undisturbed linear electrical field. Since the microelectrode was only 3 mm from the electrode surface, frequency dispersion and capacitive pick-up were minimized.

Figure 3 shows examples of oscilloscope traces obtained with this equipment. The traces shown here were selected in order to demonstrate the advantage of using a micro reference-electrode over a macro-electrode and the advantages of a differential oscilloscope input over a single ended one. The traces are voltage-time curves. The sweep speed was 20 μsec/cm. The voltage scale was 5 mv/cm. The square wave current used had a frequency of 6250 cps and was 10 ma peak to peak.

Trace 1 was obtained using a conventional macro reference electrode and differential oscilloscope input (type 53/54 D Tektronix plug-in preamplifier). Here the electrolyte path between the reference

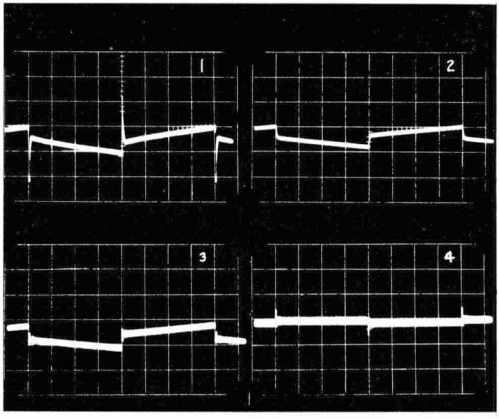

Fig. 3. Oscilloscope traces of voltage-time curves. Abscissa: time (20 μsec/cm); ordinate: voltage (5 mv/cm).

electrode and the working electrode was a Luggin capillary 8 cm long. Clearly visible is the overshoot of the trace due to capacitive pick-up. The duration of the transient spike at the moment of current reversal is between 2-3 μsec. This obscures the determination of initial slopes of the traces.

Trace 2 shows a similar curve, but taken with a microelectrode. It can be seen that the transient spikes are completely eliminated. The rise-time of the oscilloscope preamplifier was about 1 μsec in the 5 mv/cm range used here, and the reference electrode shows a perfect frequency response for this rise time. [When a wider band pass amplifier was used (type 53/54 B Tektronix plug-in unit), the rise time of the traces was found to be 0.1 μsec, or as good as the rise time of the square wave current used.] This shows that the arrangement used here is capable of following extremely fast electrochemical phenomena.

Trace 3 shows the effect of using a single-ended preamplifier (type 53/54 D Tektronix unit, used single ended) instead of a differential amplifier. The traces show extensive ringing and noise pick-up. At the low voltage signal levels used here even the resistance of the copper wires of the cable shields and the ground return paths represent considerable impedances. Even though all ground connections are made at the working electrode, high-frequency cable oscillations are detectable and a-c ground loops are set up.

Trace 4 was obtained by connecting the single ended amplifier between the square wave generator ground and the working electrode, which were short circuited by the cable shield. Trace 4 represents the difference between trace 2 and 3. In trace 2 the effects of all ground loops and spurious pick-up have been eliminated or cancelled electronically.

Pure silver sheet (99.99%) was etched in dilute nitric acid, washed with triple-distilled water, and air dried. The sample was cathodized at 3 ma/cm^2 in 30% KOH at 28°C for several minutes whereby hydrogen was evolved to remove any surface films of silver oxide. The current was reversed and the electrode anodized. The potentials were recorded and pictures were taken with the camera on the oscilloscope to determine the double layer capacity and resistance at rapid intervals during the anodization period of 5 min. Then the current was reversed and the oxide film discharged.

In a second phase of this investigation of the silver-silver oxide system, a microvolumetric study of oxygen evolved during the open-circuit decay of oxygen overvoltage was made. The oxygen evolved at constant temperature and pressure was measured as a function of time simultaneously with the decay of potential. The experimental set-up for this study has been described recently (17).

A standard AgO storage battery plate as produced by the Industrial Division of The Electric Storage Battery Company, containing 7 g of silver, was charged over prolonged periods of time at 50 ma in 30% KOH. The current was then interrupted and the potential allowed to decay to 0.52 v vs. Hg/HgO or 20 mv positive to the reversible AgO/Ag$_2$O potential. The plate was then charged at various

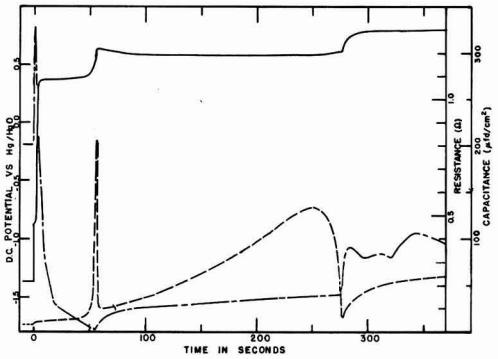

Fig. 4. Electrode potential (solid line), ohmic resistance (dashed line), and double layer capacity (dotted-dashed line) of silver during anodization at 3 ma/cm^2 as a function of time.

constant currents from 10 ma to 250 ma and the build-up of oxygen overvoltage recorded. After 24 hr of overcharge the currents were interrupted and the cell sealed simultaneously. The gas evolved during overvoltage decay was measured by the displacement of a drop of liquid in a calibrated capillary.

Results

The anodization curve of a 1 cm^2 sheet silver electrode is shown as the solid line in Fig. 4. The curve starts out at hydrogen evolution at 3 ma/cm^2. At $t = 0$ the current was reversed and the potential rose rapidly. After a sharp rise of 450 mv there was a slight arrest and then the potential rose smoothly to the Ag/Ag$_2$O potential at about +0.35 v.

After about 40 sec, the potential increased to a peak of +0.62 v, and decreased subsequently to about +0.57 v. The potential rose again after 250 sec to +0.6 v, after which a sharp break occurred, and the potential increased to +0.8 v. At the point of the sharp rise a cloud of fine gas bubbles was seen rising in the electrolyte.

The electrode film resistance calculated from the oscilloscope traces as recorded by the camera is plotted as a dotted line. The initial resistance is very low, about 0.03 Ω, and is due primarily to the gas bubbles adhering to the surface, and reducing the effective cross section of the electrolyte. As the current is reversed, the resistance shows a slight jump, but remains relatively constant at 0.04 to 0.05 Ω for about 40 sec.

At this time, the resistance builds up quite rapidly to a very high value of 0.8 Ω, and probably higher, indicating a rapid passivation of the surface. At the moment the potential reaches its peak, the resistance falls off such that within 1 sec the resistance has fallen to 0.1 Ω. During the course of the Ag$_2$O/AgO voltage plateau the resistance increases smoothly to a point about 30 sec before the third step in the voltage-time curve, or where O_2 is evolved. Here, rather than increasing as at the beginning of the Ag$_2$O/AgO plateau, the resistance takes a sharp dip, falling to a value of 0.06 Ω. After the oxygen evolution starts, the resistance builds

up smoothly as the oxide film thickness continues to increase slowly.

The curve showing the differential capacitance (as determined from the initial slope of the voltage-time oscillographs) is plotted as a dot-dash line. This curve reflects in a general way the inverse of the resistance-time curves, with several noteworthy exceptions. The initial capacity during H_2 evolution is about 200 μfd/cm^2, indicating a roughness factor of about 10 (assuming a double layer capacity of 20 μfd/cm^2 of true surface area). The momentary high capacity after reversal shows that some highly reversible reaction is in progress, but after the first 10-15 sec the capacity decreases nearly linearly to very low values of 1-2 μfd/cm^2. After the Ag_2O/AgO plateau is reached the capacity rises rapidly to 25 μfd/cm^2 and then more slowly to about 40 μfd/cm^2. When oxygen evolution starts the capacity increases abruptly and erratically, rising to a peak and decaying, rising to a peak and decaying, rising again, etc.

The discharge curve of a specimen that had been held at the oxygen evolution potential at 3 ma/cm^2 for 3 min is shown by the solid line in Fig. 5. The potential falls in about ½ sec to the Ag_2O/AgO plateau, but this drop is *not* instantaneous. The AgO plateau lasts for 100 sec, at 3 ma/cm^2 and then drops to the Ag_2O/Ag discharge potential. This second plateau lasts for 170 sec (longer than the first plateau) and then the potential falls off rapidly. A slight arrest is noted, at −0.75 v and then the potential drops to the H_2 evolution value.

The resistance curve during discharge shows a very different behavior from that obtained on anodization. The resistance of 0.3 Ω at oxygen evolution shows an initial rise which levels off at about 0.5 Ω. A more gradual increase sets in, which slowly accelerates until values as high as 2.5 Ω or more are reached. The resistance breaks down completely within 1/6 of a second, or the repetition rate of the camera we used, at the moment when the potential drops to the lower voltage plateau. The resistance falls to 0.04 Ω and gradually decreases to unmeasurably low values during the Ag_2O/Ag plateau.

After a sharp initial peak, the capacitance decreases about linearly as passivation progresses, decreasing to 1 or 2 μfd/cm^2 at the transition point. As the Ag/Ag_2O step progresses, the capacitance increases more or less linearly to very high values (greater than 4000 μfd/cm^2) and drops off sharply at the end of the second voltage plateau. A further peak in capacitance occurs during the small potential arrest, and then the capacitance decreases rapidly at H_2 evolution. It might be noted that the capacitance at this point is about 400 μfd/cm^2 as compared to 200 at the start of the run, indicating a roughening of the surface by a factor of 2.

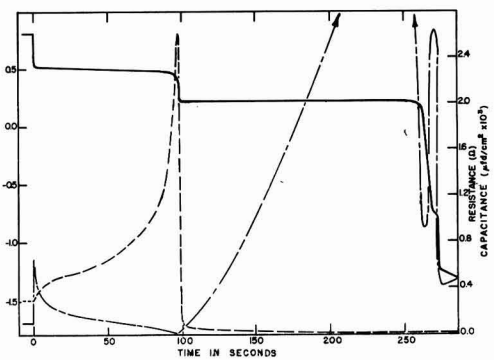

Fig. 5. Electrode potential (solid line), ohmic resistance (dashed line), and double layer capacity (dotted-dashed line) of a silver oxide film (produced by previous anodization of silver in KOH) during discharge at 3 ma/cm^2, as a function of time.

The results of the microvolumetric studies during oxygen overvoltage decay are shown on Fig. 6. These results were obtained with porous large-area electrodes. Figure 6A shows the plots of electrode potential vs. time on a logarithmic scale, for open-circuit decay from three different prepolarizing currents. Also shown is a plot of oxygen evolved vs. time during overvoltage decay on open circuit. Figure 6B shows a similar curve for the decay of oxygen overvoltage on PbO_2 in sulfuric acid. The results for PbO_2 (Fig. 6B, 6D, and 6F) are included here for purposes of comparison only, because they are representative of the decay of overvoltage on an inert electrode (17). Similar curves are obtained for decay of oxygen overvoltage on nickel in KOH, decay of hydrogen overvoltage on Zn and Cd in KOH, and Pb in H_2SO_4.

Figure 6C is a plot of the electrode potential during oxygen overvoltage decay vs. relative excess of oxygen, or vs. $V_T - V_X$, where V_T is the total volume of oxygen evolved to a potential 20 mv above the open-circuit potential, and V_X is the volume of oxygen evolved to any intermediate potential. Figure 6D shows a similar plot for decay of oxygen overvoltage on PbO_2 (17). Figure 6E illustrates a charging curve for build-up of oxygen overvoltage on AgO. The large-area electrodes were charged after being allowed to decay to a potential 20 mv above the reversible open-circuit potential, at different currents. Similar charging curves are shown in Fig. 6F for PbO_2.

Discussion

These results permit a detailed analysis of the mechanisms of the silver oxide electrode. In particular, the effects of the resistance of the surface films on silver are brought out clearly. The lower oxide, Ag_2O, has a very high electrical resistivity. Ag_2O powder was compressed into a hard, shiny pellet at 62,500 psi. The resistance was measured with an electrometer ohmmeter to be $7 \cdot 10^6$ Ω cm. (Using this value, a 1 cm^2 monolayer would have a calculated resistance of about 1 Ω. The extrapolation is, of course, very approximate, since a monolayer has different properties from bulk material.) From the length of the Ag/Ag_2O plateau in Fig. 4 and a surface roughness factor of about 10, the thickness of the Ag_2O film produced during the plateau is roughly 50-100 monolayers thick. It is apparent that the surface film of Ag_2O is nonuniform and that at the moment of complete coverage, the resistance must rise to relatively high values. This causes the sharp peak in the resistance curve.

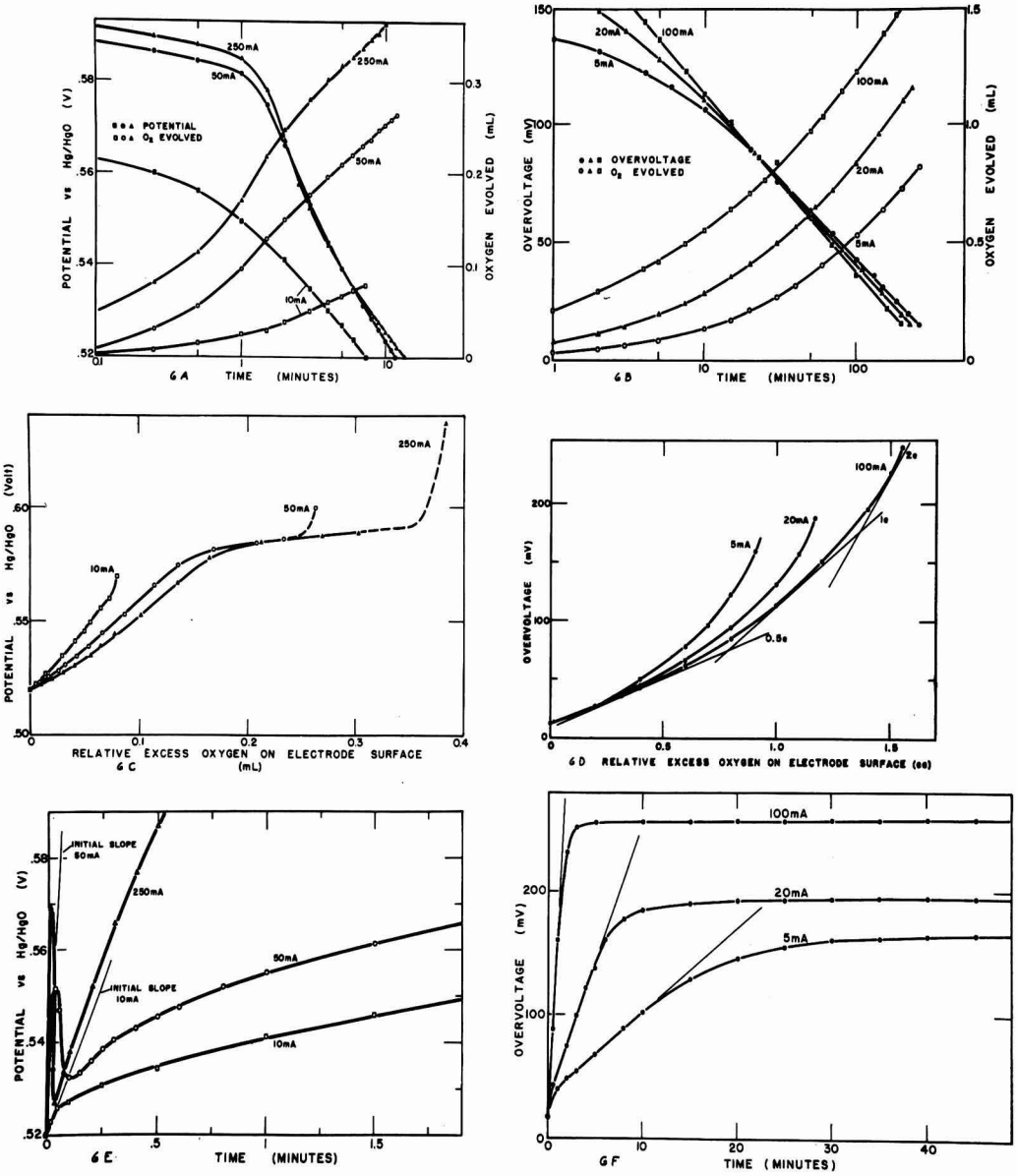

Fig. 6. Comparison of overvoltage and gas evolution data on AgO and PbO_2 electrodes. Fig. 6A, overvoltage decay and gas evolution during open-circuit decay of an AgO electrode in KOH. Fig. 6B, overvoltage decay and gas evolution during open-circuit decay of a PbO_2 electrode in H_2SO_4. Fig. 6C, electrode potential of AgO in KOH during decay as a function of gas evolved. Fig. 6D, electrode potential of PbO_2 in H_2SO_4 during decay as function of gas evolved. Fig. 6E, charging curves for oxygen overvoltage build-up on AgO electrodes. Fig. 6F, charging curves for oxygen overvoltage build-up on PbO_2 electrodes.

The peak observed in the voltage-time curve at the beginning of the AgO step is not directly due to an ohmic resistance effect since the ohmic resistance is in the order of 1 Ω and would produce a voltage increase of only 3 mv at 3 ma/cm². The peak is much higher and is produced rather by a concentration of the current into small localized areas, where the conversion of Ag_2O to AgO can proceed. This causes an increased overvoltage for the conversion reaction. The points where Ag_2O first converts to AgO are those where the Ag_2O film is thinnest and which were covered last. From these points the conversion spreads until the Ag_2O film is substantially oxidized. Simultaneously a further attack of metallic silver takes place. Any Ag_2O which is formed during this stage must be rapidly oxidized and can have only a transitory existence.

The resistivity of AgO was measured in the same

way as for Ag_2O, and was found to be $5 \cdot 10^8$ Ω cm. This is five orders of magnitude smaller than for Ag_2O.

During the upper plateau 0.6 coulombs of electricity are used in forming a film of AgO of "average" thickness of approximately $5 \cdot 10^{-5}$ cm. Since the resistivity is $5 \cdot 10^8$ Ω cm, the resistance of the film should be of the order of 0.25 Ω. This is of the order of the resistance actually measured, 0.53 Ω. This resistance value shows that there *cannot* be at any time during anodization a significant complete interface layer of Ag_2O present. On open circuit, a heavier film of Ag_2O can be present, formed by local action cells between AgO and Ag.

It is pointed out here that the limiting film thickness roughly of $5 \cdot 10^{-5}$ cm is of particular importance for the manufacturing of porous silver oxide electrodes for silver-zinc batteries. It is evident that only particles with a diameter less than 10^{-4} cm (1 μ) are readily and completely converted from metal to oxide.

At the end of the AgO plateau the resistance drops to values of 0.08 Ω. This drop should not be interpreted as a physical rupture of the layer and an exposure of silver to the electrolyte, because the oxidation of metallic silver has been shown to be small once a complete AgO film is formed, and ruptures therefore should not occur. It is proposed that a further incorporation of oxygen in the AgO film has taken place, producing a highly unstable film of a higher oxide than AgO. It is not clear how the additional oxygen is adsorbed in the individual crystallites. However, in any case, the resistivity of the film is changed.

Although little accurate data is available, it is often observed that when a metal oxide exists in several valence states, the resistivity decreases with increasing valence state. For example, PbO has a resistivity of $2\text{-}5 \cdot 10^7$ Ω cm and PbO_2 of 1 to $5 \cdot 10^{-4}$ Ω cm. Similarly, AgO has much lower resistivity than Ag_2O, and a possible higher oxide would have an even lower resistivity. Although this rule is not without exceptions, it could possibly account for the sharp drop in resistance observed at 250 sec in Fig. 4. Only very small parts of the AgO surface film need be converted to a highly conducting compound in order to produce the observed effect.

The rise in potential at the point of oxygen evolution is not due to an ohmic-resistance passivation, but rather to oxygen overvoltage on the limited number of sites of the higher, unstable oxide, concentrating the current to small local areas.

The capacitance peak at the beginning of the anodization curve shows that the reaction is here very reversible. The linear decrease during the first voltage plateau is due to a decrease in the available surface area. The capacity during the AgO step is small. This indicates that the surface film is now conductive, and that the capacitance is again due to the solid-liquid double layer. The erratic behavior of the capacitance during oxygen evolution is due to the instability of the higher silver oxide sites which may vary in number and size.

During discharge of the silver oxide film, shown in Fig. 5, the resistance is low at the beginning and increases quickly as the higher silver oxide sites disappear. The further increase in resistivity is due to build-up of Ag_2O on the surface toward the electrolyte, blocking the underlying AgO from reaction. The resistance rises to values greater than 2.5 Ω. When the electrode is substantially covered with Ag_2O, the local high current density polarizes the electrode to a potential where metallic silver can be produced. At this point, the resistance drops sharply due to the formation of filamentary crystals of silver, providing good electrical contact. The first voltage plateau during discharge is always observed to be substantially shorter than the second plateau, although the film consisted initially of almost pure AgO, and the total capacity to the end of the second plateau corresponds to a two-electron change. As explained above, this is due to a covering of AgO by Ag_2O. As the passivating layer of Ag_2O is converted to silver, further AgO can be discharged, by formation of more Ag_2O from a local cell of Ag and AgO. The energy corresponding to the 250 mv difference between the two plateaus is lost internally as heat. The electrochemical reactions for the oxidation of Ag and the reduction of AgO are fast. Thus internal local action in an electrode between Ag and AgO should proceed rapidly. The utilization of AgO in discharge of silver-zinc cells is illustrated in Fig. 7. Two standard commercial cells were made using chemically produced AgO in the positives. In one of these cells (upper circuit), a special inert conductive matrix[1] was incorporated which could establish electric contact to each individual AgO particle. In this manner, the passivation due to Ag_2O was greatly minimized, and all the AgO was utilized at the

[1] Subject matter of patent application.

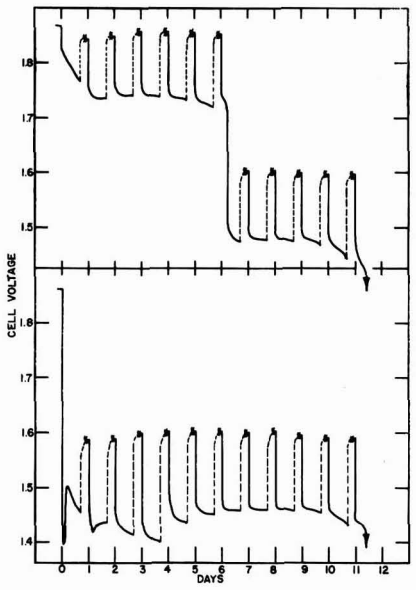

Fig. 7. Discharge curves of commercial silver-zinc cells with and without conductive, inert matrix in the silver electrode. The solid line is the cell voltage during discharge. The dotted line represents the recovery of cell voltage on open circuit.

higher voltage plateau, at close to 100% efficiency.

These cells were discharged for 6 hr/day and allowed to recover overnight. The discharge is shown in Fig. 7 by the solid line and the recovery by the dotted line. The initial sharp drop in voltage for the lower cell shows the insulating effect of the Ag_2O film, which quickly covered the surface of the AgO electrode. The voltage recovered somewhat as soon as some silver was produced. Overnight, most of the silver was reoxidized by the remaining AgO.

The upper curve is for an identical cell but with the conductive matrix. The discharge occurs at the higher plateau for the theoretical time, namely one half of the discharge. This results in an increase of 10% in the watt-hour output.

The decay of oxygen overvoltage on open circuit on an inert electrode is in general expected to follow, after an initial time period, a linear relationship with the logarithm of time, having a slope equal to the negative of the Tafel slope (17). It is noticed in Fig. 6A that the decay curve from 10 ma charge shows this normal behavior, while the decay curves from 50 and 250 ma show a characteristic inflection. The curves for evolved oxygen show similar inflections. The curves approach the same slope toward the end of decay only. The electrode potential tends to remain higher than normal for an initial period of time. Figure 6C shows this even more clearly. Several tenths of a cubic centimeter of oxygen are evolved while the potential remains at 0.585 ± 0.005 v, independent of the value of the prepolarizing current. This quantity of oxygen corresponds to 10 micromoles. No such potential plateau is observed for a "normal" electrode like PbO_2 (Fig. 6D).

The decay from 10 ma/cm^2 for AgO (Fig. 6C) also shows no such arrest, indicating that the charging potential was not sufficiently high to produce the higher oxide.

The arrest in oxygen overvoltage decay on AgO has been observed by other investigators (2, 15) but has been interpreted sometimes to be caused by hydroxyl-hydroperoxide ion couples and/or hydroxyl-oxygen couples (8, 15). This interpretation does not explain the high conductivity of the film at the point of oxygen evolution and, furthermore, the potential of such couples would not coincide with the plateau observed.

The charging curves of large-area AgO electrodes (Fig. 6E) which had previously been kept slightly above the Ag_2O/AgO potential, but below the potential of the plateau mentioned above, show a sharp initial peak unlike the smooth build up of oxygen overvoltage on PbO_2. These peaks possibly correspond to a nucleation phenomena for the higher oxide or the active sites of oxygen evolution.

Conclusions

1. The mechanism responsible for the peak in the anodization curve of Ag in KOH solution at the beginning of the AgO step (Fig. 4) is due to passivation, forcing the currents to small areas and producing a high overvoltage. It is *not* due directly to an ohmic resistance.

2. The reason for the shortness of the AgO step on discharge of an AgO electrode is an isolation of AgO by an Ag_2O film which is highly resistive.

3. By special electrode formulation the length of the AgO plateau can be extended to the theoretical length of ½ of the discharge time.

4. Evidence is presented for the existence of a conductive, unstable oxide of silver with an oxidation state higher than AgO. Because of its transitory nature, identification by means of x-ray diffraction techniques is difficult, if not impossible.

5. The use of an adequately designed cell and microreference electrode, together with a differential amplifier, permits single electrode studies at high frequencies, with electrode voltage rise-times better than 0.1 μsec.

Acknowledgments

The authors are indebted to Captain C. G. Grimes, Director of Research of The Carl F. Norberg Research Center of The Electric Storage Battery Company, for the permission to publish this paper.

Manuscript received Feb. 26, 1960. This paper was prepared for delivery before the Columbus Meeting, Oct. 18-22, 1959.

Any discussion of this paper will appear in a Discussion Section to be published in the June 1961 JOURNAL.

REFERENCES

1. A. Hickling and D. Taylor, *Discussion Faraday Soc.*, **1**, 277 (1947).
2. P. Jones, H. R. Thirsk, and W. F. K. Wynne-Jones, *Trans. Faraday Soc.*, **52**, 1003 (1956).
3. A. B. Neiding and I. A. Kazarnovskii, *Dokl. Akad. Nauk SSSR*, **78**, 713 (1951).
4. T. P. Dirkse and G. J. Werkema, *This Journal*, **106**, 88 (1959).
5. P. Rüetschi and P. Delahay, *J. Chem. Phys.*, **23**, 556 (1955).
6. T. P. Dirkse, *This Journal*, **106**, 453 (1959).
7. B. N. Kabanov and D. I. Leikis, *Z. Elektrochem.*, **62**, 660 (1958).
8. C. P. Wales and J. Burbank, *This Journal*, **106**, 885 (1959).
9. Yu. V. Pleskov, *Doklady Akad. Nauk. SSSR*, **117**, 645 (1957).
10. K. Nagel, R. Ohse, and E. Lange, *Z. Elektrochem.*, **61**, 795 (1957).
11. F. Bonk and A. B. Garret, *This Journal*, **106**, 612 (1959).
12. T. I. Borisova and V. I. Veselovskii, *Zhur. Fiz. Khim.*, **27**, 1195 (1953).
13. T. I. Borisova, *Trudy Sov. Elektrokhim. Akad. Nauk. SSSR Otdel Khim Nauk* 1950, 386 (1953).
14. I. N. Pospelova, A. A. Rakov, and S. Ya. Pshezhetskiy, *Zhur. Fiz. Khim. SSSR*, **30**, 1433 (1956).
15. T. P. Dirske, *This Journal*, **106**, 920 (1959).
16. B. D. Cahan and P. Rüetschi, *ibid.*, **106**, 543 (1959).
17. P. Rüetschi, J. B. Ockerman, and R. Amlie, *ibid.*, **107**, 325 (1960).

The High-Temperature Aqueous Corrosion Resistance of the Uranium-5% Zirconium -1½% Niobium Alloy

J. E. Draley, S. Greenberg, and W. E. Ruther

Argonne National Laboratory, Lemont, Illinois

ABSTRACT

The ~~uranium-5% zirconium-1½% niobium~~ U/5% Zr/1½% Nb alloy shows good corrosion resistance, as gamma quenched, in water to about 315°C. Optimum heat treatment results in a rate of about 6 mg/cm²/day at 290°C. Moderate aging, e.g., 400°C for 2 hr, results in reduced corrosion rates in the initial stages of corrosion; however, corrosion resistance can be destroyed by overaging. After protracted exposure, samples fail; this is believed due to absorbed corrosion product ~~hydrogen~~. H.

Operation of heterogeneous water-cooled nuclear reactors at high temperatures would be facilitated if the fuel were corrosion resistant. Since unalloyed uranium corrodes very rapidly in high-temperature water, considerable effort has been devoted to the development of corrosion resistant alloys of reasonably low alloy content and to the understanding of the corrosion mechanism. Much of this work has been summarized (1-5).

The development of a group of "distorted" alpha phase alloys of relatively low alloy content has been described (6). In this class, niobium has appeared to be the most valuable alloying element. Its loss of as-quenched corrosion resistance during heat treatment can partly be prevented by the ternary addition of zirconium. This paper is concerned with the detailed corrosion behavior of the uranium-5% zirconium-1½% niobium alloy.

This alloy was chosen as the fuel for the Argonne Experimental Boiling Water Reactor. The properties of a fissionable material are profoundly affected by nuclear radiation. Its effect on the corrosion behavior, as well as on some physical and mechanical properties, of this alloy has been described in detail elsewhere (7-9). It is sufficient to mention here that only small amounts of radiation greatly increase the corrosion rate of relatively resistant material.

Experimental Procedure

Alloys were vacuum melted and cast by the Foundry and Fabrication Group of the Argonne Metallurgy Division. The compositions of all those studied during this investigation, together with the crucible and mold material, are given in Table I.

Most samples were gamma quenched by heating at 1000°C in vacuum (suspended in tantalum wire basket) and quenching in Woods Metal at 125°C. Other samples were gamma treated by heating to 850°C in liquid metal or salt and quenching in various media. The method of heat treatment is indicated in the data.

Relatively low-temperature treatments subsequent to quenching are referred to as aging treatments. Because of the wide variation in times and temperatures of aging, three methods were used: (*a*) sample in an evacuated ampoule placed in electric oven (low temperatures, long times); (*b*) sample placed in Vycor tube furnace with flowing argon or helium (low and medium temperatures, short and medium times); and (*c*) sample immersed bare in liquid metal (high temperature, short time).

Samples were air cooled after aging. There were enough samples aged by two of these methods to indicate that the method used was not a significant variable.

Samples are described by the original casting number and the location (when known) with relation to the ingot, indicated as T (top), B (bottom), or C (center). Preparation of the material is described as c (as cast) or r (rolled). Thus L-170B-r indicates the bottom section of casting L-170 in the rolled condition. Compositions are given in weight per cent.

The high-temperature corrosion tests were conducted in stainless steel autoclaves, placed in forced convection ovens. In most tests, samples were insulated from electrical contact with a stainless steel

Table I. Composition of alloys tested†

Alloy	Zr	Nb	C, ppm	N, ppm	Si, ppm	Crucible material‡
H-203-T	3.93	1.77	10	35	200	
B	4.70	1.73				Magnesia
H-317-T	5.40	1.57	65	46	50	
B	5.36	1.60	23	26	60	Magnesia
H-416-T	4.88	1.71	25	11		
B	4.81	1.67	22	10	100	Graphite
H-419-T	5.80	1.80	15	13	200	
B	4.95	1.62	78	34	150	Graphite*
L-157-T	7.00	1.60	64	41	100	
B	6.00	1.65	43	134	100	Magnasite*
L-170-T	5.70	1.95	12	10		
B	5.20	1.60	21	16	100	Magnasite*

† Unless otherwise indicated, composition is given as weight per cent. Analyses by Chemistry Division, ANL.

‡ Most casting was done into a water-cooled copper mold.

* Denotes those which were cast into heated graphite molds.

holder by means of synthetic sapphire rods. Some corrosion tests performed in the Argonne Reactor Engineering Division are also reported here. In these tests the alloy samples were allowed free contact with the bodies of the stainless steel test autoclaves. There was no noticeable effect of such contact.

Before the first period of test, samples were wet-ground to 400 grit metallurgical paper. Whenever the sample shape made this procedure impractical, it was electropolished in a perchloric-acetic acid (1 to 10) bath. Results indicate that there was no significant difference in corrosion behavior caused by this difference in procedure. Surface areas were measured, after which the samples were degreased in methyl alcohol, washed in distilled water, and weighed. After each test period each sample was cleaned of loose oxide with wet Kleenex, dried under vacuum, and weighed. Since very little of the corrosion product remained on the sample, weight losses closely approximated actual metal corroded. These values were plotted as a function of time, and the slopes of the curves so obtained are described as the "corrosion rate" (areas used in the computations were the original sample areas). These rates are expressed as mg/cm²/day (mcd).

Distilled water was used as the corroding medium unless otherwise indicated. This water was double distilled, passing through a cation exchange resin between the two distillation steps. The resistivity of the water was equal to or greater than one megohm-cm at the tap. The autoclave was filled with this water, heated to boiling, and the water discarded. The sample and its holder were placed in the autoclave; water was then added and again heated to boiling. A water sample was withdrawn and the autoclave sealed while the water was still boiling. The specific resistance of this water sample was measured as a check on water quality and cleanliness of the autoclave. The value was typically several hundred thousand ohm-cm. Fresh water was added in this way for each exposure so that during long tests the water was replaced each time the sample was examined.

Hydrogen analyses were performed in an apparatus in which the uranium alloy sample was heated into the gamma phase region (about 850°C). By means of two Toepler pumps the hydrogen was passed, through a paladium valve, into a calibrated volume where its pressure was measured. That the evolution of hydrogen is complete has been demonstrated by corroborative analyses run by combustion. For analyses of samples after corrosion test, the corrosion product was sometimes removed by grinding the samples clean, and sometimes it was left on and simply dried by evacuation at room temperature. For a few cases where both procedures were used on similar samples, the results were the same, inferring that the drying procedure adequately removed moisture, so that errors from this source are unlikely.

For metallographic examination the majority of samples were electroetched with the Ames solution at 15-30 ma/cm² at room temperature. This solution consists of eight parts (by volume) concentrated phosphoric acid, five parts ethyl alcohol, and five parts ethylene glycol. In some cases, electroetching was carried out in a 10% (by weight) chromic acid solution at room temperature using a current density of 10-15 ma/cm².

Results

Heat Treatment

Necessity for gamma quench.—The uranium-zirconium-niobium system has been thoroughly studied and analyzed (10, 11). The discussion here is limited to that necessary for an understanding of the relationship between heat treatment and corrosion resistance.

Between 677°C and the melting point the alloy (5 Zr + 1½ Nb) consists of a single phase (gamma). A two-phase (beta plus gamma) region exists in the narrow temperature range of 666°-677°C. Below 666°C, the structure depends on the heat treatment received by the material.

Alpha uranium is orthorhombic and lacks high-temperature corrosion resistance. The beta phase has a complex structure of tetragonal symmetry. Gamma uranium has a body-centered cubic lattice and has shown good corrosion resistance when retained by alloying.

Isothermal quenching from the gamma to the beta-plus-gamma region (and holding there for, say, 24 hr) followed by rapid quenching to room temperature produces alpha plus a martensitic (distorted alpha) phase. This structure is not corrosion resistant.

If the above procedure is followed except that the temperature of the isothermal quench is reduced to about 660°C, the room temperature structure consists of normal alpha and retained (metastable) gamma. This structure also lacks corrosion resistance.

Rapid quenching from the gamma phase to temperatures close to room temperature produces the martensitic (distorted alpha) structure. This structure is corrosion resistant. It is not known if the alloying elements are present as a submicroscopic dispersion or are in supersaturated solution. However, a second phase has not been detected at 2000X. This treatment and resulting structure is necessary for high-temperature corrosion resistance.

The rate of quench is very important. One typical method of heat treatment consists of holding the sample at 1000°C for 1 hr and then quenching in molten Woods Metal at 125°C. In one such operation the sample caught up in such a position that only about one-half was immersed in the Woods Metal. A subsequent three-day corrosion test at 300°C resulted in almost complete disintegration of that part of the sample which was not immersed.

Additional experiments confirmed the importance of quenching rate. A series of samples were heated in lead at 800°C and quenched in water, molten Woods Metal at about 125°C, oil, and liquid nitrogen. The first two groups of samples were satisfactory in water at 290°C. The latter two disintegrated in less than four days. It is indicated that the rate of quenching in oil and liquid nitrogen is lower than some critical required value. In the latter case

this is probably due to the presence of a vapor blanket.

Corrosion-resistant material is produced by quenching from temperatures in the range 725°-1000°C. The materials tested apparently were homogeneous at these temperatures, since corrosion behavior was independent of time at temperature during gamma treatment, in the range of a few minutes to 5.5 hr.

Aging characteristics.—The aging characteristics of the alloy are of importance from the point of view of particular uses. Of equal interest is the fact that a study of the aging process can lead to an understanding of the nature of the corrosion resistance and the mechanism of the loss of corrosion resistance.

Overaging destroys the corrosion resistance of the alloy. Failure of the alloy can take place either by complete disintegration or by cracking or spalling into several pieces. The latter is apparently a stage in the former. If an apparently sound piece which has cracked off is subjected to a short additional exposure, further severe cracking or complete disintegration usually takes place. This statement refers to cracking into several relatively equivalent pieces and not to minor chipping from the bulk of a sample.

As an arbitrary measure of the aging resistance of the alloy it was decided that a sample was resistant to the given combination of time and temperature if it did not fail in either of the above ways in two weeks of testing in degassed, distilled water at 290°C.

In Fig. 1, the area above the curve represents heat treatments which caused failure in less than two weeks. Combinations of time at temperature below the curve did not cause failure as it has been defined. This curve is based on castings H-317, H-416, H-419, and L-170 in the as-cast and rolled conditions. Samples were quenched from 1000°C (in vacuum) and aged in vacuum, argon, helium, or molten lead. Aging for times insufficient to cause "failure" reduced short-time corrosion rates, with the optimum close to 2 hr at 400°C. This effect is illustrated in Fig. 2. Satisfactory samples had a dark brown surface uniformly interspersed with shallow pits.

As the time of exposure was increased the corrosion rates of gamma quenched and gamma quenched

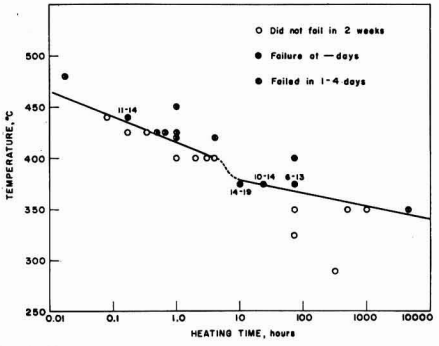

Fig. 1. Effect of heat treatment on corrosion life at 290°C of gamma quenched U-5% Zr-1½% Nb alloys.

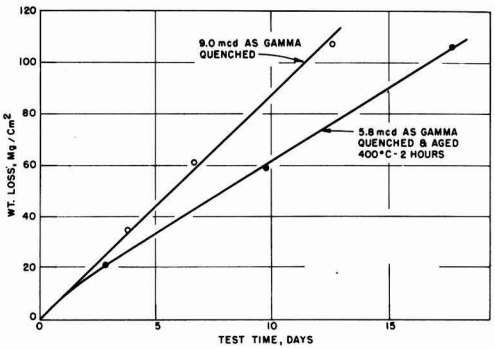

Fig. 2. Short-time effect of aging on corrosion rate of L170BC in water at 290°C.

and aged material generally became equal. In some cases the corrosion rate of gamma quenched material decreased (Fig. 3, curve 3). (This figure is also used to illustrate other ideas and will be referred to again.) It also appears that aging at 400°C decreased the corrosion life of the few samples tested for sufficient times.

To eliminate the possibility that aging occurred during test, cast samples of alloy H-317 were tested as quenched, as quenched and aged at 400°C for 2 hr, and as quenched and aged at 290°C for 312 hr. All samples showed appreciable periods of approximately equal corrosion rates.

Effect of hydrogen.—The standard heat-treatment procedure includes heating in a vacuum tube furnace at 1000°C. Considerable gas (believed to be largely hydrogen) is evolved in this process. In an effort to learn whether corrosion behavior is influenced by this gas, adjacent samples from the same rolled ingot were treated in vacuo and in molten lead.

The corrosion of these samples in water at 290°C is shown in Fig. 4. The sample heat treated in helium was included to reproduce the thermal history of the vacuum-treated sample. It is inferred that the gas content of the metal, as received, is detrimental to its corrosion properties.

A similar conclusion can be deduced from the corrosion of the sample quenched from salt (the

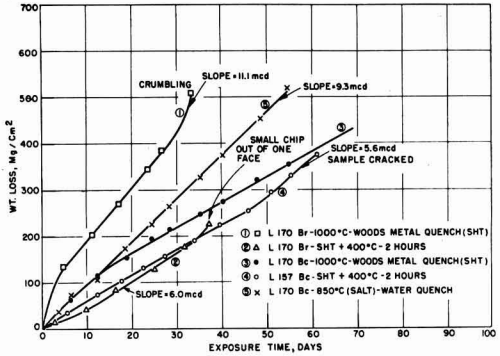

Fig. 3. Effect of heat treatment on corrosion resistance of U-5% Zr-1½% Nb alloys.

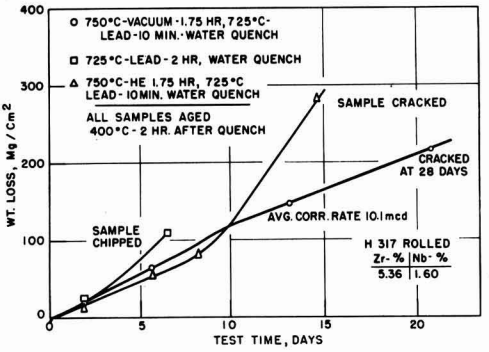

Fig. 4. Effect of gas removal on corrosion in water at 290°C of U-5% Zr-1½% Nb alloy.

eutectic of Li_2CO_3 and K_2CO_3), as shown in Fig. 3, curve 5. For the first twelve days its corrosion rate was the same as the sample, differing only by having the vacuum heat treatment. Subsequent to that time, however, the salt-treated sample continued to corrode at the same rate while the corrosion rate of the vacuum-treated sample decreased by 40%. The hydrogen content of this particular salt-treated sample was not determined; however, similar samples given the same treatment contained about 35 ppm hydrogen. Vacuum-treated metal contains little or no hydrogen.

Hydrogen can also be introduced into the sample by exposing it as the cathode in a hydrogen discharge tube. Such a sample (after 24-hr bombardment) was cracked after exposure to water and steam (because of autoclave leakage, part of the test involved a steam exposure) at 300°C for three days. A similarly tested, but nonbombarded, sample corroded in the normal manner.

Hydrogen analyses of corroded samples show direct correlation with the amount of metal corroded. In Table II such data have been treated to show the per cent of the hydrogen produced which was absorbed in the alloy. After a short initial period the percentage of hydrogen absorbed remained constant for similar samples from the same piece.

When samples from different sources were corroded, there was not always the same fraction of

Table II. Hydrogen build-up as function of corrosion time (Water, 290°C; Alloy H-416C-c, gamma quenched, aged 2 hr at 400°C)*

Time, hr	Metal corroded, mg	H_2 in corroded sample, ppm	% of total H_2 produced that is found in sample
113	234	4.0	1.14
274	692	6.5	0.71
401 (Chip out of sample)	848	7.6	0.69
642 (Sample cracked into 3 pieces)	1127	13.9	0.71

* Four identical samples were tested for the times indicated. Initial hydrogen content (after heat treatment) was 0.9 ppm.

Table III. Hydrogen absorption in corroding alloy (Water, 290°C)

Sample and heat treatment	Test time, days	Average corrosion rate, mcd	% of H_2 produced that entered metal	Rate of hydrogen build-up in metal, $\mu g/cm^2$/day	Condition after test
H-416C-c Gamma quenched from vacuum, aged 400°C, 2 hr	26.7	8.6	0.7	1.09	Cracked
L-170B-c Gamma quenched from salt	18.9	9.4	0.6	0.95	No cracks
H-419B-r Gamma quenched from vacuum, aged 400°C, 2 hr	48.9	6.7	0.96	1.07	Cracked
L-170B-c Gamma quenched from vacuum	47.9	6.5	0.97	1.06	No cracks

the produced hydrogen absorbed into the metal. It is interesting to observe in Table III, however, that the rate at which the hydrogen accumulated was approximately the same for all the samples, independent of their corrosion rates. The data from the second sample show that "loading" the material with hydrogen (by treatment in salt) before corrosion caused a higher corrosion rate. However, the absolute rate of hydrogen pickup by the sample (during corrosion) was not increased. As indicated above, an identical sample of the "loaded" material continued to corrode at the initial rate for at least 55 days, so that the shorter exposure time for the second sample in Table III does not invalidate the argument.

Although the rate of hydrogen pickup was approximately the same, the corrosion-induced cracking was not. Assuming that this type of cracking is caused by corrosion product hydrogen, it must be supposed that high local hydrogen concentrations in the metal cause it, rather than the total amount present. The following experimental results support this hypothesis.

A quenched and aged specimen contained 0.9 ppm hydrogen. After about eleven days of testing at 290°C the sample was cut in half and analyzed for hydrogen. The results were 5.7 and 8.1 ppm (±0.1 ppm). It is significant that the piece with the higher hydrogen content had a subsurface crack which was revealed in sample preparation.

The salt-treated sample referred to in Table III contained about 35 ppm hydrogen after heat treatment. Very likely this was uniformly distributed in the body-centered cubic gamma uranium during the treatment. After an additional hydrogen build-up of 8 ppm during the corrosion test there was no evidence of cracking. Thus a total quantity of hydrogen which causes cracking in a sample in which it is not uniformly distributed did not cause cracking here. Perhaps the original (uniformly distributed) hydrogen enhanced the diffusion of the corrosion product hydrogen so that it too was uniformly distributed.

Table IV. Effect of aging on corrosion in water at 290°C and on hydrogen absorption

Sample*	Aging time at 400°C, hr	Corr. rate, mcd	Hydrogen content after 3-day test, ppm	Appearance of sample after test
1	0	13.5	60	Dull. Pitted
2	1	337†	832	Sample cracked into irregularly shaped piece and slurry. This piece in good condition.
3	2	450†	1220	Same as above.
4	3	616†	1340	Same as above.
5	4	—	—	Completely disintegrated.

* L-170BC—quenched from salt at 850°C.

† Based on remaining piece.

A group of samples which had been simultaneously quenched from salt were aged in a helium atmosphere at 400°C for various periods of time and tested for 71 hr in degassed, distilled water at 290°C. The aging times bracketed that for optimum corrosion resistance of a vacuum-treated sample, i.e., approximately 2 hr. Results are shown in Table IV.

The as-quenched sample reacted typically, indicating that the samples were adequately quenched. The behaviors of the aged samples were completely different from that of vacuum quenched and similarly aged metal in that the corrosion resistance was destroyed.

It seems likely that during the aging process the hydrogen concentrated, perhaps at grain boundaries. These concentrations might act as nuclei for further local hydrogen build-up, especially if the hydrogen is present as hydride. The analytical samples consisted of small pieces of metal close to cracked surfaces. As expected, very high hydrogen contents were found. It is also possible that the hydrogen content of the specimen increased the rate of transformation of the strained alpha to normal alpha, with resultant increase in corrosion.

When the hydrogen content of the alloy becomes greater than its solubility, it has been expected that a hydride phase will form. Efforts to observe such a phase in a number of samples of the sort previously discussed were unsuccessful. It was therefore attempted to obtain higher total hydrogen content as follows. A sample of L-170B-c was quenched from salt at 850°C and aged in helium at 400°C for 3 hr. It was then exposed to degassed, distilled water at 290°C for 24 hr. At the end of this period the sample had a rough, heavily pitted, irregular surface; it had corroded at an average rate of 2126 mcd. The hydrogen content was 1100 ppm. The unexpectedly high corrosion rate (as compared with data in Table IV) could have been due to an inadequate quench. However, the object of obtaining a sample with high hydrogen content for metallographic study was achieved.

The sample was examined metallographically after heat treatment, after corrosion, and after hydrogen analysis.[1] The respective hydrogen contents

[1] The hydrogen analysis produces a slow cooled alloy and the resultant structure is very complex. The sample was therefore gamma quenched and aged after analysis in order to produce a structure more conducive to evaluation.

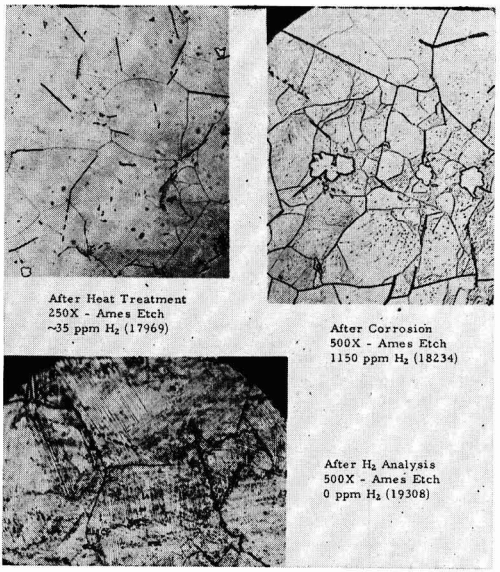

Fig. 5. Effect of hydrogen on structure of U-5% Zr-1½% Nb alloy.

were approximately 35, 1100, and 0 ppm. The photomicrographs appear in Fig. 5. Only the sample with the high hydrogen content has what may be described as a "salt and pepper" effect. This structure has been found in this alloy only in samples containing high hydrogen contents. It is therefore inferred that the structure is hydride.

The difficulty of forming the (proposed) hydride is in line with the report that the addition of as little as 0.5% zirconium to 10.5 and 12% molybdenum alloys virtually eliminates the precipitation of hydride (4).

It would be desirable to identify the new phase as the hydride in a more rigorous manner, for instance by x-ray or neutron diffraction. However, the highest hydrogen concentrations produced to date are below the threshold (2000 ppm or greater) of detection and identification by these methods. The particles are too small to be identified by standard microfocus x-ray equipment.

Effect of temperature.—Water temperature affects both the corrosion rate and the useful life of this alloy. As indicated earlier, simultaneous aging may occur at sufficiently high temperatures. Figure 6 is

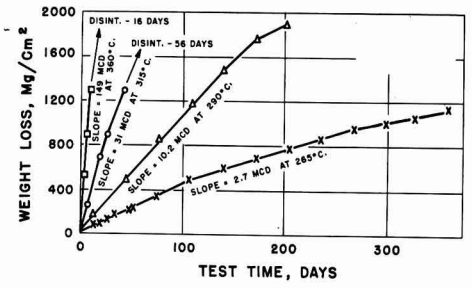

Fig. 6. Effect of temperature on aqueous corrosion behavior of gamma quenched alloy (H203r).

representative of tests performed by the Reactor Engineering Division. The effects of temperature on corrosion rate and life are illustrated.

Discussion

Structural Aspects

The quenched alloy has a martensitic "strained alpha" structure. Although optical metallography up to 2000X shows only a single phase structure, we have postulated a sub-microscopic second phase. Such a structure is possible if the rate of cooling is not great enough to prevent some decomposition before the temperature of the martensitic transformation is reached (12).

Moderate aging would complete precipitation of the second phase, if it were not already complete, and cause a slight growth of the second phase particles already present. We have attempted to confirm or disprove the existence and growth of the second phase by means of the optical microscope, x-ray diffraction, and electron microscope techniques.

Optical metallography has not been fruitful in revealing the relations between aging and corrosion behavior. Moderate aging produces a "cellular" structure within the martensite. Severely overaged samples, i.e., 475°C for 3 min, show what appears to be gross precipitation at grain boundaries. These changes are illustrated in Fig. 7, 8, and 9.

Several comments should be made concerning these figures. The dark lines are probably borides. This casting had an unusually high boron content, i.e., 15 ppm. The "overaged" sample also had the "cellular" structure, but it was impossible to show both the "cellular" structure and grain boundary effect with one etch, i.e., a longer etching time was required to develop the "cellular" structure. Neither the "cellular" structure nor the grain boundary precipitation could be shown to exist on the as quenched sample. The grain boundary effect was revealed only on the "overaged" sample.

Fig. 7. L-170BC-gamma quenched. Chromic acid etch, VHN-382, 30 kg. Magnification 500X before reduction for publication.

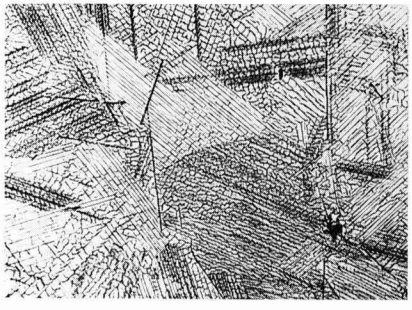

Fig. 8. L-170BC-gamma quenched and aged 400°C, 2 hr (moderate aging); Ames etch, VHN-566, 30 kg. Magnification 500X before reduction for publication.

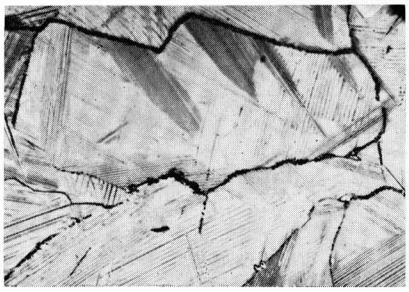

Fig. 9. L-170BC-gamma quenched and aged 475°C, 3 min (overaged), Ames etch, VHN-563, 30 kg.

X-ray diffraction results for a group of quenched and aged samples are more interesting. In Table V it is indicated that a significant return toward the lattice parameters of α-uranium accompanies increased aging. At the same time enough line sharpening was observed to indicate strain relief. These observations are consistent with the hypothesized growth of a fine precipitate. It would thus appear that agglomeration of the precipitate and return of the lattice dimensions to those of α-uranium are responsible for loss of corrosion resistance.

Etched surface textures, as revealed by electron microscopy (using direct, i.e., negative, carbon replicas) suggest that a precipitate is present in the as-quenched alloy, and that particle size increases as the alloy is aged. Figures 10, 11, and 12 are representative of quenched and aged samples, as seen at high magnification.

Any theory relating corrosion resistance to structure must explain the observation that resistance of the zirconium-niobium ternaries to aging is considerably greater than that of binary alloys containing up to about 6% niobium (6). There are at least two ways to explain the beneficial effect of zir-

Table V. (13) Effect of aging on lattice parameters and corrosion resistance

Aging† Temp, °C	Time	2θ Angle for (111)	Corrosion resistance at 290°C*
As-quenched		39.1	Good
425	10 min	39.3	Good
425	20 min	39.3	Good
425	40 min	39.35	Bad
425	2 hr	39.4	Bad
425	4 hr	39.5	Bad
440	5 min	39.35	Good
475	3 min	39.4	Bad
(α-Uranium)		39.5	Bad

* Good and bad indicate no failure and failure, in two weeks' exposure to water, respectively.

† All alloys quench from 1000°C.

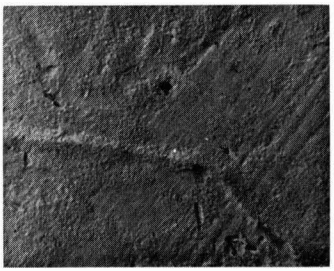

Fig. 10. L-170BC-gamma quenched, Ames etch, 16,100X —5227B.

Fig. 11. L-170BC-gamma quenched and aged 400°C, 15 min, Ames etch, 16,100X—5282A.

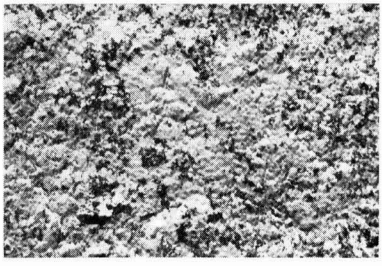

Fig. 12. L-170BC-gamma quenched and aged 400°C, 6 hr, Ames etch, 16,100X—5326C.

conium as an additive to the uranium-niobium binary alloy. In the first, the addition of several per cent of zirconium will augment the grain refining action of the niobium and will very likely slow down agglomeration of the second phase during aging. Hence the distribution of the second phase will perhaps be more favorable initially, and the unfavorable effects of overaging will be retarded.

The second explanation deals with the nature of the second phase formed. At equilibrium the ternary alloy consists of alpha uranium and about 10% γ_1 (10), which is gamma uranium saturated with niobium and zirconium. The corresponding structure of the niobium binary alloys is α-uranium and γ_2 (niobium saturated with uranium). γ_2 is not found in the ternary system. It is entirely possible that the γ_1 phase agglomerates slower than the γ_2 phase; hence the ternary alloy overages more slowly.

Role of Hydrogen

Aqueous corrosion of uranium.—It is considered helpful to discuss some aspects of the mechanism of the aqueous corrosion of uranium and then to show how the situation is modified by alloying. The results of this investigation will be used to support the belief that hydrogen produced as a product of the corrosion reaction has a considerable influence on corrosion behavior.

As unalloyed uranium corrodes in air-saturated distilled water at room temperature it forms a thin continuous and protective film of uranium dioxide. Samples of the metal in this environment develop typical interference-color films, and the progress of corrosion can be estimated from the apparent film thickness. After sufficiently long exposure, however, points of local breakdown of this film are observed. At these points the corrosion product is fine granular uranium dioxide. Where this type of product is formed, the rate of corrosion is considerably higher. With further exposure these points of breakdown gradually spread, and it is inferred that eventually most of the surface would be corroding at the more rapid rate characteristic of the situation where the relatively unprotective corrosion product is formed (1). It is considered, and the idea is developed in a publication by two of us (14), that these points of local breakdown represent places at which corrosion product hydrogen reacts beneath the protective film to form uranium hydride. This hydride then prevents bonding between the oxide film and the metal. Since this bonding appears to be a necessary requirement for the stability of thin oxide films of this type, the corrosion product takes its more stable form, a mass of fine crystals.

It is essential that there be some oxygen dissolved in the water in order to have the protective film. The means by which the oxygen acts cannot be stated unequivocally, but it appears reasonable to suppose that oxygen adsorbed on the protective oxide film will prevent the entry of hydrogen into the film and, hence, will prevent access of hydrogen to the uranium surface. The fact that breakdown ultimately occurs indicates that the prevention of the entry of hydrogen into the oxide film is not complete. In the absence of dissolved oxygen, corrosion always proceeds on initially clean metal at the rate characteristic of the situation where there is no stable protective film (1).

As the temperature is increased it is perhaps more difficult to prevent the access of some of the hydrogen to the metal surface, and the solubility of oxygen in the water is reduced. Consequently there is a temperature above which the formation of the highly protective film is not observed on unalloyed uranium. In air-saturated water this temperature is about 60°-70°C. The addition of hydrogen peroxide to the water apparently increases this temperature somewhat (1).

Alloying.—By the addition of more than a minimum amount of zirconium the apparent sensitivity to the hydrogen effect can be considerably reduced, so that the protective film forms in boiling distilled water on a uranium-5% zirconium alloy (15, 16). The behavior of this alloy in boiling distilled water can be described in exactly the same terms as was the corrosion of unalloyed uranium in air-saturated distilled water at room temperature. Ultimately local breakdown of the oxide film occurs, and the film

does not form if oxygen is rigidly excluded from the water.

There are three mechanisms which appear reasonable as explanation for the effect of the alloying zirconium. In the first the incorporation of zirconium into the UO_2 lattice could make an inherently more stable film and could also make the process of hydrogen migration through it more difficult. That this is at least reasonable is indicated by the fact that the presence of zirconium in the oxide produced on these alloys has been observed to reduce the UO_2 lattice dimensions (16).

The second proposal for the protective action of zirconium is that a zirconium-containing phase in the surface layers of the metal acts as a getter for that hydrogen which does reach the metal surface. If, then, this zirconium phase is distributed in such fashion that it can getter all of the hydrogen reaching the surface, no uranium hydride should be formed, at least until the zirconium becomes saturated. According to this picture the ultimate breakdown of the oxide film occurs when this saturation is effected. Presumably the zirconium-rich phase can absorb hydrogen only at a given maximum rate. Oxygen might be effective by maintaining the rate of arrival of corrosion product hydrogen below this limit.

If the alloy content is increased so that the total rate at which the zirconium-rich phase can absorb hydrogen at the surface is equal to or greater than the rate at which hydrogen gets there (without any retardation, as by oxygen), then there should be no requirement for dissolved oxygen. 7.5% zirconium is apparently sufficient for this purpose in boiling water (15). Some gettering action by zirconium is indicated in uranium alloys, since it has been reported (4) that as little as 0.5% zirconium virtually eliminates the formation of internal hydride crystals during corrosion in gamma-phase alloys.

The third alternative considers that hydrogen diffuses rapidly into the strained phase (martensitic). Hence the entire surface would be gettering the hydrogen. This proposal is in accord with the fact that the strained lattice has larger parameters than the normal alpha structure (Table V). In other studies (17, 18), increasing lattice parameters (by tension) has been observed to cause the rate of hydrogen diffusion to increase, sometimes strikingly.

As previously noted (16), the altered properties of the oxide appear to be insufficient to explain the observed phenomena. There would be no obvious explanation for the sensitivity of the 5% alloy to oxygen in boiling water, nor would it be clear why there should be a critical minimum zirconium content to achieve corrosion resistance. The proposals relating to the disposal of hydrogen are therefore preferred and will be emphasized in the remainder of this discussion. Of these, the one based on the action of the precipitated phase is preferred. In addition to the observed activity of zirconium (as a getter) referred to above, the greater effectiveness of increased percentages of zirconium seems more readily explained on the basis of this hypothesis. (The martensitic transformation always seems to be at least nearly complete, as indicated by x-ray diffraction and the observed topography of corroded specimens.)

A fine random dispersion of the second phase is desirable for its most efficient operation. Improved dispersion of the second phase produced by aging the quenched material is accompanied by some production of normal α-uranium. This perhaps explains the reduced corrosion lifetime of those aged samples which have lower corrosion rates. Perhaps niobium is better than zirconium both as a hydrogen getter and as a grain refiner, explaining its observed superiority as an alloying constituent (1).

Damage by hydrogen.—Presumably the niobium and/or zirconium do not do a perfect job in providing protection. It is assumed that a small amount of hydrogen is available to the surface uranium. Very possibly this influences the corrosion rate, either by the formation of a small amount of uranium hydride or perhaps even by some disruption of the oxide by gaseous hydrogen formed beneath it.

When samples of the alloy described in this report are corroded in water they frequently become pock-marked or etched. Sometimes such localized corrosion is observed to make rather deep pits. This is probably an indication of the presence of impurity phases; whether the interface between such phases and the matrix are preferred sites for hydride formation is not known, but might be suspected. Subsequent reaction with the water could change the hydride to oxide.

It is known that some hydrogen diffuses into the metal. Thus, a constant rate of hydrogen pickup by corroding samples was observed, in terms of micrograms of hydrogen per square centimeter of corroding surface. It is presumably this hydrogen which initiates the formation of cracks (perhaps by formation of internal hydride) after prolonged corrosion exposure. The growth of oxide within the cracks probably leads to rupture and ultimate failure by a wedging action.

Both reduction of the corrosion rate and increase of the corrosion lifetime might be induced by the use of more efficient material (for hydrogen disposal), or its better distribution. In addition, it would be desirable to have the hydrogen in the metal uniformly distributed. This should provide increased corrosion lifetimes over those now observed for the reference alloy. Both objectives are perhaps at least partly achieved in those alloys in which the gamma phase is stabilized. The body-centered cubic gamma phase has a much higher multidirectional hydrogen diffusion rate than does the α-uranium; it might also provide a more efficient surface for the formation and liberation of hydrogen. Active cathodes on its surface should provide additional benefit, and apparently do (3).

Acknowledgment

The cooperation and interest of the following were of great aid in this study: C. R. Breden and A. H. Roebuck of the Reactor Engineering Division, ANL, directed the experiments on the long-time corrosion tests; G. Dragel performed the corrosion tests and is responsible for some of the photomicrographs;

E. J. Silk, on loan to the Metallurgy Division from Babcock and Wilcox, is responsible for some of the photomicrographs and aided in their interpretation.

Manuscript received Dec. 18, 1959. This paper was prepared for delivery before the Columbus Meeting, Oct. 18-22, 1959. Work on the paper was performed under the auspices of the USAEC.

Any discussion of this paper will appear in a Discussion Section to be published in the June 1961 JOURNAL.

REFERENCES

1. J. W. McWhirter and J. E. Draley, "Aqueous Corrosion of Uranium and Alloys: Survey of Project Literature," ANL-4862 (May 1952).
2. J. T. Waber, "A Review of the Corrosion of Uranium and Its Alloys," LA-1524 (Nov. 1952).
3. R. K. McGeary, *et al.*, "Development and Properties of Uranium Base Alloys Corrosion Resistant in High Temperature Water. Part I, Alloys without Protective Cladding," WAPD-127 (April 1955).
4. E. W. Cawthorne, *et al.*, "Corrosion in 650°F Degassed Water of Uranium-Molybdenum Alloys Containing Impurity Additions," BMI-1045 (Oct. 1955).
5. J. E. Draley "Preliminary Report on Low Columbium: Uranium Corrosion Resistant Alloys," ANL-5078 (June 1953).
6. J. E. Draley, S. Greenberg, and W. E. Ruther, "The High Temperature Aqueous Corrosion of Uranium Alloys Containing Minor Amounts of Niobium and Zirconium," ANL-5530 (Oct. 1956).
7. J. H. Kittel, S. Greenberg, S. H. Paine, and J. E. Draley, *Nuclear Sci. and Engrg.*, **2**, 431 (1957).
8. S. Greenberg and J. E. Draley, *ibid.*, **4**, 319 (1958).
9. S. Greenberg, *ibid.*, **6**, 159 (1959).
10. A. E. Dwight and M. Mueller, "The Constitution of the Uranium-Niobium Binary and the Uranium-Zirconium-Niobium Ternary Alloys," ANL-5581 (Dec. 1957).
11. A. E. Dwight, "Kinetic Transformations in the Uranium Rich Uranium-Niobium and Uranium-Niobium-Zirconium Alloy Systems," ANL-5582, to be published.
12. Morris Cohen, "Phase Transformation in Solids," Chap. 17, "The Martensitic Transformation," John Wiley & Sons, Inc., New York (1951).
13. M. Mueller, Private communication (May 1955).
14. J. E. Draley and W. E. Ruther, *This Journal*, **104**, 329 (1957).
15. H. A. Pray and W. E. Berry, "Corrosion of Uranium Alloys in High Temperature Water," BMI-874 (Oct. 1953).
16. J. E. Draley, J. W. McWhirter, F. Field, and J. Guon, "The Corrosion of Low Zirconium-Uranium Alloys in Boiling Water," ANL-5030 (April 1953).
17. D. P. Smith, "Hydrogen in Metals," University of Chicago Press, Chicago (1948).
18. M. W. Burkart, Editor, "The Corrosion Mechanisms of Uranium Base Alloys in High Temperature Water," WAPD-127-Part III (Oct. 1956).

Inhibition of Acid Attack on Steel by Heavy Metal Ions

Joseph A. Shropshire

Products Research Division, Esso Research and Engineering Company, Linden, New Jersey

ABSTRACT

Ions of ~~lead, tin,~~ and ~~cadmium were shown to~~ inhibit ~~the~~ dissolution of steel in acid solutions in the absence of metal plating. A mechanism was postulated whereby sulfide ions produced by metal dissolution combined with the heavy metal ions to form a protective coating on the dissolving surface. Analytical studies indicated that both lead and tin ions were removed from acid solutions in contact with iron filings, in quantities too great to be explained by adsorption. Studies on the effect of increased acid concentration and varying sulfur content of the dissolving metal tended to substantiate the mechanism. The order of effectiveness of inhibition of ions of lead, tin, and cadmium was shown to coincide with the order of solubility of the respective metal sulfides.

Although the effect of foreign ions on the corrosion resistance of various metals has been studied extensively for a number of years, some controversy remains concerning the action of certain metal cations in reducing the attack on iron and steel by nonoxidizing acids. The action of As^{+++} in this respect has been recognized for many years (1, 2). More recently, Sn^{++} has been shown to exhibit an effect similar to arsenic in 1*N* H_2SO_4 and 1*N* HCl (3). As yet, however, no completely satisfactory mechanism to explain these phenomena has been advanced. The present work studies the effect produced by Sn^{++}, Pb^{++}, and Cd^{++} on the acid dissolution of steel and proposes a mechanism for inhibition applicable to these ions as well as to As^{+++}.

The rate of dissolution of iron or steel in a nonoxidizing acid such as H_2SO_4 or HCl has been shown to increase in the presence of certain ions capable of being reduced at local cathode potentials (3-5). In contrast, the presence of As^{+++} or Sn^{++} greatly reduces the attack on steel by 1*N* H_2SO_4 or 1*N* HCl. The action of As^{+++} has been attributed by previous investigators (2) to the high hydrogen overvoltage of metallic arsenic. Gatos (3) has established, however, that the presence of metallic arsenic alone on the steel sample does not cause a decrease in rate of dissolution. He has further studied the effects of As^{+++} and Sn^{++} and concludes that the inhibition is due to the following reactions at anodic sites on the metal surface:

$$Sn^{++} \rightarrow Sn^{++++} + 2e^-$$

$$5As^{+++} \rightarrow 3As^{+++++} + 2As^\circ$$

These reactions are postulated to compete with and suppress the primary reaction, the oxidation of iron.

In the present study, a comparison of the effects of Sn^{++} and Pb^{++} on the corrosion of steel in 1*N* HCl solution has been made. These two ions were chosen in light of the oxidation mechanism proposed to account for the effect of Sn^{++}, and the fact that Pb^{++}, while similar to Sn^{++} in most respects, differs greatly in oxidation stability. Thus the respective standard oxidation potentials indicate that Pb^{++} should not inhibit in the manner proposed for Sn^{++}.

$$Sn^{++} \rightarrow Sn^{++++} + 2e^- \qquad E^\circ = +0.15 \text{ v}$$

$$Pb^{++} \rightarrow Pb^{++++} + 2e^- \qquad E^\circ = +1.69 \text{ v}$$

Experimental Procedure

Weight loss measurements.—Corrosion rates were determined by conventional weight loss measurements. Two types of metal specimens were used: (*a*) SAE 1010 steel coupons measuring 1 x 1.5 x 1/16 in., (*b*) disk-shaped specimens (3/4 in. diameter, 1/8 in. thick) of vacuum melted electrolytic iron to which had been added varying amounts of sulfur. Elemental analysis of the 1010 steel gave the following results: C, 0.08%; S, 0.019%; P, 0.01%; Cu, 0.007%; Mn, 0.25%. Analyzed sulfur contents of the electrolytic iron samples ranged from 0.001 to 0.021%. Corrosion tests were carried out individually in stoppered Erlenmeyer flasks containing 500 ml of test solution. Specimens were suspended vertically from a small glass rod through a 1/8 in. hole near the top of the metal coupon. Prior to immersion, the test specimens were sand-blasted, scrubbed with powdered detergent, rinsed with cold water and acetone, and finally degreased with benzene and desiccated. All corrosion tests reported in this paper were carried out at 25.0° ± 0.5°C, and all test times were of the order of 20 hr.

Baker's Analyzed lead chloride and metallic tin were used to prepare the necessary stock solutions, and test solutions were obtained by appropriate dilution. The simple deaeration of test solutions (as used in Fig. 1) was effected by prolonged bubbling with nitrogen, after passing the gas through identical solutions for vapor content equilibrium. After bubbling of nitrogen was stopped, a slow stream of the gas was passed over the top of the solutions during weight loss runs. Constancy of rate for the dissolution reaction was established independently by following the cross-sectional area change of a 1010 steel probe via resistance measurements.

Experimental Results and Discussion

Effect of Sn^{++} *and* Pb^{++} *on the Corrosion of Steel in* 1*N* HCl

Both Pb^{++} and Sn^{++} inhibit the dissolution of steel in 1*N* HCl. The results of the rate studies, shown in Fig. 1, indicate that Pb^{++} is just as effective as Sn^{++}, and that, in fact, the data for both metal ions fall on the same curve. At this low *p*H, dependence of rate on the state of aeration was neither expected nor found. Microscopic inspection (500X) revealed no plating of metal in either case at these low ion concentrations and high acidity. (Later studies indicated that metal plated under similar conditions formed crystals which were easily visible at this magnification.) Utilizing standard methods, measurement of the potential of 1010 steel in 1*N* HCl as a function of plumbous ion concentration indicated no significant change from the value found in 1*N* HCl alone. The identical nature of the inhibition curves for Pb^{++} and Sn^{++} and the fact that oxidation to the plumbic state is impossible under such mild conditions suggest that most of the inhibition in both cases is attributable to a different mechanism than that previously proposed.

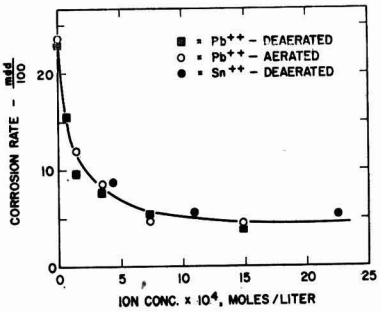

Fig. 1. Corrosion rate of 1010 steel in 1N HCl as a function of stannous and plumbous ion concentration.

Ion Removal Studies

Since no metal plating was observed, it was felt that the inhibition evidenced by both stannous and plumbous ions could be due to protection of the metal surface by the formation of an impervious layer of material. Studies were therefore carried out to determine if stannous and plumbous ions were removed from acid solution by contacting with iron filings. Two methods of contacting were employed: [1] percolation of 50 ml of the M^{++} — 1*N* HCl solutions through 30.0 g of Fisher 20 mesh iron filings (0.10% S) contained in a column with a glass wool filter, and subsequent analysis for changes in M^{++} concentration, and [2] agitation of 50 ml of the M^{++} — 1*N* HCl solutions with 30.0 g of Fisher 20 mesh iron filings in a separatory funnel, immediate filtration through glass wool, and subsequent analysis. Contact times in both cases averaged 5 min. Metal ion concentrations of the test solutions were identical to those which were shown to inhibit acid attack on steel.

Analyses for Pb^{++} were carried out by the dithizone method with final colorimetric determination. Tin determinations were made by a low concentra-

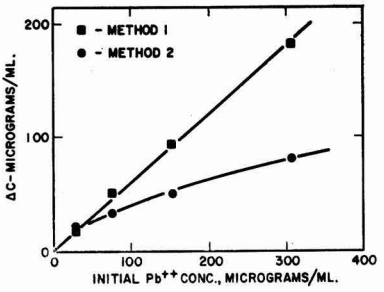

Fig. 2. Removal of plumbous ion from 1N HCl solution by contacting with iron filings. T = 25°C.

tion air-free iodine titration with complete reduction to the stannous state in a closed system with a carbon dioxide atmosphere. Due to analytical difficulties encountered at low concentrations, studies on tin were carried out at a single ion concentration known to give effective inhibition. All duplicate determinations agreed within 1%.

The change in lead ion concentration caused by contacting with iron filings is shown in Fig. 2, and the data obtained for Sn^{++} at a single concentration are given below:

Method	Initial Sn^{++} conc $\mu g/ml$	ΔSn^{++} conc $\mu g/ml$
1	534	320
2	534	249

The results indicate that more than half the metal ion can be removed from solution. If a surface area for the iron filings of 500 cm^2 is assumed (estimated on the basis of 30.0 g of spheres of radius 0.042 cm and density 7.86 g/cm^3), the amount of, e.g., Sn^{++} removed from solution corresponds to approximately three hundred times that needed for monolayer coverage of the surface. Thus, the removal of ions cannot be ascribed to adsorption phenomena. If metal ions were plated during this contacting process, the amount of ions removed would not be expected to decrease with agitation of the system. These facts led to the belief that metal ions were removed from the solution by precipitation as an insoluble species.

Mechanism

Examination of the possible reactions which could occur in the system led to the postulate that the steel (or iron) has a sulfur content sufficient to precipitate the sulfides of both lead and tin. Common steels have a sulfur content of 0.02-0.05%, the sulfur being in the form of metal sulfides. Dissolution of the surface of the metal in acid solution then results in the formation of hydrogen sulfide in the immediate vicinity of the surface. The hydrogen sulfide equilibrium is such that in 1*N* HCl solution, in which the dissociation is suppressed, sulfide ion concentrations of the order of 10^{-23} moles/liter can exist (6). Solubility products of plumbous and stannous sulfides (1.0×10^{-29} and 8×10^{-29}, respectively) (7) show that this sulfide ion concentration is sufficient to initiate the precipitation of the metal ions, even from 0.0001M solutions. Such sulfide concentrations are not grossly in excess since these divalent metal halides ionize incompletely (e.g., $[PbCl]^+ \rightarrow Pb^{++} + Cl^-$; $K_a = 0.03$) (8). The increase of sulfide ion concentration in the layer adjacent to the surface should cause the solubility limits of the heavy metal sulfides to be exceeded at distances near enough to the surface to create a protective layer. The formation of such a layer would naturally depend on the distance from the surface at which precipitation occurs, and thus become a combined function of sulfide ion diffusion and metal ion concentration. This layer is looked on as being a barrier to diffusion of the participants in the partial reactions occurring at the surface, thus causing the over-all rate of dissolution to decrease. A further consequence of the buildup of sulfide ion in the diffusion layer is that a heavy metal ion approaching the surface would probably be converted to the sulfide before approaching closely enough for electron transfer, i.e., reduction to the metal, to occur. Direct reduction of the sulfides of lead and tin is considerably more difficult than reduction of the ions themselves and, thus, is not a likely reaction (9).

Table I. Corrosion rate of 1010 steel in 1N HCl in the presence of Cd^{++}

Molarity Cd^{++}	Rate— mdd / 100	Relative rate
0.00	23.8	1.00
0.01	12.8	0.54
0.10	10.7	0.45

Since the heavy metal sulfides exhibit a marked tendency toward colloid formation when precipitated from dilute solution, it is possible that agitation of the solutions while contacting with iron filings could result in precipitation of the sulfides at greater distances from the surface and in concentrations at which colloid formation would be favored. Thus a nonfilterable dispersion could give rise to the observed variation in ion removal by the two methods used. (It is felt that the "ion removal" data are such that adsorption as well as metal plating are improbable as explanations. It must be realized, however, that these data provide no positive evidence of sulfide formation.)

Cadmium Ion

If the sulfide formation mechanism as postulated above is the correct one, cadmium ion should also act as an inhibitor for the corrosion of steel in 1*N* HCl solutions. For cadmium, the solubility product of the sulfide (1.4×10^{-28}) (7) is such as to make it a borderline case, i.e., a lesser degree of inhibition is to be expected. More important, the second ionization constant for $CdCl_2$ as reported by Harned (8) is 0.01. Thus the $CdCl_2$ concentration required to produce precipitation of the sulfide in a solution approximately 1*N* with respect to Cl^- is increased one hundredfold. Results of weight loss measurements carried out in the presence of cadmium ion at two concentrations (Table I) indicate that concentrations of cadmium ion up to one hundred times those used for Pb^{++} and Sn^{++} produce only a 50% inhibition, and thus, the foregoing conclusions are qualitatively confirmed.

Effect of Solution Acidity

The degree of inhibition afforded by Sn^{++} and Pb^{++} was found to be greatly reduced in 3*N* HCl solution, as shown in Fig. 3. This evidence reinforces the sulfide mechanism, since the increase in acidity causes a sharp increase in the solubility of the sulfides of tin and lead. It is doubtful that the observed decrease in effectiveness of the metal ions would occur if metal plating were a major factor here, since the increase in acidity from 1*N* HCl to 3*N* HCl would result in a change of hydrogen discharge potential at a cathodic site of only a few millivolts. The same change in acidity, however, causes a ninefold decrease (ideally) in the sulfide ion concentration in the acid solution.

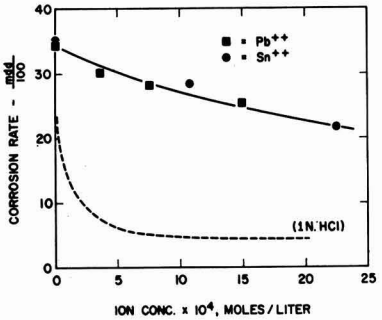

Fig. 3. Corrosion rate of 1010 steel in 3N HCl as a function of stannous and plumbous ion concentration.

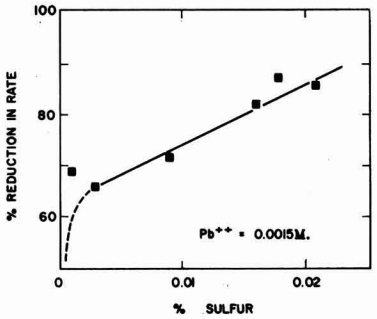

Fig. 4. Effect of sulfur content of electrolytic iron specimens on corrosion rate in IN HCl —0.0015M Pb^{++}. Per cent reduction calculated against rate in IN HCl alone.

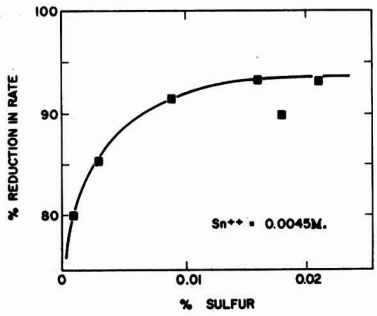

Fig. 5. Effect of sulfur content of electrolytic iron specimens on corrosion rate in IN HCl —0.0045M Sn^{++}. Per cent reduction calculated against rate in IN HCl alone.

The rate of dissolution of 1010 steel in 3*N* HCl in the presence of 0.01 mole/liter of cadmium ion was found to be 92% of the rate of dissolution in pure 3*N* HCl. This is undoubtedly due to the fact that cadmium forms the most soluble sulfide of the metals investigated. It is to be expected that cadmium ion would exhibit no effect whatsoever in solutions of slightly greater acidity.

Effect of Sulfur Content of the Metal

If the postulated sulfide formation mechanism is correct, it follows that sulfur content of the metal should play a determining role in the inhibition. Accordingly, a series of vacuum melted electrolytic iron samples which differed only in sulfur content was obtained. Weight loss measurements were carried out on these samples in 1*N* HCl alone and in 1*N* HCl containing low concentrations of Pb^{++} and Sn^{++}. The results of this study indicate that high levels of inhibition are obtained, and that the degree of inhibition in both cases increases with sulfur content of the sample (Fig. 4 and 5).

It is of interest to note that a saturation level is obtained with the use of a Sn^{++} concentration somewhat higher than that of Pb^{++}. Such a level admits to several possible explanations in light of the proposed mechanism. It is possible that maximum surface coverage has been realized and that the remaining attack represents reaction occurring by diffusion of reactants through the sulfide layer. Alternatively, it could be assumed that the majority of impurities and the majority of attack are centered about the grain boundaries of the metal lattice and that while this attack is inhibited by sulfide formation, a residual dissolution remains at crystal faces.

The apparent inconsistency of the data at 0.001% S in Fig. 4 is explained by the fact that microscopic examination (500X) revealed relatively large crystals of lead on this sample only. This observation conforms to the previous hypothesis that metal plating should not occur in the presence of an appreciable amount of sulfide ion. The plated lead in itself appears to be an effective inhibitor, probably due to its high overvoltage for hydrogen discharge. It is of interest to note that this behavior was observed only with Pb^{++}, which is reduced only slightly more easily than Sn^{++}.

The plating of metal ions at very low sulfur contents was reconfirmed by the observation that both lead and tin were plated from their 1*N* HCl solutions on electrolytic iron powder (trace sulfur) which had been sintered into coupons with a density of 6.5 g/cm³.

Conclusion

The presence of plumbous, stannous, and cadmium ions has been shown to inhibit the dissolution of iron and steel in 1*N* HCl. With the exception of iron specimens with extremely low sulfur content, no evidence of plating of any of the metals on the iron or steel samples has been detected. Both plumbous and stannous ions are removed from acid solutions in contact with iron filings, in amounts dependent on the mode of contacting. The removal of plumbous ion is linear with initial ion concentration. As yet, no satisfactory explanation for the linearity can be advanced. The inhibition afforded by Pb^{++} and Sn^{++} is markedly decreased by small increases in acidity of the solutions, and has been shown to be dependent on the sulfur content of the dissolving metal.

In view of these facts, it is postulated that the dissolution of a steel surface in a strong nonoxidizing acid produces sufficient sulfide ions to precipitate the respective heavy metal sulfides at the surface. This metal sulfide formation probably occurs at distances from the surface which are too great for iron discharge, and thus precludes metal plating. The precipitated layer of sulfide then restricts diffusion to and from the surface and causes a decrease in rate of the partial reactions. Since As^{+++} forms a sulfide which is insoluble even in strong acid solu-

tion, it is believed that the well-known inhibition effects of As^{+++} are accounted for by a similar mechanism. The concentration of ions required for maximum effectiveness appears to increase in the order $As^{+++} < Pb^{++} \simeq Sn^{++} < Cd^{++}$. This order is in agreement with the respective metal sulfide solubility products (7).[1]

A puzzling factor in the experimental results is that corrosion rates characteristic of each metal ion concentration were obtained after the first few minutes of reaction. The continued release of sulfide ions during the period of reaction would be expected to increase the thickness of the protective layer and thus cause a decrease of corrosion rate with time. It is possible that the film is established quite rapidly at the period when reaction rate is high and that subsequent reaction by slow diffusion of ions through the film does not add measurably to the "effective" film thickness. This would occur if the metal sulfide formed in the latter case by diffusion of $S^{=}$ through the film were loosely bound at relatively large distances from the surface.

It should be emphasized that, in accord with Gatos' observations on Sn^{++}, no plating of tin, lead, or cadmium on ordinary steel coupons was observed in these systems. Observation of the plating on electrolytic iron specimens and on steel coupons in less acid systems indicated that the metal deposits were semi-adherent and crystalline, and that even the most minute deposits were readily observable under the microscope.

Oxidation at anodic sites, as postulated by Gatos, is certainly not a factor in the inhibition evidenced by plumbous ion, although it could play a minor role in the case of Sn^{++}. Cadmium ion, at low concentrations, is probably stable in acid solutions insofar as reduction is concerned, and cannot conceivably function by the oxidation mechanism previously postulated for Sn^{++}.

The inhibition effects produced by As^{+++}, Sn^{++}, Pb^{++}, and Cd^{++} through formation of a sulfide layer at a dissolving steel surface are, of course, limited to a definite range of acidity. The upper limit of this range is governed by the solubility of the respective metal ion sulfides, being greatest for As^{+++} and lowest for Cd^{++}. The lower limit of the range is largely determined by the pH at which the sulfide in the test metal specimen becomes soluble in the corroding medium.

It should be mentioned that many metal ions (e.g., Cu^{++}) form sulfides of such low solubility as to make inhibition by this mechanism possible. However, if the system is capable of causing deposition of a low-overvoltage metal, either through reduction of the ions themselves or sulfides, then the concurrent increase in local cell current and subsequent galvanic cell action overshadows any possible inhibition effects. For Ni^{++}, indications exist that, dependent on the metal ion concentration of the system, both phenomena may occur (3).

[1] The author can find no published value for the solubility product of As_2S_3. However, it is well known that HgS and As_2S_3 are the most insoluble of the heavy metal sulfides (10).

Acknowledgments

The author gratefully acknowledges the helpful suggestions of Dr. J. S. Batzold, Dr. J. O'M. Bockris, and Dr. P. J. W. Debye during the course of this investigation.

Manuscript received Sept. 8, 1959.

Any discussion of this paper will appear in a Discussion Section to be published in the June 1961 JOURNAL.

REFERENCES

1. U. R. Evans, "Metallic Corrosion, Passivity and Protection," p. 536, Edward Arnold & Co., London (1948).
2. A. Wachter, R. S. Treseder, and M. K. Weber, *Corrosion*, **3**, 406 (1947).
3. H. C. Gatos, *ibid.*, **12**, 322t (July 1956).
4. W. R. Buck and H. Leidheiser, *ibid.*, **14**, 308t (1958).
5. H. C. Gatos, *This Journal*, **103**, 286 (1956).
6. H. T. S. Britton, "Hydrogen Ions," Vol. II, p. 115, Chapman & Hall Ltd., London (1942).
7. H. H. Uhlig, Editor, "Corrosion Handbook," p. 1138-9, John Wiley & Sons, Inc., New York (1948).
8. H. S. Harned and B. B. Owen, "The Physical Chemistry of Electrolytic Solutions," 3rd ed., p. 560-1, Reinhold Publishing Co., New York (1958).
9. W. M. Latimer, "Oxidation Potentials," 2nd ed., pp. 148, 153, Prentice-Hall, Inc., New York (1952).
10. P. C. L. Thorne and E. R. Roberts, "Inorganic Chemistry," p. 545, Interscience Publishers, New York (1949).

Addendum

H. A. Laitinen, R. P. Tischer, and D. K. Roe wish to add the following acknowledgment to their paper "Exchange Current Measurements in KCl-LiCl Eutectic Melt" which was published in the June issue of the *Journal*, Vol. 107, pp. 546-555 (1960):

This work was supported by the office of Ordnance Research, U. S. Army.

Bridged Complexes and the Deposition of Tin-Nickel Alloys

Robert L. Rau[1] and John C. Bailar, Jr.

Department of Chemistry and Chemical Engineering, University of Illinois, Urbana, Illinois

ABSTRACT

The method of continuous variations has been used to determine the nature of the complex in solutions containing tin(II), nickel(II), and fluoride ions. This indicates the formation of SnF_4^{2-}, which in turn forms $NiSnF_4$. Other complexes of the type $NiSnF_x^{4-x}$, where x is 1, 2, or 3, have been shown to form also. These complexes may contain one or more fluoride bridges. There is no indication of complex formation in the absence of fluoride.

Since the introduction of a bright tin-nickel alloy plate by Parkinson in 1951, much interest has been aroused in the nature of the species responsible for the nearly constant one to one atomic ratio of tin-nickel in the plate.

Parkinson (1) has shown that tin and nickel are deposited in roughly equal atomic proportions, over a wide range of conditions, from solutions containing stannous chloride, nickel chloride, sodium fluoride, ammonium fluoride, and enough hydrochloric acid to give the solution of *p*H of 2.5. This plate is the intermetallic compound NiSn, which has been unattainable by any other method (2).

A more detailed study of the electrolyte used in the plating process has led to several interesting qualitative conclusions (3). When the cathode potential was plotted against current density for a series of solutions containing a constant amount of stannous chloride and increasing amounts of sodium fluoride, it was observed that the cathode potential became increasingly negative, indicating complex formation between stannous and fluoride ions. A similar study using nickel chloride in place of stannous chloride indicated little or no complexing between nickel and fluoride ions. A third study, in which increasing amounts of nickel chloride were added to a solution containing constant amounts of stannous chloride, sodium fluoride, and ammonium bifluoride, indicated that the addition of nickel chloride caused the potential at which tin plates out to become more negative. It was suggested that this could be due to the formation of a complex containing both tin and nickel.

Davies (4) has studied the interaction between fluoride and stannous ions by determining the effect of a change in fluoride ion concentration on the nature of the alloy deposit. The solutions studied had a constant nickel concentration but contained varying amounts of stannous and stannic tin (the latter being due to the air oxidation of the stannous ion). At low fluoride concentrations the deposits obtained had a matte surface and a tin content higher than that of the bright alloy, but with fluoride concentrations above certain critical values the typical bright appearance of the tin-nickel alloy was obtained. The fluoride concentration range in which this change took place was quite narrow. The bright tin-nickel alloy could be obtained only from solutions in which each stannous ion was associated with four fluoride ions and each stannic ion with six fluorides ions.

Further studies (4) have indicated that $SnF_6^{=}$ is more stable than $SnF_4^{=}$ and is not involved in the deposition of the tin-nickel alloy. If the tin-nickel electrolyte contains an insufficient amount of fluoride to complex all the stannous and stannic ions, there is uncomplexed stannous ion in the electrolyte, and the bright alloy is not deposited.

By comparing the transport numbers of the metallic ions in the electrolyte with calculated values for the simple metallic ions, the existence of a tin(II)-fluoride complex seemed to be confirmed (5). For solutions containing nickel chloride, the difference between the experimental and calculated values of the transport number of Ni(II) suggested that the nickel ion was part of a negatively charged ion. Since there is no evidence for complex formation between nickel(II) and fluoride in aqueous solution (6), Brook, *et al.* suggested that Ni(II) was associated with the stannous fluoride complex.

In spite of the reluctance of nickel(II) to form fluoride complexes, some combination of $SnF_4^{=}$ with Ni(II) seems to occur, but conclusive evidence for this has not been established. It was the object of this investigation to determine the nature of the species formed in the tin-nickel electrolyte, using the method of continuous variations (7-9) with refractive index as the measured property.

Experimental

The Zeiss dipping refractometer, which was used in this investigation, does not give a direct reading of refractive index, but for our purposes it was not necessary to convert the readings to refractive index values. The instrument is easily read to ± 0.03 scale units; if desired, these can be converted to refractive index values having an accuracy of 0.00002 units.

In a typical study, solutions approximately 0.1M were prepared by direct weighing of analytical grade reagents. In some cases concentrations were determined analytically (10). Portions of these so-

[1] Present address: Minnesota Mining and Manufacturing Co., St. Paul, Minn.

lutions were measured into glass stoppered flasks in such a manner that the first flask contained 90% by volume of solution A and 10% of B. The second flask contained 80% of A and 20% of B and so on up to 10% of A and 90% of B. In every case the total volume was 10 ml.

After the solution had been in a thermostat for 30 min, it was placed in the refractometer cup, the prism of the refractometer was put in position, and the assembly was immersed in the water bath for 20 min prior to reading. All readings were taken at 25°C.

The continuous variation curves were obtained by plotting the solution readings (n) minus the reading of pure water (n_o) vs. volume per cent of the two constituents. The deviation curves were obtained by plotting the difference between the values used in the continuous variation curves and the values obtained by assuming no interaction between the constituents against per cent composition. Such a plot gives a maximum deviation at the point corresponding to the ratio in which the two constituents react.

Preparation of solutions.—To eliminate the possibility of atmospheric oxidation of the stannous ion, the distilled water was boiled and saturated with nitrogen. All stannous solutions were stored under an atmosphere of nitrogen and were used within 24 hr after preparation.

To duplicate the optimum plating conditions (4), all solutions were brought to a pH of 2.5. In the preparation of standard stannous solutions, it was necessary to add acid to prevent hydrolysis. This gave the solution a negative pH. If, however, two moles of fluoride ion were added per mole of stannous ion, it was possible to prepare stannous solutions of pH 2.5. A Beckman model G pH meter was used.

In cases in which ammonium fluoride was a constituent of the solution, it was necessary to take into account the two ionization constants of hydrofluoric acid (11) in order to prepare an acid solution having a known unassociated fluoride ion concentration.

Continuous Variation Studies

Study No. 1—$SnCl_2$:$2NH_4F$ vs. NH_4F—In order to determine the nature of the complex formed between stannous and fluoride ions, a continuous variation study of $SnCl_2$:$2NH_4F$ vs. NH_4F was undertaken (Fig. 1). The deviation curve shows a maximum at 33% $SnCl_2$:$2NH_4F$, indicating a [Sn(II) + $2F^-$]:F^- reaction ratio of 1:2; the complex must have the composition $SnF_4^=$.

Study No. 2—$NiCl_2$ vs. NH_4F—The data are plotted in Fig. 2. The figure shows no deviation, indicating no reaction between the constituents under the existing conditions.

Study No. 3—$SnCl_2$:$4NH_4F$ vs. $NiCl_2$—This study was undertaken to determine whether there is any interaction between the constituents in a solution containing Sn(II), Ni(II), and F^- (Fig. 3). The deviation curve indicates a [Sn(II) + $4F^-$]:Ni(II) reaction ratio of 1:1.

Study No. 4—$SnCl_2$:$3NH_4F$ vs. $NiCl_2$—In order to determine whether four fluoride ions are necessary for Sn(II) and Ni(II) to become part of the same species, a solution containing Sn(II) and F^- in the ratio 1:3 was used in a continuous variations study. The deviation curve shows a maximum (and thus indicates compound formation) at a ratio of [50% Sn(II):$3F^-$] and 50% Ni(II).

Studies 2, 3, and 4 were repeated using SnF_2 and $Ni(ClO_4)_2$ instead of the chlorides. Where a greater difference in successive readings was desired, an

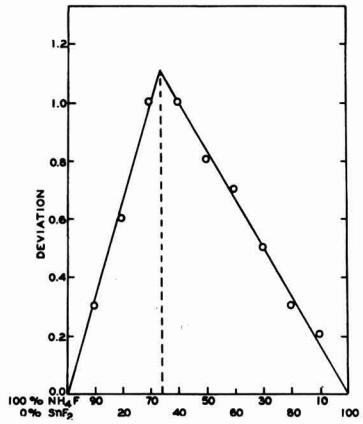

Fig. 1. 0.1M SnF_2($SnCl_2$:$2NH_4F$) vs. 0.1M NH_4F

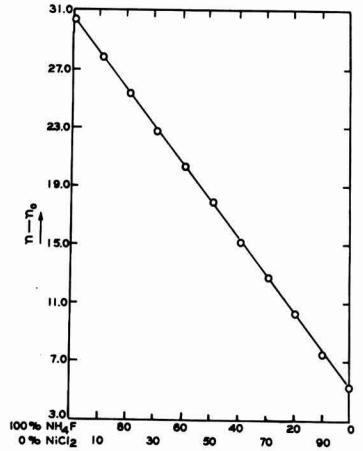

Fig. 2. 0.1M $NiCl_2$ vs. 0.1M NH_4F

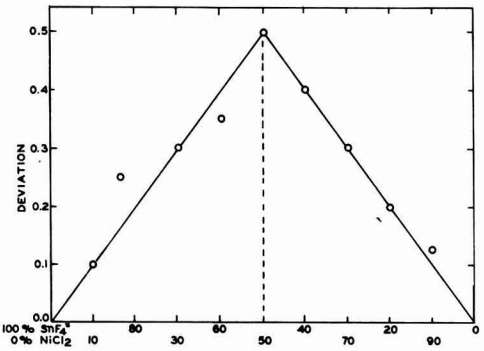

Fig. 3. 0.1M SnF_4($SnCl_2$:$4NH_4F$) vs. 0.1M $NiCl_2$

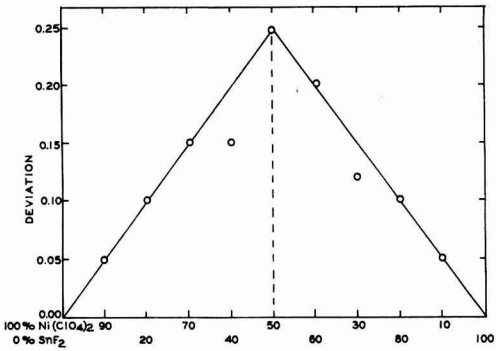

Fig. 4. 0.1M SnF_2 vs. 0.1M $Ni(ClO_4)_2$ + $NaClO_4$

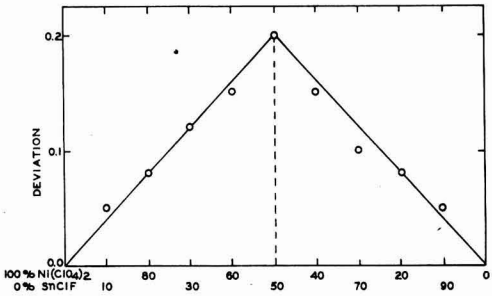

Fig. 5. 0.1M SnClF vs. 0.1M $Ni(ClO_4)_2$ + $NaClO_4$

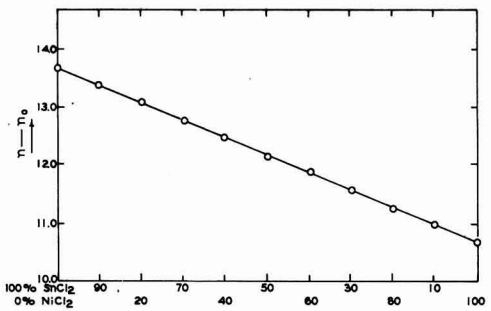

Fig. 6. 0.1M $SnCl_2$ vs. 0.1M $NiCl_2$

inert salt such as $NaClO_4$ was added to one of the solutions. In all cases the results were exactly the same as those obtained with chloride ion present.

Study No. 4a—SnF_2 vs. $Ni(ClO_4)_2$ + $NaClO_4$—The data obtained using a solution of Sn(II) and F^- in a ratio of 1:2 as one of the constituents are plotted on Fig. 4. The curve shows a maximum deviation at 50% SnF_2 and 50% $Ni(ClO_4)_2$.

Study No. 5—SnClF vs. $Ni(ClO_4)_2$ + $NaClO_4$—To determine whether one fluoride ion is sufficient to allow Sn(II) and Ni(II) to become part of the same complex, a study of tin(II) chlorofluoride vs. nickel perchlorate was undertaken.

A 0.1M solution of tin(II) chlorofluoride (12) had a *p*H of 2.3 due to partial hydrolysis of the stannous ion. The nickel perchlorate solution was brought to a *p*H of 2.3 by the addition of perchloric acid.

After standing for 30 min the SnClF solution became slightly turbid, so the refractometer was immersed in the solutions for only 10 min. The readings for 100% SnClF before and after the formation of the turbidity did not change by more than the maximum experimental error. Figure 5 shows a maximum deviation at 50% SnClF and 50% $Ni(ClO_4)_2$ indicating a SnF^+:Ni(II) reaction ratio of 1:1.

Study No. 6—$SnCl_2$ vs. $NiCl_2$—To ascertain whether the presence of fluoride ions is necessary for the formation of the complex species, a continuous variation study of tin(II) chloride vs. nickel chloride was undertaken.

To prevent the hydrolysis of the stannous ion, the calculated quantity of stannous chloride was dissolved in a solution of 25 ml of water containing 2 ml of concentrated hydrochloric acid. The resulting solution had a *p*H less than zero. The nickel chloride solution was prepared in a similar manner.

The curve (Fig. 6) shows no deviation, indicating no reaction between stannous chloride and nickel chloride under existing conditions.

Discussion

In order to explain the constant composition of the tin-nickel alloy which is obtained over a wide range of conditions, several investigators have postulated the existence of a tin-nickel complex (3, 4). Except for the work previously cited, however, no evidence has been offered in support of this hypothesis.

Study No. 1 indicates a $[Sn(II) + 2F^-]:F^-$ reaction ratio of 1:2, which is consistent with the formation of $SnF_4^=$. Davies (4) and Brook (5) have postulated the existence of $SnF_4^=$ from experimental data obtained by entirely different methods.

Study No. 2 indicates that Ni(II) forms no complex with fluoride ions under the conditions investigated. Similar results have been obtained by other investigators (6), although there have been some claims of complex formation between Ni(II) and fluoride (13).

Study No. 3 indicates that Sn(II) and Ni(II) are present in a 1:1 ratio in the complex species. If we assume that the only anions associated with either tin(II) or nickel(II) are the fluoride ions of $SnF_4^=$, the formula for the complex is $NiSnF_4$. Davies (4) and Brook have postulated the existence of such a complex.

If a metal ion and a complexing agent form a series of complexes for which the successive stability constants do not differ greatly, a solution of the constituent ions may contain appreciable amounts of all the possible complexes (14). If such a relationship exists in the tin(II)-fluoride system, a solution of constituent ions may contain SnF_3^-, SnF_2, and SnF^+ as well as $SnF_4^=$. The existence of all of these complexes has not been definitely established, but studies of tin(II) chloride and bromide systems indicate the simultaneous existence of successive complexes. Duke and Courtney (15) obtained values for the stability constants of $SnCl^+$, $SnCl_2$, $SnCl_3^-$, and $SnCl_4^=$, and concluded that an acid solution of the constituent ions contains some of each of these complexes. The determination of stability constants of Sn(II)-Br^- complexes led Vanderzee (16) to a

similar conclusion; the stability constants of the bromide complexes are smaller than those of the chloride complexes. We should therefore expect a solution of tin(II) and fluoride ions to contain all the ions $SnF_n^{(2-n)}$ (where $n = 0, 1, 2, 3$, and 4), each of these being more stable than the corresponding chloride or bromide complex. The concentration of each complex would be determined by the ratio of the concentrations of the tin and fluoride ions and the relative stability constants of the various complexes.

The electrolyte used by Parkinson in his studies of the tin-nickel alloy doubtless contains some of each of the possible tin(II)-fluoride complexes. The continuous variation studies reported here indicate that even one fluoride ion is sufficient to bind a tin(II) ion and a nickel(II) ion into a complex in which the metal ions are present in a 1:1 ratio.

Study No. 6, in which stannous chloride and nickel perchlorate were the constituents, showed no deviation from the "no reaction" curve, and it is assumed that $SnCl_2$ and Ni(II) do not form a complex under the conditions studied. It should be pointed out, however, that the conditions of Study No. 6 are not identical to those of previous studies. Because of the absence of fluoride ions, it was necessary to keep the *p*H below 2.5 in order to prevent the hydrolysis of the stannous ion.

As previously shown, $SnF_4^=$ is the predominant species in solutions containing an excess of fluoride ion, but other tin(II)-fluoride complexes may be present in the commercial electrolyte. Evidence for the formation of a 1:1 tin(II)-nickel(II) complex was obtained in all cases in which fluoride ions were present, but in the absence of fluoride ions there was no indication of tin-nickel complex formation. The conclusion that fluoride ions are necessary for complex formation is consistent with previous observations that the bright alloy plate cannot be obtained from solutions which do not contain fluoride (4).

The consistent 1.1 ratio of Sn(II):Ni(II) obtained in the continuous variation studies can be explained most easily by assuming that fluoride ions serve as bridging groups between the metals. Fluoride ions have not previously been shown to serve as bridging groups, but compounds which may contain fluoride bridges are known. Under extreme thermal conditions, the fluorides and chlorides of some alkaline earth elements combine to form compounds of the type $CaF_2 \cdot CaCl_2$, $SrF_2 \cdot SrCl_2$, and $BaF_2 \cdot BaCl_2$ (17). The complex $[Co(NH_3)_4BeF_4]^+$ (18) probably contains fluoride bridges.

From the continuous variation studies, we have concluded that only one fluoride ion is necessary for bridging in the tin-nickel complex, but we cannot be sure that only one fluoride ion acts as a bridging group when more are available.

Throughout this discussion it has been assumed that nickel(II) does not form complexes with fluoride ions, but that in the presence of a tin(II)-fluoride complex some type of association takes place. Apparently, no other similar cases have been reported, and we can offer no explanation for this seemingly inconsistent behavior. Because the phenomenon is of both theoretical and practical importance, other examples are being sought in the hope that they will shed light on the nature of the bonding in such mixed complexes. Fluoride complexes of Ni(II) have been reported, but their existence is not shown by the method of continuous variations. Evidently the conditions prevailing in this work were not conducive to their formation.

The formation of a tin(II)-nickel(II)-fluoride complex does not preclude the simultaneous existence of the individual ions in the electrolyte. Cuthbertson, *et al.* (3) have shown that complex species as well as the individual ions are present in the commercial electrolyte. It is, therefore, not illogical to assume the existence of the equilibria

$$NiSnF_x^{4-x} \rightleftharpoons Ni^{+2} + SnFx^{2-x}$$
$$\Updownarrow$$
$$Sn^{+2} + X\,F^-$$

Under normal conditions, the simple ions are not discharged because their potentials are too high. If the concentrations of the constituent ions are high enough, the equilibrium shifts in favor of the formation of $NiSnF_x^{4-x}$, but in dilute solutions very little of the tin-nickel complex is formed. Electrolysis of such a solution would not be expected to give the tin-nickel alloy.

Manuscript received Oct. 2, 1959.

Any discussion of this paper will appear in a Discussion Section to be published in the June 1961 JOURNAL.

REFERENCES

1. N. Parkinson, *J. Electrodepositors' Tech. Soc.*, **27**, 129 (1951).
2. H. P. Rooksby, *ibid.*, **27**, 153 (1951).
3. J. W. Cuthbertson, N. Parkinson, and H. P. Rooksby, *This Journal*, **100**, 107 (1953).
4. A. E. Davies, 4th International Conf. on Electrodeposition and Metal Finishing, April 1954.
5. P. A. Brook, A. E. Davies, and J. W. Price, *J. Appl. Chem.*, **5**, 81 (1955).
6. E. R. Sheffer and E. M. Hammaker, *J. Am. Chem. Soc.*, **72**, 2575 (1950).
7. H. W. Bond, Thesis, University of Illinois (1938).
8. P. F. Cundy. Thesis, University of Illinois (1939).
9. N. Costachescu and T. Apostoi, *Ann. Sci. Univ. Jassy*, **7**, 101 (1912); *J. Chem. Soc.*, (Abs. of papers), **102**, II, 528 (1912).
10. "Scott's Standard Methods of Chemical Analysis," **1**, 1207 (1925) D. Van Nostrand Co., New York (1939).
11. H. H. Broene and T. De Vries, *J. Am. Chem. Soc.*, **69**, 1644 (1947).
12. W. H. Nebergall, G. Baseggio, and J. C. Muhler, *J. Am. Chem. Soc.*, **76**, 5533 (1954).
13. A. Kurtenacker, W. Finger, and F. Hey, *Z. anorg. Chem.*, **211**, 281 (1933).
14. I. V. Tananayev and E. N. Duchman, *Bull. Acad. Sci. U.S.S.R.*, Div. Chem. Sci., **6**, 591 (1947), (Russian) *C. A.*, **42**, 4025i (1948); K. E. Kleiner, *J. Gen. Chem. U.S.S.R.*, **21**, 19 (1951) (English); A. K. Babko and K. E. Kleiner, *J. Gen. Chem. U.S.S.R.*, **17**, 1259 (1947) (English Summary); C. Brosset and B. Gustaver, *Svensk Kem. Tidskr.*, **54**, 185 (1942) (English); C. Brosset and J. Orring, *Svensk Kem. Tidskr.*, **55**, 101 (1943) (English).
15. F. R. Duke and W. G. Courtney, *J. Sci.*, **24**, 397 (1950).
16. C. E. Vanderzee, *J. Am. Chem. Soc.*, **74**, 4806 (1952).
17. G. A. Buhalova and A. G. Bergman, *J. Gen. Chem.*, U. S. S. R., **21**, 1723 (1951) (English).
18. A. B. Ray, S. Banerjie, and H. Ray, *J. Indian Chem. Soc.*, **31**, 731 (1954).

Retention of Chloride in Zinc Sulfide during Phosphor Preparation

A. Kremheller, S. Faria, P. Goldberg, and D. J. Bracco

General Telephone & Electronics Laboratories Inc., Bayside, New York

ABSTRACT

A concentration cell procedure, based on the method of Furman and Low, is employed to study chloride retention in ~~zinc sulfide~~ powders. ~~Amounts of 0.001% by weight of chloride in 1 g of zinc sulfide can be determined quantitatively.~~ Zinc sulfide powders with physically admixed or coprecipitated chloride are processed in open boats with variations in firing time and temperature; the retained chloride is determined. The chloride retained after displacement of surface chloride is defined as "volume chloride." It is found that the retention of volume chloride in ~~zinc sulfide~~ is similar whether ~~zinc chloride or sodium chloride~~ is used as the flux; a peak concentration is observed in both cases after processing near 500°C. ~~The~~ experimental results are interpreted and found significant in elucidating the mechanism of the incorporation of chloride into ~~zinc sulfide~~ powder during phosphor preparation.

Although Tiede and Schleede (1) and recently Riehl and Ortmann (2) report that they have obtained luminescent zinc sulfide phosphors without employing a fluxing agent, commercial zinc sulfide phosphors are usually prepared with a fluxing agent, such as zinc chloride or sodium chloride. The presence of flux exerts a pronounced influence on the luminescence emission, crystal structure, and particle size. It is well known that the use of chloride flux has a beneficial effect during zinc sulfide phosphor preparation; however, the particular mechanism by which the chloride enhances the luminescence emission is not yet fully understood.

Schleede and Gantzckow (3) propose that a thin film of flux dissolves small particles of the base material with subsequent precipitation on large particles, and that the thin film sets up strain and disorder in the host lattice during cooling. The resulting lattice imperfections are considered by these authors as the cause of luminescence.

Guntz (4) is probably the first researcher who considers the possibility of flux action within the volume of the phosphor. Following a suggestion by Gugel (5), Smith (6) shows that the flux is able to form a solid solution with the base material. Kroeger and Hellingman (7) assume that chloride, i.e., the flux anion, is incorporated substitutionally into the host lattice. They find by quantitative chemical analysis 2 to 27 x 10^{-5} g atoms of chloride per mole of zinc sulfide in various phosphor samples. Their investigations aim at correlating the incorporated coactivator with the activator concentration and the luminescence mechanism; however, the authors point out that experimental difficulties lead to a ± 50% error in the determination of incorporated chloride, especially, since a certain part of the chloride may be too tightly bound for removal. Bube (8) was aware of this difficulty and removed 10% of the sample with nitric acid to dispose of occluded surface chloride before conducting a quantitative chloride analysis; in this case the possible error is given as ± 20%. There are some objections to Bube's procedure of removing surface chloride, in that small particles, corners, edges, specific crystallographic planes, and similar singularities may dissolve preferentially. Some chloride may still be held by surface forces. This fraction may not be completely removable by fractional dissolution and water washing; reprecipitation may also occur.

Froelich (9) observes that much of the initially added activator remains with the zinc sulfide phosphor after processing while almost all flux is lost, although it is apparent that coactivators have a beneficial effect on the phosphor obtained.

An attempt is made in the present paper to define and determine the amount of volume chloride that becomes incorporated into zinc sulfide during the process of phosphor preparation. The present study is considered as the first step in investigating and establishing the mechanism by which chloride helps to change a finely divided, nonluminescent zinc sulfide powder into a well crystallized, brightly luminescent phosphor. While the final objective of the investigation will be an attempt to correlate quantitatively the amount of chloride on and within the base material with luminescence emission and related properties of phosphors, this introductory exploration should establish a procedure for chloride determination and present some data on the quantitative chloride retention in zinc sulfide powder during phosphor preparation.

Experimental

In studying the incorporation of chloride into a phosphor, it is necessary to distinguish between chloride on the external surfaces and that which becomes incorporated into the volume. Palumbo and Levine (10) have shown that washing zinc sulfide powder with water until the filtrate shows no chloride does not assure that the surface is free of chloride. In a typical example, a sample of zinc sulfide powder precipitated in the presence of chlo-

ride may contain more than 1% by weight of chloride after water washing. The authors (10) find, however, that on leaching the water-washed sample with sulfate solution an appreciable fraction, for instance 30%, of the chloride appears in the leachate. It seems reasonable to assume that the sulfate ions displace chloride ions from the surface of zinc sulfide powder, so that the chloride remaining after displacement washing can be defined as volume chloride, i.e., that which is retained on enclosed internal surfaces and in the host crystal lattice. Accordingly, the determination of volume chloride is an experimental process during which the sample approaches asymptotically, after successive leachings with sulfate ion, a constant amount of retained chloride which is called volume chloride. The latter is, therefore, defined experimentally as the amount retained when the filtrate does not contain any detectable chloride, and when the retained chloride is found constant after additional displacement washings.

Chloride is determined by the concentration cell method of Furman and Low (11); this technique may also be employed in determining the concentration of other halides. The analysis is conducted by measuring the emf between two silver-silver chloride electrodes (Fig. 1) which are suspended in chloride solutions of different concentrations. One electrode is immersed in a chloride solution of concentration x and the other in a solution of concentration $0.01 + x$, where x is the chloride to be determined and the concentrations are in moles per liter. Electrochemical theory leads to the following equation at 25°C:

$$E = 0.0591 \log \frac{2(x + 0.01)}{x + (x^2 + 4P_o/f^2)^{1/2}} \qquad [1]$$

where E is the emf, x is moles of chloride per liter, P_o is the solubility product of AgCl in pure H_2O, and f is the activity coefficient. The value of the activity coefficient is found experimentally by using a solution with $x = 0$ and measuring the emf. A graph of Eq. [1] facilitates the determination of x. For chloride analysis, zinc sulfide is washed in deionized water to remove the zinc sulfate and is then dissolved in hot dilute nitric acid. The acid solution is digested until the hydrogen sulfide is expelled; the sulfur which forms is removed by filtration. The volume is adjusted to 100 ml; two 25-ml aliquots are taken, to one 5 ml of water are added, to the other 5 ml of 0.06M NaCl. The aliquots are then placed into the arms of the concentration cell and the emf is measured. Bancie-Grillot and Grillot (12) indicate that chloride is lost if hot $4N$ HNO_3 is employed in dissolving zinc sulfide; however, in this laboratory careful checks with blanks containing known amounts of added chloride have shown no loss within the limit of chloride detection.

The results obtained by the concentration cell technique have been found to be reproducible and accurate. As little as 0.001% by weight of chloride in 1 g of zinc sulfide can be determined; the limit of detection is 0.0005%. In many cases gravimetric analyses have been run on selected zinc sulfide samples, with results that confirm the usefulness of the concentration cell procedure.

The zinc sulfide powders, zinc chloride, and sodium chloride used in these experiments are free of heavy metals to the limit of spectrographic detectability. Some of the zinc sulfide powders contain coprecipitated chloride in amounts specified below. The zinc sulfide described as chloride-free contains 0.0015 ± 0.0005% (Fig. 2) by weight of chloride. During phosphor preparation the samples are held in transparent quartz boats and heated in transparent quartz combustion tubes in an atmosphere of helium. Conductivity-grade deionized water is used for washing. The zinc sulfate used for leaching and the nitric acid for dissolution of zinc sulfide powder contain no chloride to the limit of detectability.

Results

The amount of added halide has a marked influence on the luminescence intensity and spectral distribution of the emission. Accordingly, it appears desirable to study quantitatively the history of added chloride during zinc sulfide phosphor syntheses. The mechanism by which chloride carries out its function of enhancing luminescence has not yet been established. Previous investigators have examined only the finished product. Our results show that the phosphor passes during its preparation through stages in which the amount of incorporated

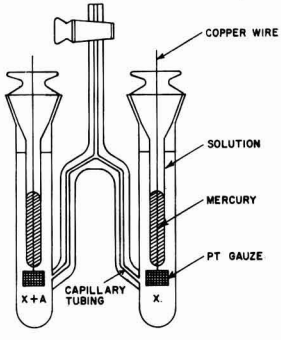

Fig. 1. Concentration cell with silver-silver chloride electrodes.

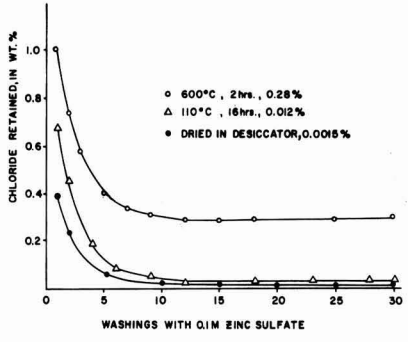

Fig. 2. Volume chloride retained after successive leachings with 0.1M zinc sulfate solution.

volume chloride is several orders of magnitude higher than that in the final phosphor. Data will be presented on the incorporation and retention of chloride in the volume of zinc sulfide as found during various steps of phosphor preparation from zinc sulfide powders with physically admixed or coprecipitated chloride coactivator.

Experimental definition of volume chloride.—Chloride-free zinc sulfide is mixed with 5% by weight of zinc chloride in solution. To check possible effects at room temperature, the slurry is placed in a vacuum desiccator at 25°C until it is completely dry. The dried mixture is then divided into eight 2-g portions. The first portion is leached once with 35 ml of 0.1M zinc sulfate, a second portion is leached twice with successive 35 ml portions of solution, and the remaining portions are leached in the same way for 5, 10, 15, 20, 25, and 30 times, respectfvely. The powder was separated from the leach solution by filtering through fritted glass filters and successive water washings. After separation, each portion is dissolved in nitric acid and the chloride content is determined as described above. The portion that had been leached only once contains 0.39% by weight of chloride, and after twenty leachings the retained amount decreases gradually (Fig. 2) to a constant value of 0.0015% by weight of chloride. Since this is the chloride content of the chloride-free zinc sulfide, it can be concluded that none of the added chloride became incorporated into the volume on drying at 25°C.

The same study is repeated on samples which are processed in a quartz combustion tube in one case for 16 hr at 110°C, and in another case for 2 hr at 600°C. After leaching, the samples are dissolved and their chloride contents are determined. Figure 2 indicates the number of times each sample has been leached and the resulting asymptotically attained volume chloride. It is seen that, in contrast to the result obtained by drying at room temperature, chloride is now incorporated into the volume of zinc sulfide powder during the heat treatment.

Influence of duration of heat treatment.—The amount of chloride incorporated into the volume of zinc sulfide, when zinc sulfide with physically admixed zinc chloride is heated at 600°C for 2 hr, is found above to be 0.28% by weight. In order to determine how the amount of incorporated volume chloride depends on the duration of heat treatment, zinc sulfide samples with 5% by weight of zinc chloride are heated at 750°C for 1, 4, 10, 20, and 30 min, and for 1, 2, 3, 4, and 8 hr. These samples are treated as above to determine the volume chloride. The data, which are presented in Fig. 3, show that chloride incorporation proceeds very rapidly. A peak value is attained within the first 10 min of heat treatment at this temperature. Thereafter, chloride begins to leave the volume as the sample remains at temperature. It should be noted that the amount of chloride in the volume of zinc sulfide after processing at 750°C for 2 hr is smaller than that incorporated during processing at 600°C for the same time. This result indicates the importance of the firing temperature, as discussed in the next part.

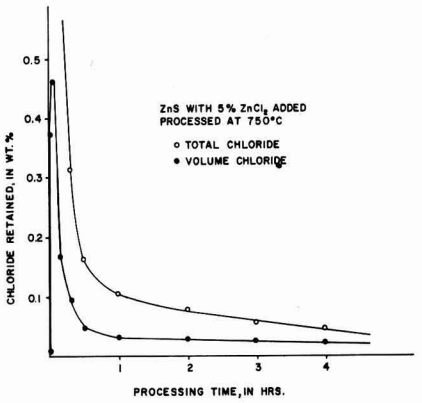

Fig. 3. Retention of total chloride and volume chloride as a function of processing time at 750°C.

Influence of the temperature of heat treatment.—It has been shown above that chloride is incorporated into the volume of zinc sulfide when heated with 5% zinc chloride. It is qualitatively clear from the above data that the amount of volume chloride incorporated first increases with temperature and then decreases as the temperature increases further. The present study is concerned with the quantitative nature of this temperature dependence. Zinc sulfide with 5% zinc chloride admixed is heated for 2 hr at various temperatures between 200° and 1100°C. External surface chloride is removed by the zinc sulfate leaching procedure, and the chloride content of the samples is determined; data are given in Fig. 4.

The peak value for the incorporation of chloride into the volume of zinc sulfide occurs near 500°C. The chloride retention curve rises about linearly to a maximum, and falls off so that the volume chloride diminishes to about 0.01% by weight at 800°C and to about 0.003% at 1100°C.

Usually a chloride other than zinc chloride is employed in phosphor synthesis; therefore chloride retention has been investigated when sodium chloride is added as the flux. The zinc sulfide samples with sodium chloride admixed are prepared in the same way as those containing zinc chloride. However, the amount of sodium chloride is changed to

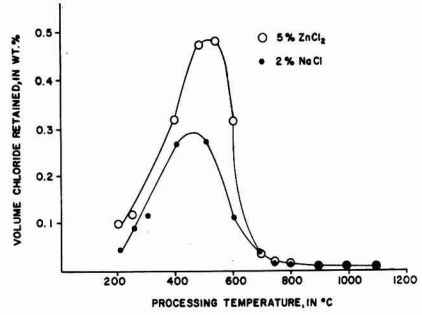

Fig. 4. Retention of volume chloride as a function of processing temperature for $ZnCl_2$ and NaCl addition; processing time is 2 hr.

2% by weight to approach a flux concentration often used in commercial practice. The zinc sulfide powders with the admixed sodium chloride are heated for 2 hr in the temperature range from 200° to 1100°C. The heat-treated powders are leached with zinc sulfate and then analyzed for volume chloride as before. The data, which are presented in Fig. 4, show the same general dependence of volume chloride on processing temperature as observed with zinc chloride, which has a much lower melting point than sodium chloride.

Retention of volume chloride in zinc sulfide containing coprecipitated chloride.—Chloride may be added to zinc sulfide either as a chloride salt after zinc sulfide precipitation from solution, as described above, or as coprecipitated[1] chloride formed when zinc sulfide is precipitated in the presence of a soluble chloride. In the latter case, amounts of about 1% by weight of chloride become incorporated into the volume of zinc sulfide during its formation.

As another, complementary part of studying the history of chloride incorporation during phosphor preparation, it appears of interest to observe the retention of volume chloride when coprecipitated chloride is present in the volume of zinc sulfide powder. For this purpose, zinc sulfide is prepared by passing hydrogen sulfide through a solution of zinc chloride acidified to pH 2.5 with hydrochloric acid. The zinc sulfide precipitate is filtered and leached with zinc sulfate solution until it attains a constant chloride content after several successive washings. The constancy of chloride is determined by analysis of the zinc sulfide sample as well as by the absence of chloride in the filtrate. The zinc sulfide prepared by this method contains 0.82% by weight of chloride which is all present in the volume.

Samples of zinc sulfide containing coprecipitated chloride are placed in quartz boats and heated in a quartz combustion tube at 400°C for 1, 4, and 16 hr, respectively, in an atmosphere of helium. Each specimen is leached twenty times with 0.1M $ZnSO_4$ after heating and then is dissolved to determine the chloride content. Figure 5 presents the data; almost all the volume chloride remains in zinc sulfide under the above processing conditions. The same experiment is performed by maintaining the zinc sulfide powder with coprecipitated chloride for various periods of time at 600°, 800°, and 1100°C, as shown in Fig. 5. It is found that the amount of retained volume chloride decreases rapidly with increasing processing temperature. The amounts of chloride remaining incorporated in the volume after heating for 4 hr at 600°C are comparable to the amounts of volume chloride incorporated when the chloride is introduced in the form of zinc chloride or sodium chloride by physical admixture.

[1] The term "coprecipitated" is used in the sense as given by I. M. Kolthoff and E. B. Sandell, Textbook of Quantitative Inorganic Chemistry, The MacMillan Co., New York, 1948, pp. 110-112.

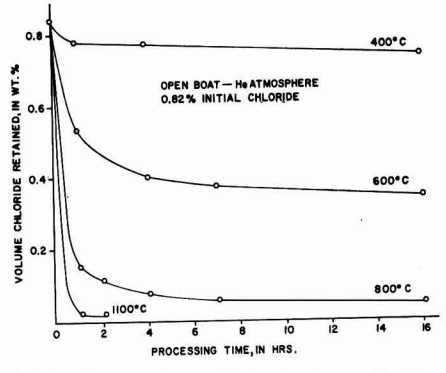

Fig. 5. Retention of coprecipitated volume chloride as a function of processing time and temperature.

Discussion

As part of the present investigation, it has been found that it is possible to define volume chloride as chloride not removed by successive leachings. One obtains reproducible values of volume chloride; these values depend on the conditions to which zinc sulfide powders containing either physically admixed or coprecipitated chloride have been subjected.

Following the explanation of Leverenz (13) for particle growth of Zn_2SiO_4, one can explain the incorporation of chloride into the volume of zinc sulfide as an attendant effect of particle growth. The admixed chloride coats the surface of the zinc sulfide grains which grow together and include chloride on contiguous surfaces. Chloride included in intergranular boundaries cannot be removed by leaching with sulfate ions and is, therefore, volume chloride as above defined. As the temperature increases (Fig. 4) to about 500°C, the number of intergranular boundaries also increases so that additional chloride becomes incorporated. When the processing temperature is increased above 500°C, the walls of the intergranular boundaries may start to sinter together so that chloride is expelled. At high temperatures many grain boundaries disappear, and particle growth takes place. A part of the volume chloride is then displaced to the external surface and volatilizes, while some may be retained on interior surfaces and some may become incorporated into the host lattice.

Sodium chloride flux shows essentially the same behavior as zinc chloride with respect to chloride incorporation into zinc sulfide. However, the two fluxes differ considerably in physical properties, such as vapor pressure and melting point. The similarity in behavior may indicate that chloride incorporation into the volume of zinc sulfide is essentially a property of the host material and the chloride ion, and to a lesser extent a property of the flux cation. The fact that zinc chloride has a lower melting point than sodium chloride, yet shows the same temperature dependence of chloride incorporation, tends to cast doubt on a mechanism of flux action that depends on the dissolving (3) of zinc sulfide by the fluxing agent. This result is in agreement with Bube (8) who finds that the amount of chloride retained is the same regardless of whether sodium chloride or hydrochloric acid is present during preparation of a copper-activated zinc sulfide phosphor. The concentration of retained chloride is about the same whether it is present origi-

nally as a coprecipitate or is admixed with the sulfide before firing. For this reason one is led to suspect that the actual mode of retention is the same in both cases.

As shown in Fig. 4, the volume chloride is a function of firing temperature for a given firing time. The volume chloride does not, however, by itself, determine the obtainable luminescence; maximum luminescence is usually obtained by firing at temperatures well above 500°C. Therefore, if a numerical correlation between the amount of incorporated chloride and luminescence is to be expected, one must consider the volume chloride to be composed of at least two kinds, one of which is effective in promoting luminescence. One hopes that future explorations will make it possible to distinguish between the various fractions of volume chloride, so that quantitative correlation with luminescence can be established. A first goal (14) will be to differentiate between lattice chloride and internal surface chloride.

Acknowledgment

Grateful acknowledgment is made to A. K. Levine for many helpful discussions, R. Bastian for conducting some additional chloride analyses, and J. T. Ragusin for valuable assistance with the experimental work.

Manuscript received March 14, 1960. This paper was prepared for delivery before the Cincinnati Meeting, May 1-5, 1955.

Any discussion of this paper will appear in a Discussion Section to be published in the June 1961 JOURNAL.

REFERENCES

1. E. Tiede and A. Schleede, *Berichte,* **53B,** 1921 (1920).
2. N. Riehl and H. Ortmann, *J. Phys. Radium,* **17,** No. 8-9, 620 (1956).
3. A. Schleede and H. Gantzckow, *Z. Phys. Chem.,* **106,** 37 (1923).
4. A. A. Guntz, *Ann. Chim.,* **5,** 157 (1926).
5. V. M. Gugel, *Bull. Acad. Sci. USSR,* Ser. Phys., **9,** 539 (1945).
6. A. L. Smith, *J. (and Trans.) Electrochem. Soc.,* **96,** 75 (1949).
7. F. A. Kroeger and J. E. Hellingman, *ibid.,* **93,** 156 (1948); **95,** 68 (1949).
8. R. H. Bube, *J. Chem. Phys.,* **19,** 985 (1951).
9. H. C. Froelich, *This Journal,* **100,** 280 (1953).
10. D. T. Palumbo and A. K. Levine, *ibid.,* **102,** 181 (1955).
11. N. H. Furman and G. W. Low, *J. Am. Chem. Soc.,* **57,** 1585 (1935).
12. M. Bancie-Grillot and E. Grillot, *Compt. rend.,* **237,** 171 (1953).
13. H. W. Leverenz, "Luminescence of Solids," John Wiley & Sons, Inc., New York, (1950).
14. A. Kremheller and A. K. Levine, The Release of Chloride from Zinc Sulfide by Grinding, paper presented at The Electrochemical Society Meeting, San Francisco, May 1956.

Study of Ball Milling and the Determination of Lattice Chloride in Zinc Sulfide

A. Kremheller, S. Faria, and A. K. Levine

General Telephone & Electronics Laboratories Inc., Bayside, New York

ABSTRACT

Ball milling, followed by displacement washing, permits a distinction to be made between lattice chloride and internal surface chloride as parts of volume chloride. The surface area, which is determined by gas adsorption methods, increases rapidly in the beginning and then in a linear manner as a function of milling time. The extent of linearity between surface area and milling time is considered to be a measure of crystallinity. The data indicate that the maximal amount of lattice chloride becomes incorporated at a processing temperature near 700°C after a processing time of 2 hr. Zinc sulfide gradually loses its ability to luminesce under ultraviolet (u.v.) irradiation during milling; the logarithm of the luminescence emission is about proportional to the newly formed surface. It appears that the luminescence centers consist of lattice regions of about 0.2 μ in diameter, as is indicated by the observed minimal size of luminescent particles. The luminescence emission of milled samples can be restored by reprocessing, although the degree of restoration is highly sensitive to impurities introduced during milling.

Lenard and Klatt (1) were probably the first to observe that photoluminescence is considerably decreased during the destruction, e.g., by crushing, of phosphor particles. Wecker (2), Frey (3), and Broser and Reichardt (4) among others have confirmed this observation. Many researchers (5) have attempted to correlate the decay of luminescence intensity during phosphor destruction with the particle size, extent of destruction, and related parameters. However, some conclusions which have been attained are confounded by the method of particle size determination, as zinc sulfide particles usually agglomerate if they are below 1 μ in diameter. For instance, Frey (3) concludes from microscopic observations that the grain size of zinc sulfide approaches a constant value of 4 μ during ball milling, although he observes small particles (about 0.1 μ) when an electron microscope is used. Short and

Steward (6) attempt a correlation between photoluminescence intensity and crystal structure changes during grinding of zinc-cadmium sulfides. They find that the residual photoluminescence is an exponential function of the retained hexagonal structure fraction. Broser and Reichardt (4) were probably the first to consider the surface increase during ball milling of zinc sulfide phosphors. They determined the surface change and degree of destruction of the phosphor particles by an optical procedure based on reflection.

Results on grinding of zinc sulfide are only incidental to the present investigation, which is mainly concerned with a distinction between chloride present on internal surfaces and within the lattice. Zinc sulfide particles are destroyed in order to expose the incorporated volume chloride. The various fractions of chloride have been discussed in a previous publication (7), in which the need for determining lattice chloride and its possible implication on luminescence properties of zinc sulfide also have been indicated. The present paper consists essentially of the continuation of previous researches looking into the mechanism of flux action during zinc sulfide phosphor preparation. The present incidental results on ball milling appear, however, to be of such general interest in considering the mechanism of photoluminescence that their inclusion seems desirable.

Experimental

The zinc sulfide powder, processing procedure, and fluxing agent used have been specified in a previous publication (7) which also explains the determination of small amounts of chloride by the concentration cell procedure.

The ball milling is performed in 4-oz glass bottles with screw caps; 0.5 in. diameter procelain balls are employed for crushing the zinc sulfide particles. The speed of the ball mill, the number of balls, and the sample size are kept constant in all experiments. Dry milling is employed to avoid the decomposition of zinc sulfide which takes place, for instance, in the presence of water. It is found that the chloride contamination introduced by milling for 300 hr is below the limit of detectability, i.e., 0.0005% by weight, by the concentration cell procedure (7); however, amounts near 10 ppm each of copper, iron, lead, and silicon are detected. These impurities affect the restoration of luminescence during refiring of ball milled samples, as will be shown.

A simplified gas adsorption method (8) was employed for determining the newly formed surface area after ball milling. The simplified procedure reduces the time for one surface area determination by a factor of about ten when compared with the general Brunnauer-Emmett-Teller (B.E.T.) method, makes routine determinations feasible, and permits one to obtain a quantitative measure of the extent of destruction of phosphor particles during ball milling. Optical and electron microscope studies, as well as the general B.E.T. gas adsorption method, have been employed to confirm and supplement results obtained by the simplified method.

A semi-quantitative measure of the blue, green, and red luminescence intensity was obtained with a laboratory plaque tester (9) in which u.v. radiation from two germicidal lamps excites the phosphor to be tested. The emission from the phosphor is filtered, and the emission within the corresponding spectral range is measured with a photomultiplier tube, thus permitting a comparison of the luminescence emission from different phosphor samples to be made. We have found this method to be accurate, and the results are reproducible within ± 2%.

Results

Ball Milling and Surface Area

The average particle diameter of zinc sulfide decreases during milling, but the rate of decrease diminishes with milling time, as shown in Fig. 1. In this figure, three different initial particle sizes are represented; the size in microns is given for average equivalent spherical diameters. If one assumes that the crystallites are perfect, Rittinger's law (10) applies. This law states that the work consumed in particle-size reduction is directly proportional to the area of the newly formed surface. If the material is hard, which means that the cohesive forces are large, much work is needed to expose a given surface area.

The determination of the particle size is quite difficult and represents only an average value that is confounded by the fact that the particles are actually not spherical and are distributed over a variety of shapes according to their sizes (11). An improved sensitive index of the effect of milling is therefore the increase in surface area with milling time. Figure 2 represents this relationship. It is interesting to observe that the curves consist of two distinct regions. During the initial milling period the specific surface area increases rapidly, while there exists a linear relationship with extended milling times. The slope in the linear part is very nearly the same in all five cases, and the fracture of particles is still proceeding at the same rate after 100 hr of ball milling. The increase in specific surface area is larger for smaller particles than for the larger ones during the initial part of milling.

These results are readily amenable to an interpretation. The data can be explained tentatively by assuming that during the early stages of milling the increase in surface area is predominantly due to the breaking of particle aggregates, such as fracture along grain boundaries and similar imperfections,

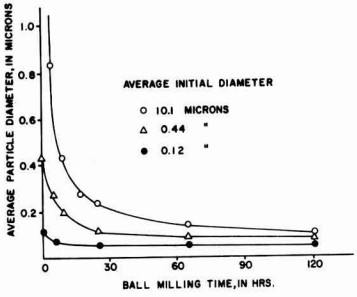

Fig. 1. Dependence of average particle diameter on milling time.

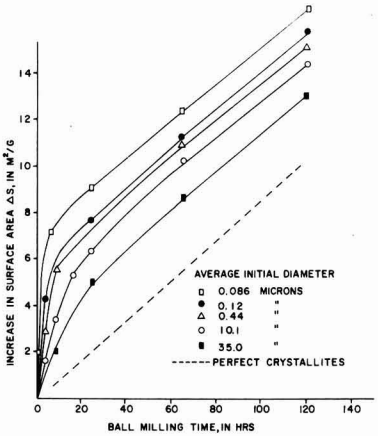

Fig. 2. Increase in surface area with milling time for various initial particle sizes.

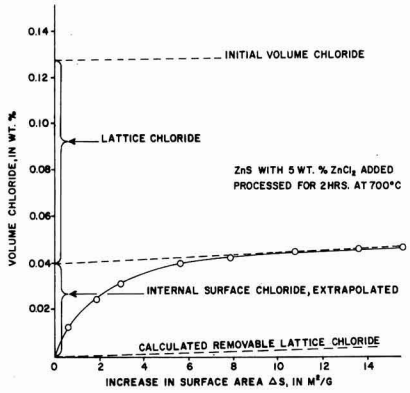

Fig. 3. Distinction between chloride on internal surfaces and within the lattice.

while in the later stages of milling it is the fracture of single crystallites that is dominant. This explanation is also in agreement with the sequence of the curves in that the large particles can be expected to exhibit better crystallinity and fewer imperfections than the small ones. Generally, it may well be feasible to compare the crystallinity and degree of perfection of crystalline materials by evaluating these relationships, as given in Fig. 2.

Distinction between Internal Surface Chloride and Lattice Chloride

When the agglomerates and crystallites are broken up, the surface area of the powder increases. A portion of the volume chloride becomes exposed, and this can be replaced by displacement washings with zinc sulfate solution. Most of the chloride that becomes removable is exposed in the early stages of milling when agglomerates and imperfections are broken up. There will also be some loss of lattice chloride during the initial stage of ball milling; however, this amount can be estimated readily. If one assumes that the lattice chloride is uniformly distributed throughout the lattice, e.g., in a 1-g sample, one finds that about 1% of the volume chloride present will be exposed as lattice chloride if the increase in specific surface area is 10 m²/g. On the other hand, if a portion considerably larger than 1% of the volume chloride becomes displaceable, essentially internal surface chloride must be exposed. In addition, one may expect also from Fig. 2 that mainly internal surface chloride becomes exposed during the initial stages of milling when agglomerates break up.

In a practical case, one would expect therefore that a diagram of the volume chloride as a function of the increase of specific surface area Δs will initially show an amount of chloride exposed per newly formed specific surface area, which is determined essentially by internal surface chloride which becomes displaceable; one can see this exemplified in Fig. 3. However, during subsequent milling essentially lattice chloride becomes exposed when the single crystallites fracture. The sample represented in Fig. 3 was processed for 2 hr at 700°C after 5% by weight of zinc chloride as a flux had been added. The volume chloride is 0.127% by weight, as indicated by the dashed horizontal line. After milling is started one finds that an increasing amount of chloride becomes exposed as the surface area is increased. After the increase in specific surface area is about $\Delta s = 10$ m²/g, the amount of exposed chloride becomes a linear function of Δs. Since single crystallites rather than agglomerates fracture on further milling, it appears likely that lattice chloride is essentially exposed from here on. The straight part of the curve can be extended toward the ordinate of Fig. 3, so that an extrapolation to indicate the amount of lattice chloride present becomes possible. It is assumed in this estimate that the lattice chloride is uniformly distributed within the lattice and is exposed at a linear rate from the start of milling. In the sample shown in Fig. 3, the amount of internal surface chloride is found to be about 0.04% by weight, so that the incorporated lattice chloride amounts to 0.09%.

Other samples were treated in the same manner in order to distinguish between lattice chloride and internal surface chloride as parts of volume chloride. Results are given in Table I. The amount of internal surface chloride decreases as the crystallinity is improved at elevated processing temperatures. The lattice chloride concentration appears to have a peak near 700°C, although one could hardly draw definite conclusions because the determination of lattice chloride is not possible in a direct manner after sample processing at 500°C. In this case the slope does not change as in Fig. 3, but one obtains the impression that internal surface chloride is exposed even after a ball milling time of 350 hr. The

Table I. Chloride retained in zinc sulfide processed with 5% by weight of zinc chloride for 2 hr

Processing temp, °C	Wt % of chloride in Volume	Lattice	Internal surfaces
600	0.303	0.08	0.22
700	0.13	0.09	0.04
800	0.017	0.014	0.003
900	0.0065	0.0055	0.001
1000	0.0030	0.0025	0.0005

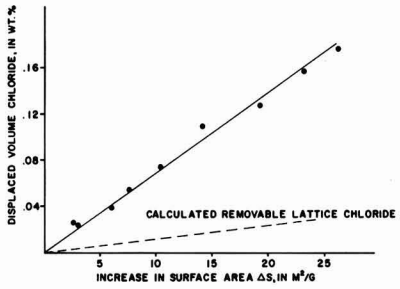

Fig. 4. Removal of coprecipitated volume chloride from precipitated zinc sulfide after milling.

behavior of this sample is very similar to that of zinc sulfide containing coprecipitated chloride,[1] as seen in Fig. 4.

The chloride flux, which is beneficial in preparing zinc sulfide phosphors, may also be present in the coprecipitated form. This is common commercial practice, for the same quality of phosphor is attained with a smaller amount of coprecipitated chloride as with admixed flux. It therefore appears valuable to know the way in which chloride is distributed in this case. A zinc sulfide powder containing 0.80% by weight of coprecipitated chloride was carefully washed with zinc sulfate solution until the amount of volume chloride was at the constant value of 0.73%. Portions of this material were milled for successive periods after which the surface increase and the amounts of displaceable chloride were determined. Figure 4 represents the amount of exposed volume chloride as a function of the increase in surface area during milling. The largest Δs corresponds to 350 hr of milling, during which time about 20% by weight of the initial volume chloride is rendered displaceable. From the nearly linear character of the curve one can surmise that all the chloride rendered displaceable is of one type. If this were uniformly distributed lattice chloride, one should expect a relationship between Δs and exposed chloride as shown by the dashed line in Fig. 4. When this is compared with the experimental results plotted in the upper line, it appears that the coprecipitated chloride is not uniformly distributed within the lattice. The data can be taken to mean that the chloride lies for the most part on internal surfaces of tightly agglomerated particles of the precipitated zinc sulfide powder. This incidental result is of importance to analytical chemists who are concerned with the manner in which coprecipitated ions are incorporated into a precipitate.

When the same zinc sulfide powder is processed for 2 hr at 700°C, one finds about 0.25% by weight of volume chloride of which about one half is lattice chloride. Therefore, the incorporation of volume chloride into the lattice is very similar in this case to that observed with zinc sulfide containing physically admixed chloride flux.

Decay of Luminescence Intensity during Milling

Several experimental samples of a luminescent zinc sulfide phosphor were milled for various lengths

[1] "Coprecipitated" is used in the sense as indicated in ref. (7).

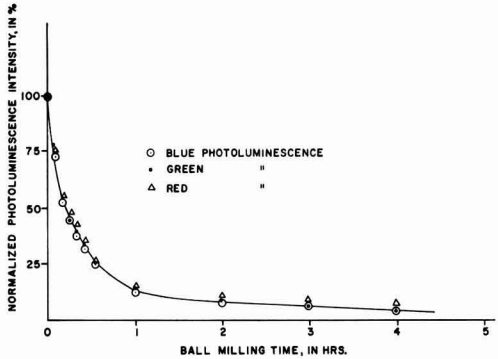

Fig. 5. Decay of photoluminescence intensity of zinc sulfide phosphor during milling.

of time; results are presented in Fig. 5. The blue and green photoluminescence emission decay somewhat faster than the red component. This different behavior of the red part of the emission after ball milling was also observed by Wecker (2). One finds that the ability to luminesce is essentially destroyed during the first 10 hr of milling when the agglomerates are broken up and the internal surfaces (cf. Fig. 2) are exposed.

Therefore, it appears that the exposure of internal surfaces may be intimately connected with the decay of luminescence intensity during the milling process. This consideration led us to plot the logarithm of the luminescence intensity B as a function of the increase of surface area Δs exposed during the ball milling. The resulting Fig. 6 indicates that the luminescence decreases about exponentially with increasing surface area. This means that the decrease in luminescence with the change in Δs is proportional to the instantaneous luminescence emission, i.e., $dB/d(\Delta s) = -aB$.

Another interesting result is that no particles below 0.2 μ were found to be photoluminescent in these very extensive experiments. It appears that a

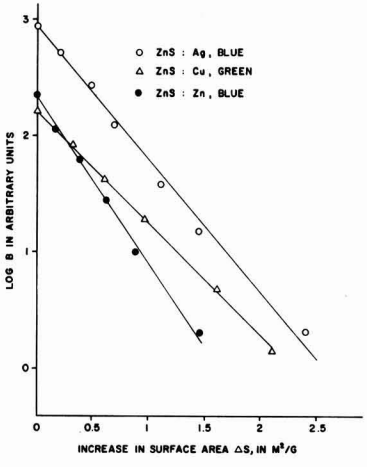

Fig. 6. Logarithm of the photoluminescence intensity B as a function of the increase in surface area Δs during milling.

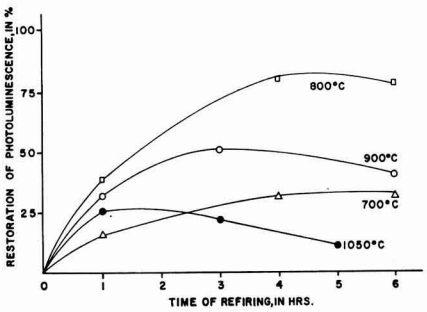

Fig. 7. Restoration of photoluminescence intensity by refiring after milling.

minimum cell size is required for photoluminescence; this is in agreement with conclusions stated by other authors (12-15).

Restoration of Luminescence Emission after Milling

Some experiments have been conducted to explore the restoration of photoluminescence by heat treatment of the milled phosphor. Figure 7 presents some data on recovery of photoluminescence by reprocessing at various temperatures. The extent of restoration is given in per cent of the green luminescence emission before milling as a function of processing time, and the temperature as parameter. If a sample that becomes nonluminescent during milling is held at 800°C for 4 hr the original luminescence is nearly restored, while on extended firing the intensity decreases again. The luminescence recovery was found to be optimum at 800°C. The restored luminescence intensity can be further increased by about 20% if chloride flux, such as 2% by weight of zinc chloride, is admixed or if the sample is quenched rapidly after refiring.

The average particle size increases during the refiring process, as can be determined readily by the gas adsorption method or by microscopic observation (11). The particle size also increases, however, in cases where the restoration of luminescence emission is counteracted by other processes, such as the diffusion of "killer" impurities introduced during ball milling; the extent of this contamination is indicated above. The degree of luminescence recovery and especially the maxima found for various processing temperatures and times become self-evident if impurity diffusion is assumed, as can be seen from Fig. 7. It appears likely that the degree of contamination was smaller in our samples than in those used by Broser and Reichardt (4), since they obtain maximum restoration with a 30-min heat treatment at 500°C.

Summary and Discussion

A study of the mechanism of flux action on the luminescence behavior of zinc sulfide has led to a method that permits one to distinguish between internal surface and lattice chloride. Previous investigations have led to ambiguous results because difficulties arose from the presence of occluded and internal surface chloride. The present study is based on the displacement of chloride ion by sulfate ion, surface area determination by the simplified gas adsorption method, and the use of milling as a means of exposing lattice chloride and internal surface chloride.

It was found that the internal surfaces are exposed mainly during the initial stages of milling, so that internal surface chloride becomes exposed preferentially and can be removed by ion-exchange washings. The slope of the curve of displaceable chloride as a function of the increase in specific surface area gradually approaches a constant value with additional milling, when essentially lattice chloride is rendered displaceable. Simple extrapolation permits one to obtain a quantitative estimate of the amounts of lattice chloride and internal surface chloride.

The instantaneous luminescence intensity of milled zinc sulfide phosphors is found to be an exponential function of the increase in specific surface area. The decrease in luminescence occurs essentially during the exposure of internal surface chloride. When luminescence emission is no longer perceptible, about 80% of the original lattice chloride is still incorporated within the phosphor lattice. It may therefore be concluded that the presence of lattice chloride alone is not sufficient for photoluminescence. A possible correlation may exist between the occurrence of luminescence and the requirement of a certain minimum cell size, since no photoluminescent particles have been observed below 0.2 μ in diameter. It appears possible that the exposure of internal surfaces is accompanied by the creation of trapping levels that lead to the observed decrease in luminescence with the increase in specific surface area.

Acknowledgment

Grateful acknowledgment is made to D. J. Bracco for many helpful discussions, and to J. T. Ragusin for valuable assistance with the experimental work.

Manuscript received March 14, 1960. This paper was prepared, in part, for delivery before the San Francisco Meeting, Apr. 29-May 3, 1956.

Any discussion of this paper will appear in a Discussion Section to be published in the June 1961 JOURNAL.

REFERENCES

1. P. Lenard and V. Klatt, *Ann. Physik*, **12**, 439 (1903).
2. F. Wecker, *ibid.*, **42**, 561 (1942); **43**, 607 (1943).
3. F. Frey, *ibid.*, **2**, 147 (1948).
4. I. Broser and W. Reichardt, *Z. Physik*, **134**, 222 (1953).
5. H. Meier, *Z. Elektrochem.*, **60**, 1007 (1956).
6. M. A. Short and E. G. Steward, *Z. Physik. Chem.* (Neue Folge), **13**, 298 (1957).
7. A. Kremheller, S. Faria, P. Goldberg and D. J. Bracco, *This Journal*, **107**, 749 (1960).
8. D. T. Palumbo, F. M. Starkweather, and D. J. Bracco, "A Simplified Gas Adsorption Method for the Determination of the Surface Area of Fine Powders," presented at The Electrochemical Society Meeting, Cincinnati, May, 1955.
9. K. H. Butler and R. W. Mooney, Private communication.
10. P. Rittinger, "Lehrbuch der Aufbereitungskunde," Berlin (1867).
11. Results on "Particle Growth during Phosphor Preparation" will be published in the near future.

12. P. D. Johnson and F. E. Williams, *J. Chem. Phys.*, **18**, 1477 (1950).
13. I. O. M. Poltorak and A. V. Lavrov, *Zhur. Fiz. Khim.*, **29**, 1254 (1955).
14. A. Smekal, "Ueber den Aufbau der Realkristalle," Bologna (1927).
15. A. J. Dekker, "Solid State Physics," p. 410, Prentice Hall, Inc., New York (1959).

Donor Concentration at the Surface of a Diffused N-type Layer on P-type Germanium

R. Glang[1] and W. B. Easton[2]

Diamond Ordnance Fuze Laboratories, Washington, D. C.

ABSTRACT

Four methods of evaluating the donor concentration at the surface of a diffused N-type layer on P-type germanium have been investigated. All methods assumed a complementary error function (erfc) distribution in the diffused layer. The methods required the use of experimental data for junction depth and sheet resistivity, and of published data for diffusion coefficients of group V elements and electron mobilities in germanium. The methods were applied to calculate the donor concentrations at the surfaces of a number of diffused samples. Under diffusion conditions, which were expected to result in an erfc impurity distribution, the actual concentration profile in the vicinity of the junction was shown to deviate from the erfc law. Due to this deviation, one of the methods of calculating the surface concentration was ruled out. With the other three methods, calculated surface concentrations agreed within a factor of 2 or 3. The disagreement is mainly caused by lack of precise information in respect to the electron mobilities in the diffused layer. Therefore, all the methods represent approximations only.

The preparation of diffused PN-junctions has become a widely used technique in the fabrication of semiconductor devices (1, 2). The electrical characteristics of these devices depend to a large degree on the properties of the diffused layer (3). Therefore, a quantitative knowledge of these properties is essential to the design of devices as well as to the experimental direction of the diffusion process. Some of these properties, for instance the junction depth and the sheet resistivity of the layer, are amenable to direct experimental determination. The concentration of the diffused impurity at the surface, however, cannot be measured directly; it has to be derived from other measured parameters. This concentration is generally referred to as surface concentration. There are several ways of determining the surface concentration (4), and the actual choice of the method will depend on the types of experimental data which are available.

The following discussions concern a special case of the diffusion process, characterized by the diffusion of a donor element from a source of constant vapor pressure into P-type germanium of uniform acceptor concentration. The diffusion temperature is maintained constant during the entire experiment. Furthermore, it is assumed that the indiffusion is not complicated either by a rate-determining layer or by evaporation from the germanium surface. If Fick's second equation of diffusion is solved for these boundary conditions, the complementary error function (erfc) is obtained as the general type of the impurity distribution (5):

$$N(x) = N_0 \text{erfc}\ (x/2\sqrt{Dt}) \qquad [1]$$

where $N(x)$ is the concentration of donors in the germanium at a certain distance, x, from the surface; N_0 is the donor concentration immediately at the surface; t is the diffusion time; and D is the diffusion coefficient of the donor element in germanium.

Figure 1 shows the concentration profile of the donors and, in addition, the initial acceptor concentration A, as functions of x. At a certain depth w, where these concentrations are equal and no excess charge carriers are available, the PN-junction is formed; at this depth

$$N(w) = A \qquad [2]$$

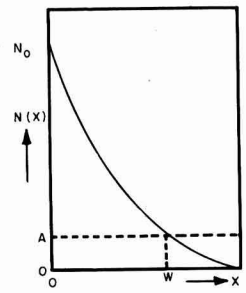

Fig. 1. Concentration of donors N(x) and initial concentration of acceptors A as a function of distance x from the surface of a diffused layer.

[1] Present address: International Business Machines Corp., Kingston, New York.

[2] Present address: Cornell University, Ithaca, New York.

Determination of the Surface Concentration

1. From the erfc distribution.—The simplest treatment of the problem of the surface concentration is obtained by substituting Eq. [2] in Eq. [1] and solving for N_0:

$$N_0 = \frac{A}{\operatorname{erfc}(w/2\sqrt{Dt})} \qquad [3]$$

Values of the diffusion coefficients D for group V donor elements in germanium have been published frequently (6-10). The junction depth w can be determined experimentally, for instance by the techniques described by Bond and Smits (11). The initial acceptor concentration A can be obtained from Hall measurements on the P-type material prior to diffusion. Unfortunately, this simple method was found to be completely unsatisfactory, as will be shown and explained later on.

2. By differential etching.—N_0 may also be expressed in terms of conductivity of the surface layer. Four-point-probe measurements (12, 13) on diffused layers can be expressed in terms of the sheet conductivity σ_s of the entire diffused layer. Since the carrier concentration in the layer varies with depth, the total sheet conductivity is the integral of the differential

$$d\sigma_s = e \cdot \mu(N_i) \cdot n(x) \cdot dx \qquad [4]$$

where $\mu(N_i)$ is the electron mobility at a certain distance x from the surface and is a function of the total impurity concentration N_i at that depth; e is the electron charge. Assuming that all donors are ionized and that a fraction of them equal to the number of acceptors is not available for the conduction process,

$$n(x) = N(x) - A \qquad [5]$$

To obtain the sheet conductivity of a layer of finite thickness, Eq. [4] is integrated. For this purpose, the layer which is closest to the surface and extends into a depth Δx, small compared to the total junction depth w, will be considered. Within this shallow layer, an average value $\bar{\mu}$ can be used to approximate the mobility. Furthermore, the error function is expanded into a series, of which only the first term has to be considered as long as $x/2\sqrt{Dt}$ is small compared to 1. Then

$$N(x) \cong N_0 \left[1 - \frac{2}{\sqrt{\pi}} \cdot \frac{x}{2\sqrt{Dt}} \right] \qquad [6]$$

With these simplifications, the sheet conductivity of the first surface layer of thickness Δx follows from integration of Eq. [4].

$$\Delta\sigma_s = e \cdot \bar{\mu} \left[N_0 \cdot \left[\Delta x - \frac{(\Delta x)^2}{2\sqrt{\pi Dt}} \right] - A\Delta x \right] \qquad [7]$$

Equation [7], solved for the surface concentration, yields

$$N_0 = \frac{\dfrac{\Delta\sigma_s}{e \cdot \bar{\mu}} + A\Delta x}{\Delta x - \dfrac{(\Delta x)^2}{2\sqrt{\pi Dt}}} \qquad [8]$$

Frequently it will be tolerable to further simplify this expression by neglecting second order terms.

The numerical solution of Eq. [8] requires knowledge of the differential sheet conductivity $\Delta\sigma_s$. This information is obtained by measuring the sheet conductivity of the diffused layer with a four-point-probe, then briefly etching the surface and taking another four-point-probe measurement on the new surface. The difference between the two sheet conductivities is $\Delta\sigma_s$. The thickness Δx of the removed surface layer may be determined either by using a calibrated etch or by another junction depth measurement after the etch. Attempts to derive Δx from the difference in the weight of the unetched and etched sample did not give satisfactory results. The average mobility in Eq. [8] has to be estimated either on the basis of a Hall measurement (14, 15) on the diffused layer, or by comparing the average resistivity $\Delta x/\Delta\sigma_s$ of the removed layer with resistivities obtained from published mobility data (16-18).

3. From average mobility approximations.—It is also possible to relate the surface concentration to the total sheet conductivity of the layer, if one succeeds in integrating Eq. [4] over the entire junction depth, i.e., from zero to w. This integration can be done algebraically by using the simplifying approximation of a constant average mobility throughout the entire layer. Obviously, this assumption will affect results more seriously than it did in the foregoing method, where it was applied for a thin sublayer only. With this simplification, the sheet conductivity of the diffused layer is represented by

$$\sigma_s = e\bar{\mu} \cdot [N_0 2\sqrt{Dt} \int_0^{w/2\sqrt{Dt}} \operatorname{erfc} u \, du - \operatorname{erfc}(x/2\sqrt{Dt})\, d(x/2\sqrt{Dt}) - \int_0^w A \, dx] \qquad [9]$$

The first integral term can be transformed according to

$$\int_0^z \operatorname{erfc} u \, du = \frac{1}{\sqrt{\pi}} - \int_z^\infty \operatorname{erfc} u \, du \qquad [10]$$

Numerical values of the function $\int_z^\infty \operatorname{erfc} u \, du$ have been published by Kaye (19), who uses the symbol "ierfc z" for this first repeated integral of the complementary error function. Introducing his symbol, with the understanding that

$$z = w/2\sqrt{Dt} \qquad [11]$$

and, furthermore, substituting the more commonly used sheet resistivity ρ_s for the sheet conductivity, where

$$\rho_s = \frac{1}{\sigma_s} \qquad [12]$$

the surface concentration follows from Eq. [9]

$$N_0 = z \cdot \frac{\dfrac{1}{w \cdot \rho_s \cdot e \cdot \bar{\mu}} + A}{1/\sqrt{\pi} - \operatorname{ierfc} z} \qquad [13a]$$

For numerical solution, A, w, z, and ρ_s are determined as before. The product

$$w \cdot \rho_s = \bar{\rho} \qquad [14]$$

represents the average resistivity of the layer. Since data relating the electron mobility to the donor concentration are published for germanium (16-18) one may derive a graph giving μ as a function of the resistivity. This graph may be used to estimate the average mobility in the layer from the experimental value of the average resistivity as given by Eq. [14].

A more elegant way of interpreting Eq. [13a] requires a Hall measurement instead of a resistivity measurement on the diffused layer. The Hall measurement yields the average excess carrier concentration directly in the following terms:

$$\bar{n} = \frac{3\pi}{8} \cdot \frac{H \cdot I}{w \cdot e \cdot V_H} \qquad [15]$$

where H is the magnitude of the magnetic field, I is the current through the sample, and V_H is the measured Hall voltage. The average electron concentration $\bar{n}$ is given by:

$$\bar{n} = \frac{1}{w \cdot \rho_s \cdot e \cdot \bar{\mu}} \qquad [16]$$

and when substituted in Eq. [13a] leads to:

$$N_0 = z \cdot \frac{\bar{n} + A}{1/\sqrt{\pi} - \text{ierfc } z} \qquad [13b]$$

Further simplifications of Eq. [13a] or [13b] are possible, since A in most practical cases will be very small compared to $\bar{n}$. In addition, the term ierfc z converges rapidly to zero; for $z = 1.6$, for instance, the value of ierfc z is only 1% of $1/\sqrt{\pi}$, and therefore may be neglected.

4. From computer approximations.—The accuracy of the method described in the foregoing paragraph is limited by the assumption of a constant average mobility over the entire layer. Better results are to be expected if the variation of the mobility within the layer is considered. This consideration necessitates the use of a computer. For diffused layers in silicon and various types of impurity distributions, Backenstoss (20) has computed and published curves which relate the surface concentration to the average layer resistivity $\bar{\rho} = \rho_s \cdot w$. For germanium, however, similar data have not been published. In the following discussion, the individual steps of the computation process, which has been applied to obtain analogous curves, are outlined briefly. Only diffused N-layers on P-type germanium and erfc-distributions are considered.

In the general conductivity equation

$$\frac{1}{\bar{\rho}} = \frac{1}{\rho_s \cdot w} = \frac{1}{w} \cdot e \cdot \int_0^w \mu(N_i)\,[N(x) - A]\,dx \qquad [17]$$

$N(x)$ is assumed to be given by Eq. [1]. The mobility $\mu(N_i)$ is taken from the data of Conwell (17). This implies the assumption that the total impurity concentration approximately equals the excess donor concentration: $N_i \simeq N(x) - A$, which is true only if $N(x)$ is large compared to A. The integral was evaluated by Simpson's rule, using an IBM 704 computer. The computation is greatly simplified by the change of variable, $x = wu$. On substituting the latter and Eq. [1] in Eq. [17]

$$\frac{1}{\bar{\rho}} = e \cdot \int_0^1 \mu\,(N_0 \text{ erfc } zu - A) \cdot [N_0 \text{ erfc}(zu) - A] \cdot du \qquad [18]$$

where $z = w/2\sqrt{Dt}$. The value of z is determined by assuming Eq. [1] as a first approximation for $x = w$, and solving for z by Newton's iteration method. This procedure defines an effective diffusion coefficient D, which has the advantage of making the resistivity a function only of the initial and surface concentrations. It will be shown later on that Eq. [1] does not give a true picture of the impurity distribution in the region close to the junction, and therefore the effective diffusion coefficient will not be a true value. However, diffusion coefficients of group V elements in germanium, published by different authors (6-10), vary within rather wide limits. Therefore, for the problem at hand, the effective D-value is certainly as good as one of the published values.

The complementary error functions used in the calculations were evaluated by means of the Rand approximation (21) of the form:

$$\text{erfc } y = \frac{2}{\sqrt{\pi}} \int_y^\infty \exp(-v^2)\,dv =$$

$$[1 + a_1 y + a_2 y^2 + a_3 y^3 + a_4 y^4 + a_5 y^5]^{-8}$$

An unsuccessful attempt was made to find a simple approximation for $\mu(n)$ or $n \cdot \mu(n)$. The latter was found to be approximately proportional to $(\log n)^4$, but the approximation was not close enough for computation. The values of $\mu(n)$ were therefore taken from Conwell's graph (17) in which they are plotted as a function of $\log n$. The mobilities were found during computation by four-point Lagrange interpolation. The values of the average conductivity of the diffused layer, $1/\bar{\rho}$, were computed for various values of A and N_0. Results are shown in Fig. 2. The truncation and round-off errors in the calculation are negligible. Sources of possible errors are therefore the mobility data and the use of Eq. [1] to compute z.

Application of Methods and Discussion of Results

Numerous diffusion experiments were conducted in accordance with the conditions stated in the introduction. The source of the diffusing impurity and the wafers to be treated were kept together in a covered quartz boat, which was located in a vacuum tube furnace and heated to varied diffusion temperatures. The diffusion tube containing the boat was mantled by a graphite cylinder to pick up RF energy from an induction coil. Heating and cooling periods prior to and after the experiment were in the order of only 10 min. The diffusing donor im-

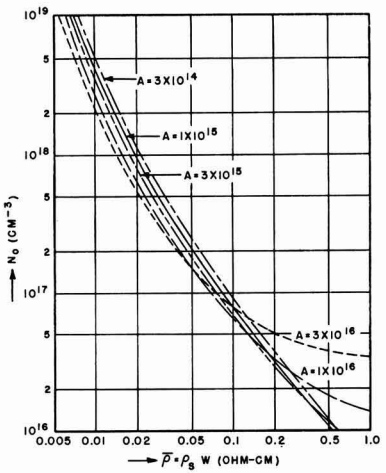

Fig. 2. Surface concentration N_0 vs. average resistivity $\bar{\rho}$ for several initial acceptor concentrations A; computed for diffused N-type layers with an erfc distribution in germanium.

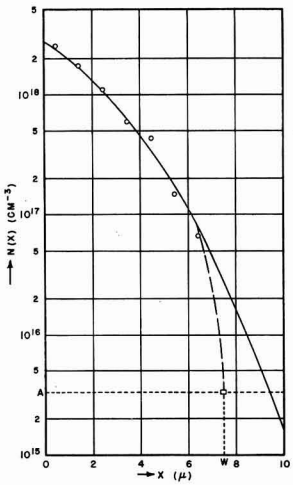

Fig. 3. Actual impurity distribution N(x) (circles, dashed line, and square) and ideal erfc distribution (solid line) vs. distance x from the surface of a diffused N-type layer on P-type germanium. Arsenic indiffusion: 1 hr at 800°C.

purity was arsenic obtained by evaporation from powdered master alloys containing arsenic in germanium.

Numerical values of the diffusion coefficients were based on data given by Smits (6); only in the computer approximations were effective D-values used. Junction depths were determined by angle lapping the diffused sample, depositing copper to delineate the junction, and subsequently making interference depth measurements (11). The average mobilities needed for solution by methods 2 and 3 were estimated from the average resistivity, again using the mobility data published by Conwell. In one case, the mobility was determined experimentally by Hall measurement on the diffused layer.

Experimental data and results of the calculations for 13 samples diffused in various runs are listed in Table I. On comparing the surface concentrations shown in the last four columns of the table, the most striking fact is that all values obtained by direct evaluation of the erfc equation (method 1) are unreasonably small. In order to investigate this phenomenon further, a few diffused layers have been analyzed by a method which has been mentioned by Smits (4). It consists of etching away the diffused layer in small steps and taking four-point-probe conductivity measurements between steps. In this way the average donor concentrations for each individual sublayer can be evaluated. In the immediate neighborhood of the junction, measurements are not possible, because the resistance of the remaining and extremely thin layer becomes very high and unreproducible.

An example of such a layer analysis is shown in Fig. 3. The circles indicate concentrations derived from measurements. The solid line is an erfc curve, calculated to fit the experimental points most closely.

Table I. Parameters of germanium diffused with arsenic

Sample No.	Diffusion time, min	Diffusion temp, °C	A[a], 10^{15}/ccm	w[b], 10^{-4} cm	ρ_s[c], ohm/sq	Surface concentration N_0 10^{17}/ccm Calculated by methods 1	2	3	4
H5-48-34	60	800	3	7.5	11.3	0.6	36	17	54
H5-61-36	360	700	3	5.6	17.6	1.2	20	15	36
V21-30-46	60	800	2	5.8	29.3	0.2	—	4.4	12
P1-47	60	750	5	2.6	120	0.2	—	1.7	3.5
P1-48	40	750	5	1.5	154	0.1	—	2.1	5.6
P1-49	40	750	5	1.5	169	0.1	—	1.8	4.8
P1-50	40	750	5	1.5	210	0.1	—	1.4	3.4
P1-51	242	800	10	10.6	22.9	0.6	2.7	2.6	4.7
P1-52	241	800	10	10.4	30.9	0.6	3.3 5.8[d]	1.8 4.0[d]	3.0
SM1-53	30	750	1.5	2.0	115	0.1	—	2.6	7.0
SM1-54	61	800	1.5	6.6	65	0.2	—	1.3	2.6
SM1-55	37	800	1.5	3.8	90	0.1	—	1.5	3.7
SM1-56	45	800	1.5	3.8	116	0.1	—	1.0	2.5

[a] Initial acceptor concentration.
[b] Depth at which A = donor concentration $N(w)$.
[c] Sheet resistivity.
[d] Derived from Hall measurements.

The small square indicates the depth where the junction was determined to be located, using the angle lapping technique. From this figure, it can be seen that the true impurity distribution in the vicinity of the junction deviates strongly from the erfc curve; the true distribution in this vicinity is indicated by a dashed line. This deviation is larger than a possible error in the junction depth determination.

Other samples which have been investigated in the same way gave similar results. In the numerical evaluation of Eq. [3], too small a value of w will give an erfc value which is too high and, therefore decrease N_0. This effect has been observed in all cases and, therefore, it must be concluded that for diffusion conditions, as explained previously, the resulting impurity distribution follows the erfc curve in the major part of the layer, but deviates strongly in the neighborhood of the junction. Since the determination of the surface concentration by method 1 depends strongly on the validity of the erfc law exactly at the junction, this method is not suitable for a reasonable estimate of N_0.

The mechanism which causes this deviation of the impurity distribution is not fully understood. On a few samples, which had been used for a layer analysis, the acceptor concentration A was determined by Hall measurement after the diffused layer had been etched off completely. It was found that A was larger than it had been prior to diffusion, in one extreme case by a factor of two. This may be an indication of simultaneous indiffusion of copper during the diffusion process. It is well known that copper is a rapidly diffusing acceptor impurity in germanium, and the complete exclusion of traces of copper from the surface of the sample during the cleaning operations is extremely difficult (22). Copper atoms in the order of 10^{16}/ccm in the layer may at least partially account for the observed deviation in the distribution of excess donors. Near the surface the contamination with copper is negligibly small compared to that with arsenic. In greater depths, however, the arsenic concentration decreases and eventually becomes even smaller than the copper concentration. This happens close to the junction, and that is the region where the deviations appear.

The fact that the impurity distribution does not exactly follow the erfc law raises the question of how this deviation affects the other methods of calculation. There is obviously no influence on the differential etching method because all measurements involve only the region nearest to the surface of the diffused layer. The accuracy of this method therefore depends entirely on the accuracies of the estimate of the mobility and the thickness of the etched-off layer. Results are nearly independent of the value of the diffusion coefficient, since in Eq. [8], D occurs in a second order term only. This deviation certainly influences the results of methods 3 and 4 in some degree. However, these methods involve integration over all donors in the diffused layer. The small region near the junction, where the deviation from the erfc law becomes noticeable, does not contribute a substantial fraction of the total integral. Therefore, the effect of this deviation will be minor.

The accuracy of methods 2, 3, and 4 is limited mainly by the lack of precise information about the electron mobility in various parts of the diffused layer. The mobility data of Conwell, used for most of the calculations, refer to samples of homogeneous doping with no concentration gradient and as little compensated impurities as possible. Therefore, these values may not hold well for the diffused layers. For example, the electron mobilities for concentrations between 10^{16} and 5.10^{17}/ccm should range from 3000 to 1500 cm^2/v sec, according to Conwell. The average Hall mobility, however, has been measured on a sample of corresponding concentrations and was found to be only 930 cm^2/v sec. Because of the mobility values used for most of the calculations, results may be in error by a factor in the order of two. On the other hand, it may very well be that the experimental mobility value is too low, because the Hall measurements were made on N-type layers adjoining P-type bulk material, and the measured voltage depends on the effectiveness of the junction as an insulator between different regions. If a small leakage current passes through the junction, the Hall voltage will be affected by the presence of holes in the P-type region.

The rather crude assumption of a constant mobility throughout the entire layer is reflected in the last two columns of Table I. All data obtained according to method 3 are smaller than those of method 4 by a factor of about 2.5, whereas the values of the differential etching method are somewhere in between.

On comparing the surface concentrations of different samples calculated by the same methods, minor differences will be noted. These differences are due to the fact that master alloys with slightly varying amounts of arsenic, in the order of 10^{19}/ccm, have been used as sources of the diffusant. The first two samples listed in Table I, i.e., those bearing the designation "H5—", were diffused in the presence of a master alloy which was richer in arsenic than the other sources by a factor of about 10.

Summary and Conclusions

Four methods have been investigated in order to obtain data of the surface concentrations in diffused layers. These methods are not equally suitable for the purpose. The first method involves a junction depth measurement and the assumption of an erfc distribution extending throughout the entire layer and into the junction region. It leads to numerical results which disagree by more than one order of magnitude with resistivity and Hall measurements and with all calculations based on these measurements. The complete experimental analysis of diffused layers, by determining sheet conductivities and excess electron concentrations of individual partial layers, indicates that the distribution of donors in the neighborhood of the junction deviates from the erfc distribution. Therefore, the erfc equation fails to give true values of the surface concentration.

The remaining three methods rely on the fact that the conductivity of the diffused layer is related to the number of excess electrons in the N-type region. The fraction of the conductivity which is due to

carriers in the deviating part of the distribution curve is either not involved (method 2), or is negligibly small compared to the total quantity (methods 3 and 4). Therefore, these methods are not sensitive to deviations of the donor distribution in the region of the junction. Their accuracy depends, rather, on how closely the true relation between excess electron concentration and conductivity of the layer can be approximated. These methods allow fairly accurate calculations of the surface concentration. The major limitation of method 3 is that it employs the concept of a constant mobility. However, the relation between electron concentration and conductivity requires knowledge of electron mobilities in the diffused layer, and these are amenable to experimental determination only to a limited extent. Therefore, in the preceding calculations, the electron mobilities had to be estimated by comparison with data referred to germanium of similar but not exactly the same impurities as in the diffused layers. Consequently, these three methods can give only an estimate of the surface concentration. Considering the uncertainty in the mobility data as the main source of error, the surface concentrations obtained by either method 2 or 4 should not deviate from the true value by a factor larger than 2.

Manuscript received Jan. 12, 1960.

Any discussion of this paper will appear in a Discussion Section to be published in the June 1961 JOURNAL.

REFERENCES

1. L. P. Hunter, "Handbook of Semiconductor Electronics," Chap. 7, p. 12, McGraw-Hill Book Co., Inc., New York (1956).
2. F. J. Biondi, "Transistor Technology," Vol. III, p. 64ff, D. Van Nostrand Co., Inc., New York (1958).
3. *Ibid.*, p. 245 ff.
4. F. M. Smits, *Proc. IRE*, **46**, 1055 (1958).
5. *Ibid.*, p. 1049 ff.
6. *Ibid.*, 1052.
7. K. B. McAfee, W. Shockley, and M. Sparks, *Phys. Rev.*, **86**, 137/38 (1952).
8. C. S. Fuller, *Phys. Rev.*, **86**, 136/37 (1952).
9. J. A. Burton, *Physica*, **20**, 845 (1954).
10. W. Bösenberg, *Z. Naturforsch.*, **10A**, 285 (1955).
11. W. L. Bond and F. M. Smits, *Bell System Tech. J.*, **35**, 1209 (1956).
12. L. B. Valdes, *Proc. IRE*, **42**, 420 (1954).
13. F. M. Smits, *Bell System Tech. J.*, **37**, 711 (1958).
14. O. Lindberg, *Proc. IRE*, **40**, 1414 (1952).
15. L. J. van der Pauw, *Philips Research Repts.*, **13**, 1 (1958).
16. H. E. Bridgers, J. H. Scaff, and J. N. Shive, "Transistor Technology," I, p. 79, D. van Nostrand Co., Inc., New York (1958).
17. E. M. Conwell, *Proc., IRE*, **40**, 1331 (1952).
18. P. P. Debye and E. M. Conwell, *Phys. Rev.*, **93**, 693 (1954).
19. J. Kaye, *J. Math. Phys.*, **34**, 119 (1955).
20. G. Backenstoss, *Bell System Tech. J.*, **37**, 699 (1958).
21. C. Hastings, Jr., "Approximations for Digital Computers," p. 186, Princeton University Press, Princeton, N. J. (1955).
22. L. P. Hunter, "Handbook of Semiconductor Electronics," Chap. 7, p. 15, McGraw-Hill Book Co., Inc., New York (1956).

A Study of the Thorium-Tungsten-Boron System

Douglas T. Pitman and Dilip K. Das

Spencer Laboratory, Raytheon Company, Burlington, Massachusetts

ABSTRACT

A phase diagram for the Th-W-B system has been determined by x-ray diffraction of samples fired to a brightness temperature of 1800°C and furnace-cooled. A ternary compound was found with a probable composition of $ThWB_4$. This compound is monoclinic, with lattice parameters: $a = 12.25$, $b = 3.75$, $c = 6.14$Å, and $\beta = 104.1°$. The stability of the thorium and tungsten borides and their reaction with ThO_2 were also investigated.

The hexaborides of the alkaline earth and rare earth metals and thorium with the general formula MB_6 have been investigated by Lafferty (1). He found that these borides had certain desirable properties that might make them good thermionic emitting materials. The hexaborides were found to be unstable in the presence of refractory metals such as Mo and W, and certain precautions had to be used to prevent their decomposition. However no work has been reported on the Th-W-B ternary system and the stability of the tungsten borides and thorium borides in the presence of thorium or boron. This information would be of importance for the design and conception of high-temperature cathodes and the interpretation of the emission mechanisms. The phase diagram of W-B has been reported by Kiessling (2) and Brewer, *et al.* (3). It has four intermediate phases: W_2B_5, W_2B, and a high- and low-temperature form of WB. The Th-B system has been reported in the literature by various authors (3-6) and has two intermediate phases: ThB_4 and ThB_6. Th and W do not form any compounds or solid solution and their eutectic composition is about 8 atomic per cent (a/o) tungsten with a melting point of 1475°C (7). Also of interest is the role of ThO_2 as an impurity in the thorium and its effect on the phases present in the ternary diagram.

Experimental

The ternary compositions were synthesized by reactive sintering of pressed powder compacts. The boron obtained from U. S. Borax Research Corporation had a maximum impurity of less than 0.4%. Westinghouse thorium had a maximum impurity

Table I. Spectrographic analysis of B, Th, W, and ThB_4

o/o	B	Th	W	ThB_4
Al		0.3-0.03	0.001-0.0001	0.3-0.03
B		0.003-0.0003		
Ba			0.001-0.0001	
Ca	0.001-0.0001	0.3-0.03	0.01-0.001	0.001-0.0001
Cr		0.001-0.0001	0.001-0.0001	0.003-0.0003
Cu	0.01-0.001	0.01-0.001	0.01-0.001	0.001-0.0001
Fe	0.01-0.001	0.1-0.01	0.03-0.003	0.1-0.01
Ga		0.003-0.003		
K			0.01-0.001	
Mg	0.01-0.001	0.3-0.03	0.01-0.001	0.003-0.0003
Mn	0.1-0.01	0.03-0.003	0.03-0.003	0.003-0.0003
Na			0.001-0.0001	
Ni			0.003-0.0003	
Pb		0.01-0.001	0.001-0.0001	
Si	0.3-0.03	1.00-0.10	0.01-0.001	0.03-0.003
Sr			0.001-0.0001	
Ti	0.003-0.0003		0.003-0.0003	
Zn			0.001-0.0001	

content of less than 2.2%. X-ray diffraction analysis showed that there was about 1.0% thoria in the thorium. The tungsten was obtained from Fansteel Metallurgical Corporation with a purity better than 99.8%. The particle size of these materials was less than 100 mesh. Spectrographic analyses of the starting materials B, Th, and W are given in Table I.

Ten-gram samples were weighed out and thoroughly spatulated. Five grams was then pressed at 10,000 psi to form a compact with a ¼ in. diameter and a thickness of about ½ in. These compacts were vacuum-fired to a brightness temperature of 1800°C for ½ hr and furnace cooled at a pressure of 10^{-4}-10^{-5} mm Hg. The sample temperature dropped from 1800° to 700°C in about 90 sec after the heat was turned off.

The small furnace in which the compacts were fired was placed inside a vacuum bell jar. The heater was a 1 in. diameter by 1½ in. long helix of six turns made from 0.080 in. tungsten wire. Three molybdenum heat shields were mounted around the heater coil. A viewing port was cut into the shields to allow the temperature of the sample to be measured with an optical pyrometer. The sample rested on a ThO_2 disk of a special design to give a minimum contact area between the compact and the disk. The disk was placed on a molybdenum pedestal that brought the sample up to the middle of the heater coil directly in line with the viewing port in the molybdenum radiation shields. This experimental arrangement avoided contamination of the sample and the loss of boron by diffusion into the container. Temperatures were measured with a L&N optical pyrometer, and all temperatures reported in the body of the paper are brightness temperatures. As many as three compacts could be fired simultaneously without physical contact between the individual specimens.

X-ray diffractometer traces or Debye-Scherrer powder photographs were made of all the fired samples in order to identify the crystalline phases. The powder photographs were taken with a 114.59 mm radius camera. Filtered copper Kα radiation was used for all x-ray work. Several samples were examined in the diffractometer using a high temperature camera (8) capable of reaching 2000°C in a vacuum of 10^{-5} to 10^{-6} mm Hg.

Table II. Phase analysis of Th-W-B system

Sample No.	Composition (mole %) intended Th	W	B	Heat treatment Br Temp, °C	Time, min	Crystalline phases present as identified by x-ray diff.*
1	7.9	61.4	30.7	1800	30	W_2B, Th, W
2	25.0	50.0	25.0	1800	30	W_2B, Th, W
3	49.5	32.9	17.6	1800	30	Th, W_2B, W
4	50.0	25.0	25.0	1800	30	Th, W_2B
5	50.0	20.0	30.0	1800	30	Th, W_2B
6	50.0	14.4	35.6	1800	30	Th, W_2B
7	35.0	10.0	55.0	1800	30	$ThWB_4$, Th, ThB_4
8	20.0	30.0	50.0	1800	30	W_2B, $ThWB_4$, Th
9	20.0	20.0	60.0	1800	30	$ThWB_4$, W_2B
10	12.5	25.0	62.5	1800	30	WB, $ThWB_4$, ThB_4
11	15.1	23.9	61.0	1800	30	$ThWB_4$, WB
12	16.6	16.7	66.7	1800	30	ThB_4, $ThWB_4$, WB
13	18.0	18.5	63.5	2100	30	$ThWB_4$, WB
14	22.5	15.0	62.5	2100	30	$ThWB_4$
15	23.5	12.5	64.0	1800	30	$ThWB_4$, ThB_4
16	21.0	10.5	68.5	1800	30	$ThWB_4$, ThB_4
17	17.3	13.8	68.9	1800	30	ThB_4, $ThWB_4$, WB
18	21.0	13.0	66.0	1800	30	$ThWB_4$, ThB_4, WB
19	25.0	3.0	72.0	1800	30	ThB_4, $ThWB_4$
20	18.7	6.0	75.3	1800	30	ThB_4, $ThWB_4$, WB
21	12.7	11.1	76.2	1600	30	W_2B_5, ThB_4
22	13.6	4.7	81.7	1600	30	ThB_n, ThB_4, W_2B_5
23	12.0	20.2	67.8	2100	30	ThB_4, WB

* All the samples have ThO_2 present in an amount of not more than 3%.

Results and Discussion

The phase equilibrium data used to determine the Th-W-B ternary diagram are given in Table II. This table lists the composition in atomic per cent, the firing temperature and time, and the crystalline phases as identified by x-ray diffraction.

Figure 1 is the proposed ternary diagram as determined by this experiment.

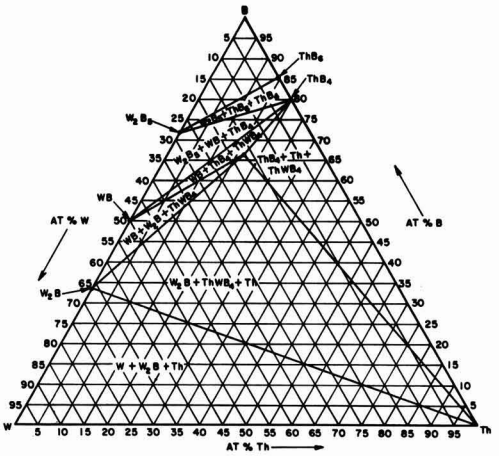

Fig. 1. Phase diagram of the system Th-W-B based on samples fired at 1800°C and furnace cooled.

It is known from the binary phase diagrams that the homogeneity ranges of WB and W_2B_5 are 48-51 a/o and 66.6-68.0 a/o B, respectively, while the homogeneity ranges of the other existing phases are too narrow to be measured. The assumption was made that all the compounds and elements in the binary systems could be represented as points on the ternary phase diagram.

The initial samples were chosen in order that their composition would fall on the intersections of lines drawn in the ternary field for all possible combinations of phase co-existence. This reduced the number of fired samples needed to establish the phase diagram. The analysis of these strategic samples showed which two phases could or could not co-exist, thus determining the locations and contents of every three-phase field, barring the existence of ternary compounds in these regions.

A ternary compound was found which could be represented by the formula $ThWB_4$. A number of samples were required to ascertain its composition. This phase was found to co-exist with W_2B, WB, ThB_4, or Th. Since the lattice constants did not vary with composition the homogeneity range is believed to be very narrow.

The ternary phase has the approximate composition $ThWB_4$ based on the following evidence. The sample, 50 m/o ThB_4 and 50 m/o W, was fired in the usual manner. Weight loss during the firing was found to be 2 w/o. The composition of the evaporant was found to be Th and B. X-ray diffraction and metallographic examination of this sample showed it to be primarily the ternary phase with a combined total of less than 2 w/o ThO_2 and WB. Also using the molecular formula, $ThWB_4$, and calculating the theoretical density on the basis of two molecules per unit cell, (crystal structure studies are described in the next paragraph), good agreement is obtained between the calculated and measured density. For the reasons above the most probable composition is $ThWB_4$.

Small crystals of the ternary phase could be obtained on the surface of samples which were in the vicinity of $ThWB_4$ in the phase diagram by firing them to 2100°C. Precession photographs were made using a small crystal 0.05 mm by 0.15 mm (Mo Kα, λ = 0.7107 Å). These photographs showed $ThWB_4$ to be monoclinic with a = 12.25 Å, b = 3.75 Å, c = 6.14 Å and β = 104.1°. The probable space groups are P_2, $P_{2/m}$, or Pm. The x-ray density, assuming two molecules per unit cell, is 5.6 g cm^{-3} while the measured density is 5.8 g cm^{-3}. The pycnometric value of the density is high because of the presence of a small amount of WB. The melting point of this phase is 2175° ± 25°C which is lower than the melting points of the surrounding borides: ThB_4, W_2B, and WB.

The diffraction data and the calculated hkl values for monoclinic $ThWB_4$ are presented for comparison along with those of ThO_2 and ThB_4 in Table III. It was also found that other refractory metals such as Mo or Re react with ThB_4 to form ternary compounds which are isomorphous with $ThWB_4$.

In the presence of W, ThB_4 is unstable with the result that W_2B is always the first product formed along with free Th. This reaction was examined by means of the high-temperature camera mounted on the Geiger counter diffractometer. It was found that in a 50 m/o W and 50 m/o ThB_4 sample, W_2B first appeared at a temperature of 1100°C with a decrease in the intensity of ThB_4 and W lines. As the temperature was raised the amount of W_2B continued to increase until at 1600°C the W_2B began to decrease with the formation of $ThWB_4$. Holding the sample at this temperature for 1 hr showed the components to be $ThWB_4$ with a small amount of W_2B. As the temperature was further increased to about 1800°C WB started to appear and $ThWB_4$ decreased slightly in intensity indicating that both B and Th were evaporating off from the surface.

Table III. X-ray diffraction data for $ThWB_4$, ThB_4, and ThO_2

$ThWB_4$			ThB_4			ThO_2*		
hkl	I/I_o	d	hkl	I/I_o	d	hkl	I/I_o	d
200	3	5.92	110	4	5.159			
			001	61	4.091			
010	41	3.748	200	53	3.636			
			210	77	3.252	111	100	3.234
			111	7	3.200			
400	100	2.963	201	61	2.718	200	35	2.800
211	5	2.655	211	100	2.546			
			310	14	2.301			
401, 402	30	2.423	221	32	2.177			
41$\bar{1}$	81	2.324	002	19	2.046			
51$\bar{1}$, 60$\bar{1}$	32	2.033	311	21	2.008	220	58	1.980
			112	4	1.905			
103, 402	9	1.880	321	7	1.809			
020	20	1.873	202	19	1.783			
601	12	1.753	410	40	1.765			
			212	32	1.731			
113	3	1.682	330	12	1.714	311	64	1.689
61$\bar{2}$	7	1.676	411	35	1.619	222	11	1.616
60$\bar{3}$	9	1.612	222	7	1.601			
32$\bar{1}$	18	1.587	331	19	1.581			
71$\bar{1}$, 42$\bar{1}$	24	1.582	312	5	1.528			
80$\bar{1}$	22	1.532	430	2	1.455			
800	3	1.483	322	4	1.436			
70$\bar{3}$	12	1.480	510	3	1.428	400	8	1.400
711	20	1.422	431	7	1.371			
			511	7	1.347			
			412	32	1.337			
			332	16	1.314	311	26	1.284

* Data from Swanson and Tatge, National Bureau of Standards Circular 539.

The following reactions and stability tests were made at elevated temperatures in a vacuum of 10^{-4}-10^{-5} mm Hg. The reaction products studied were those which could be identified by x-ray diffraction, i.e., crystalline materials. No attempt was made to determine the gaseous products of such reactions.

Boron reacted with ThO_2 to form ThB_6 at a temperature of less than 1600°C. When the temperature was raised to 2100°C, ThB_6 disappeared and was replaced by ThB_4, with two moles of boron reacting with excess ThO_2.

Firing ThB_4 in contact with ThO_2 at 2300°C resulted in no reaction, reduction, or solid solution,

contrary to the postulations by Brewer, *et al.* (3). The phase ThX_2, which was reported by Brewer to be a solid solution between ThO_2 and ThB_4, was not found in any of the samples examined during this investigation, and it is quite probable that this phase involves some element other than B.

ThB_6 fired to 1600°C in vacuum showed no decomposition. The apparent instability that Brewer proposes for ThB_6 may be partly due to diffusion of boron into the molybdenum boride crucible that he used.

WB fired in contact with ThO_2 to 2100°C showed no apparent reduction of the ThO_2. X-ray examination revealed WB, W_2B, and ThO_2 to be present in the sample.

X-ray examination of mixtures of W_2B and ThO_2 fired to 1800°C showed only W_2B and ThO_2.

$ThWB_4$ was found to be inert to ThO_2 at a temperature of 2100°C.

During this investigation pure ThB_4 and ThB_6 were prepared. The preparation of ThB_4 by firing powder compacts of the elements was found to be mainly a problem of obtaining equilibrium. This was achieved by regrinding and refiring the sample. In the case of ThB_6, boron was lost when the reaction became strongly exothermic at 1050°-1150°C. To compensate for the loss of boron in the resultant ThB_6-ThB_4 mixture, a calculated amount of B was added to convert all the samples to ThB_6 on refiring at 1800°C. The calculations were based on a calibration curve obtained with the x-ray diffractometer from known mixtures of the two compounds. The impurities of the synthesized ThB_4 and ThB_6 were those of the elemental starting materials although substantially reduced by the vacuum firing. The amount of ThO_2 which was the main impurity in the Th has been practically eliminated. The spectrographic analysis of the ThB_4 is included in Table I for comparison.

Acknowledgments

The authors are indebted to Dr. L. Lesensky for his encouragement and helpful discussion during the course of this investigation. They also wish to acknowledge the efforts of Dr. L. E. Alexander who took and interpreted the precession photographs of the ternary phase and Mr. N. J. Aubert and Mr. W. Y. Tye for their skilled assistance.

Manuscript received Aug. 21, 1959. Portions of this paper have been presented at the Nineteenth Annual Conference on Physical Electronics held at the Massachusetts Institute of Technology on March 26-28, 1959.

Any discussion of this paper will appear in a Discussion Section to be published in the June 1961 JOURNAL.

REFERENCES

1. J. M. Lafferty, *J. Appl. Phys.*, **22**, 299 (1951).
2. R. Kiessling, *Acta. Chem. Scand.*, **1**, 893 (1947).
3. L. Brewer, D. L. Sawyer, D. H. Templeton, and G. H. Dauben, *J. Am. Ceram. Soc.*, **34**, 173 (1951).
4. A. Zalkin and D. H. Templeton, *Acta Cryst.*, **6**, 269 (1953).
5. R. Kiessling, *Acta Chem. Scand.*, **4**, 163, 209 (1950).
6. F. Bertaut and P. Blum, *Compt. rend*, **234**, 2631 (1952).
7. H. A. Wilhelm, A. S. Newton, A. H. Doane, and G. Neher, "Thorium Metallurgy," CT-3714 (February 1946).
8. D. K. Das and D. T. Pitman, Pittsburgh Diffraction Conference (Nov. 1959).

Theory of Faradaic Distortion

K. B. Oldham

King's College, University of Durham, Newcastle upon Tyne, England

ABSTRACT

The passage of a pure a.c. across an electrode gives rise to a cell potential containing sinusoidal components of frequencies which are multiples of the fundamental. The first harmonic is predominant and expressions are derived for its amplitude and phase angle. The magnitude of the effect is similar to that of faradaic rectification, but its measurement may offer advantages over the latter in the determination of the kinetic parameters of some electrode reactions. The effect of the double layer is considered, and an apparatus is described which enables faradaic admittance, rectification, and distortion to be measured simultaneously.

Two effects of the passage of an alternating current across an electrode have been employed to determine the rates of the two electrode reactions and their dependence on potential. The first of these effects, faradaic admittance (1), is usually exploited by placing the cell[1] in one arm of an a-c bridge: the kinetic parameters are calculated from the magnitudes of the resistance and capacitance which must be inserted into a balancing arm to achieve a null signal across the bridge (2, 3). The second effect, faradaic rectification (4), is assessed by measuring the change in d-c potential which the alternating current produces, either directly (5, 4) or by supplying the cell with an intermittent high-frequency signal, the resultant square-wave potential being nullified by application of an intermittent current (6, 7). A third effect is now described: this too may be employed for the determination of the kinetic parameters of the electrode reaction.

[1] The design of the cell is such that one electrode remains depolarized. One method of achieving this result is to employ two electrodes similar in all respects except area, of which one electrode has incomparably more than the other. The equilibrium potential of such a cell is, of course, zero and therefore if the passage of a current through the cell causes a change v in the potential of the smaller electrode, the cell potential is directly equal to v plus an ohmic potential V_o caused by the passage of the current through the resistance R_s of the cell solution. The potential across a cell having chemically dissimilar electrodes is, however, equal to the sum of three terms, $(v + V_o + V_e)$, V_e being the equilibrium potential of the polarizable electrode versus the reference (depolarized) electrode.

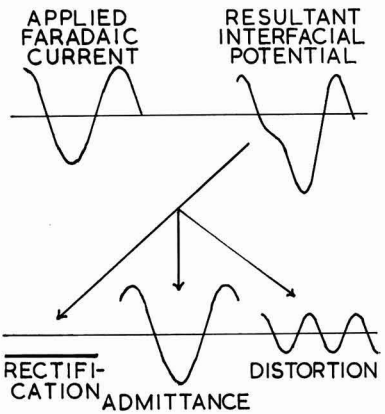

Fig. 1. Wave forms of the applied faradaic current (a pure sine wave) and the resultant interfacial potential. The latter contains three major components having the wave forms shown in the three lower diagrams.

If the instantaneous anodic magnitude of the faradaic component of the applied alternating current is $I \cos \omega t$, its effect is to change the electrode potential from its equilibrium value E_e to $(v + E_e)$. It will be shown in the *Mathematical Derivation* below that v has the form

$$v = \Psi + V \cos(\omega t + \theta) + V_2 \cos(2\omega t + \theta_2) + (\text{much smaller terms}) \quad [1]$$

and the unknowns Ψ, V, θ, V_2, and θ_2 in this equation will be evaluated there. The upper two diagrams in Fig. 1 show typical plots of the quantities $I \cos \omega t$ and v against time; the three lower diagrams correspond to the three leading terms on the right hand side of Eq. [1] into which v can be resolved. The d-c potential Ψ, which has been termed the redoxokinetic potential (8), arises from faradaic rectification. The ratio V/I is termed the faradaic impedance of the electrode and since θ turns out to take values between 0 and $-\pi/4$, this impedance is best represented by a pure resistance in series with a Warburg impedance (1). The third term on the right hand side of [1] arises in the same way as Ψ: from the nonlinearity of electrode reaction rate with potential, and it is suggested that the effect giving rise to this harmonic content in v be termed "faradaic distortion." The primary object of the present communication is the derivation of an expression for V_2, the amplitude of the faradaic distortion.

Electrode Reaction

Established expressions for the cathodic and anodic currents associated with the electrode reaction

$$Ox + ne^- \rightleftharpoons Rd$$

are

$$\vec{i} = nA\mathbf{F}ka_o \exp\{-\alpha n\mathbf{F}E/RT\} \quad [2]$$

and

$$\overleftarrow{i} = nA\mathbf{F}ka_o' \exp\{(1-\alpha)n\mathbf{F}E/RT\} \quad [3]$$

where a_o and a_o' are the activities of Ox and Rd at the electrode surface. E is the potential of the electrode vs. the standard Ox/Rd electrode and k is a standard rate constant (9), being equal to the actual rates of both forward (cathodic) and reverse reactions at a standard Ox/Rd electrode in equilibrium. The term α denotes the transfer coefficient of the forward reaction.[2]

If equilibrium is established at the electrode, the surface activities will be equal to a and a', the bulk activities of Ox and Rd; moreover, the forward and reverse currents are then equal to each other and to the quantity termed the equilibrium exchange current I_e. Therefore,[3]

$$a \exp\{-\alpha n\mathbf{F}E_e/RT\} = I_e/nA\mathbf{F}k = a' \exp\{(1-\alpha)n\mathbf{F}E_e/RT\} \quad [4]$$

For many purposes I_e is a more convenient kinetic parameter than k, but it must be appreciated that the equilibrium exchange current (unlike the standard rate constant k) is itself a function of the activities of Ox and Rd and, to a lesser extent, is also dependent on the concentrations of other constituents of the solution.

In the next three sections, cases are considered in which Rd is a pure phase of invariant activity. The reaction $Cu^{2+} + 2e^- \rightleftharpoons Cu$ occurring at a copper electrode would be an example: in such situations it is usual to set the invariant activity equal to unity.

The bulk activity a of Ox may be set equal to fC, where C is the concentration (mole cm^{-3}) of Ox in the bulk of the cell solution[4] and f is its activity coefficient.[5] In such cases equation [4] shows that the relationship between I_e and C is $I_e = nA\mathbf{F}k(fC)^{1-\alpha}$.

The section *Soluble Reductant Case*, below, deals with the more general case in which the activity of Rd is not constant. Examples of such reactions include $Fe^{3+} + e^- \rightleftharpoons Fe^{2+}$ and $Cd^{2+} + 2e^- \rightleftharpoons Cd(Hg)$. For such cases Eq. [4] gives $I_e = nA\mathbf{F}k(f'C')^{\alpha}(fC)^{1-\alpha}$, where C' is the bulk concentration and f' the activity coefficient[5] of Rd.

Mathematical Derivation

Let it be supposed that at time $t = 0$ the circuit is made and that for $t > 0$ the faradaic cell current is given by

$$i = I \cos \omega t + (\text{transients important only at small } t) \quad [5]$$

If r represents the dimension normal to the electrode

[2] Equations [2] and [3] may be applied directly only to electrode reactions which take place in a single step. Nevertheless, these equations often apply in cases where the reaction mechanism is complex, although the terms k and α no longer have the simple significances ascribed to them in the text. Approximate expressions for the apparent k and α terms may be deduced by constructing the mechanism's equivalent reaction pair (10).

[3] Note that Eq. [4] also embodies the Nernst equation for the system.

[4] The present theory is limited to cases in which the cell solution is of high ionic strength. Furthermore, if Ox is an ion, C must be much less than the ionic strength. These restrictions are needed to ensure that transport of Ox shall be by diffusion and not by migration. A high concentration of supporting electrolyte is also useful in reducing R_s and in keeping the double layer capacity constant.

[5] The activity coefficient of Ox (and also that of Rd in cases where the latter dissolves in the cell solution) will be effectively constant in a solution of high ionic strength,[4] even though the concentration of Ox is subject to local variation. Moreover, if a series of experiments is conducted in which the bulk concentration C of Ox is varied, it would be natural to maintain the ionic strength constant throughout the series: thus f would be constant from one experiment to the next as well as within any one experiment.

surface,[6] $C(r, t)$ will signify the concentration of Ox at a distance r at time t. It will be assumed that the surface concentration can be represented by the Fourier series

$$C(0, t) = \sum_{j=0}^{\infty} \mu_j \cos j\omega t + \sum_{j=1}^{\infty} \lambda_j \sin j\omega t \qquad [6]$$

where the μ's and λ's are undetermined coefficients.

Fick's second law of diffusion, $\partial C(r, t)/\partial t = D\partial^2 C(r, t)/\partial r^2$, must apply to the system,[4] D being the diffusion coefficient of Ox. Solution of this equation under the boundary condition [6] and the initial condition $C(r, 0) = C = C(\infty, t)$ is[7]

$$C(r, t) = C + \mu_0 \operatorname{erfc} [r/2(Dt)^{1/2}]$$

$$+ (2/\pi^{1/2}) \sum_{j=1}^{\infty} \int_{r/2(Dt)^{1/2}}^{\infty} \{\mu_j \cos (j\omega t - j\omega r^2/4Dp^2) + \lambda_j \sin (j\omega t - j\omega r^2/4Dp^2)\} \exp (-p^2)\, dp$$

On differentiation (13), this gives

$$\partial C(r, t)/\partial r = -(\pi Dt)^{-1/2} \exp (-r^2/4Dt) \sum_{j=0}^{\infty} \mu_j$$

$$+ (2/\pi^{1/2}) \sum_{j=1}^{\infty} \int_{r/2(Dt)^{1/2}}^{\infty} (j\omega r/2Dp^2) \cdot \exp (-p^2)$$

$$dp \{\mu_j \sin (j\omega t - j\omega r^2/4Dp^2) - \lambda_j \cos (j\omega t - j\omega r^2/4Dp^2)\} \cdot$$

which may be evaluated for $r = 0$, $t > 0$, since the integral then has a zero lower limit.[8] The expression thus obtained for the surface concentration gradient is

$$\partial C(0, t)/\partial r = -(\pi Dt)^{-1/2} \sum_{j=0}^{\infty} \mu_j$$

$$- \sum_{j=1}^{\infty} (j\omega/2D)^{1/2} \{(\mu_j + \lambda_j) \cos j\omega t - (\mu_j - \lambda_j) \sin j\omega t\}$$

From Fick's first law of diffusion, an expression may now be derived relating the concentration gradient at the electrode surface to the flux of Ox and hence to the anodic faradaic current in the form $i = -nA\mathbf{F}D\, \partial C(0, t)/\partial r$. Comparison of this equation with [5] shows that $\mu_j = 0 = \lambda_j$ for $j = 0$, $j \geq 2$ and that $\mu_1 = \lambda_1 = I/nA\mathbf{F}(2D\omega)^{1/2}$, whence [6] becomes

$$C(0, t) = C(1 + Q \sin \omega t + Q \cos \omega t) \qquad [7]$$

where $Q = I/nA\mathbf{F}C(2D\omega)^{1/2}$. Clearly, since $C(0, t)$ cannot be negative, $Q \leq 2^{-1/2}$; however, it will be convenient to place a more severe restriction on Q, *viz.* $Q \leq 0.1$.

[6] The electrode need not be planar provided its radius of curvature is everywhere large compared with the "diffusion layer thickness" (11). This latter quantity may be taken as the value of r at which the amplitude of the concentration oscillations has fallen to 1% of its surface value. Now, the concentration amplitude can be shown (2-4) to be proportional to $\exp[-r(\omega/2D)^{1/2}]$, and taking $D = 10^{-5}$ cm^2 sec^{-1}, $\omega/2\pi \geq 10$ cps, we see that the diffusion layer cannot exceed 2.5×10^{-3} cm in thickness. A lower limit to the radius of curvature might thus be set at 0.1 mm.

[7] The analogous problem in heat conduction is considered by Carslaw and Jaeger (12).

[8] Rejecting small values of t, the limit may be taken to approach zero before the integrand. The integration is then carried out with the aid of transformations akin to those discussed by Carslaw and Jaeger (14).

The current $I \cos \omega t$ must be equal to the difference $(\overleftarrow{i} - \overrightarrow{i})$ obtained by subtracting Eq. [2] from [3]. Therefore, since a' is equal to unity and f is constant,[5]

$$I \cos \omega t = nA\mathbf{F}k \exp \{(1 - \alpha)n\mathbf{F}(E_e + v)/RT\}$$

$$- nA\mathbf{F}ka[C(0, t)/C] \exp \{-\alpha n\mathbf{F}(E_e + v)/RT\}$$

This equation may be simplified by substituting for $C(0, t)$ from Eq. [7] and for E_e and k from [4]. The result is

$$I \cos \omega t = I_e \exp \{(1 - \alpha)n\mathbf{F}v/RT\}$$

$$-I_e(1 + Q \sin \omega t + Q \cos \omega t) \exp \{-\alpha n\mathbf{F}v/RT\} \qquad [8]$$

It will be convenient to define a new parameter y by $y = I/I_eQ$. This new parameter is dimensionless and can take values between 0 and $+\infty$; it is a measure of the ability of the electrode reaction to keep pace with the alternating electrode potential. At low y values the electrode is able to follow the potential variation, whereas at high values of y this is not possible and $C(0,t)$ assumes an almost constant value; the changeover between these two extremes occurs in the vicinity of $y = 1$.

Provided that $n\mathbf{F}v/RT << 1$, *i.e.*, if the total magnitude of the perturbation v never exceeds a few millivolts, a simplification of the exact Eq. [8] may be achieved by making series expansions of the two exponential terms and rejecting all but the first few members of these series. However, since both faradaic distortion and faradaic rectification are second order effects, the retention of only two terms, *viz.*

$$\exp \{-\alpha n\mathbf{F}v/RT\} \approx 1 - \alpha n\mathbf{F}v/RT \qquad [9a]$$

$$\exp \{(1 - \alpha)n\mathbf{F}v/RT\} \approx 1 + (1 - \alpha)n\mathbf{F}v/RT \qquad [9b]$$

is inadequate to give a reliable expression for v. Nevertheless, as a first approximation, it is instructive to insert the approximations [9] into Eq. [8]. This approach yields[9]

$$n\mathbf{F}v/RT \approx [(y + 1)Q \cos \omega t + Q \sin \omega t](1 + \alpha Q \sin \omega t + \alpha Q \cos \omega t)^{-1}$$

$$\approx [(y + 1)Q \cos \omega t + Q \sin \omega t](1 - \alpha Q \sin \omega t - \alpha Q \cos \omega t)$$

$$\approx (y+1)Q \cos \omega t + Q \sin \omega t - \tfrac{1}{2}\alpha(y+2)Q^2 - \tfrac{1}{2}\alpha y Q^2 \cos 2\omega t - \tfrac{1}{2}\alpha(y+2)Q^2 \sin 2\omega t \qquad [10]$$

Recalling that $Q \leq 0.1$ and that $0 < \alpha < 1$, inspection of Eq. [10] will show that the rms values of the two terms $(y+1)Q \cos \omega t$ and $Q \sin \omega t$ always account for more than 87% of the rms value of $n\mathbf{F}v/RT$. Therefore, approximation [9a] can be vastly improved by adding a third term in which $n\mathbf{F}v/RT$ is replaced by the two most important terms in [10], *i.e.*,

$$\exp \{-\alpha n\mathbf{F}v/RT\} = 1 - \alpha n\mathbf{F}v/RT + \tfrac{1}{2}\alpha^2[(y+1)Q \cos \omega t + Q \sin \omega t]^2$$

[9] It will be noted that the inclusion of additional terms in the binomial expansion of $(1 + \alpha Q \sin \omega t + \alpha Q \cos \omega t)^{-1}$ would have introduced additional harmonics (terms in $\sin 3\omega t$, $\cos 4\omega t$, etc.) of very small amplitude, but would not have affected the magnitude of any of the five final terms in [10] by more than 1%.

A similar improvement may be made to [9b] and if these amended equations are then inserted into expression [8], the following result can be obtained

$$n\mathbf{F}v/RT = (y+1)Q\cos\omega t + Q\sin\omega t$$
$$-\tfrac{1}{2}[(1+y+\tfrac{1}{2}y^2)-\alpha(y+y^2)]Q^2$$
$$+\tfrac{1}{2}[\alpha(y+y^2)-(y+\tfrac{1}{2}y^2)]Q^2\cos 2\omega t$$
$$-\tfrac{1}{2}(1+y-\alpha y)Q^2\sin 2\omega t + \text{terms in } Q^3$$

This expression for v is readily transformed into [1] and the five unknowns in the latter equation are thus found to be

$$\Psi = -(RTQ^2/4n\mathbf{F})(y+z+yz+2)$$
$$V = (RTQ/n\mathbf{F})(y^2+2y+2)^{1/2}$$
$$\theta = -\operatorname{arccot}(1+y)$$
$$V_2 = (RTQ^2/4n\mathbf{F})(y^2+2y+2)^{1/2}(z^2+2z+2)^{1/2}$$
$$\theta_2 = -\operatorname{arccot}\frac{y+z+yz}{y+z+2}$$

where $z = (1-2\alpha)y$.

The expressions given above for V and θ have been derived previously (4). The equation for Ψ is in agreement with that given by Barker, Faircloth, and Gardner (6), but differs from an expression derived earlier by the present author (4), which was in error (15). For fast electrode reactions y approaches zero and therefore $\Psi = -RTQ^2/2n\mathbf{F} = -n\mathbf{F}V^2/4RT$. This last relationship has been experimentally verified for the $Hg_2^{2+} + 2e^- \rightleftharpoons 2Hg$ reaction (4).

Magnitude of the Distortion

It is convenient to express V_2 in terms of the amplitude V of the fundamental interfacial potential. In this form the amplitude of the first harmonic potential (the faradaic distortion) is given by

$$V_2 = \frac{n\mathbf{F}V^2}{4RT}\left(\frac{z^2+2z+2}{y^2+2y+2}\right)^{1/2} \qquad [11]$$

This equation predicts that if $V = 10$ mv, $T = 300°K$, and $n = 2$, then the magnitude of V_2 will lie between 0 and 2 mv, depending on the magnitudes of the parameters k, α, C, f, D, and ω.

For a given system at constant temperature, Eq. [11] shows that V_2 depends on V and ω only, varying directly as V^2 but showing a complicated dependence on frequency. Figure 2 shows how the ratio V_2/V^2 varies with y for various values of α. Since y is proportional to the square-root of ω, a change in y from 0.1 to 10 corresponds to a ten-thousandfold increase in frequency. The shape of the curves in Fig. 2 is seen to be very dependent on α, especially when the latter is greater than 0.5. If the transfer coefficient exceeds 0.64, the curves exhibit minima at characteristic values of y. It will be apparent that I_e and α may readily be determined if a curve of the type shown in Fig. 2 is constructed. An apparatus which enables V_2 to be measured as a function of ω at constant V is described below.

The faradaic distortion method of determining the kinetic parameters of an electrode reaction shares with faradaic rectification the advantage over the classical a-c method (faradaic admittance) that a knowledge of the double-layer capacity is not needed; uncertainties associated with the double-layer often lead to difficulties when a-c studies are made at electrodes other than mercury (3, 16). Faradaic distortion offers two advantages over faradaic rectification in the determination of α and I_e. First, as a comparison of Fig. 2 and 3 shows, curves of V_2 against frequency are far more characteristic of α than the corresponding plots of Ψ. Second, whereas several effects can be envisaged which might cause spurious d-c potentials to exist across the cell, thereby interfering in the measurement of Ψ, only one effect[10] other than faradaic distortion is likely to introduce alternating potentials of frequency ω/π. On the other hand, faradaic rectification does not suffer from the severe limitations which are the subject of the next section.

The close parallelism between faradaic distortion and faradaic rectification is illustrated by a comparison of the values acquired by V_2 and Ψ in the limiting cases $y << 1$ and $y >> 1$. In the former case $V_2 = n\mathbf{F}V^2/4RT = -\Psi$ while in the latter, $\Psi = (2\alpha-1)n\mathbf{F}V^2/4RT = \pm V_2$.

[10] If the double-layer capacity is potential dependent, then the passage of an a.c. across the electrode will introduce harmonic frequencies in the interfacial potential. The first harmonic is the most serious and its amplitude is $(V^2/4c)(\partial c/\partial E)$. This effect is unlikely to interfere in the determination of faradaic distortion except in the vicinity of the electrocapillary maximum, where the double-layer capacity does change appreciably with potential (17).

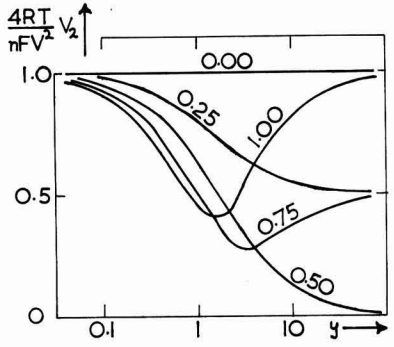

Fig. 2. Dependence of faradaic distortion on the parameter y (proportional to the square root of frequency) for values of the transfer coefficient α = 0.00, 0.25, 0.50, 0.75, 1.00.

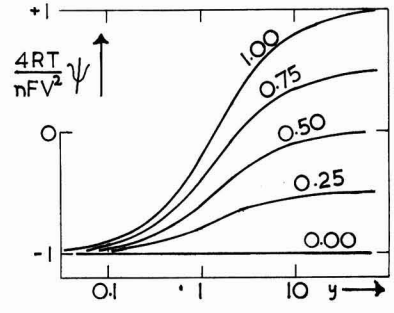

Fig. 3. Dependence of faradaic rectification on the parameter y for values of the transfer coefficient α = 0.00, 0.25, 0.50, 0.75, 1.00.

Effect of the Double Layer

As yet the fact has been ignored that, in addition to the faradaic path, an alternative route, the charging and discharging of the electrical double layer, is accessible to a.c. crossing the electrode/solution interface. Usually this nonfaradaic path is considered as a pure capacity,[11] proportional to electrode area but otherwise constant (19); its capacitance will be equated to cA.

The production by faradaic distortion of an alternating potential of frequency ω/π across the electrode interface will cause a current of the same frequency to flow across the double layer capacity. However, this harmonic current must be shunted back via the faradaic path, as illustrated in Fig. 4, since no harmonic frequencies are present in the current flowing in the external circuit. The presence of this harmonic component in the faradaic current cannot be ignored unless the nonfaradaic impedance is much greater than the faradaic impedance; if this is not the case, the appropriate correction terms must be inserted into Eq. [5] and the entire derivation of V_2 repeated. The result is

$$V_2=\frac{n\mathbf{F}V^2}{4RT}\cdot\left(\frac{z^2+2z+2}{y^2+2y+2}\right)^{1/2}\cdot\frac{x}{[(y+2^{-1/2})^2+(x+2^{-1/2})^2]^{1/2}} \qquad [12]$$

where $x = n^2\mathbf{F}^2D^{1/2}C/RTc(2\omega)^{1/2}$. Also,

$$\theta_2=\operatorname{arccot}\frac{(y+2^{-1/2})(y+z+2)-(x+2^{-1/2})(y+z+yz)}{(x+2^{-1/2})(y+z+2)+(y+2^{-1/2})(y+z+yz)}$$

The term x is a measure of the ratio of the nonfaradaic impedance to the faradaic.[12] Therefore, for a sufficiently large x value [12] reduces to Eq. [11]. However, as x becomes small V_2 decreases and this may be interpreted as the shorting out of the faradaic distortion by the decreasing double layer impedance.

[11] However, Bockris and Conway (18) regard the nonfaradaic path as equivalent to a condenser with a relaxing dielectric. In their terms, the present treatment is only valid at frequencies low enough that $1/\omega$ is large compared with the relaxation time of the dielectric.

[12] In fact, $2x$ is the ratio of the reactances of the two paths.

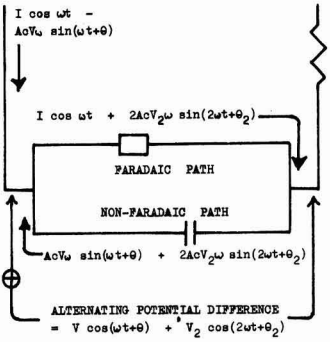

Fig. 4. Distribution of currents between the faradaic and and nonfaradaic paths. The resistor shown represents the solution resistance R_s.

Inspection of Fig. 2 shows that $y \leq 10$ covers the region most useful for the determination of kinetic parameters by faradaic distortion. In this region the final fraction in [12] exceeds 0.95 if $x \geq 35$. Taking the following representative values: $T = 298°K$, $c = 39$ μfd. cm^{-2} (20), $n = 2$, and $D = 10^{-5}$ cm^2 sec^{-1}; this restriction becomes $C/\omega^{1/2} \geq 4 \times 10^{-8}$ mole sec$^{1/2}$ cm^{-3}. On the other hand, the final fraction in [12] is less than 0.1 if $x \leq 0.11$ which implies $C/\omega^{1/2} \leq 1.2 \times 10^{-10}$ mole sec$^{1/2}$ cm^{-3}. The practical consequences of these limitations are shown below.

C (mole cm^{-3}):	10^{-9}	10^{-8}	10^{-7}	10^{-6}	10^{-5}	10^{-4}
Double layer effect can be ignored and Eq. [11] is obeyed for frequencies less than	....	....	1.0 cps	100 cps	10 kc/s	1.0 Mc/s
Double layer capacity effectively shorts out all faradaic distortion if the frequency is in excess of	10 cps	1.0 kc/s	100 kc/s	10 Mc/s	....	....

Three conclusions can be drawn immediately. First, faradaic distortion will not interfere in conventional admittance measurements provided low enough concentrations (about 10^{-6} M) are employed: higher concentrations can be tolerated provided a low frequency limit is set at a value greater than 10 cps.[13] Second, since the double layer shorting effect becomes very pronounced at low concentrations, the analytical applications of faradaic rectification (7, 21) are unlikely to be paralleled by similar developments of faradaic distortion. Third, if faradaic distortion is to be employed quantitatively (to measure k or α, for example), the concentration range available will be seen to be severely limited. An audio-frequency bridge has a range of about 10 cps to 10 kc/s and the table shows that full use can be made of this range only for concentrations greater than 10^{-5} mole cm^{-3}. An upper concentration limit (about 0.1 M, i.e., $C = 10^{-4}$) is set by the requirement that the Ox concentration shall be much less than the supporting electrolyte.[4] Taking all factors into consideration it would appear that the faradaic distortion method is a useful one for determining kinetic parameters over a thousandfold range of reaction rates, suitable exchange current densities ranging from about 20 ma cm^{-2} to 20 amp cm^{-2}. Although this range is rather narrow, it does encompass some important electrode reactions: thus the $Cu^{2+} + 2e^- \rightleftharpoons Cu$ reaction is reported to have $I_e/A \approx 2$ amp cm^{-2} at $C = 10^{-5}$ mole cm^{-3} in an acidified KNO_3 solution (22).

Soluble Reductant Case

Cases in which Rd is not a pure phase but is a species soluble in the cell solution (or in the electrode in the case of amalgam electrodes) can be treated in a manner which exactly parallels the method described above under *Mathematical Deri-*

[13] In any case, since V_2 is proportional to V^2, a lower percentage of distortion can always be realized by decreasing the signal across the cell.

vation. Since no new principles are involved it will suffice to present the results; these are

$$\Psi = -(RT/4n\mathbf{F})\,(Q^2-Q'^2)\,(Y+Z+YZ+2)$$

$$V = (RT/n\mathbf{F})\,(Q+Q')\,(Y^2+2Y+2)^{1/2}$$

$$\theta = -\operatorname{arccot}(1+Y)$$

$$V_2 = (RT/4n\mathbf{F})\,(Q^2-Q'^2)\,(Y^2+2Y+2)^{1/2}(Z^2+2Z+2)^{1/2}$$

$$\theta_2 = -\operatorname{arccot}\frac{Y+Z+YZ}{Y+Z+2}$$

where $Q' = I/nA\mathbf{F}C'(2D'\omega)^{1/2}$, $Y = I/I_e(Q+Q')$, and $Z = (1-2\alpha)Y(Q+Q')/(Q-Q')$. Each of these equations reduces to the corresponding equation already given above as Q' tends to zero. The above expression for Ψ differs from that obtained previously by the present author (4) but is in agreement with equations derived by Barker (7) and (for the special case $C = C'$, $D = D'$) by Doss and Agarwal (23, 5). The equations for V and θ are well established (2, 3). The expression for the amplitude of faradaic distortion can be cast into a particularly simple form when $CD^{1/2} = C'(D')^{1/2}$:

$$\pm V_2 = \frac{n\mathbf{F}V^2}{4RT}\cdot\frac{(1-2\alpha)Y}{(Y^2+2Y+2)^{1/2}} = \frac{(1-2\alpha)VI}{4I_e}$$

Moreover, θ_2 then equals θ, showing that the fundamental interfacial potential is perfectly in phase with its first harmonic.

Again, the double layer affects V_2 and θ_2. The equation analogous to [12] is

$$V_2 = \frac{n\mathbf{F}V^2}{4RT}\left(\frac{Z^2+2Z+2}{Y^2+2Y+2}\right)^{1/2}\frac{X}{[(Y+2^{-1/2})^2+(X+2^{-1/2})^2]^{1/2}}$$

and

$$\theta_2 = \operatorname{arccot}\frac{(Y+2^{-1/2})(Y+Z+2)-(X+2^{-1/2})(Y+Z+YZ)}{(X+2^{-1/2})(Y+Z+2)+(Y+2^{-1/2})(Y+Z+YZ)}$$

where $X = n\mathbf{F}I/RTAc(2\omega)(Q+Q')$.

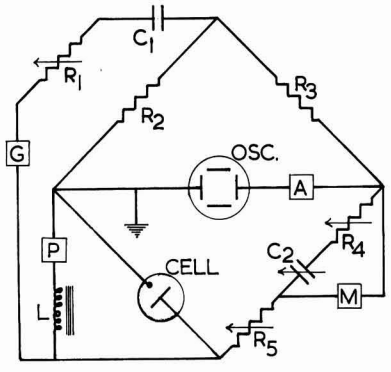

Fig. 5. Circuit for measuring all three faradaic effects. Suitable component values are G: 10 c/s-10 kc/s, 100 v; R_1: 0-100kΩ; C_1: 1 μfd; R_2: 5 kΩ; R_3: 5 kΩ; A: 10000 X; R_4: 0-100Ω; C_2: 0-5 μfd; M: 10 mv f.s.d.; R_5: 0-10Ω; P: to read to 10 μv; L: 10 H.

Measurement

The circuit shown in Fig. 5 permits the amplitude V_2 of faradaic distortion to be measured without the use of filter networks or tuned amplifiers. Faradaic rectification may also be measured with this apparatus and, provided that the double layer capacity is known, the faradaic admittance can be determined as well. Rough measurements with a circuit of this type have confirmed the predicted parallelism between faradaic rectification and distortion.

The pure sinusoidal potential produced by G, a generator of variable frequency and high voltage output, is fed through the high resistance R_1 to produce a pure a.c. of frequency $\omega/2\pi$. Since R_2 and R_3 are equal resistors, if R_4 and C_2 are adjusted[14] so that the impedance of the R_4-C_2-R_5 arm is identical in both phase angle and magnitude to the impedance of the cell, no signal of frequency $\omega/2\pi$ will appear across the amplifier A and cathode ray oscilloscope OSC. However, a signal of the harmonic frequency ω/π remains and if the resistance of R_2 is much greater than the cell impedance, the whole of the distortion voltage V_2 will be developed across the A-OSC arm. V_2 can be calculated from the height of the oscilloscope trace if the gain of A and the sensitivity of OSC are known.

A series of measurements of V_2 at a constant known value of V, the fundamental alternating interfacial potential, but varying frequency can be made by adjusting R_5 to equal the solution resistance R_s. With the bridge balanced the a-c millivoltmeter M then measures V directly and R_1 can be repeatedly adjusted to give any predetermined M reading.

The potentiometer P enables Ψ to be measured, V_e being subtracted if necessary.[1] The choke L restricts the passage of a.c. through P and d.c. is prevented from flowing through the cell by P being balanced and by the presence of the condensers C_1 and C_2.

Symbols

A	area of the electrode, cm²
C,C'	bulk concentrations of Ox and Rd, mole cm⁻³
$C(r,t)$	concentration of Ox at a distance r from the electrode surface at time t, mole cm⁻³
D,D'	diffusion coefficients of Ox and Rd, cm² sec⁻¹
E	potential of the electrode vs. standard Ox/Rd electrode, v
E_e	equilibrium (null) value of E, v
$\mathbf{F}$	the faraday, 9.65×10^4 coulomb equivalent⁻¹
I	amplitude of applied faradaic a.c., amp
I_e	equilibrium exchange current, amp
Ox	an electroreducible species
Q,Q'	dimensionless parameters defined in sections on *Mathematical Deviation* and *Soluble Reductant Case*
R	gas constant, 8.32 joule mole⁻¹ deg⁻¹
Rd	an electroöxidizable species formed by reduction of Ox
R_s	resistance of the cell solution, ohm
T	absolute temperature, °K
V	amplitude of that component of the interfacial potential having the fundamental frequency ($\omega/2\pi$), v
V_2	amplitude of that component of the inter-

[14] Under certain conditions a parallel arrangement of R_4 and C_2 may be more convenient.

facial potential having the harmonic frequency (ω/π), v

V_e equilibrium cell potential, v

V_o potential generated by the passage of current through R_s, v

X,Y,Z dimensionless parameters defined in section *Soluble Reductant Case.*

a,a' bulk activities of Ox and Rd, treated as dimensionless

a_o,a_o' surface activities of Ox and Rd, dimensionless

c double layer capacity per unit area, farad cm^{-2}

e^- an electron

f,f' activity coefficients of Ox and Rd, liter $mole^{-1}$

$\overleftarrow{i}, \overrightarrow{i}$ anodic and cathodic currents resulting from the faradaic reaction at the electrode surface, amp

j a running index

k standard rate constant, mole cm^{-2} sec^{-1}

n number of faradays needed to reduce one mole of Ox, equivalent $mole^{-1}$

p an integration variable

r normal distance from the electrode surface, cm

t time, sec

v total interfacial potential, v

x,y,z dimensionless parameters defined in sections *Mathematical Deviation* and *Effect of the Double Layer*

α transfer coefficient of the cathodic reaction

θ phase angle by which the fundamental component of the interfacial potential leads the faradaic current

θ_2 phase angle by which the harmonic component of the interfacial potential leads the faradaic current

λ,μ surface concentration amplitudes, defined by Eq. [6], mole cm^{-3}

Ψ potential due to faradaic rectification, sometimes termed the redoxokinetic potential, v

ω angular frequency of the applied current, sec^{-1}

Manuscript received Oct. 12, 1959.

Any discussion of this paper will appear in a Discussion Section to be published in the June 1961 JOURNAL.

REFERENCES

1. D. C. Grahame, *This Journal*, **99**, 370C (1952).
2. J. E. B. Randles, *Discussion Faraday Soc.*, **1**, 11 (1947).
3. P. Delahay, "New Instrumental Methods in Electrochemistry," Chap. 7, Interscience Publishers Inc., New York (1954).
4. K. B. Oldham, *Trans. Faraday Soc.*, **53**, 80 (1957).
5. K. S. G. Doss and H. P. Agarwal, *Proc Indian Acad. Sci.*, **34**, 263 (1951).
6. G. C. Barker, R. L. Faircloth, and A. W. Gardner, *Nature*, **181**, 247 (1958).
7. G. C. Barker, *Anal. Chim. Acta*, **18**, 118 (1958).
8. K. S. G. Doss and H. P. Agarwal, *J. Sci. Ind. Res. India B*, **9**, 280 (1950).
9. J. E. B. Randles, *Trans. Faraday Soc.*, **48**, 828 (1952).
10. K. B. Oldham, *J. Am. Chem. Soc.*, **77**, 4697 (1955).
11. L. L. Bircumshaw and A. C. Riddiford, *Quarterly Rev.*, **6**, 157 (1952).
12. H. S. Carslaw and J. C. Jaeger, "Conduction of Heat in Solids," Chap. II, Oxford University Press, London (1947).
13. G. A. Gibson, "An Elementary Treatise on the Calculus," p. 458, MacMillan, London (1933).
14. H. S. Carslaw and J. C. Jaeger, *Op. cit.*, footnote on page 47.
15. M. Fleischmann and K. B. Oldham, *Ann. Reports*, **55**, 67 (1958).
16. H. A. Laitinen and R. A. Osteryoung, *This Journal*, **102**, 598 (1955).
17. I. M. Kolthoff and J. J. Lingane, "Polarography," p. 110, Interscience Publishers Inc., New York (1941).
18. J. O'M. Bockris and B. E. Conway, *J. Chem. Phys.*, **28**, 707, (1958).
19. D. C. Grahame, *J. Am. Chem. Soc.*, **68**, 301 (1946).
20. D. C. Grahame, *ibid.*, **71**, 2975 (1949).
21. K. S. G. Doss, K. Sundararjan, U. H. Narayanan, and S. Visvanathan, *Electrochim. Acta*, **1**, 22 (1959).
22. P. J. Hillson, *Trans. Faraday Soc.*, **50**, 385 (1954).
23. K. S. G. Doss and H. P. Agarwal, *Proc. Indian Acad. Sci.*, **35**, 45 (1952).

Correction

In the paper by M. P. Korver, R. S. Johnson, and N. C. Cahoon, "Study of the Recuperation Reaction in the Leclanché Dry Cell," which appeared on pp. 587-591 of the July JOURNAL, the line drawings for Figures 1 and 2 on pp. 588 and 589 were reversed. The captions for the figures are correct, however.

The Electrolytic Formation and Dissolution of Oxide Films on Platinum

H. A. Laitinen and C. G. Enke

Noyes Chemical Laboratory, University of Illinois, Urbana, Illinois

ABSTRACT

The extent of surface oxidation of a smooth platinum electrode and the electrode capacitance were measured for various conditions of anodization. The electrolytic formation of the surface platinum oxide is shown to be a highly irreversible reaction. A mechanism which involves a hydroxyl radical intermediate of the oxygen evolution reaction is proposed for the surface oxide formation reaction. This mechanism is supported by the shapes of the anodic and cathodic charging curves on platinum and the interrelationships of the electrode potential, the electrode capacitance, and the extent of surface oxidation. From these same interrelationships it was also concluded that the steady-state evolution of oxygen occurs on a surface which has at least one atom of oxygen per surface platinum atom and that the rate-determining step in the oxygen evolution reaction is the electrolytic discharge of oxygen-containing radicals which are adsorbed on the electrode surface. The surface oxide is reduced at potentials several hundred millivolts cathodic to the potential required to form the oxide. The reduction of the surface oxide is shown to be a first order reaction. The rate of the reduction increases with increasingly cathodic electrode potential.

It has been well substantiated that a surface oxidation occurs on a platinum electrode which is functioning as an anode in water solutions (1-17). The surface oxide thus formed on platinum has the unusual ability to transfer charge from the metal to a reactant in the solution without an appreciable increase in the thickness of the film. The film is electron conducting rather than ion conducting, and therefore does not grow beyond one or two atomic layers. The presence of the surface oxide alters the behavior of platinum indicator electrodes to such an extent that almost all investigators using such electrodes have had to adopt a standard anodic or cathodic pretreatment in order to obtain reproducible results. The formation of the surface oxide layer has been shown to affect considerably the results obtained with platinum indicator electrodes in potentiometry (14), chronopotentiometry (1), polarography (10), and kinetics determinations (18). A knowledge of the chemical nature of the surface oxide as well as the mechanism of its formation is a prerequisite to the understanding of the behavior of platinum indicator electrodes.

Historically, three experimental approaches have been taken in an effort to arrive at a conclusion regarding the composition of the surface oxide on platinum. These are cathodic stripping (3-5, 7-9, 15, 17,), chemical attack (2), and potentiometry 10-12, 16). In the first case, the number of coulombs of electricity required to completely reduce the surface oxide is determined. If the exact electrode area and the number of platinum atoms per square centimeter are known, and if it is assumed that the oxide is a monomolecular film, the oxidation state of the oxidized platinum surface can be calculated. Because of the assumptions required for such calculations, the results are indicative but not conclusive. In the case of the chemical attack the oxide film is dissolved and the solution analyzed spectroscopically for platinum(II) and platinum(IV). Here one must be certain that during the chemical attack the oxidation state of the platinum has not been changed. Finally, the potentials of the plateaus in the anodic and cathodic charging curves have been equated to the thermodynamic standard potentials of Pt-PtO or Pt-PtO_2 to demonstrate the existence of these species on the electrode surface. Giner (8) has discounted all such comparisons by pointing out the physical and chemical differences between a monomolecular layer of PtO on platinum and crystalline platinum(II) oxide [and similarly platinum(IV) oxide]. Such a monolayer may be regarded as identical to a chemisorbed oxygen atom layer. Furthermore, it will be shown here that the reaction of the formation of the surface oxide is so irreversible that it is incapable of determining the potential of the platinum electrode even under conditions of no electrode current.

Cathodic and Anodic Charging Curves

It is worthwhile at this point to make a critical evaluation of the interpretation of the shapes of the cathodic and anodic charging curves on platinum. Typical charging curves for oxygen and hydrogen free solutions are shown in Fig. 1. Potentials in this figure and throughout the paper are referred to the normal hydrogen electrode. A constant anodic current is passed while the potential of the electrode is followed as a function of time (or coulombs). The potential rises slowly (region Ha) until all the hydrogen adsorbed on the electrode has been oxidized. The potential then rises rapidly through region Ca

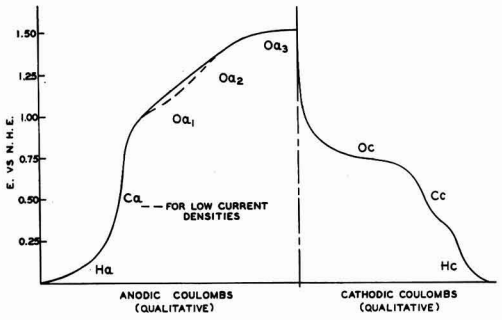

Fig. 1. Anodic and cathodic charging curves

where the only process is the charging of the electrical double layer. At about 0.9 v an anodic process begins and the potential increases more gradually through regions Oa_1 and Oa_2. Eventually the oxygen evolution potential is reached, causing a leveling off of the potential (region Oa_3). If the current is reversed and the electrode thus anodized is now made the cathode, the cathodic charge curve of Fig. 1 is observed. The potential drops very rapidly to about 0.7 v where there is a plateau (region Oc) due to the reduction of the substance formed during regions Oa_1 and Oa_2 of the anodization. When all of the oxidation product has been reduced, the potential drops rapidly again through region Cc and then enters the hydrogen evolution region Hc.

The shapes of the cathodic and anodic charging curves on platinum were one of the first indications of a surface oxidation (5) and they have been of interest to many investigators subsequently (3, 4, 6-9, 11, 15-17). A comparison of the anodic and cathodic charging curves shows that they are not the same shape. If the difference in their shapes were the effect of polarization due to a slow reaction, the curves would become more similar as the current density is decreased. However, very low current density studies (15-17) have shown that the hysteresis is not decreased significantly with decreasing current density. Such an intrinsic hysteresis suggests a reaction which is so irreversible that the oxidation and reduction occur by different mechanisms.

A comparison of the charging curves also shows that the region Oa_1-Oa_2 is always larger than the region Oc indicating that more electricity is used to form the oxide than is required to remove it. Vetter and Berndt (15) who found a ratio of anodic to cathodic coulombs of nearly two postulated the oxidation of water to the oxide during the anodization and the reduction of the oxide to hydrogen peroxide during the cathodization. However, no chemical evidence for the presence of hydrogen peroxide has been reported. Other investigators using slightly different conditions have not observed a ratio of anodic to cathodic coulombs of two. Furthermore, it is unlikely that the oxidation of water to oxide would occur at a higher potential than the reduction of the oxide to peroxide. Another explanation lies in the possibility of a mixed anodic process where a reaction (such as the evolution of oxygen) occurring simultaneously with the oxide formation reaction consumes some of the electricity.

The following mechanism for the electrolytic formation and dissolution of the surface oxide on platinum gives a satisfactory explanation of the shapes of the anodic and cathodic charging curves. When a constant anodic current is applied to the platinum electrode, any hydrogen present at the electrode surface will be oxidized. When the hydrogen has been exhausted the first step in the oxidation of the water occurs. The oxidation product (which is an intermediate in the oxygen evolution reaction) may react with the surface platinum atoms to form a surface oxide, or it may react to evolve oxygen. In this way the unoxidized portion of the electrode surface on which the oxidation of water can occur most readily decreases, causing an increase in the potential due to increased polarization (region Oa_1). When the entire surface of the platinum has reacted with the oxygen evolution intermediate, the oxidation of water must take place on the oxidized platinum surface. The presence of the oxide partially counteracts the positive charge of the platinum thus causing the oxidation of water to occur at a higher electrode potential (region Oa_2). Giner and Lange (19) observed a substantial increase in the work function and a corresponding decrease in the volta potential of platinum when the surface was oxidized, showing that the oxygen imparts a negative charge to the surface. When sufficient intermediate has been formed on the surface of the oxidized platinum, the intermediate will be further oxidized to oxygen and the steady-state oxygen evolution region of the charging curve is reached (region Oa_3). At higher current densities the break between regions Oa_1 and Oa_2 is not observed because the increased polarization overvoltage causes the electrode potential to become sufficient to oxidize the water on portions of the oxide layer before the entire platinum surface has become oxidized.

When the current is reversed making the oxidized electrode the cathode, the potential follows the reduction of the surface oxide and then, when the oxide is exhausted, the potential drops to the hydrogen evolution potential.

Experimental

The cell.—Perchloric acid electrolytes of different concentrations were used exclusively. Perchloric acid was chosen because it was not expected to influence the surface reactions on platinum either by direct chemical interference or by adsorption. If the acid concentration was high enough, the solution was effectively buffered. Unless otherwise stated, the solution was continuously swept with a stream of purified nitrogen in order to keep the solution free from dissolved oxygen and hydrogen. The presence of oxygen is undesirable because it affects the open-circuit potential of an oxidized electrode, and it acts as a depolarizer when treating the electrode cathodically. Hydrogen reacts chemically with the oxygen on the platinum electrode surface and acts as a depolarizer for anodic electrode treatment.

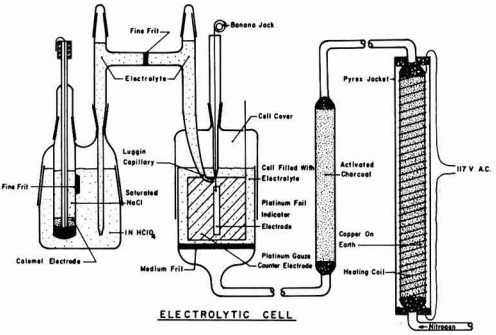

Fig. 2. Electrolytic cell

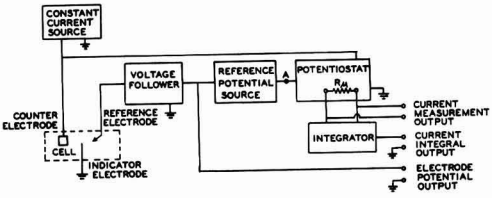

Fig. 3. Complete instrumentation

The cell arrangement is shown in Fig. 2. The cell itself was a filter funnel of 50-ml capacity, provided with a medium porosity glass frit. The indicator electrode was a 36 x 2.5 mm piece of 3 mil platinum foil welded to a 30-ga platinum wire sealed in a soft glass tube. Within the soft glass tube, the platinum wire was silver-soldered to a No. 20 ga copper wire connected to a banana jack.

The platinum foil electrode was cut from a 50-cm^2 piece of previously unused platinum foil. The surface roughness of this foil was determined in the laboratory of Professor Norman Hackerman at the University of Texas by the gas adsorption method (20). Professor Hackerman has perfected an apparatus to work with small areas making this determination economically practical on platinum. The results obtained in his laboratory on the platinum foil indicate a roughness factor of 1.12 within 10% accuracy. The true indicator electrode area was 2.0 cm^2 since both sides of the foil were exposed. The counter electrode was a platinum gauze cylinder placed concentrically around the indicator electrode. The calomel electrode was connected to the cell through an elaborate salt bridge which was designed to prevent any significant diffusion of chloride ions from the calomel compartment into the measurement cell during the course of an experiment. The cell arm of the salt bridge terminated in a luggin capillary which was placed up against the indicator electrode. The other arm of the salt bridge had a drawn-out tip which was immersed in a compartment of 1*N* $HClO_4$. This compartment served to connect the arm of the salt bridge to the frit on the side of the calomel compartment as well as to reduce the concentration gradient of chloride ions between the calomel and the salt bridge. The nitrogen which was bubbled through the cell electrolyte was passed first through a heated column of of copper-on-earth and then through a column of activated charcoal packed with glass wool. The copper-on-earth was prepared in this laboratory by M. S. Chao according to the method of Meyer and Ronge (21).

The equipment.—Figure 3 shows a block diagram of the equipment used in this investigation. A complete description of each piece of equipment and its operation is available (22). The constant current source was used to obtain constant current anodic or cathodic charging curves. The voltage follower allowed the electrode potential to be followed accurately on a recorder or oscilloscope without drawing more than 10^{-10} amp from the indicator electrode. When the potentiostat was turned on, the voltage applied to the counter electrode was such that the potential at point A (Fig. 3) was equal to that of the indicator electrode. Thus the potential between the reference electrode and the indicator electrode was precisely equal and opposite to the potential of the reference potential source. The current required to maintain this electrode potential was measured by measuring the potential across R_m and the time integral of the current was obtained at the output of the integrator. A system of relays was arranged so that when a key was pressed, a signal would trigger the oscilloscope sweep and shortly thereafter the reference potential would change by a preset value of 10 mv. Using a Tektronix Model 502 Dual Beam Oscilloscope, it was possible to observe the number of coulombs necessary to effect this potential change (at the integral output) as well as the shape of the current-time curve. The potentiostat was capable of rising to an output of 50 ma in as little as 50 μ sec.

Surface Oxide Determination by Cathodic Stripping

Chronopotentiometry was used to determine the extent of surface oxidation of the platinum indicator electrode. The indicator electrode was grounded and the saturated calomel reference electrode was connected to either the oscilloscope or the recorder. The constant current source, which was connected between the counter electrode and ground, was turned on and the potential of the indicator electrode was recorded as a function of time. The shape of the curve was that of the cathodic chronopotentiogram shown in Fig. 1. The amount of charge per unit area, Q/A, of oxide on the platinum surface was calculated by multiplying the current density by the time required to reach the middle of region Cc. A current density of 15 $\mu a/cm^2$ was used. This current density was chosen because it was at least one hundred times the current withdrawn by the potential measuring circuit. It is very likely that current densities in the region of 100 $\mu a/cm^2$ would cause the apparent amount of surface oxidation to be decreased due to premature polarization to the hydrogen evolution potential. However, no difference in the quantity of surface oxidation measured was observed between determinations using cathodic current densities of 15 and 30 μa. The cathodic current was turned off as soon as the electrode potential reached the potential of the inflection point of

the region Cc. This procedure avoided the evolution of hydrogen. The discharge of hydrogen on the platinum was observed to have an effect on subsequent anodizations.

If the surface oxidation is thought of as a compound or mixture of compounds obeying the law of small whole numbered ratios of atomic constituents, it is desirable to be able to convert millicoulombs per square centimeter to atoms of oxygen per surface atom of platinum. To make this conversion it is necessary to know the number of surface atoms of platinum per square centimeter. Using the lattice constants in Wyckoff (23) for crystalline platinum one calculates 1.3 x 10^{15} atoms/cm^2 for the 100 plane and 1.5 x 10^{15} atoms/cm^2 for the closest packed 111 plane. If one takes the two-thirds power of the number of platinum atoms per cubic centimeter as calculated from the density of platinum, 1.5 x 10^{15} atoms/cm^2 is obtained. The predominant crystal face on a polycrystalline surface would be the 111. Using 1.5 x 10^{15} atoms/cm^2 it was calculated that about 0.5 millicoulombs/cm^2 are required to provide each surface platinum with an oxygen atom. An accuracy of 10% is all that should be claimed for this number.

Potentiostatic Formation of Surface Oxide

Two methods are available for controlling the anodic treatment given to the electrode: namely, electrolysis at constant anodic current and electrolysis at constant anodic potential. Both methods were tried in this study. It was found that the constant potential anodization yielded a more reproducible quantity of surface oxidation as determined by cathodic chronopotentiometry. If the quantity of oxide on the electrode surface is a function of the anodization potential, the better reproducibility of the constant potential is reasonable. The potential of the electrode follows the shape of the anodic chronopotentiogram, as shown in Fig. 1, during constant current anodization. The steady-state potential of the electrode (region Oa_s) is reached slowly, and therefore only at long times are the two anodization methods equivalent. Another consideration is the shape of the steady-state anodic current-voltage curve. In the region of interest which is negative to the rapid evolution of oxygen, the current increases slowly with increasing potential. It would be difficult then to obtain a reproducible steady-state potential (and thus a reproducible surface oxidation) by applying a constant current.

Constant potential anodization was used throughout this work. With the indicator electrode grounded, the calomel reference electrode was connected to the input of the voltage follower. The reference potential source was connected between the output of the voltage follower and the input of the potentiostat. The potential was established within milliseconds after turning on the potentiostat.

Effect of Varying the Time of Anodization

The quantity of oxide on the surface of the electrode was measured as a function of the time of anodization at a given potential. The purpose of this experiment was to determine how long it takes the surface coverage to come to a constant value at a given applied potential. Before each anodization, the electrode had been freed of oxide by the previous chronopotentiometric determination and then allowed to drift until the open-circuit potential reached a steady value. This potential was between 0.8 and 0.85 v. The cathodic constant current was switched on immediately after the potentiostat was turned off. The quantity of oxide per square centimeter vs. the time of anodization was determined for five potential values. Results are shown in Fig. 4. Each of the curves shown actually has a point on the origin of the graph, but the initial rise is too steep to be shown. The potentiostat could pass 1 millicoulomb in 20 msec, a time very short compared to 1 sec, the shortest time interval plotted.

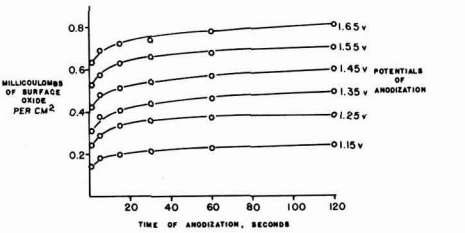

Fig. 4. Variation of amount of surface oxide with time of anodization at constant potential.

The amount of oxide on the surface increased quite rapidly during the first 15 sec of anodization at each potential. The subsequent increase in surface oxide was gradual. Apparently some slow process was causing a slow increase in the oxidation. Since steady-state coverage was not reached within a reasonable time of anodization, an anodization time of 30 or 60 sec was chosen for subsequent experiments. An anodization of 30 sec yielded a coverage which was at least 90% of that for a 2-min anodization.

Post-Anodization Behavior of Electrode

When the potentiostat was turned off after an anodization, the electrode did not remain at the anodization potential. The electrode potential dropped suddenly at first and then decreased slowly to about 0.85-0.95 v. The time required to reach a steady-state open-circuit potential increased with increasing potential of anodization. For an anodization at 0.95 v, steady state was reached in about 10 min. For anodizations at 1.3-1.7 v, over an hour was required to reach steady state. Despite the large drop in potential during an hour, the amount of surface oxide decreased by only about 0.2 millicoulombs/cm^2. Approximately the same amount of oxide was lost during an hour regardless of the anodization potential. The range studied was from 1.15 to 1.75 v. In this case the electrode was anodized for 3 min at each potential.

Experiments were also performed relating the decay of the open-circuit potential and the surface coverage for shorter times. The electrode was anodized for 30 sec at 1.25 v, 1.45 v, or 1.65 v. After the potentiostat had been turned off, the open-circuit

potential was followed for an amount of time t_d. At time t_d the constant cathodic current was applied and the quantity of oxide was determined. Thus the open-circuit potential and the surface coverage were determined for various values of t_d up to 15 min for all the three anodization potentials. The potential fell off rapidly during the first minute of drift. The drop in potential was 0.2 v for the 1.25-v anodization, 0.3 v for the 1.45-v anodization, and 0.35 v for the 1.65-v anodization. A decrease in surface charge was not noticeable for the first minute. At the end of five min, 0.015 millicoulombs had been lost; after 15 min, 0.045 millicoulombs were lost. The absolute value of the oxide loss was the same for all three anodization potentials. If the surface coverage decay is linear at 0.045 millicoulombs/cm²/15 min, at the end of an hour, the amount lost would be 0.18 millicoulombs/cm². This value is in reasonable agreement with the result cited for a 1-hr drifting time. It was thus demonstrated that an electrode may be left at open circuit after the anodization for times up to 1 min without appreciably affecting the amount of surface oxide.

The lack of correlation between oxide loss and potential decay throws considerable doubt on the notion that the post-anodization open-circuit potential is a function of the type or quantity of oxide on the electrode surface. It has been claimed that the potential decay is caused by the decomposition of an unstable surface oxide whose presence affects the open-circuit potential (16). If this were the reason for the potential decay, the rate of loss of the surface oxide would decrease as the quantity of unstable oxide decreases. Furthermore, it seems unlikely that the amount of unstable oxide on the platinum would be independent of the potential of anodization or the quantity of total oxide on the electrode surface.

In the mechanism of the oxide formation suggested in the discussion of the charging curves above, the potential of the electrode during anodization is controlled by the oxygen evolution process and not by a redox couple established between the platinum and the oxide layer. The anodic potential, then, would be dependent on the partial pressure of oxygen. In solutions swept free of oxygen, when the anodization is stopped, the electrode potential will drop rapidly as the oxygen diffuses away from the electrode surface. Eventually the oxygen partial pressure becomes so small that the oxygen-water couple can no longer establish an electrode potential. It is experimentally observed that the open-circuit potential of a platinum electrode, oxidized or reduced, eventually drifts to about 0.8 v. This potential is established by a very slow exchange since it is immediately polarized several tenths of a volt by an applied current density of a half-microampere per square centimeter. This explanation of the potential decay is supported by an experiment reported by Giner (8) who noted that the open-circuit potential of a partially oxidized platinum electrode is increased about 200 mv when the solution is saturated with oxygen. The extent of electrode oxidation was not increased by the presence of the oxygen gas, which shows that the oxidation process requires the passage of an electrical current.

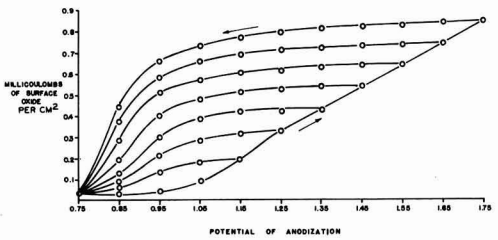

Fig. 5. Variation of amount of surface oxide with potential and direction of potential change.

The slow disappearance of oxide from the electrode surface will be shown later to be due to the diffusion of the oxygen atoms from the electrode surface to the interior of the platinum along grain boundaries. Such a diffusion satisfies the observed conditions of being a potential independent process, of being a process independent of the extent of surface oxidation (once a significant portion of the first oxidation product has formed), and of being a very slow process.

Effect of the Anodization Potential

The electrode was anodized for 30 sec, allowed to remain at open circuit for 30 sec, and then the quantity of surface oxide was determined chronopotentiometrically. The number of millicoulombs of oxygen per square centimeter as a function of the potential of anodization is shown as part of Fig. 5. The quantity of oxide increases with increasing potential of anodization. Between about 1.2 v and 1.75 v the amount of surface oxide increases linearly with potential.

The hysteresis curves of Fig. 5 result from the following experiment. The electrode was anodized for 30 sec and then the electrode potential was reduced to a lower value for 30 sec. The electrode was left at open circuit for 30 sec and then the quantity of oxide was determined. It was found that the quantity of oxide which was present at the first anodization potential remained when the potential was decreased except at potentials below 0.95 v where the surface oxide began to be removed. To determine whether or not this hysteresis might be caused by a slow equilibrium a reduced electrode was put at 1.05 v for 1 hr without obtaining an increase in surface oxide over that shown in Fig. 5. The electrode was also preanodized at 1.45 v for 1.5 min and then put at 1.05 v for 1 hr. The quantity of oxide was only 0.135 millicoulombs less than that shown in Fig. 5 for the same pretreatment with a 30-sec anodization at 1.05 v. The loss of surface oxide at a reduced potential was less than that of an oxidized electrode left at open circuit for the same period.

This hysteresis substantiates several interesting conclusions reached earlier on other bases. (*A*) The electrode potential is not determined by the degree of surface oxidation. (*B*) To reduce a substance on an electrode, electrons must be supplied to the electrode either from an oxidation occurring on the same electrode or from an external current source.

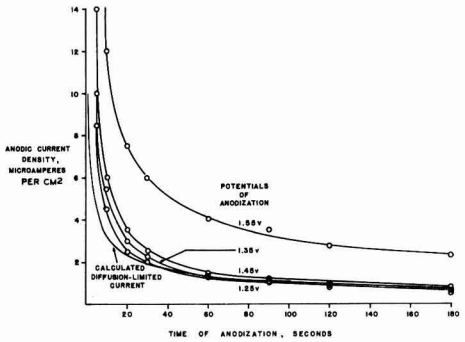

Fig. 6. Anodic current density as function of time

When the surface oxide is not reduced at open circuit, it may be due to the lack of an electron source. When the surface oxide is not reduced when the potentiostat is still connected, it is proof that the oxide is not reduced at the potential applied. (*C*) Since two steps are not observed in the oxide removal curves, that oxidation in excess of one oxygen per platinum is reduced at the same potential and thus probably by the same mechanism as the lower oxide.

Anodic Current as a Function of Anodization Time

When a constant anodic potential was applied to the unoxidized electrode, the current was very large but rapidly decayed to a small value. A plot of the current as a function of the time of anodization is shown in Fig. 6 for four potentials of anodization. Note that the current for the anodizations at 1.25, 1.35, and 1.45 v are almost identical after the first 60 sec of anodization. The current for the anodization at 1.55 v is much higher than that for the other potentials at all times. Apparently the process which requires current at the longer times of anodization is independent of potential. The anodic current at 3 min for anodizations from 1.25 to 1.45 v was also independent of the rate of stirring in the cell as provided by the nitrogen bubbling.

We suggest that an explanation for this behavior may be the diffusion of oxygen atoms into the platinum. Evidence of the penetration of platinum by oxygen has been presented in the literature (9, 24). The diffusion of a surface oxygen atom into the electrode interior would leave a vacancy on the electrode surface which requires current to become refilled. The rate of diffusion would decrease with increasing time of anodization, as was observed. The rate of diffusion would be independent of potential as long as the surface is saturated with oxygen atoms. The greatly increased current at 1.55 v is due to the evolution of oxygen. The solution of Fick's laws for the boundary condition of constant surface concentration is $i = n\mathbf{F}C^\circ \sqrt{D/\pi t}$. A surface concentration of one oxygen per platinum corresponds to a concentration C° of 0.11 moles/cm^3. For an observed i equal to 0.8 μa/cm^2 at $t = 180$ sec, D is equal to 10^{-18} cm^2/sec. This estimate must be regarded as very crude because a linear diffusion model is assumed for what is probably a grain boundary diffusion.

A value for the diffusion coefficient of oxygen in platinum has not been reported previously. The activation energy E for self-diffusion in the platinum lattice has been determined as 68.2 kcal/g-atom (25). The diffusion coefficient D is obtained from the relation $D = D_o \exp(-E/RT)$ where D_o is a constant which can be estimated as 1. Thus the self-diffusion coefficient of platinum at room temperature has a value of about 10^{-49} cm^2/sec. The activation energy of self-diffusion along grain boundaries in silver (which has the same crystal structure as Pt) is about 0.45 times the activation energy of lattice diffusion (25). The self-diffusion of Pt along grain boundaries can thus be estimated to be within several orders of magnitude of 10^{-22} cm^2/sec. Considering the smaller size of an oxygen atom than a platinum atom the uncertainties in the estimation made above, and the effect of chemical bond formation, the observed value of 10^{-18} cm^2/sec for the grain boundary diffusion of oxygen in platinum at room temperature is a reasonable one. The theoretical current due to the replacement of diffused oxygen atoms for $D = 10^{-18}$ cm^2/sec is plotted on Fig. 6.

The grain boundary diffusion of oxygen atoms is preferred by the authors over the loss of surface oxygen into the solution for the following reasons: (*A*) The loss of surface oxidation by combination of bonded (chemisorbed) oxygen atoms requires the rupture of platinum-oxygen bonds, a process not likely to be independent of the electrode potential or of the extent of surface oxidation in excess of one oxygen per surface platinum atom. (*B*) Recent photomicrographic evidence (26) indicates preferential attack of grain boundaries upon severe anodic treatment of platinum.

Photographic records were made of oscilloscopic measurements of the electrode current during the first 0.1 sec of anodization at constant potential. The potential was established on the electrode within 2 msec. The area under the current-time curve, expressed as coulombs, was always larger than the amount of surface oxide determined chronopotentiometrically after a 30-sec anodization at that same potential. Anodization potentials from 0.95 to 1.75 v were studied. In some cases the current-time integral was equivalent to as much as twice the quantity of oxide found on the surface after a 30-sec anodization. The ratio would be even greater if the quantities of surface oxide for a 1-sec anodization (Fig. 4) were used.

The fact that considerably more current was used for an anodization than could be accounted for by the amount of oxide formed substantiated the notion that another process occurs while the oxide layer is being formed. At potentials of 1.45 v and lower, the anodization current at long times can all be accounted for by the diffusion of oxygen along the platinum grain boundaries. Therefore, the reaction that occurs during the formation of the surface oxide is inhibited by the formation of the oxide. If the concurrent process is the evolution of oxygen, the overvoltage of oxygen evolution on platinum is thus explained.

Double Layer Capacity as a Function of Potential

The potentiostat was turned on to apply a constant potential to the indicator electrode. The current-integrator was connected, and the step potential was set at 10 mv. The output voltage of the current-integrator was measured on the oscilloscope. Using the second beam of the oscilloscope, the electrode current was also observed. The initiation of the potential step triggered the oscilloscope sweep. No current other than the double layer charging current was observed over the entire potential range except at high anodic and cathodic potentials where oxygen and hydrogen evolution occur, respectively. The step potential was applied in both directions with the same results.

Currents lower than 1 μa could not be observed with the equipment employed because of the noise level of the potentiostat and the voltage follower. For a reaction which is as irreversible as Fig. 5 shows the oxide formation to be, the rate of the reaction would be expected to be too slow for the reaction current to be observed with this equipment. Thus the kinetic parameters of the oxide formation reaction are not obtainable with the potential step apparatus used here. Only the double layer charging current will be integrated by the current-integrator when the integration is performed over very short times (10^{-3} sec).

The double layer capacity was measured by the method described above. The current integrator was calibrated for this purpose using a decade of large standard capacitors. The double layer capacity was shown to be a function of potential, with a distinct hysteresis behavior depending on the direction of potential change. The relationship is shown in Fig. 7. The minimum capacity of the electrode was about 20 μf/cm^2. The capacity rose as the potential increased until a value of about 60 μf was reached at about 1.25 v. The capacity varied between 60 and 55 μf for potentials above 1.25 v. The capacity remained high as the potential was decreased until the potential had reached a value of about 0.95 v. The capacity then rapidly returned to the minimum value. The similarity between the capacity-potential curve (Fig. 7) and the surface oxide-potential curves (Fig. 5) is obvious. It is evident that the presence of the surface charge causes the double layer capacity to increase up to three times its normal value.

It has been postulated by Llopis and Colum (27), who also observed this capacity hysteresis, that the reason for the increase of the electrode capacity of a

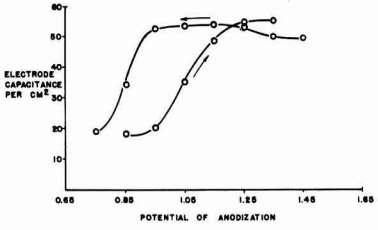

Fig. 7. Hysteresis behavior of electrode capacitance

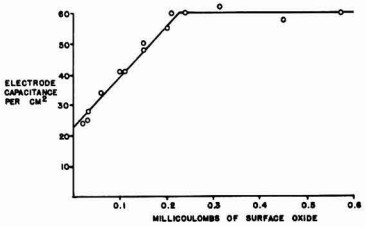

Fig. 8. Relation between electrode capacitance and amount of surface oxide.

platinum electrode at the beginning of surface oxide formation is due to the presence of dipoles such as Pt . . . O at the electrode solution interface. The negative end of the dipole may be adsorbed oxygen or some other intermediate in the oxygen evolution reaction. The capacity across this dipole would be of such a magnitude that the relative effect of the ionic double layer in the solution would be small. Furthermore, a large portion, if not all, of the potential gradient between the electrode and the solution would be developed across the dipole at the electrode surface.

Dependence of Double Layer Capacity on Surface Oxidation

Electrode capacities were again measured for the various conditions of anodizations and preanodization studied in the section above. After each capacity was measured, the current-integrator was disconnected as quickly as possible, the potentiostat was turned off, and the amount of charge on the electrode surface was determined chronopotentiometrically. Figure 8 shows the results of this experiment. The double layer capacity was found to be a linear function of the amount of surface oxide until a capacity value of 55-60 μf was reached. The double layer capacity then remained constant, independent of the amount of surface oxide. The line drawn on Fig. 8 was determined by an analysis by the method of least squares.

On the basis of the explanation advanced above for the increase in the electrode capacity as a result of the electrode oxidation it is possible to account for the capacity vs. surface charge curve (Fig. 8). For an unoxidized electrode in 1*N* perchloric acid at about 0.8 v, the double layer capacity is about 20 μf/cm^2. Highly polar groups, which might be represented as $Pt^+ \ldots O^-$ (27), $Pt^+ \ldots OH$, or $Pt^+ \ldots OH_2^+$ may exist at the metal-solution interface of the "oxidized" metal surface. These dipoles replace the water molecules and ions which form the electrical double layer at the reduced electrode surface. To account for the experimentally observed increase in electrode capacity from 20 to 60 μf/cm^2, a threefold increase in capacity due to the presence of the highly polar groups is required. For a partially covered surface, the total electrode capacity may be thought of as many capacitors in parallel (sites of hydroxyl adsorption and dipole formation) and some of low value (a double layer formed of ions and water molecules). The electrode capacity is thus a linear function of the fraction of the sur-

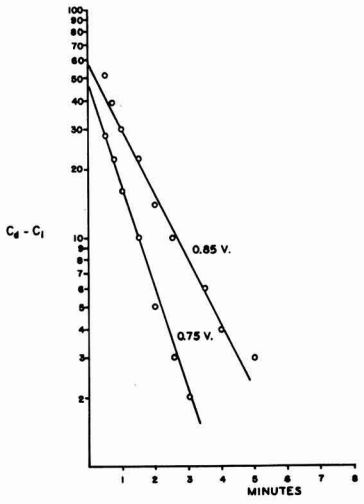

Fig. 9. Decay of surface capacitance in unstable region

face which is covered by the dipoles as demonstrated by Fig. 8.

It can be further postulated that the dipole at the electrode surface is primarily Pt...O, that is, that the electric field across the dipole is largely across the planes of the Pt^+ and O^- atoms, respectively, and is independent of the state of protonation or hydration of the O^- atom. If the surface oxidation continues and the $Pt^+...O^-$ dipole becomes a $Pt^{++}...O^=$ dipole, the capacity will not change. The permittivity of the dipole has a linear dependence on the ratio of the dipole moment to the electric field strength. When the $Pt^+...O^-$ dipole becomes a $Pt^{++}...O^=$ dipole, the dipole moment is doubled, but so is the electric field strength across the dipole. If the permittivity remains unchanged, the capacity will also remain unchanged. This explanation of the electrode capacity accounts for the linearity of capacity with surface oxidation until a surface charge of 0.25 millicoulombs (equivalent of one electron per surface platinum) has been reached as well as the constant electrode capacity observed for higher surface charge.

The postulation of the formation of the polar group as an explanation for the capacity increase is preferred over explanations involving the usual ionic double layer. One reason for this preference is that the capacity is a function of electrode oxidation (Fig. 8), but independent of potential since points on Fig. 8 were taken from both the oxide formation and dissolution curves. There is an electrode potential difference of about 200 mv between equivalent oxidation states on the oxide formation and dissolution curves. The ionic double layer capacity is known to vary with potential and therefore cannot appreciably affect the electrode capacity which is measured for the oxidized surface. The ionic double layer capacity also varies with ionic strength but, as it will be shown later, the electrode capacity of an oxidized electrode is independent of ionic strength.

Rate of Surface Oxide Dissolution

The fact that the double layer capacity is a linear function of the surface coverage was used to advantage to determine the rate of surface oxide dissolution. The electrode was put at 1.25 v until the double layer capacity came to a steady-state value (requiring about 1 min). The electrode potential was then shifted suddenly to 0.85 v and the double layer capacity was followed as a function of time. The capacity jumped to a value higher than that measured at 1.25 v and then dropped off and eventually reached a steady-state value. When the steady-state value of capacity was subtracted from all of the measured capacity values and the logarithm of the difference was plotted against time (Fig. 9), a straight line resulted. The same experiment was repeated using a removal potential of 0.75 v. Another straight line of steeper slope resulted. The conclusions to be drawn from these experiments are that the dissolution reaction is a first order reaction, and that the rate of dissolution increases with increasing cathodic electrode potential. The "half-life" of the oxide is 1 min at an electrode potential of 0.85 v and 2/3 of a minute at 0.75 v.

Effects of Acidity and Ionic Strength

Perchloric acid of 0.01M concentration was used in the cell and salt bridge for some measurements. The surface oxide was measured as a function of potential and the dissolution potential curve for anodization at 1.25 v was made. The results were identical to those shown in Fig. 5 except that the potential axis was shifted 0.12 v in the increasing positive direction. In other words, an anodization of 1.25 v in 0.01M $HClO_4$ corresponds to an anodization of 1.37 v in 1M $HClO_4$.

The double layer capacity measurement at the lower electrolyte concentration was rather difficult to make. The increased solution resistance caused the potentiostat to respond slowly due to the potential drop in the solution between the electrode and the luggin capillary. For this reason the capacity could be measured only roughly. If the experimental error is taken to be 10%, the capacity-potential curve is the same as that for 1M $HClO_4$ (Fig. 7) except for the same potential shift which was noted above for the surface oxide. The capacity-charge relationship observed in 1M $HClO_4$ solutions was also reproduced within 10% for 0.01M $HClO_4$ solutions.

The independence of the electrode capacity over a hundredfold change in ionic strength is another indication that the electrode capacity is not determined by the ionic double layer. The electrode capacity must then arise from the highly polar nature of the adsorbed surface layer.

Conclusions

On the basis of the observed anodic behavior of the platinum electrode, a mechanism for the surface oxidation and oxygen evolution reactions can be proposed. The first step is the formation of an oxygen evolution intermediate which is adsorbed on the electrode surface. The choice of an intermediate

is limited because only one electron is used in its formation from water. Possible intermediates are ·OH, ·O⁻, ·OH_2^+. The hydroxyl radical has been chosen to represent the intermediate in the reaction equations.

$$Pt + H_2O \rightleftharpoons Pt...OH + H^+ + e^- \qquad [1]$$

The Pt...OH thus formed[1] can further react in either of two ways. First, an oxygen evolution reaction may be written which removes the surface hydroxyl, presumably through the intermediate formation of surface ·OOH, forming a bare platinum site:

$$Pt...OH + H_2O \rightarrow Pt...OOH + 2H^+ + 2e^-$$

$$Pt...OOH \rightarrow Pt + O_2 + H^+ + e^- \qquad [2a]$$

Second, the surface hydroxyl may be converted to a surface oxygen atom which is firmly held

$$Pt...OH \rightarrow PtO + H^+ + e^- \qquad [2b]$$

Bare platinum sites produced by reactions [2a] are reoxidized by reaction [1], so that eventually all the surface is covered with firmly held PtO. Subsequently oxygen evolution must occur on the PtO surface, as has been also postulated by Llopis (27). Once again, surface hydroxyl formation may be postulated, with competitive reactions to form oxygen molecules, or to further oxidize the surface.

An important consideration here is the finding of Rosenthal and Veselovskii (13) by isotope experiments that oxides formed at lower potentials (0.8-1.2 v) do not appear in oxygen gas subsequently evolved from the surface. Oxides formed at higher potentials were found to make a partial contribution to oxygen molecules formed at the surface. This finding suggests that the first oxygen atom per surface platinum atom is held more firmly than additional oxygen atoms. Moreover, the oxygen evolution reaction cannot involve combination of oxygen atoms if one of the atoms is of the firmly held type, and the present finding of the stability of even the higher surface oxidation at open-circuit forces the rejection of an atom-combination mechanism for oxygen evolution.

A similar reaction sequence as postulated above for a bare platinum surface may be written for oxygen evolution at a PtO surface, in which the PtO bonds are not disrupted:

$$PtO + H_2O \rightarrow Pt^0...OH + e^- + H^+ \qquad [3a]$$

$$Pt^0...OH + H_2O \rightarrow Pt^0...OOH + 2e^- + 2H^+ \qquad [3b]$$

$$Pt^0...OOH \rightarrow PtO + H^+ + e^- + O_2 \qquad [3c]$$

According to the above mechanism the oxidation of the platinum surface occurs only when oxygen is being evolved concurrently. From the principle of microscopic reversibility it follows that the formation of the oxide is energetically possible at potentials less positive than the potential of oxygen evolution, but it appears that the oxide is not formed at an appreciable rate except in the presence of the oxygen evolution intermediates. In order to dissolve the surface oxide, however, it would be necessary to put the electrode at a potential for which the oxide is unstable. At such a potential, the instantaneous rate of oxide dissolution would be proportional to the instantaneous quantity of oxide on the surface. A first order reduction of the surface oxide was confirmed experimentally. The hysteresis of the potential vs. surface oxidation curve is direct evidence that oxide formed at potentials of 1.2-1.7 v is reduced only at potentials of about 0.95 v and below. The standard potential of the surface oxide formation on platinum would be closer to the reduction potential than to the oxidation potential, that is, about 0.8-0.9 v.

[1] Reaction [1] has been postulated by Bockris and Huq (28) as being the rate-controlling process.

Manuscript received Feb. 1, 1960.

Any discussion of this paper will appear in a Discussion Section to be published in the June 1961 JOURNAL.

REFERENCES

1. F. C. Anson and J. J. Lingane, *J. Am. Chem. Soc.*, **79**, 1015 (1957).
2. F. C. Anson and J. J. Lingane, *ibid.*, **79**, 4901 (1957).
3. M. Becker and M. Breiter, *Z. Elektrochem.*, **60**, 1080 (1956).
4. M. Breiter, C. A. Knorr, and W. Volkl, *ibid.*, **59**, 681 (1955).
5. J. A. V. Butler and G. Armstrong, *Proc. Roy. Soc.*, **A137**, 604 (1932).
6. B. V. Ershler, *Discussions Faraday Soc.*, **1**, 269 (1947).
7. A. L. Ferguson and M. B. Towns, *Trans. Electrochem. Soc.*, **83**, 271, 285 (1943).
8. J. Giner, *Z. Elektrochem.*, **63**, 386 (1959).
9. A. Hickling, *Trans. Faraday Soc.*, **41**, 333 (1945).
10. I. M. Kolthoff and N. Tanaka, *Anal. Chem.*, **26**, 632 (1954).
11. J. K. Lee, R. N. Adams, and C. E Bricker, *Anal. Chim. Acta*, **17**, 321 (1957).
12. G. Radlein, *Z. Elektrochem.*, **61**, 727 (1957).
13. K. I. Rosenthal and V. I. Veselovskii, *Doklady Akad. Nauk S.S.S.R.*, **111**, 637 (1956).
14. J. W. Ross and I. Shain, *Anal. Chem.*, **28**, 548 (1956).
15. K. J. Vetter and D. Berndt, *Z. Elektrochem.*, **62**, 378 (1958).
16. S. E. S. El Wakkad and S. H. Emara, *J. Chem. Soc.*, **1952**, 461.
17. Ts. I. Zalkind and B. V. Ershler, *Zhur. Fiz. Khim.*, **25**, 565 (1951).
18. S. Glasstone and A. Hickling, *Chem. Revs.*, **25**, 407 (1939).
19. J. Giner and E. Lange, *Naturwissenchaften*, **40**, 506 (1953).
20. S. Brunauer, P. H. Emmett, and E. Teller, *J. Am. Chem. Soc.*, **60**, 309 (1938).
21. F. R. Meyer and G. Ronge, *Angew. Chem.*, **52**, 637 (1939).
22. C. G. Enke, Doctoral Dissertation, University of Illinois (1959).
23. R. W. G. Wyckoff, "Crystal Structures," Interscience Publishers, New York (1948).
24. A. D. Obrucheva, *Zhur. Fiz. Khim.*, **26**, 1448 (1952).
25. C. E. Birchenall, *Metallurgical Revs.*, **3**, 235 (1958).
26. D. G. Davis, Jr., *Talanta*, **3**, 335 (1960).
27. J. Llopis and F. Colum, "Proceedings of the International Committee on Electrochemical Thermodynamics and Kinetics, Eighth Meeting, 1958," pp. 414-427, Butterworths, London.
28. J. O'M. Bockris and A. K. M. S. Huq, *Proc. Roy. Soc. (London)*, **A237**, 277 (1956).

Technical Notes

Electrode Assembly for Electrochemical Measurements

Milton Stern[1] and A. C. Makrides

Metals Research Laboratories, Union Carbide Metals Company, Division of Union Carbide Corporation, Niagara Falls, New York

The isolation of electrical contacts from the test solution is a common problem in electrochemical measurements. It may be circumvented in some cases by using leads of the same material as the electrode. Such an arrangement, however, produces an ill-defined current density distribution and introduces an extraneous vapor-metal-solution interface.

Electrical connections are masked frequently with tape, wax, or thermosetting plastics. All these substances contaminate the solution to some degree. Wax is probably least objectionable. In corrosive solutions, however, it often causes preferential attack next to the masked surface. Contamination of solution can be avoided with wire electrodes sealed in glass. The method is limited to tungsten and platinum since only these metals give leakproof seals. These difficulties may be eliminated with a demountable electrode assembly in which only glass and a fluorinated plastic (Teflon), besides the electrode, are exposed to solution. The assembly has been used with considerable success for several years in these Laboratories.

A diagram of the assembly is shown in Fig. 1. The electrode is tapped, threaded, and attached to a stainless steel rod through a Teflon washer machined to a narrow edge at the end next to the electrode. The rod is isolated from solution with a heavy-wall glass tube ground at the lower end at an angle of approximately 60°. The assembly is made leakproof by tightening a nut at the top of the steel rod. Sufficient pressure is exerted to produce liquid-tight seals at both the glass-Teflon and Teflon-electrode junctions. A thin Teflon washer is used between the retaining nut and the tube to avoid cracking the glass.

An assembly will remain leakproof for several weeks and has been used in boiling acid solutions. Although Teflon washers can be used more than once, they are deformed to a certain extent after each run and have to be replaced after a few runs. Their life can be extended by remachining the lower edge.

The glass tube is attached eccentrically to a ground glass joint which is inserted, again eccentrically, in a second ground glass joint on the cell (see insert in Fig. 1). The distance between electrode and a Lugin capillary probe can thus be easily adjusted within rather wide limits. Mercury or water-sealed joints are used to avoid contamination from lubricant.

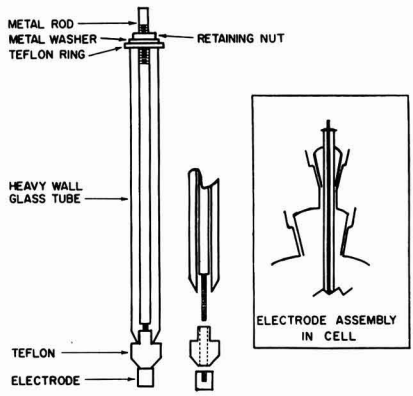

Fig. 1. Electrode assembly

A number of modifications of the basic design have been employed. For example, in experiments with a rotating electrode, a cylindrical sample was secured to the steel rod in the usual way and recessed and threaded at the lower end. A V-shaped Teflon section, which rode in a glass cup fused to the bottom of the cell, was attached at this end. The Teflon bearing minimized eccentric motion of the electrode and isolated the bottom surface of the cylinder from solution. At the top of the assembly, an inverted steel cup rotating in a pool of mercury sealed the system from the atmosphere while providing electrical contact to the electrode.

The basic assembly described above can be used with any metal or semiconductor electrode which can be attached securely to a metal rod. It can be used in practically every common test solution since only glass and Teflon come in contact with solution. Furthermore, it can be cleaned in any of the usual ways, for example, with a saturated chromic-sulfuric acid solution (cleaning solution).

Manuscript received May 9, 1960.

Any discussion of this paper will appear in a Discussion Section to be published in the June 1961 JOURNAL.

[1] Present address: Speedway Laboratories, Linde Co., Indianapolis, Indiana.

Identification of the Diffusing Species in Uranium Oxidation

J. G. Schnizlein, J. D. Woods,[1] J. D. Bingle, and R. C. Vogel

Chemical Engineering Division, Argonne National Laboratory, Lemont, Illinois

As part of an extensive study of the kinetics of uranium oxidation, experiments have been designed to establish whether uranium or oxygen diffuses through the oxide film during the oxidation reaction at 200°C in 200 mm oxygen. Two distinctly different types of marker experiments have been used to demonstrate the same conclusion.

In the first method, metallographic examination was used to establish whether an inert marker would become buried in the oxide and whether or not two impinging oxide films would fuse together. Other investigators (1-4) have shown that in cases of metal ion diffusion during oxidation, as with copper (1), an inert marker will become buried in the oxide. Similarly, two oxide surfaces growing against one another will fuse into a continuous oxide layer (2). The lack of burial of a wire or lack of fusion of the impinging oxides is generally accepted as indication of the absence of metal-ion diffusion.

The second method used involved an alpha-counting technique to locate a marker of enriched uranium. Although the use of inert markers in metal oxidation studies is common, the use of a radioactive isotope of the metal as a marker is a recent (5), extremely useful innovation. The metal isotope marker is not inert but becomes a part of the oxidation process, thereby avoiding the danger of altering the reaction under examination. In these experiments an enriched uranium film was sputtered onto the surface of normal uranium. The higher percentage of uranium-234 and -235 gives the marker considerably more alpha activity than normal uranium. After oxidation the active marker can be located by direct counting of the surface. The location of the marker indicates whether uranium or oxygen is the diffusing species.

Experimental

The uranium specimens were cubes 1 cm on an edge prepared by the Metallurgy Division of Argonne National Laboratory from high-grade biscuit metal. The metal contained approximately 250 ppm total analyzed impurities. The cubes were β-quenched to assure uniform grain structure and random orientation. The oxidation of the samples was conducted at constant temperature and constant pressure in an apparatus in which the consumption of oxygen was measured volumetrically.

Metallographically determined marker.—Two uranium cubes were polished through 1-μ diamond paste and wired together with 640-μ diameter (22-gauge) Inconel wire with a 25-μ (1-mil) platinum wire separating the cubes near one edge. Thus, a V-shaped space was left between the cubes ranging in width from zero to approximately 30 μ.

[1] Special Scientific Employee in 1957 from Drake University.

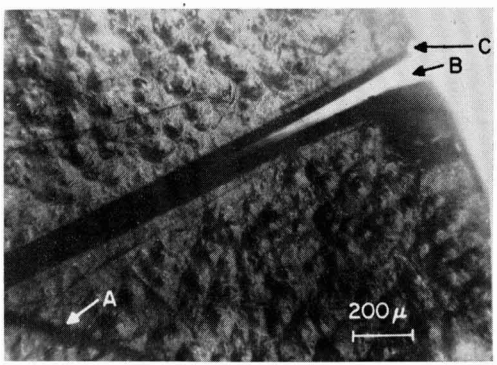

Fig. 1. Open V-shaped space between oxidized uranium cubes. A, 25 μ diameter platinum wire (out of focus); B, V-shaped space still unfilled with oxide; C, notch on edge of oxidized cube.

The sample was then oxidized at 200°C in 200 mm oxygen until the oxygen consumed was equivalent to 5150 μg/cm^2. The study of the kinetics of oxidation (which will be published at a later date) indicates that uranium dioxide is produced under these conditions and that an essentially linear oxidation rate is achieved after a brief, much lower initial rate. After cooling in vacuum, microscopic examination (Fig. 1) showed that the V-shaped space between the cubes was still not closed by oxide. The 25-μ platinum wire (A) can be seen, out of focus, in the corner opposite the open edge (B). The interesting notch (C) in the oxide at the edge of the cube should be noted. This is an indication of the absence of uranium diffusion in the oxidation mechanism (6, 7). Other related uranium oxidation experiments have shown even more clearly than Fig. 1 that the raised surfaces of the oxide are approximately of the same dimensions as those of the original sample, with notches clearly evident at each edge.

An additional oxidation of 12,500 μg/cm^2, to a total of 17,650 μg/cm^2, was completed to close the gap. Examination of the edge of the oxide contact was not satisfactory because of the notch developed on each cube edge. To obtain a cross-section view the sample was mounted in "Scotchcast," a low-temperature thermosetting plastic. After polishing through 600 grit silicon carbide paper, the section was examined.

A view of the cross section showing the platinum wire (A) separating the two cubes and locating the original metal surfaces is presented in Fig. 2. It is obvious that the two oxides have not fused, in fact, the oxide layers (C and D) from the first and second oxidations are distinctly separate. The thickness of these oxide layers is approximately proportional to

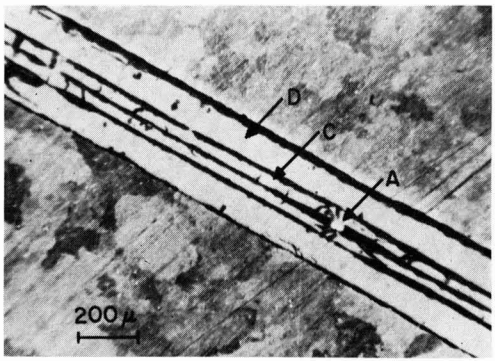

Fig. 2. Cross section of impinging oxide from two uranium cubes. A, cross section platinum wire; C, oxide produced in first oxidation; D, oxide produced in second oxidation.

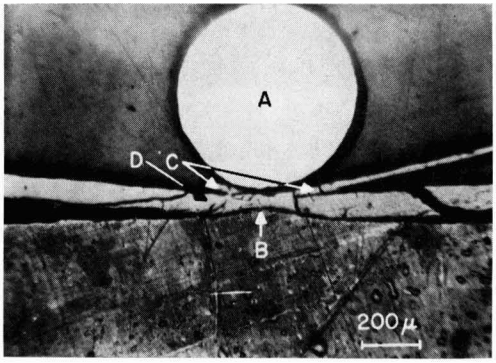

Fig. 3. Cross section of Inconel binding wire on oxidized uranium cube. A, originally 640 μ diameter Inconel wire; B, hump in uranium surface where partial protection is afforded by wire; C, oxide produced in first oxidation; D, oxide produced in second oxidation.

the extent of each oxidation. Two other interesting observations are: (*a*) the metal surfaces are now parallel instead of forming the V-shape of the original assembly, and (*b*) the 25-μ diameter platinum wire (A) has been flattened into an oval cross section approximately 17 x 38 μ. Both of these observations demonstrate the tremendous pressure of the oxide film as the gap was closed.

Figure 3 illustrates the lack of burial of the 640-μ diameter Inconel binding wire (A). It appears that the uranium was partially protected during the oxidation so that a hump (B) is observed in the surface. The oxide produced during the first oxidation (5,150 μg/cm²) becomes diminishingly thin under the wire (C), whereas that produced during the second oxidation (D) (12,500 μg/cm²) is continuous. There is no tendency of the oxide to grow up around the wire.

Radioactive marker.—For the experiments utilizing the marker of enriched uranium, two approaches were used. In the first, the active marker was initially on the exterior of the cube. After oxidation the activity should either remain on the surface or be distributed through the oxide, depending on whether oxygen or uranium was the diffusing species. In the second, the sputtered film of enriched uranium was covered with a film of normal uranium. In this case, if oxygen were diffusing, the activity would remain buried as a thin band, whereas if uranium diffused, the activity would be distributed throughout the oxide.

The normal uranium cubes were polished through 1-μ diamond paste and then electropolished. The sputtering of the enriched uranium marker onto the cubes was accomplished in a vacuum bell-jar with a glow discharge in 25-μ argon pressure using 30 to 50 ma at 2.2-2.6 kv. Although there was not any way of measuring the actual thickness of the sputtered films, previous experiments would indicate that, under the conditions used, the films of enriched uranium were approximately 1 μ thick. In the second approach this 1-μ film of enriched uranium was covered with several microns of normal uranium.

The samples were oxidized at 200°C in 200 mm oxygen. The oxidation was continued to approximately 1000 μg/cm², or a thickness of 8 μ, assuming ideal density and uniform oxidation.

The oxidized samples were hand polished on 2/0 emery paper and one face of the cube was counted with an alpha-beta-gamma proportional counter after successive polishing strokes. Although this polishing technique was only semiquantitative, experience indicated that approximately four strokes removed 1 μ of oxide. The shape of the curve obtained by plotting counts per minute vs. number of strokes (Fig. 4) clearly indicates the location of the marker in each case.

Discussion of Results

Each of two types of marker experiments demonstrate conclusively that ~~oxygen~~ oxygen, rather than ~~uranium~~ uranium, diffuses through the oxide layer during the course of oxidation at 200°C in 200 mm oxygen.

In the metallographically determined marker experiment, all of the observations indicate an absence of uranium diffusion through the oxide. The most noteworthy of these observations are: (*a*) the lack of tendency for the oxide to grow up around the Inconel binding wire; (*b*) the lack of fusion of the

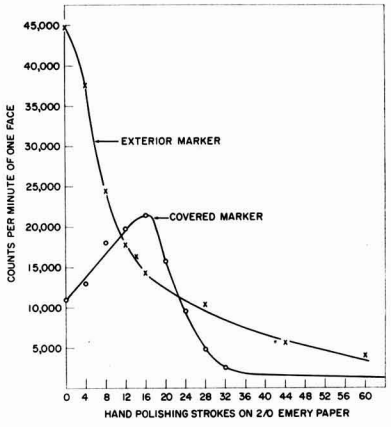

Fig. 4. Activity within the oxide layer: enriched uranium marker experiment.

oxides layers impinging on each other; and (c) the notch in the oxide which occurs at an edge of the cube.

Both approaches to the radioactive marker experiment also demonstrate that oxygen is the diffusing species since uranium diffusion would have caused the active marker to be distributed throughout the exterior oxide. In the first case, the initially exterior enriched uranium marker remained on the outside surface and was readily polished off. In the second case, the covered enriched marker remained covered and in a narrow band. The uniform increase of activity as the sample was polished would be expected as the alpha-absorbing oxide was removed from the enriched marker.

Acknowledgment

The authors wish to express their indebtedness to S. Rothmann of the Metallurgy Division, Argonne National Laboratory, for his aid in the uranium sputtering technique.

Manuscript received Feb. 29, 1960. Work was performed under the auspices of the U. S. Atomic Energy Commission.

Any discussion of this paper will appear in a Discussion Section to be published in the June 1961 JOURNAL.

REFERENCES

1. A. O. Dravnieks and H. J. McDonald, *J. (and Trans.) Electrochem. Soc.*, **93**, 177 (1948).
2. J. Chirigos and D. E. Thomas, WAPD-53 (1952).
3. C. E. Birchenall, *Ind. Eng. Chem.*, **46**, 893 (1954).
4. O. Kubaschewski and B. E. Hopkins, "Oxidation of Metals and Alloys," pp. 85-86, Academic Press, Inc., New York (1953).
5. J. Bardeen, W. H. Brattain, and W. Shockley, *J. Chem. Phys.*, **14**, 714 (1946).
6. O. Kubaschewski, *loc cit.*, p. 207.
7. H. Inouye, ORNL-1565 (1953).

Surfaces: Leveling Phenomena

Further Studies of Leveling Using Radiotracer Techniques

Seward E. Beacom and Bernard J. Riley

Research Laboratories, General Motors Corporation, Warren, Michigan

In a previous paper (1), it was shown by radiotracer techniques that the organic addition agent, sodium allyl sulfonate, which imparts leveling characteristics to a bright nickel plating solution, is preferentially adsorbed onto the peaks of an irregular surface. This was considered to be verification of a part of leveling theory which assumes that the leveling process is initiated by this preferential adsorption on peaks.

The cathodes, which were machined to exhibit a surface of alternate peaks and valleys, had rather large peak-to-peak separations (0.16 cm) and peak-to-valley heights (0.077 cm). Because of questions which have been raised about making interpretations based on cathodes of these dimensions, it seemed important to determine experimentally the limit to which this concept of preferential adsorption could be extended. Thus, a series of machined cathodes of decreasing surface roughness has been prepared and plated in solutions containing the addition agent tagged with S-35. Within the limits of the techniques available, the results show that the concept of preferential adsorption may be extended to include those surfaces which more nearly approach a microprofile dimension.

To establish further the reliability of the results being reported, it was considered desirable to show that the radioactivity observed in the deposits comes from the pure S-35 isotope only and not from some other radioactive impurity. Also, it seemed necessary to show, by an exchange study, that the observed activity comes directly from the sulfonate part of the tagged addition agent and not indirectly by way of an exchange with the sulfate ions present in the plating bath. The results of the investigation demonstrate that the observed activity is due to the presence of pure S-35 and that it comes directly from the sulfonate group.

Experimental and Results

Radiochemical purity of sodium allyl sulfonate.—Several samples of sodium allyl sulfonate tagged with S-35 were prepared (1) and the chemical purity verified by infrared analysis.

To assure that there was no complicating radiochemical impurity present in the compound, decay measurements were carried out over a period of approximately eight months. The agreement of the experimentally obtained half-life value of 87.4 days with the accepted published value of 87 days indicated that, within the limits of counting statistics, there was no appreciable radioactive impurity present.

As further evidence of the presence of pure S-35, a determination of the energy value of the isotope was obtained using the standard technique of the absorption curve. The average half-thickness corresponded to an energy of 0.172 Mev as calculated from the published range energy value (2). This energy agrees, within experimental error, with the literature value of 0.167 Mev.

Plating cell.—Some trouble with stirring patterns, edge effects, and addition agent depletion had been experienced with the 80 ml cell used previously (1). A new round cell, 13.97 cm in diameter by 8.89 cm high, and holding a liter of plating solution, was constructed from Lucite. To accommodate the anode and cathode, slots 2.54 cm wide by 0.32 cm deep were cut vertically into opposite sides of the cell. When used with a propeller stirrer rotating at 100 rpm, edge effects and stirring patterns have been virtually eliminated, and many plating runs can be made before addition agent depletion becomes serious.

Further work on grooved cathodes.—The surface features of representative machined cathodes, as well as the Precision Reference Specimens of Surface Roughness (3), are recorded in Table I. The sulfa-

Table I. Cathode data

Cathode	Machined cathodes Peak-to-peak separation, cm	Peak-to-valley height, cm	Number of peaks/cm of width
A	0.058	0.028	17
B	0.086	0.043	12
Precision reference-specimens of surface roughness			
SR(350)[a]	0.039	0.0041	26
SR(125)[b]	0.0096	0.0011	102

[a] 350-μin. average roughness.

[b] 125-μin. average roughness.

Table II. Plating, counting, and autoradiographic data

Foil No.	Cathode	Foil thickness, cm	Counts, cpm/cm^2 Top[a]	Bottom[b]	Exposure time, hr	Detail
87	A	0.0049	3885	3197	25	Good
81	B	0.0052	4732	5137	25	Excellent
85	SR(350)	0.0054	4170	3416	93	Excellent
86	SR(125)	0.0054	4914	4870	93	No detail

Bath composition and plating conditions: nickel sulfate, 300 g/l; nickel chloride, 30 g/l; boric acid, 30 g/l; proprietary wetting agent, 5 ml/l; sodium allyl sulfonate (total) 2 g/l; N-allyl quinaldinium bromide, 4 mg/l; pH of 3.0; temperature, 60°C; mild agitation; current density, 7 amp/dm^2; activity in bath, 1.1 × 10^6 cpm/ml of solution.

[a] Surface of foil next to solution during plating.

[b] Surface of foil next to grooved cathode during plating.

mate nickel-plated brass cathodes of known roughness were cleaned, passivated, and then plated in the radioactive plating bath. The plate was removed as a foil which was thoroughly rinsed, dried, and retained for examination of radioactivity (1). A summary of the plating conditions and the counting and autoradiographic data is given in Table II. All autoradiography was done with Eastman Kodak Autoradiographic A film. Figure 1 is the autoradiogram and densitometer trace for foil number 85 which was chosen as representative of the results obtained. It is apparent from this autoradiogram that

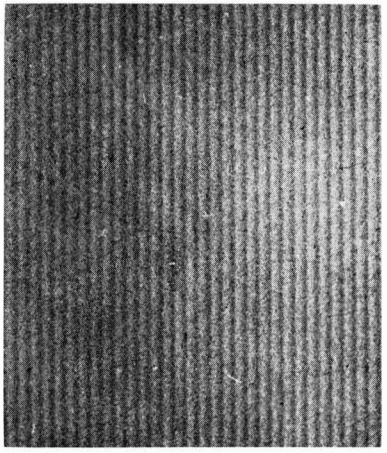

Fig. 1a. Autoradiogram of the bottom of foil number 85 with 26 peaks/cm of width.

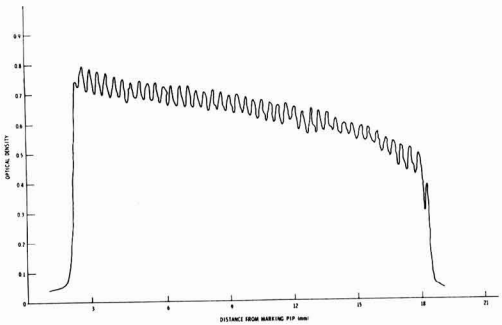

Fig. 1b. Densitometer trace of the autoradiogram shown in Fig. 1a.

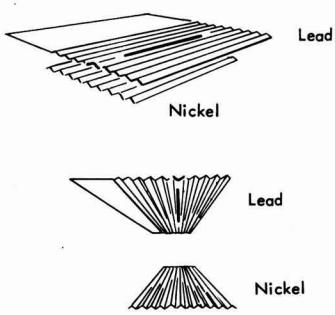

Fig. 2. Sketch of slitted lead foil counting arrangement. The heavy line on the accented peak locates the slit.

the degree of surface roughness does not affect the results within the limits of resolution of the film. Due to this limitation, however, it has not been possible to obtain a satisfactory autoradiogram from the 125-μin. specimen.

Figure 2 shows a stylized sketch of the slit-counting arrangement which has been used to supplement autoradiography (1). Matching slitted lead foils were prepared for the machined cathodes listed in Table I. Data from the counting profiles of portions of the foils, as shown in Table III, also indicate preferential adsorption on the peaks. It was not possible

Table III. Lead slit counting data

Peak	Top Recess	Cathode A Bottom Obverse of peak	Bottom Obverse of recess
301	240	219	200
316	279	257	254
305	281	347	323
291	232	278	301
294	293	395	326
286	270	359	308
425	327	383	315
		Cathode B	
692	664	720	685
642	514	628	555
570	568	652	502
535	524	679	517
521	494	569	576
487	484	637	534
549	493	553	528
499	484	536	527

Table IV. S-35 tagged sulfate plating and counting data

Foil No.	Activity, cpm/ml of soln.	Counts Top[a]	Counts Bottom[b]	Counts per minute/cm² Top[a]	Counts per minute/cm² Bottom[b]
93	7.5×10^5	58	69	6	7
94	7.5×10^5	52	56	6	6
95	1.5×10^6	86	97	9	10
96	1.5×10^6	89	86	9	9
97	3.0×10^6	165	181	18	19
98	3.0×10^6	144	152	15	16
99	6.0×10^6	238	280	25	30
100	6.0×10^6	240	260	25	28

[a] Surface of foil next to solution during plating.

[b] Surface of foil next to cathode during plating.

to prepare slitted lead foils for examination of the Precision Reference Specimens of Surface Roughness.

Sulfate ion exchange.—Using S-35 tagged sulfate (as H_2SO_4), 1 in.² steel shim stock samples were plated under conditions identical to those used with the S-35 tagged sodium allyl sulfonate. The radioactive H_2SO_4, with a specific activity of 50 mc/ml, was added in increasing amounts to the bright nickel plating bath. The starting concentration of 7.5×10^5 cpm/ml of plating solution represented an activity which was close to that used for the S-35 tagged sodium allyl sulfonate experiments. A summary of the results is given in Table IV. At an activity level of 1.5×10^6 cpm of the tagged sulfate per milliliter of plating solution, approximately 9 cpm/cm² of sulfate pickup is observed. This is compared with the 5000 cpm/cm² pickup from the tagged sodium allyl sulfonate at the same level of activity. It appears from the small amount of sulfate activity recovered that the exchange reaction, if it occurs at all, must be quite negligible, and that the source of activity found in the deposits comes directly from the sulfonate and not by exchange from the sulfate ions. The very low remaining activity due to sulfate may result from a slight general surface adsorption of sulfate ion.

Discussion

The concept of the preferential adsorption of addition agents on the peaks of irregular surfaces which is verified experimentally in this work is additional support for results previously reported (1). It seems likely that this adsorption produces at least in part the polarization effects, noticed by other investigators, which may lead to the leveling phenomenon.

Experimental work in this laboratory has shown that leveling occurs on surfaces which have an average surface roughness of 125, 50 and 20 μin. If leveling theory is correct, then it seems reasonable to assume that preferential adsorption also occurs on the peaks of these surfaces which possess a more nearly microprofile dimension. It appears that only experimental difficulties have prevented verification of this assumption.

Manuscript received March 16, 1960.

Any discussion of this paper will appear in a Discussion Section to be published in the June 1961 JOURNAL.

REFERENCES

1. S.E. Beacom and B. J. Riley, *This Journal*, **106**, 309 (1959).
2. C. Coryell and N. Sugarman, "Radiochemical Studies: The Fission Products," Vol. I, p. 18, McGraw-Hill Book Co., Inc., New York (1951).
3. J. D. Thomas, *Proc. Am. Electroplaters' Soc.*, **43**, 60 (1956).

Electrochemiluminescence at a Silicon Anode in Contact with an Electrolyte

Allen Gee

Semiconductor Division, Texas Instruments Inc., Dallas, Texas

In the study of stain films on single-crystal silicon, emission of light has been observed during the anodic oxidation of the film. This film can be formed from the substrate either electrochemically when HF is the electrolyte by the method of Turner (1) or chemically by the method of Archer (2). This note deals principally with the chemically formed film designated as Type I amorphous silicon by Archer because luminescence is more easily observed.

Experimental

A slice of 5 ohm-cm, boron-doped, p-type silicon having 1.2 cm² of its 111 face exposed is sealed with wax to the bottom of a polyethylene cell. Two ohmic contacts to the silicon are made on the under side. After the cell is filled with electrolyte, a platinum electrode and a saturated calomel electrode are inserted from the top. A constant current source is connected between one ohmic contact and the platinum electrode. The voltage between the other ohmic contact and the calomel electrode is fed to a recorder.

Before forming the film, the chemically polished surface of the silicon is treated for a few seconds with a slow etch (10 volumes 70% HNO_3 to 1 volume 49% HF) and then thoroughly rinsed with water. The film is grown by treatment with a 49% HF solution containing about 0.1% HNO_3 until a blue interference color is visible.

Results

With almost any neutral or acid electrolyte, the voltage of the film-covered silicon electrode at constant anodic current increases with time in the manner shown in Fig. 1. The plateau between 0.5 and 1 v represents a region where ready oxidation occurs. Visible light is emitted in the last half to the last fourth of this region, and passivation, indicated by

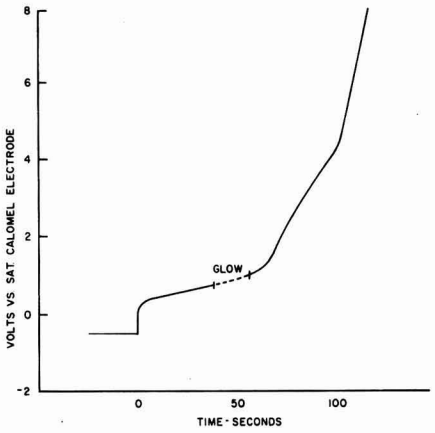

Fig. 1. Voltage of 5 ohm-cm p-type silicon anode coated with Type I film in 1M H_2SO_4. Current density, 1.6 ma/cm^2 after time zero. Period of luminescence shown on curve.

the sharp voltage rise, always sets in as soon as the luminescence disappears. On the same scale, a film-free silicon electrode gives a near vertical trace.

The faint, reddish glow usually starts at a single point, expands to cover the entire surface, and then contracts to a point away from the area where it started. On some occasions, various areas of the surface glow successively. The luminescence is responsive to short pulses of current, and the pattern of glow is not changed by current interruptions. Color of the emitted light has not been found to vary perceptibly and is not a function of the electrolyte. In subdued lighting, a rather bright flash is seen when the current density is 10 ma/cm^2. In near darkness, a prolonged glow is detectable at 0.2 ma/cm^2.

Attempts to obtain quantitative data to correlate with such parameters as the thickness of the film (2) have been disappointing. For many measurements, the entire plateau of Fig. 1 corresponds to the passage of 30-100 millicoulomb/cm^2. Within such wide limits, the exact procedure for forming the film is not critical.

Luminescence occurs in any indifferent electrolyte such as 1M solutions of KCl, LiCl, H_2SO_4, HNO_3, and acetic acid. Basic solutions (such as 1M NH_4OH), as well as 1M KF, or 20% NH_4HF_2 dissolve the film so that the film-free characteristics are obtained. When the electrolyte is HF, no luminescence or passivation occurs, but light is emitted when the electrolyte is 0.5M KF in acetic acid buffer.

Treatment of the film with most oxidizing agents (dilute solutions of dichromate, permanganate, copper salts; 30% H_2O_2, 70% HNO_3, Br_2 vapor) decreases the amount of oxidizable materials as measured anodically and reduces or eliminates the luminescence. Neutral or acid persulfate and reducing agents in general have little effect. Allowing the film to dry in room air for 16 hr does not alter its properties.

The emission of light accompanies anodic oxidation and is not the result of local heating. By making contact to the film with mercury instead of an electrolyte, current can be passed through the film without evidence of glow. Passage of 25 ma/cm^2 through the film in either direction for several minutes does not produce any significant change in the subsequent anodic behavior.

The original blue film becomes scarcely visible after anodic treatment. A fresh amorphous silicon film can be grown without etching off the anodized film. When formed in this manner, normal anodic behavior is observed except that the interference colors are now only slightly affected. Unlike the original film, the anodized film seems not to dissolve in dilute bases with evolution of gas even though there is a slight change in appearance.

Passage of cathodic currents until hydrogen evolution is visible has little effect on the original film and does not reduce the anodized film. A p-type semiconductor electrode is known (1, 3) to offer lower resistance to current flow in the anode direction. Application of 60 cycle power instead of d.c. to the silicon electrode produces the same luminescence effect for a comparable level of rectified current.

The amorphous silicon film formed anodically in 49% HF simply by shorting the silicon to a platinum electrode exhibits different and more erratic properties. Luminescence has been detected only at current densities greater than 5 ma/cm^2 and sometimes not at all.

Luminescence has not been observed on film-covered n-type silicon. Since only a few samples of silicon have been examined, no definite statement relating the phenomenon to the nature of the substrate can yet be made. Further efforts are directed toward locating the region within the film from which light is emitted and toward elucidating the mechanisms involved.

Manuscript received April 29, 1960.

Any discussion of this paper will appear in a Discussion Section to be published in the June 1961 JOURNAL.

REFERENCES

1. D. R. Turner, *This Journal*, **105**, 402 (1958).
2. R. J. Archer, Second Conf. on Semiconductor Surfaces, Washington, D. C., Dec. 1959.
3. W. H. Brattain and C. G. B. Garrett, *Bell System Tech. J.*, **34**, 129 (1955).

A PNP High-Frequency Silicon Transistor

W. A. Little

Texas Instruments Inc., Dallas, Texas

NPN high-frequency silicon transistors were described originally by Tanenbaum and Thomas (1), and more recently a switching transistor was described by Aschner, *et al.* (2). The need for complementary-type switching transistors has led to the development of a PNP silicon double-diffused transistor which is described, in this paper. The essential features of this transistor are shown in Fig. 1. Solid-state diffusion techniques are used to obtain the high degree of control required for high-frequency devices. Oxide masking techniques are used to provide exposed emitter and base areas at the surface and to control the emitter geometry. Contact of the exposed regions is obtained by evaporated metal stripes. Electrical characteristics of transistors prepared in this manner are described.

Fabrication

Transistors are fabricated by starting with 1-3 ohm-cm p-type silicon wafers that have been lapped and optically polished flat to provide a uniform surface. An n-type layer with a surface concentration of between 10^{17} and 10^{19} atoms/cm^3 is diffused into the parent p-type material to a depth of 4-5 μ. This is accomplished by an open-tube diffusion process similar to the one described by Frosch and Derick (3). Red phosphorus is used as a diffusant to obtain these values of surface concentration.

This base layer diffusion actually is done in two steps as is shown schematically in the diagram of Fig. 2, which is adapted from Fig. 2 of Aschner, *et al.* (2). First, a thin concentrated n-layer is deposited on the silicon wafer. In the second step, the source of phosphorus is removed from the combustion tube and wet oxygen is used to grow an oxide layer 5000-8000Å thick. During this time, the n-layer is diffused into the wafer to the desired depth.

The purpose of the oxide layer is to provide a mask against the subsequent emitter diffusion on portions of the exposed surface where direct contact to the base region is required. In order to produce the selective mask to accomplish this, a photographic process is used to remove the oxide selectively. This is the same type of process that is used to form the etched wiring of printed circuit boards. A photosensitive liquid, termed the resist, is applied to the surface of the oxidized silicon wafer. Upon drying, this liquid forms a thin photosensitive coating which adheres strongly to the oxide coating of the wafer. The resist coating may then be exposed using ultraviolet light and contact printing, through an ordinary film negative which contains the desired pattern. The resist is then developed in trichloroethylene. The portions of the resist that were protected by the opaque regions of the film negative

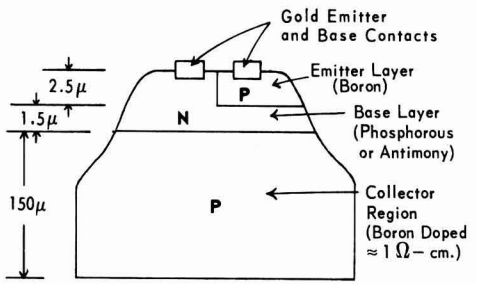

Fig. 1. Geometry of PNP transistor

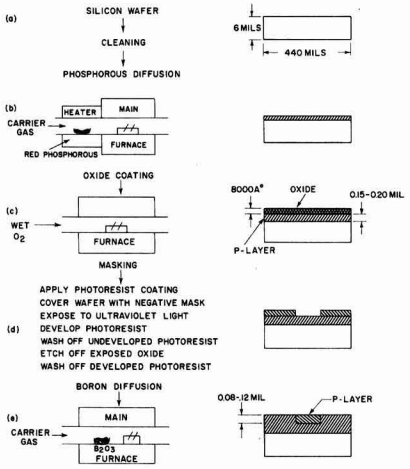

Fig. 2. Detail of diffusion and oxide masking techniques

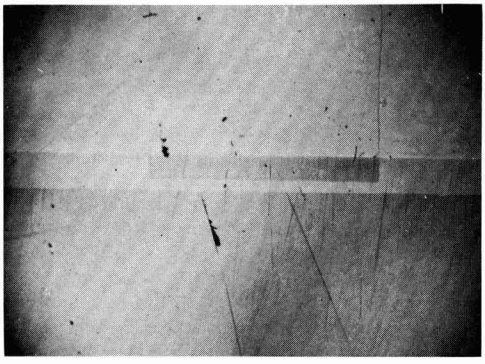

Fig. 3. Photomicrograph of an oxide masked double-diffused wafer. The junctions have been exposed by bevel lapping and polishing at an angle of about 5° and staining the p regions.

and, hence, were not exposed to the ultraviolet light, are washed away by the developer. The resist pattern thus forms a protective coating over the oxide which limits the attack of etches to those regions not covered by the resist. If the sample is placed in a weak etch, the oxide in these regions will be removed completely down to the silicon substrate. Then the developed resist can be removed easily with an organic solvent, leaving the desired oxide diffusion mask. In addition to producing extremely sharp, well-defined patterns the photo resist process allows a quick and simple method of changing device geometry merely by changing the film negative pattern. In the evaluation units fabricated to date, a simple bar pattern has been used, ultimately leading to a wafer having alternate base and emitter regions exposed.

After the wafer has been prepared with the oxide mask of suitable geometry, a diffused p-type layer 2 μ to 3 μ deep with a surface concentration of approximately 10^{20} atoms/cm^3 is superimposed on the n-layer. This is accomplished by means of an open tube diffusion process in which the source of diffusant (boric acid) was placed in the furnace beside the silicon wafers.

To illustrate the degree of control obtained in this process, a photomicrograph is shown in Fig. 3. This was made by lapping and polishing the wafers at an angle of five degrees to the surface and staining the emitter and collector with a hydrofluoric-nitric acid etch (4) to delineate the junctions clearly. In Fig. 3 it can be seen that the collector and emitter junctions are quite planar. Also, any imperfections are much less than the layer thicknesses. This photograph shows the alternately exposed emitter and base regions produced by oxide masking. Interference microscopy (5) techniques were used in measuring the thickness of the thin diffused layers.

The next step is the metal evaporation of emitter and base stripes through a mask. In order to secure proper placement of the metal stripes, the evaporation mask must be indexed with respect to the negative mask used in preparing the wafers for emitter diffusion. Close control of the vacuum deposition is necessary to secure placement of the stripes on the desired area about 0.5-1 mil from the line marking the boundary between base and emitter.

After alloying the gold emitter and base stripes in an r.f. heater at about 750°-850°C, the squares are ready for mesa masking and etching. The remainder of the fabrication process follows standard procedures for dicing of squares into individual units, bonding the collector to the header, bonding leads to the base and emitter stripes, and encapsulating the units. Figure 4 is a photomicrograph of a completed device showing emitter and base stripes and the bonded leads.

Electrical Characteristics

Electrical characteristics of a PNP silicon high-frequency transistor prepared by the techniques described above are presented here. During fabrication of experimental devices, base widths were deliberately varied from about 1 to 2 μ. The characteristics described below are for an intermediate

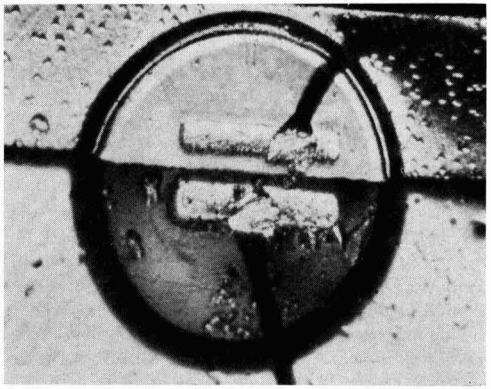

Fig. 4. Photomicrograph of completed unit showing the gold stripes and bonded leads.

base width of 1-½ μ. In such a device, typical collector-base breakdown voltage was of the order of 35 v, while the emitter-base breakdown voltage was 9 v. At a typical d-c bias condition of 10 ma emitter current, with collector-base voltage $V_{CB} = 6$ v, the d-c forward current transfer ratio h_{FE} was 35, and the d-c forward voltage drop V_{BE} was of the order of 0.8 v.

High-frequency characteristics of a typical device are illustrated by Fig. 5. The common-emitter current transfer ratio h_{fe}, shown as a function of frequency, decreases inversely with increasing frequency to a value of 1 at a frequency (f_T) of 200 mc. Common-emitter input resistance $R_e(h_{ie})$, also shown in Fig. 5, decreases with increasing frequency and appears to approach a limiting value of the order of 45 ohms at high frequencies. Hence, this value can be taken as essentially equal to the high-frequency base resistance of the unit. Collector transition capacitance at a reverse bias of 6 v is approximately 3 pf, whereas the emitter transition capacitance (at reverse bias of 3 v) is somewhat larger—3.8 pf. This reflects the fact that, even though the emitter-base area is less than the collector-base area, the emitter-base junction gradient is considerably steeper than that at the collector-base junction.

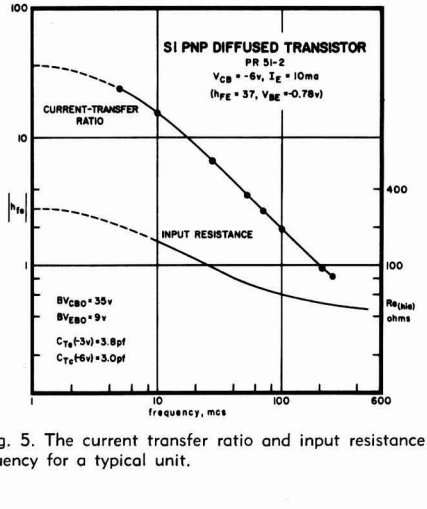

Fig. 5. The current transfer ratio and input resistance vs. frequency for a typical unit.

Acknowledgments

The writer is grateful for the helpful discussions and suggestions of R. L. Pritchard, and wishes to thank Jay W. Lathrop, L. E. Barnes, and R. L. Martin for assistance with experiments. Thanks are also due to George Pierson for measuring the parameters for the experimental transistors.

Manuscript received March 24, 1960. This paper was presented at the Washington, D. C., Meeting of Electron Devices, 1959.

Any discussion of this paper will appear in a Discussion Section to be published in the June 1961 JOURNAL.

REFERENCES

1. M. Tanenbaum and D. E. Thomas, *Bell System Tech. J.*, **35**, 1 (1956).
2. J. F. Aschner, C. A. Bittmann, W. F. Hare, and J. J. Kleimack, *This Journal*, **106**, 415 (1959).
3. C. J. Frosch and L. Derick, *ibid.*, **104**, 547 (1957).
4. C. S. Fuller and J. A. Ditzenberger, *J. Appl. Phys.*, **27**, 544 (1956).
5. W. L. Bond and F. M. Smits, *Bell System Tech. J.*, **35**, 1209 (1956).

Technical Review

Report of the Chlor-Alkali Committee of the Industrial Electrolytic Division for the Year 1959

Nelson J. Ehlers

Columbia-Southern Chemical Corporation, Pittsburgh, Pennsylvania

Clifford A. Hampel

Skokie, Illinois

Chlorine-Caustic

Production and Sales

Chlorine and caustic soda production in the U. S. was at an all-time high in 1959. With about 4,285,000 ton production of chlorine, the increase above 1958 was nearly 19%. U. S. capacity as reported by The Chlorine Institute was near 14,100 TPD at the end of the year, which means the industry operated at 83% of capacity in 1959. Apparent per capita consumption was 48.2 lb, an all-time high and double that of 1949.

After a substantial chlorine production increase in 1959, it is felt by many that prospects for future growth are good. Recent publicized estimates of growth indicate from 7 to 8.5% per year growth from 1960 to 1970. Another source estimates an increase of 70% in chlorine and 50% in caustic soda during the ten-year period.

Canadian chlorine production in 1959 was about 287,000 tons as compared to 268,000 in 1958. Indications are that about 305,000 tons will be produced in 1960.

Caustic soda production in the U. S. increased 17% above 1958, for a total of about 4,675,000 tons in 1959. The apparent per capita consumption was 50.0 lb, an all-time high, which was nearly twice that of 27.3 in 1949. Lime soda caustic production data are not available, but it is estimated such production was some 300,000 to 325,000 tons for the year.

Even though caustic is being converted to soda ash on a relatively small scale, soda ash continues to be converted to lime soda caustic. Some sources believe that caustic was more in excess during 1959 than in the previous year.

Table I. U.S. sources of chlorine

	1959 (preliminary)		1958	
	Tons	%	Tons	%
Cl_2 equiv. of NaOH	3,997,200	93.3	3,319,042	92.1
Cl_2 equiv. of KOH	58,900	1.4	48,736	1.3
Cl_2 equiv. of Na	172,500	4.0	169,857	4.7
Cl_2 equiv. (others) *	56,400	1.3	66,903	1.9
Cl_2 total gas produced	4,285,000	100.0	3,604,538	100.0

* By difference.

About 75% of the capacity of chlorine in 1959 was in diaphragm cells, 19% was in mercury cells, 5% in sodium cells, and less than 1% in nonelectrolytic processes. Two-thirds of the capacity added in 1959 was in diaphragm cells and one-third in mercury cells.

Estimated sources of chlorine comparing 1959 with 1958 appear in Table I.

New Plants and Expansions

U. S. chlorine capacity increases amounted to about 760 TPD in 1959 as compared to 640 TPD in 1958, and are believed to be as shown on p. 792.

Diamond Alkali completed modernization of facilities at Painesville, Ohio, using Diamond diaphragm cells to replace Tucker-Windecker cells, while Frontier Chemical at Wichita, Kans., completed modernization using Hooker S-3B cells. Chlorine producing plants of Gulf at Port Arthur, Texas, and West Virginia Pulp & Paper at Luke, Md., were shut down in January 1959.

Increased facilities for 1960 and 1961 are believed to be as shown on p. 792.

1959 Increase

Company	Site	Type Cells	Quantity, TPD
Diamond Alkali Co.	Deer Park, Texas	DeNora Mercury Cells	200
Jefferson Chemical Co.	Port Neches, Texas	Hooker S-3B Cells	150
Stauffer Chemical Co.	Niagara Falls, N. Y.	Hooker S-3M Cells	30
Weyerhaeuser Timber Co.	Longview, Wash.	DeNora Mercury Cells	80
Wyandotte Chemicals Corp.	Geismar, La.	Diamond Diaphragm Cells	300

1960-61 Increase

Company	Site	Type Cells	Quantity
Dow Chemical Co.	Plaquemine, La.	—	Expansion
Food Machinery & Chemical Corp.	S. Charleston, W. Va.	Hooker S-3B	Modernization and modest expansion
Hooker Chemical Corp.	Niagara Falls, N. Y.	Uhde Mercury	100 TPD
Kolker Chemical Corp.	Newark, N. J.	Hooker S	50 TPD
Olin Mathieson Chemical Corp.	McIntosh, Ala.	Mathieson (E-11) Mercury	125 TPD
Olin Mathieson Chemical Corp.	Niagara Falls, N .Y.	Mathieson (E-11) Mercury	About 50% increase
Pennsalt Chemicals Corp.	Wyandotte, Mich.	Gibbs	Modernization
Stauffer Chemical Co.	Henderson, Nev.	Hooker S	45 TPD

An estimate of chlorine capacity by companies appeared in the *Chemical & Engineering News,* December 14, 1959, p. 38.

The Canadian capacity at the end of 1959 is estimated by The Chlorine Institute of about 950 TPD. Western Chemicals Ltd., Duvernay, Alta., brought a 20 TPD diaphragm cell expansion on line in 1959. Consolidated Mining & Smelting Co. has announced plans for construction of a $2.6 million chlorine-alkali plant at Trail, B. C. Canadian Industries Ltd. has announced conversion of a number of mercury cells from NaOH to KOH. Pennsalt is apparently firming up its plans for a plant in the Vancouver, B.C., area.

Markets and End-Use Patterns

There does not appear to have been a major change in the end-use patterns for chlorine and caustic during 1959. The use of chlorine dioxide for bleaching in the pulp and paper industry is gaining in importance and is affecting chlorine usage.

The present use of chlorine in the extraction of titanium, zirconium, hafnium, columbium, and tantalum suggests the need for serious consideration of its use in the recovery of other metals. DuPont is using titanium tetrachloride for the production of titanium dioxide at its New Johnsonville, Tenn., plant. The general interest in this use for titanium tetrachloride could lead to a substantial use of chlorine in the future.

Table II. Chlorine—caustic soda end-use pattern*

Chlorine	%	Caustic soda	%
Chemicals	80.7	Chemicals	32.4
Pulp & paper	15.9	Rayon, film	14.9
Sanitation	3.2	Pulp & paper	11.4
Others	0.2	Soap, cleaners	6.0
		Petroleum refining	5.4
		Textiles	5.4
		Net exports	5.3
		Others	19.2
Total	100.0	Total	100.0

* Courtesy of Diamond Alkali Co.

The end-use pattern of caustic remains quite diversified. The alkali industry is watching the nylon-rayon battle for supremacy in the tire industry. Rayon remains the largest single use of caustic soda. The further application of caustic in the pulp and paper industry looks promising.

Table II gives a recent estimated end-use pattern for chlorine and caustic soda in 1959.

Technical Developments

With recent price reductions in power rectification units of silicon and germanium, the trend toward this type of unit will continue, especially where cell amperages are high and circuit voltages are low.

The interest of industry in platinum-titanium anodes for diaphragm and mercury cells continues. Articles of interest appeared in *Chemical Week,* December 12, 1959, p. 67, and *Chemical Week,* December 26, 1959, p. 50. The patent situation is not yet clear. Test installations exist but it is doubtful if any chlorine producer in the U. S., Canada, or England has made a decision at present for a large-scale installation.

For the first time in the U. S., liquid chlorine is being transported from a producer to a consumer in a tank truck (see *Chemical Week,* March 19, 1960, p. 31). Barge shipments of chlorine to large consumers on the Gulf and Atlantic shores, as well as on inland waterways, continue to increase.

The Chlorine Institute, Inc., continues a most aggressive program for the safe handling of chlorine in transportation and in producing and consuming plants.

Monsanto Chemical Co. continues to offer the DeNora cell for recovery of chlorine from hydrochloric acid. Although considerable interest has been shown, it is doubtful if a large-scale installation has been initiated at present.

Among articles of interest appearing recently, which have not otherwise been cited, were: "Chlorine Output Hits New High," *Chemical & Engineering News,* Dec. 14, 1959, p. 38; "Confidence Keys Chlorine Makers Outlook," *Chemical Week,* March 7, 1959, p. 113; "Chemical Forecast—1964," Chemical Market Research Association Report—*Oil,*

Paint & Drug Reporter, Sept. 28, 1959, pp. 44 and 47; "Alkalis and Chlorine Industry—Outlook for 1960 and Review of 1959," *U. S. Dept. of Commerce, BDSA, Chemical & Rubber Div.,* ER-59-86; "Cell Users Get New Fuel for Old Debate," *Chemical Week,* March 5, 1960, p. 95; "Graphitized Anodes in the Electrolysis of Aqueous Chloride Solutions," V. V. Stender and O. S. Ksenzhek, *J. Applied Chem., USSR,* **32** (1), 111 (1959);[1] "Influence of Electrolyte Composition on the Distribution of Current Inside a Graphite Anode and on Its Internal Wear," B. M. Bulygin, *J. Applied Chem., USSR,* **32** (1), 122 (1959).[1]

Among U. S. patents of interest which issued recently are: 2,868,711, electrolytic cell; 2,870,074, electrolysis of alkali metal chloride brine; 2,872,291, process and apparatus for the decomposition of alkali metal amalgams; 2,872,403, electrolytic cell; 2,884,-310, production of alkali metal hydroxides by ion exchange; 2,887,448, fused salt cell; 2,898,284, mercury cathode chlorine cell; 2,919,238, fused salt electrolytic cells.

Soda Ash

The U. S. production of soda ash increased about 13% from 1958 to 5,611,600 tons in 1959, thus reversing the downward trend since 1956. The only year of higher production was in 1956. The apparent per capita consumption was 61.6 lb for 1959, which was equal to the average of the years 1949 to 1959 inclusive. It is evident the per capita consumption of soda ash has not changed since the early 1940's. The U. S. industry operated at about 80% capacity in 1959; 12.7 % of the production was "natural soda" and 87.3% was "synthetic."

Diamond Alkali is engaged in a modernization program of its soda ash producing facilities at Painesville, Ohio. Dow Chemical Co. continues to operate its plant at Freeport, Texas, converting electrolytic caustic to soda ash. Dow is reported to be studying the possibility of increasing its capacity to produce soda ash. Considerable interest in the trona deposits in Wyoming has been indicated by several producers and potential producers of soda ash. Food Machinery & Chemical Corp. continues to expand in soda ash in Wyoming, and capacity is now in the 550,000 ton per year range.

Miscellaneous Chemicals

Potassium hydroxide.—Production of KOH (88-92%) increased about 21%, from 76,870 tons in 1958 to 92,869 tons in 1959. The trend toward high-purity KOH from mercury cells continues.

Chlorates.—The American Potash and Chemical Corp. began an expansion of its sodium chlorate facilities at Aberdeen, Miss., which will increase capacity to 25,000 tons per year. Hooker Chemical Corp. placed an additional circuit on line at its Columbus, Miss., plant, bringing capacity there to over 24,000 tons per year. Pennsalt Chemicals Corp. announced plans to expand its Portland, Oreg., sodium chlorate plant by 25%. The formation of the Penn-Olin Chemical Corp. was announced with the intent to construct a 25,000 ton per year sodium chlorate plant at Calvert, Ky. The new plant of Standard Chemical Ltd. at Beauharnois, Que., was placed in operation during late 1959. A review of markets for chlorates and perchlorates during 1958 and 1959 was published in *Chemical and Rubber,* August 1959.

Sodium chlorate production in 1959 was 87,665 tons, which was an increase of about 30% above the 67,249 ton production in 1958. Production has more than doubled since 1954.

Perchlorates. —Continued interest in solid-fueled missiles and the use of ammonium perchlorate as an oxidizer led to the announcement of plans by Pennsalt Chemicals Corp. to expand its plant at Portland, Oreg., by several thousand tons per year. During 1960, the Navy declared the ammonium perchlorate plant at Henderson, Nev., which is operated by the American Potash and Chemical Corp., as surplus to its needs, and arrangements are being made for disposal.

Miscellaneous Metals

Aluminum.—The production of aluminum in this country continues to grow. The primary production in 1959 of 1,953,000 tons set a new record; it was 25% above 1958 and 16% above 1956, the previous peak year for aluminum. Canada showed a decrease of 46,000 tons, or 7% less than 1958 production, during the past year.

At the end of 1959, total domestic capacity amounted to 2.4 million tons. New production facilities in 1959 included: (*a*) Ormet Corp. started its fifth and last pot line at its 180,000 ton per year plant at Clarington, Ohio; (*b*) Kaiser Aluminum & Chemical Corp. installed two new lines to complete its 145,000 ton per year plant at Ravenswood, W. Va.; and (*c*) Reynolds Metals Co. completed three lines at its new plant at Massena, N. Y., each having a capacity of 33,000 tons per year.

New aluminum prices established in December are 26¢ per lb for pig and 28.1¢ per lb for ingot.

Magnesium.—Consumption of primary magnesium reached about 44,000 tons in 1959, an increase of some 25% over 1958. While primary production of magnesium has been increasing steadily since 1958, the production rate of some 3,000 tons per month at the end of the year is still less than the consumption rate, although this production rate will be increased during 1960.

Alabama Metallurgical Corp., a new producer, began production of magnesium by the ferrosilicon reduction of dolomite last fall. This year, it should reach its anticipated capacity of 6 to 7,000 tons per year. The company is jointly owned by Calumet & Hecla and Brooks & Perkins.

The brightest possibility for significant expansion of the nonmilitary use of magnesium lies in its use in the engines of the lightweight automobiles. Expectations are that total consumption of primary magnesium will reach 45-50,000 tons in 1960, but the automotive die-casting outlet may cause an increase above this figure.

Sodium.—The production of sodium reached 112,-019 tons in 1959, only slightly more than the 1958 output and still much less than the 133,000 tons made in 1957. It is evident that with the production

[1] Reference pages of the English translation.

capacity at about 200,000 tons per year, the sodium industry faces for some time to come the problem of idle plant capacity.

Titanium.—During the first half of 1959, production and consumption of titanium sponge were at rates slightly greater than the 1958 average annual rate. In the second half of 1959, the steel strike cut the consumption of titanium sponge, and the production rate dropped accordingly. Imports of titanium sponge were about three quarters of the 1958 rate. In spite of the handicap of the steel strike, production of mill products increased. According to BDSA, in the near future consumption of titanium mill products will be reduced because of the cancellation of some defense aircraft programs which would have consumed substantial quantities of mill products. The growing use of titanium in construction of civilian aircraft, in missiles, and in the chemical process industries will only partly compensate for this loss. Therefore, consumption and production of titanium mill products in 1960 may be lower than in 1959. Growth in these uses and in other civilian applications is confidently expected in the future. Recently, ICI mentioned growth in the use of titanium in surgical implants, and suggests the use of titanium in nuclear applications because of the rapid dissipation of radioactivity which is formed when titanium is exposed to intense radiation. The development of new titanium alloys with improved qualities continues at a high rate.

An article of interest appears in *Chemical Engineering,* Feb. 22, 1960, p. 66

The Bureau of Mines and the Business and Defense Services Administration report the following figures:

	Sponge			Mill Products
	Production tons	Imports tons	Consumption tons	Shipments tons
1955	7,398	567	4,145 (est.)	1,898
1956	14,595	2,048	10,936	5,166
1957	17,249	3,532	8,221	5,658
1958	4,585	2,072	4,147	2,594
1959*	3,898	1,563	3,953	3,211

* Based on estimate, 10 months.

Zirconium.—The three companies, Carborundum Metals Co., Mallory-Sharon Metals Corp., and Columbia-National Corp., continue to supply zirconium sponge to the Atomic Energy Commission under contract. Columbia-National temporarily discontinued operations in December, 1959, because of a sponge quality problem with the AEC. The production of these three producers remains a little above 2,200,000 lb per year, and no future expansion of sponge producing facilities is planned at the present time.

Manganese.—The consumption of manganese metal derived by the electrolytic process amounted to 12,732 tons in 1959. This quantity would have been greater but for the long steel strike which began in July. At that time, the consumption had reached about 9,000 tons. Over 80% of this metal is used in the preparation of steel ingots, chiefly of the stainless variety.

Lithium.—The drastic cutback in the preparation of boron high-energy fuels caused the cessation in the production of lithium, as intermediate in the process, at the Olin Mathieson Chemical Corp. plant at Model City, N. Y. This plant had sufficient capacity to be a major producer of lithium by the electrolysis of fused lithium chloride admixed with potassium chloride in Downs type cells.

Beryllium.—Pure beryllium metal is made in the United States by the reduction of beryllium fluoride with magnesium. Both producers, Brush Beryllium Co. and Beryllium Corp., reported higher production of the metal in 1959 over 1958. It is estimated that production reached about 150,000 lb in 1959, compared with 50,000 lb in 1958, and it is expected that the figure will approach 300,000 lb in 1960 (*Chemical Week,* Feb. 20, 1960). Chief outlets for beryllium are in nuclear and space applications.

Chromium.—The electrolysis of ammonium chromium sulfate solution continues to be the premier source of the highest purity chromium metal. Production in 1959 probably reached about 2,000 tons, the reported capacity of the Union Carbide Metals Co.'s Marietta, Ohio plant.

Tantalum and columbium.—Tantalum production was estimated to be well over 300,000 lb in 1959, a sizable increase over the 1958 figure. Most of the metal is obtained either by the electrolysis of fused potassium fluotantalate or by sodium reduction of this and other tantalum compounds. Most of the metal is consumed in electronic applications, chiefly as capacitors. The production and use of columbium, found in all tantalum ores, are still small, probably around 60,000 lb in 1959.

Prices for tantalum were cut toward the end of the year. Capacitor grade powder dropped to $49.80 per lb from $58.60, and sheet tantalum is priced at $59.16 per lb.

Manuscript received May 31, 1960. This paper was prepared for delivery before the Chicago Meeting, May 1-5, 1960.

Any discussion of this paper will appear in a Discussion Section to be published in the June 1961 JOURNAL.

ECS Houston Meeting, October 9-13, 1960

Plans have been completed for the Fall Meeting of The Electrochemical Society to be held in Houston, Texas, from October 9 through 13, 1960, at the Shamrock Hilton Hotel. The complete program for the meeting appeared in the August JOURNAL, pp. 169C-194C.

Members of the Houston Convention Committee, under the General Chairmanship of Oliver Osborn, are: Ray M. Hurd, College Relations; Alvan E. Richey, Entertainment; C. S. Templeton, Finance; John Loeffler, General Arrangements; Emily Osborn, Ladies' Activities; Roy Post, Membership; E. J. Williams, Plant Trips; Frank Evans, Publicity; Ralph J. Hach, Registration.

Symposia Chairmen Breakfasts

From Monday through Thursday, October 10-13, special breakfasts will be held for symposia chairmen. On the day on which he presides at a technical session, each chairman should be in the Normandy Room, third floor of the hotel. A special table will be set up each morning at 7:45 A.M. Menu prices will prevail.

Sunday Deep Sea Fishing Trip

Plans have been made for a day of fishing 12 to 60 miles out in the Gulf, starting very early Sunday morning, October 9. Return to the Freeport dock will be about 5:00 or 6:00 P.M.

Sunday Evening Mixer

The Local Committee has arranged a two-hour, get-acquainted gathering for Sunday, October 9, in the Grecian Room, just off the lower lobby from the North Promenade of the hotel, from 6:00 to 8:00 P.M. All those registered for the meeting are invited to attend. Beer, soft drinks, and snacks will be served. Mixed drinks can be obtained from the bar. Admission will be by registration badge.

Monday Evening Cocktail Party and Barbecue

On Monday, October 10, a Society Mixer in combination with a traditional Texas-Style Barbecue and Equestrian Display will be held, on and around the Shamrock Hilton's triangular adjoining lawns, beginning promptly at 5:00 P.M. For those who desire, an assortment of refreshments will be available immediately on arrival; these will include cold drinks and coffee, as well as the usual cocktails. Barbecue and other food will be served at 6:00 P.M., followed by the performance of the famous Harris County Sheriff's Mounted Posse. Come early to share in the fun and entertainment at this party.

Oliver Osborn

Tuesday Acheson Medal Reception and Banquet

A Society reception honoring the recipient of the Edward Goodrich Acheson Gold Medal and Prize, Dr. Henry B. Linford, professor of chemical engineering, Columbia University, New York City, will be held on Tuesday, October 11, in the Grecian Room, at 6:30 P.M. Cocktails and soft drinks will be served. The banquet, in the Connecting Emerald Room, will begin at 7:30 P.M. The award will be presented during the banquet, after which Dr. Linford will deliver the Acheson Medal Address.

Division Luncheons and Business Meetings

The Battery Division Luncheon and Business Meeting will be held on Tuesday, October 11, at 12:30 P.M., on the glass-enclosed Terrace of the Shamrock Hilton.

The Electronics Division, Semiconductor Group Luncheon will be held on the same date and time in Castillian Room B & C, third floor.

The Electrodeposition Division Luncheon and Business Meeting will be held on Wednesday, October 12, at 12:30 P.M., on the glass-enclosed

Shamrock Hilton Hotel, Main at Holcombe Blvd., Houston, Texas.

Terrace, while, on the same date and at the same time, the Corrosion Division Luncheon and Business Meeting will take place in Castillian Room B & C, third floor.

Board and Committee Meetings that Include Luncheons and Receptions

The Electrochemical Society's Board of Directors will meet on Sunday October 9, at 12:30 P.M. in Castillian Room B & C, third floor, for a reception and cocktails. A buffet luncheon will be served promptly at 1:00 P.M. in the connecting Normandy Room. Following luncheon, the business meeting will take place at 2:00 P.M. in Castillian Room B & C.

On Monday, October 10, in Castillian Room A, a luncheon and business meeting of the Membership Committee will take place at 12:15 P.M.

The General Chairmen of Future Meetings will be served a luncheon at 12:00 M. in Castillian Room A on Wednesday, October 12, at which time they will conduct a business meeting.

Student Round Table and Reception

A round-table discussion will be conducted for the benefit of the visiting invited students and their faculty members attending the convention. This will take place on Wednesday, October 12, at 3:00 P.M., in the Normandy Room, third floor. Following the student round table, a reception and mixer will take place at 5:00 P.M. in Castillian Room B and C.

Speakers Special Breakfast

On Sunday, October 9, at 7:30 A.M., in Castillian Room A, breakfast will be served to symposia speakers. Menu prices will prevail.

Plant Trips

A novel plant inspection awaits those who visit the Diamond Alkali Corp. chlorine plant at Deer Park, on October 11. The group will board the Port of Houston's Inspection Boat, the "Sam Houston," and travel for over an hour down the Houston Ship Channel, passing many chemical plants, refineries, and process industries that form one of the most heavily industrialized areas in the South.

Disembarking at Deer Park, the group will inspect the diaphragm and deNora mercury cell rooms and the utility department of the Diamond plant.

On Wednesday, a bus trip will be made to Freeport to visit the Dow Chemical Co. A general tour of the plant will be made, and the cell rooms of the magnesium reduction plant will be visited. Following inspection of the sea-water magnesium plant, a barbecue will be served. The visitors will return to Houston Wednesday evening.

Ladies' Program

Hospitality Headquarters for the ladies will be the Nile Room, third floor. There will be daily coffee hours, and morning programs on Tuesday and Thursday. Most afternoons will be left open for individual activities.

In addition, the ladies are cordially invited to attend all of the general functions.

Swimming

The Shamrock Hilton's facilities include a magnificent Olympic-sized swimming pool. The fall weather may be as hot as mid-summer—ideal for relaxing in and around the pool —so be sure to bring a swim suit.

Poolside Hawaiian Luau Party at the Shamrock Hilton

Section News

Council of Local Sections

The following are the newly elected officers of the Council of Local Sections of the Society for the 1960-1961 term:

Chairman—A. J. Cornish (Pittsburgh)
Vice-Chairman—J. C. White (Washington)
Secretary—R. F. Bechtold (San Francisco)
Representative on Board of Directors— N. C. Cahoon (Cleveland), two-year term (1960-1962).

M. F. Quaely (New York) continues as Representative on Board of Directors (1959-1961).

Midland Section

The following have been elected officers of the Midland Section of the Society for the term June 1, 1960 through May 30, 1961:

Chairman—M. R. Bothwell, 13 Erie Court, Midland, Mich.
Vice-Chairman—D. Chapin, 3400 Bay City Rd., Midland, Mich.
Secretary-Treasurer—C. K. Bon, 2916 Swede Rd., Midland, Mich.
Councilor—R. S. Karpiuk (1960-1962).

P. F. George continues as the other Councilor (1959-1961).

Pittsburgh Section

The annual spring symposium of the Pittsburgh Local Section was held on June 17 at the Westinghouse Research Laboratories. This one-day symposium was the fourth technical meeting of the 1959-1960 season.

Westinghouse provided luncheon and a demonstration of the growing of germanium dendrites. The technical program consisted of six papers:

"Some Structural Problems Concerned with Disorder and Super-Structure in Wurtzite and Zinc Blende Mixed Valence Compounds" by G. A. Jeffery, University of Pittsburgh.

"The Growth of Dendrites" by J. W. Faust, Jr., and H. F. John, Westinghouse Research Labs.

"The Growth of Oxide Films on Tin" by W. E. Boggs, U. S. Steel Corp., Applied Research Lab.

"Some Studies of Metal-Hydrogen

Systems" by W. E. Wallace and R. S. Craig, University of Pittsburgh.

"Dissolution Kinetics at Dislocation Sites in Lithium Fluoride" by M. B. Ives and P. J. Hearth, Carnegie Institute of Technology.

"The Permeability of Solid Aluminum to Hydrogen" by C. N. Cochran, Alcoa Research Labs.

The following officers of the Section were elected for the 1960-1961 season:

Chairman—J. W. Faust, Jr., Westinghouse Electric Corp., Beulah Rd., Churchill Boro., Pittsburgh 35, Pa.

Vice-Chairman—W. E. Haupin, Alcoa Research Labs., P. O. Box 772, New Kensington, Pa.

Secretary-Treasurer—E. J. Smith, National Steel Corp., Research and Development Dept., Weirton, W. Va.

Committeemen—A. J. Cornish, Westinghouse Research Labs., Beulah Rd., Churchill Boro., Pittsburgh 35, Pa. (1960-1961); E. H. Phelps, U. S. Steel Corp., Applied Research Labs., Monroeville, Pa. (1960-1962).

W. E. Haupin,
Secretary-Treasurer (1959-1960)

San Francisco Section

The third meeting of the 1959-1960 season was held on January 27, 1960 at the University of California Men's Faculty Club. The speaker was Dr. William D. Smiley, director of research and development of Tempress Research Co., Inc. His subject was "Recent Developments in High-Temperature Materials."

Dr. Smiley discussed the relationship between structure and properties of various materials used for high-temperature applications. Included among the materials discussed were the special alloys, high-purity oxides, some of the refractory metal carbides, unusual intermetallic compounds, and the graphite and diamond forms of graphite.

The speaker at the fourth meeting was Dr. Clinton M. Kelley, chairman of the Chemical Physics Dept., Stanford Research Institute. The meeting was held at the Faculty Club on March 16, 1960. Dr. Kelley's topic was "Thermoelectric Generation of Power."

Dr. Kelley first discussed the theory and physical basis of the thermoelectric effects. The materials involved and certain applications of thermoelectric devices were described.

Dr. Scott Lynn, research engineer, Dow Chemical Co., was the speaker at the final meeting, held May 25, 1960. Dr. Lynn's talk was on "Effect of Geometry on Current Distribution in Industrial Electrolytic Cells."

Dr. Lynn described the results of his mathematical analysis of the distribution of current over the electrode surface. Relationships between the distribution and rational cell design were discussed.

The following have been elected officers of the San Francisco Section for the 1960-1961 term:

Chairman—Robert E. De La Rue, Stanford Research Institute, Menlo Park, Calif.

Vice-Chairman—Worden Waring, Fairchild Semiconductor Corp., 844 Charleston Rd., Palo Alto, Calif.

Secretary—H. F. Stout, Columbia-Geneva Steel Div., U. S. Steel Corp., Pittsburg, Calif.

Treasurer—J. E. Chilton, Stanford Research Institute, Menlo Park, Calif.

Councilors—R. F. Bechtold, 3725 Bon Homme Way, Concord, Calif. (1960-1961); R. A. Lewis, 27140 Moody Rd., Los Altos, Calif.

R. E. De La Rue, *Chairman*

Southern California-Nevada Section

The fifth regular meeting of the Section was held on June 7, 1960 at the Rodger Young Auditorium in Los Angeles. The speaker of the evening was Dr. Robert A. Osteryoung, of Atomics International, whose topic was "An Electrochemical Study of Uranium in Fused Chlorides." Dr. Osteryoung described in detail the experimental techniques for the measurement at 450°C of the standard electrode potentials for U(III) — U(0) and for U(IV) —U(III) in the $MgCl_2$ — Nacl — KCl eutectic, also for U(IV) — U(III) and UO_2(II) — UO_2(0) in the LiCl — KCl eutectic. Polarographic studies which were carried out on the behavior of U(III), U(IV), and UO_2(II) in the LiCl — KCl eutectic were outlined. The speaker concluded by briefly discussing the significance of the foregoing results with respect to a processing scheme for a liquid bismuth metal fuel reactor.

Newly elected officers of the Southern California-Nevada Section for the 1960-1961 term are:

Chairman—Matt E. Carlisle, Northrop Corp., Norair Div., Hawthorne, Calif.

Vice-Chairman—George A. Larchian, Hughes Products, Semiconductor Div., Box 278, Newport Beach, Calif.

Secretary-Treasurer—Lahmer Lynds, Atomics International, Canoga Park, Calif.

Manuscripts and Abstracts for Spring 1961 Meeting

Papers are now being solicited for the Spring Meeting of the Society, to be held at the Claypool Hotel in Indianapolis, Ind., April 30, May 1, 2, 3, and 4, 1961. Technical sessions probably will be scheduled on Electric Insulation, Electronics (including Luminescence and Semiconductors), Electrothermics and Metallurgy, Industrial Electrolytics, and Theoretical Electrochemistry.

To be considered for this meeting, triplicate copies of abstracts (*not exceeding 75 words in length*) must be received at Society Headquarters, 1860 Broadway, New York 23, N. Y., *not later than January 2, 1961. Please indicate on abstract for which Division's symposium the paper is to be scheduled and underline the name of the author who will present the paper.* Complete manuscripts should be sent in triplicate to the Managing Editor of the JOURNAL at the same address.

Presentation of a paper at a technical meeting of the Society does not guarantee publication in the JOURNAL. However, all papers so presented become the property of The Electrochemical Society, and may not be published elsewhere, either in whole or in part, unless permission for release is requested of and granted by the Editor. Papers already published elsewhere, or submitted for publication elsewhere, are not acceptable for oral presentation except on invitation by a Divisional program Chairman.

Councilors—W. M. Hetherington, Pacific Semiconductors, Inc., Culver City, Calif.; William F. Seyer, 474 Halvern Dr., Los Angeles 49, Calif.

G. A. Larchian,
Secretary-Treasurer (1959-1960)

Division News

Spring 1961 Symposium on Instrumentation

For the Spring Meeting of The Electrochemical Society in Indianapolis, Ind., April 30 to May 4, 1961, the Theoretical Electrochemistry Division is planning to organize a Symposium on "Modern Instrumentation and Techniques of Electrochemical Measurements."

The emphasis of this symposium will be on subjects like electrical circuitry for transient and steady-state experiments, instrumentation for determination of true surface areas of solid electrodes, microscopy and electron microscopy, single crystals in electrochemistry, purification of electrochemical systems, instrumentation for electrochemical calorimetry, transference numbers, and various other electrochemical quantities of interest to theoretical electrochemists.

Further information can be obtained from the Secretary of the Theoretical Division, Dr. Paul Rüetschi, Head, Electrochemistry Div., Carl F. Norberg Research Center, Electric Storage Battery Co., Yardley, Pa.

New Members

In July 1960, the following were elected to membership in The Electrochemical Society by the Admissions Committee:

Active–Sustaining Members

R. M. Hexter, Ovitron Corp., 37-05 48th Ave., Long Island City 1, N.Y. (Electronics)

Arno Stupel, Industro Transistor Corp., 35-10 36th Ave., Long Island City 6, N.Y. (Electrothermics & Metallurgy)

R. M. Wilson, Delco-Remy Div., General Motors Corp., Anderson, Ind. (Battery)

Active Members

Irving Adams, USASRDL; Mail add: 173 Garden St., Cranford, N.J. (Electronics)

P. P. Anthony, Columbia-Southern Chemical Corp.; Mail add: 188 Franks Ave., Wadsworth, Ohio (Industrial Electrolytic, Theoretical Electrochemistry)

J. E. Astier, Station d'Essais de l'IRSID, Maiziereslès Metz, Moselle, France (Electrothermics & Metallurgy)

C. D. Atkinson, E. I. du Pont de Nemours & Co., Inc.; Mail add: 3207 Swarthmore Rd., Wilmington 6, Del. (Electronics)

T. E. Ban, McDowell-Wellman Co., Vulcan Bldg., 113 St. Clair, Cleveland, Ohio (Electrothermics & Metallurgy)

R. P. Bastian, Republic Aviation Corp.; Mail add: 64 Bryan Ave., Amityville, L.I., N.Y. (Electronics)

K. A. Berberian, Sperry Semiconductor Div., Sperry Rand Corp.; Mail add: Box 26, New Canaan, Conn. (Electronics)

H. B. Berman, Engelhard Industries; Mail add: 26 Glenwood Rd., Hicksville, L.I., N.Y. (Corrosion, Industrial Electrolytic)

G. J. Biefer, Mines Branch, 568 Booth St., Ottawa, Ont., Canada (Corrosion)

F. L. Blake, Motorola, Inc.; Mail add: 455 W. 3 St., Scottsdale, Ariz. (Electronics)

J. W. Bowman, Northwestern Steel and Wire Co., Ave. B & Wallace St., Sterling, Ill. (Electrothermics & Metallurgy)

J. H. Braun, E. I. du Pont de Nemours & Co., Inc.; Mail add: 2316 Knowles Rd., Wilmington 3, Del. (Electronics)

R. J. Brumbaugh, Electric Storage Battery Co.; Mail add: Box 334A Coach Rd., R. D. #1, Langhorne, Pa. (Battery)

John Burnham, Ti-Tal, Inc.; Mail add: 10960 Verano Rd., Los Angeles 24, Calif. (Electric Insulation)

Battery Extended Abstracts, Houston Meeting

The Battery Division is making available an extended abstracts booklet containing 1000-word abstracts of most of the papers to be presented at the Division's symposia at the Houston Meeting of The Electrochemical Society, October 1960.

Copies of the booklet can be obtained from C. H. Clark, 34 Pleasant Way, Deal, N. J., after September 15, for $2.00 each.

Allan Carlson, Clevite Research Center, 540 E. 105 St., Cleveland 8, Ohio (Electronics)

H. E. Carlton, Battelle Memorial Institute; Mail add: 799 Kenworth Rd., Columbus 24, Ohio (Electrothermics & Metallurgy)

D. K. Chatterjee, Sen-Raleigh Industries of India Ltd., Po Asansol (West Bengal), India (Electrodeposition)

J. R. Conner, Jr., Allegheny Ludlum Steel Corp., Research Center, Brackenridge, Pa. (Corrosion)

J. A. Crumley, Jr., Aeronutronics, Div. of Ford Motor Co.; Mail add: 289 Camellia Lane, Costa Mesa, Calif. (Electronics)

W. J. Engel, Hughes Semiconductors; Mail add: 6504½ West Ocean Front, Newport Beach, Calif. (Electronics)

Herman Erkku, Aluminum Co. of Canada Ltd.; Mail add: 542 Normandie, Apt. 2, Arvida, Que., Canada (Electrothermics & Metallurgy, Industrial Electrolytic, Theoretical Electrochemistry)

P. S. Fay, Standard Oil Co. (Ohio); Mail add: 1163 Churchill Rd., Lyndhurst 28, Ohio (Industrial Electrolytic)

M. W. Ford, Philco Corp., Lansdale Tube Div.; Mail add: 123 Goldengate Rd., Levittown, Pa. (Electronics)

M. G. Gandel, Lockheed Aircraft Corp.; Mail add: 1885 Ednamary Way, Mountain View, Calif. (Industrial Electrolytic)

M. P. Grotheer, Columbia-Southern Chemical Corp., Corpus Christi, Texas (Industrial Electrolytic)

C. C. Habeger, Eagle-Picher Co.; Mail add: 1610 Washington Dr., Miami, Okla. (Electronics)

J. M. Harris, Sylvania Electric Products Inc., 60 Boston St., Salem, Mass. (Electronics)

P. L. Hawkes, Associated Electrical Industries (Woolwich) Ltd., Research Lab., West Rd., Templefields, Harlow, Essex, England (Battery, Electric Insulation, Electrodeposition, Electronics, Electrothermics & Metallurgy, Theoretical Electrochemistry)

W. A. Henry, Fansteel Metallurgical Corp.; Mail add: 6338 Pershing Blvd., Kenosha, Wis. (Electrothermics & Metallurgy)

F. E. Hill, Westinghouse Electric Corp.; Mail add: 1514 Pennsylvania Ave., Irwin, Pa. (Electronics)

J. M. Hirshon, Philco Corp., Lansdale Div., Lansdale, Pa. (Electronics)

J. R. Horacek, Diamond Alkali Co.; Mail add: 2107 Harper Dr., Pasadena, Texas (Industrial Electro-

lytic, Theoretical Electrochemistry)

W. P. Hornberger, General Instrument Corp., Semiconductor Div.; Mail add: 200 Haven Ave., New York 33, N.Y. (Electronics)

K. E. Johnson, University of Illinois, Dept. of Chemistry, Urbana, Ill. (Theoretical Electrochemistry)

Theodore Katan, Lockheed Missiles & Space Div.; Mail add: Box 5222, Stanford, Calif. (Battery)

L. L. Knapp, Aluminum Co. of America; Mail add: R. D. 1, Box 602, New Kensington, Pa. (Industrial Electrolytic)

G. D. Kopperl, Sprague Electric Co.; Mail add: Canterbury, N. H. (Electronics)

Zenon Kurpisz, Standard Telephones and Cables, Rectifier Div.; Mail add: 1, The Gowers, Harlow, Essex, England (Electronics)

J. H. Legg, Consulting Metallurgical Engineer, 162 Bedbrooke Ave., Montreal West, Que., Canada (Electrothermics & Metallurgy)

I. A. Liberman, Zenith Radio Corp., 6001 W. Dickens Ave., Chicago 39, Ill. (Electronics, Theoretical Electrochemistry)

Wilbur Liebson, U.S. Army, Research & Development Labs.; Mail add: 6738 Bestwick Dr., Springfield, Va. (Electronics)

R. L. Longini, Westinghouse Electric Corp., Research Labs., Pittsburgh 35, Pa. (Electronics)

R. A. Maglio, Solid State Products, Inc.; Mail add: 15 Victor Ave., Beverly, Mass. (Electronics)

R. F. Meehan, Monsanto Chemical Co.; Mail add: 830 Audubon Dr., Clayton 5, Mo. (Electronics)

J. C. Meyer, RT&E Corp.; Mail add: 119 N. 92 St., Wauwatosa 13, Wis. (Battery, Electric Insulation, Industrial Electrolytic)

E. E. Millaway, Titanium Metals Corp. of America; Mail add: 1604 E. St. Louis, Las Vegas, Nev. (Industrial Electrolytic)

G. T. Miller, Jr., Hampden-Sydney College, Box 146, Hampden-Sydney, Va. (Corrosion)

S. P. Mitoff, General Electric Co., Research Lab., The Knolls, Schenectady, N.Y. (Electric Insulation)

V. D. Mochel, Corning Glass Works, Research Lab., Corning, N.Y. (Electronics)

Willem Oser, Institute of Gas Technology, 17 W. 34 St., Chicago 16, Ill. (Battery, Electrodeposition, Electro-Organic, Industrial Electrolytic, Theoretical Eectrochemistry)

B. R. Pagel, Texas Instruments, Inc., Device Research, P.O. Box 1079, Dallas, Texas (Electronics)

Ann M. Parks, International Business Machines Corp.; 177 White Plains Rd., Apt. 9T, Tarrytown, N.Y. (Electric Insulation)

Victor Medina, Patterson Moos Div., Leesona Corp.; Mail add: 232 Frankel Bvd., Merrich, L.I., N.Y. (Battery, Electrodeposition, Theoretical Electrochemistry)

J. H. Pearson, Allied Chemical Corp., Box 405, Morristown, N.J. (Electrothermics & Metallurgy)

F. A. Pizzarello, Hughes Aircraft Co., Semiconductor Div.; Mail add: 18071 Norwood Park, Tustin, Calif. (Electronics)

P. E. Poppert, Bendix Aviation Corp.; Mail add: P.O. Box 552, Mantoloking, N.J. (Electronics)

Bernard Rabinovitch, Fairchild Semiconductor Corp.; Mail add: 3436 Green Rd., Palo Alto, Calif. (Electronics)

Alexander Rajczi, Joseph Lucas (Aust.) Pty. Ltd., Nepean Highway, Cheltenham, Victoria, Australia (Battery)

A. A. Rasch, Eastman Kodak Co., Research Lab., Kodak Park, Rochester, N. Y. (Electrodeposition, Theoretical Electrochemistry)

H. W. Rathmann, Vanadium Corp. of America; Mail add: Cedar Hills, Route 3, Cambridge, Ohio (Electrothermics & Metallurgy)

A. K. N. Reddy, Central Electrochemical Research Institute, Karaikudi 3 (S. Ry.), South India (Electrodeposition, Theoretical Electrochemistry)

T. B. Reddy, University of Illinois, 314 Noyes Lab., Urbana, Ill. (Theoretical Electrochemistry)

R. A. Rightmire, Standard Oil of Ohio; Mail add: 1064 Thistle-Ridge Dr., Twinsburg, Ohio (Theoretical Electrochemistry)

A. G. Robiette, Metallurgical Consultant, Bury Farm, Bovington, Herts., United Kingdom (Electrothermics & Metallurgy)

J. C. Rubin, John E. Fast & Co.; Mail add: 1458 S. Hasse Ave., Westchester, Ill. (Electric Insulation)

T. O. Ryland, A. O. Smith Corp., Long Range Research, 3533 N. 27 St., Milwaukee, Wis. (Theoretical Electrochemistry)

E. M. Savitski, Metallurgical Institute, Academy of Science, Leninskii Prospekt 49, Moscow, U.S.S.R. (Electrothermics & Metallurgy)

R. F. Scarr, Union Carbide Consumer Products Co., Research Center, 12900 Snow Rd., Parma 30, Ohio (Battery, Theoretical Electrochemistry)

Herman Schneider, Sprague Electric Co.; Mail add: 72 N. State St., Concord, N.H. (Electric Insulation, Electronics)

J. W. Shepard, Minnesota Mining & Manufacturing Co., 900 Bush Ave., St. Paul 6, Minn. (Electronics)

Leonard Stein, General Electric Co.; Mail add: 104 Village Dr., Syracuse 6, N.Y. (Electronics)

A. J. Stone, Battelle Memorial Institute, Process Metallurgy Research Div., 505 King Ave., Columbus 1, Ohio (Electrothermics & Metallurgy)

K. S. Tarneja, Westinghouse Electric Corp., Adv. Dev. Section, Youngwood, Pa. (Electronics, Electrothermics & Metallurgy)

G. H. Timmings, Sun Capacitors, 2554 W. Lawrence Ave., Chicago 25, Ill. (Electric Insulation, Electrothermics & Metallurgy)

M. F. Tomaino, McGraw-Hill Publishing Co.; Mail add: 786 Bronx River Rd., Bronxville 8, N.Y. (Battery, Corrosion, Electric Insulation, Electrodeposition, Electronics, Electro-Organic, Electrothermics & Metallurgy, Industrial Electrolytic, Theoretical Electrochemistry)

R. P. Totah, Westinghouse Electric Corp., Semiconductor Div., Youngwood, Pa. (Electronics)

W. W. Trainor, Titanium Alloy Div., National Lead Co.; Mail add: 611 Ferry Ave., Niagara Falls, N.Y. (Electrothermics & Metallurgy)

J. G. Tschinkel, United Aircraft Corp., Pratt & Whitney Div.; Mail add: 94 Brown St., Hamden, Conn. (Theoretical Electrochemistry)

Govind Vazirani, Scientific Control Labs., Inc.; Mail add: 5222 S. Kenwood Ave., Chicago 15, Ill. (Electro-Organic)

By action of the Board of Directors of the Society, all prospective members must include first year's dues with their applications for membership.

Also, please note that, if sponsors sign the application form itself, processing can be expedited considerably.

Notice to Members and Subscribers
(Re Changes of Address)

To insure receipt of each issue of the JOURNAL, please be sure to give us your old address, as well as your new one, when you move. Our records are filed by states and cities, not by individual names. The Post Office does not forward magazines.

R. L. von Hohenleiten, National Carbon Co., 270 Park Ave., New York 17, N.Y. (Industrial Electrolytic)

Jiro Wantanabe, OKI Electric Industry Co., Ltd., Research Lab., 4-1 Nishishibaura, Minato-ku, Tokyo, Japan (Electric Insulation)

Bernard Yurash, Fairchild Semiconductor Corp.; Mail add: 3385 Stockton Place, Palo Alto, Calif. (Electronics)

Associate Members

A. V. Gregory, Raytheon Manufacturing Co., Semiconductor Div., 150 California St., Newton, Mass. (Electronics, Electrothermics & Metallurgy)

D. H. Jurden, Strategic-Udy Metallurgical & Chemical Processes Ltd., P.O. Box 262, Niagara Falls, Ont., Canada (Electrothermics & Metallurgy)

Henry Kressel, Radio Corp. of America; Mail add: 964 Aurora St., Highland Park, N.J. (Electronics)

Willem Lambrechtse, General Electric Research Lab.; Mail add: 1511 Rugby Rd., Schenectady 8, N. Y. (Electric Insulation)

L. G. F. Ljungberg, Sandvik Steel Works Co., Ltd., Dept. TFH, Sandviken, Sweden (Corrosion)

Student Associate Members

R. C. Ayers, Jr., University of Texas, Chemistry Bldg., Rm. 126, Austin, Texas (Theoretical Electrochemistry)

J. D. Hervey, Hiram College; Mail add: Box 325, Hiram, Ohio (Electro-Organic)

R. J. Sutch, Fenn College; Mail add: 143 Chestnut St., Painesville, Ohio (Industrial Electrolytic)

Reinstatements to Active Membership

Derick Hartshorn, Jr., Enthone, Inc.; Mail add: 45 Elm Ave., Larchmont, N.Y. (Corrosion, Electrodeposition, Electrothermics & Metallurgy)

Joseph Parker, Diamond Alkali Co.; Mail add: 154 Briar Hill Dr., Painesville, Ohio (Industrial Electrolytic)

J. S. Peake, Minnesota Mining & Manufacturing Co.; Mail add: 43 Pheasant Lane, North Oaks, White Bear Lake 10, Minn. (Corrosion)

B. L. Vondra, Jr., Nuclear Materials & Equipment Corp.; Mail add: 420 Arch St., Greensburg, Pa. (Electrodeposition, Electrothermics & Metallurgy, Industrial Electrolytic)

Lawrence Whitby, Lockheed Aircraft Co., Missiles & Space Div.; Mail add: 357 Everett Ave., Palo Alto, Calif. (Corrosion)

Transfer from Student to Active Membership

G. E. Walrafen, Bell Telephone Labs., Inc.; Mail add: 479 South St., Murray Hill, N.J. (Theoretical Electrochemistry)

Deceased Member

C. W. Henson, 2nd, Worcester, Mass.

Book Reviews

Progress in Dielectrics, Vol. 1. Edited by J. B. Birks and J. H. Schulman. Published by John Wiley & Sons, Inc., 1960. 312 + IX pages; $11.00.

As the name implies, this is a compilation of the results of research in various aspects of dielectric materials. The first several chapters deal principally with dielectric breakdown of liquids, solids, and gases, and associated phenomena. There is a chapter on the properties of barium titanate, another on non-oxide ceramic dielectrics such as the nitrides of boron, silicon, and aluminum, and, finally, a chapter on electrophoretic deposition of insulating materials, a technique having interesting possibilities for applying insulation to conductors.

This is the first volume of a series which the editors hope will be continued by publishing succeeding volumes annually. The volume is unusually well documented; the bibliography for each chapter is quite extensive. This reviewer feels that it is a valuable textbook for scientists and engineers interested in dielectric materials; however, its usefulness as a reference work is impaired somewhat by omission of an index.

W. McMahon

Mechanical Properties of Intermetallic Compounds. A Symposium held by the Electrothermics and Metallurgy Division during the May 1959 meeting of The Electrochemical Society in Philadelphia. Edited by J. H. Westbrook. Published by John Wiley & Sons, Inc., New York, 1960. 435 pages; $9.50.

Intermetallic compounds long have been familiar as dispersed constituents in conventional alloys. Their structures, formation energies, and bond characters remain the objects of considerable attention as demonstrated in the 1955 American Society for Metals Seminar in Philadelphia and the 1958 National Physical Laboratory Symposium. In contrast, extensive interest in their mechanical behavior has developed only recently in response to the pressure for better high-temperature structural materials and stimulated by the hot strengths many of the compounds possess. The difficulty, as with ceramics, has been the absence of room temperature ductility. Interest in this area and in compound semiconductors has occasioned the present Symposium, which contains 17 papers, mostly original and including contributions by Soviet, Japanese, British, and German authors.

The Symposium starts with a most useful review by the editor which synthesizes what is known of the features and mechanisms of the mechanical behavior of intermetallic compounds. About half the other papers describe experimental studies of the preparation and properties of particular compounds or series of them. Some of these represent attempts at systematic exploration of mechanical properties as functions of temperature, composition, and other variables, with the apparent goal of revealing characteristic behavior patterns which will guide future efforts. Russian workers have been at this for some time. This phenomenological approach has now yielded a relatively substantial body of information on compound properties but has failed to disclose any key to the brittleness problem, and there is no indication that anyone has stumbled over a compound of practical high-temperature value. In this field, special interest attaches to fabrication and test techniques which are described in a number of the papers and in two dealing specifically with extrusion and testing. Most of the remaining contributions have some bearing on mechanisms of deformation and fracture— domain structure in CuAu, slip patterns of superlattice alloys, a review of the interaction between dislocations and the superlattice, effect of mode of deformation on the electrical properties of InSb, microscopy of fracture surfaces in NiAl and Ni_3Al. It is remarkable that nowhere outside the opening review does one find discussion or speculation, let alone enlightenment, concerning the central problem—what are the mechanisms of deformation and fracture which make these compounds brittle at ordinary temperatures and ductile only at sufficiently high temperatures; in this respect, the Symposium was a "dud." The value of this volume is, in part, that it records the results of some notable original work and, perhaps in greater part, that it displays in

one source the state of a subject heretofore treated only in widely scattered references.

The editor has noted that, in the interest of prompt publication, a full editorial review was not undertaken; the lack of editorial finish is apparent but does not diminish the book's usefulness. The author, compound, and subject indexes provided will prove helpful.

M. Metzger

News Items

1961 Palladium Medal Award, ECS

The sixth Palladium Medal of The Electrochemical Society will be awarded at the Fall Meeting of the Society to be held in Detroit, Mich., October 1-5, 1961.

The medal was established in 1951 by the Corrosion Division for distinguished contributions to fundamental knowledge of theoretical electrochemistry and of corrosion processes. It is awarded biennially to a candidate selected by a committee appointed by the Society's Board of Directors.

Sections, Divisions, and members of the Society are invited to send suggestions for candidates, accompanied by supporting information, to the National Office of the Society, 1860 Broadway, New York 23, N. Y., attention of Robert K. Shannon, Executive Secretary, for forwarding to the committee Chairman. *Deadline for submission of suggestions is March 15, 1961.*

Candidates may be citizens of any country and need not be members of the Society. Previous medalists have been: Carl Wagner, Max Planck Institut für Physikalische Chemie; N. H. Furman, Princeton University; U. R. Evans, Cambridge University; K. F. Bonhoeffer, Max Planck Institut für Physikalische Chemie (posthumous award); and A. N. Frumkin, Electrochemical Institute of the U.S.S.R.

Latest Volume in ECS Series

The Electrochemical Society is pleased to announce the availability of the following new volume in The Electrochemical Society Series:

The Surface Chemistry of Metals and Semiconductors; Proceedings of an International Symposium. Edited by Harry C. Gatos, with the assistance of J. W. Faust, Jr., and W. J. La Fleur. Price: $12.50; 526 pages. (*See* advertisement on page 210C of this issue.)

Contained in the volume are the papers and discussions of the International Symposium (held at the Columbus Meeting of The Electrochemical Society, October 1959) sponsored jointly by the Office of Naval Research and The Electrochemical Society, Inc.

The material is organized under the categories: I. Chemistry and Physics of Surfaces; II. Imperfections and Surface Behavior; III. Electrode Behavior of Metals and Semiconductors; IV. Surface Reactions in Liquid Media; V. Surface Reactions in Gaseous Media.

The volume is available from the publisher, John Wiley & Sons, Inc., 440 Park Ave. South, New York 16, N. Y. *A 33 1/3% discount is offered to ECS members only and can be obtained by ordering through Society Headquarters, 1860 Broadway, New York 23, N. Y.*

New ECS Sustaining Members

The following recently became Sustaining Members of The Electrochemical Society:

Aircraft Accessory Turbine Dept., General Electric Co., West Lynn, Mass.

Delco-Remy Division, General Motors Corp., Anderson, Ind.

Symposium on Redox Processes

A Symposium on Redox Processes, with international participation, will be held at the Chemical Laboratories, University of Allahabad, under the auspices of the Chemical Research Committee, Council of Scientific and Industrial Research, India, in the third week of January 1961. The exact dates will be announced later.

Symposium on Experimentation Below the Microgram Range

The National Academy of Sciences –National Research Council sponsored a symposium on "Experimentation Below the Microgram Range" at the Marriott Key Bridge Motor Hotel, May 15-18, 1960, in Washington, D. C. Professor Nicholas D. Cheronis of Brooklyn College was Chairman of the Planning Committee and General Chairman of the symposium. Attendance was limited to the 27 invited participants. The proceedings will be published as a separate issue of the *Microchemical Journal.*

In his opening remarks, the Chairman stated that two of the principal objectives of the symposium were to stimulate interest in this frontier field and to bring together investigators from widely separated areas of physical and biological sciences to exchange information as to approaches to problems of instrumentation, observation, and correlation of the observed data.

Consideration was given to the unique problems encountered in experimentation below the microgram range. These included: the need for nomenclature pertaining to the 10^{-15} to 10^{-30} gram range and for a general name to describe the area; need for refinement of present methods for determining all physical constants required to establish purity and identity in this range; need to determine lower limits of organic reactions; need for examination of theoretical problems involved, particularly as to what type of chemical kinetics apply at extremely low concentrations; and need for re-examination of our concepts of purity and identity.

Dean Henry Eyring of the University of Utah Graduate School closed the symposium with a lecture on the theoretical aspects of kinetics of chemical reactions in the microgram and submicrogram range. He stated that surface reactions are comparatively much more important and critical at submicrogram levels. Some of the interface reactions differ from reactions occurring in the macro-range.

Dean Eyring believes that the time will come when we will continuously monitor the atmosphere for bacteria and pollutants as we now observe the weather. Flame chromatography is one of the promising methods for such air surveillance.

Ford Foundation Grant to Polytechnic Institute of Brooklyn

The Ford Foundation has awarded a grant of $700,000 to the Polytechnic Institute of Brooklyn to establish an honors program in science and engineering.

Under the new program, exceptional students will be able to receive a doctorate in six years of full-time study. At present, science and engineering students generally take from eight to ten or more years to receive doctorates.

In announcing the receipt of the Ford grant, Dr. Ernst Weber, Polytechnic president, noted that approximately six per cent of the Institute's September freshman class will be enrolled in the honors program.

Under the new program, no strict dividing line is provided between undergraduate and graduate work. A common core curriculum, concentrating in mathematics, physics, and the humanities, will be given to all honors students in the first two years.

At the end of the second year, students will begin specialization in selected areas, including chemistry, mathematics, physics, astronautics, chemical engineering, civil engineering, mechanical engineering, or metallurgical engineering.

Although the program is designed to educate research scientists and engineers from the freshman year through the doctorate, students will be awarded a bachelor of science degree at the end of the undergraduate portion of their studies.

In addition to special curricula, the honors students will take part in seminars and special lectures given by visiting and foreign lecturers and will pursue faculty-supervised research projects early in the program.

Dr. Weber noted that the purpose of the honors program was designed for "the exceptional student whose full potential is not challenged adequately by the average college curriculum."

The Ford Foundation grant, which may be used over a five-year period, will allow Polytechnic to release faculty members from normal teaching loads, to invite visiting faculty members from other institutions, and to award fellowships and loans for graduate students in the program. It will also enable the Institute to develop new syllabi and develop experimental laboratory equipment.

Thirty-three members of approximately 500 September freshman have already been selected to take part in the program. All were at the top of their high school graduating classes, had excellent scores in the College Entrance Board Examinations, and were interviewed by the Honors Program Faculty Committee.

Oxidation of Niobium

The National Bureau of Standards, Washington, D. C., has been studying the oxidation characteristics of niobium to determine the actual cause of the metal's rapid oxidation at temperatures as low as 400°C. In the investigation, the Bureau has found that the continual formation of a porous niobium pentoxide exposes increasingly more niobium to oxygen. Although niobium is a promising metal for structural applications in aircraft, nuclear reactors, and other high-temperature equipment, its oxidation behavior restricts its uses.

BMI Experimental Gas Cell Generator

An experimental electrolytic gas cell generating an oxygen-hydrogen mixture is a promising fuel source for explosive metal-forming operations and high-temperature welding and cutting torches, according to scientists at Battelle Memorial Institute, Columbus, Ohio.

When exploded, the gas mixture creates pressure 10 times greater than the starting pressure, which is limited only by the strength of the container. For example, a 1500-psi mixture on a 2000-sq-in. working surface would produce a peak explosive force of 15,000 tons when ignited. Possible applications include forming large sheet parts of the type used in the aircraft and missile industry.

The generator consists of a number of flat nickel-plated steel electrodes placed 0.060 in. apart in a plastic or insulated-metal container holding a weak caustic solution. Current is run into the two outside electrodes with the intermediate ones functioning as bipolar electrodes.

Using gas for explosive forming operations may provide some advantages over conventional methods. When solid or liquid explosives are used, pressures of millions of pounds per square inch form the metal within a few microseconds. Shock waves are reflected and reinforce the next wave, sometimes doubling the impact and causing the workpiece to crack.

In contrast, gas explosions produce pressures up to hundreds of thousands of pounds per square inch lasting several milliseconds and have a different shock pattern. With solid explosives, the shock wave goes to a high level almost instantaneously, remains there for a few microseconds, then drops abruptly. The shock wave of a gas explosion rises to a peak within several milliseconds, then tapers off gradually.

Used in welding and cutting torches, the burning gases can produce temperatures above 2000°C—hot enough to cut and weld steels, aluminum, and nickel; melt platinum; and fuse alumina. Flame temperature can be controlled by varying the amount of moisture in the gases. Trace amounts of caustic in the gas mixture create a yellow flame, making it visible and thus easier to control.

New Process for Production of Niobium (Columbium)

A new process for the production of niobium (columbium)—a metal that may be increasingly important in future metallic nuclear reactor fuel elements—was described for the first time by a Battelle Memorial Institute scientist. Dr. Joseph H. Oxley, of the Columbus, Ohio, research center presented a report on the fluidized-bed vapor-deposition process at the First International Congress of Chemical Engineering in Mexico City on June 20, jointly sponsored by the American Institute of Chemical Engineers and its Mexican counterpart.

The Battelle process is an entirely new concept in the reduction of niobium pentachloride developed for Nova Beaucage Mines, Ltd. The process is well adapted to continuous production. Present-day chemical and electrolytic processes for producing niobium must be carried out on a batch basis.

In the process developed at Battelle, hydrogen is used to reduce niobium pentachloride. The volatile niobium pentachloride is fed into a reactor chamber containing a fluidized bed of seed niobium. Subsequent reduction by the hydrogen fluidizing gas at 1500°F produces metallic niobium which is deposited on the seed particles. Seed for the fluidized bed is replenished by grinding a portion of the end product and recycling it into the reactor.

Much of the Battelle report, written by Dr. Oxley in conjunction with Dr. George H. Kesler and Dr. I. E.

June 1961 Discussion Section

A Discussion Section, covering papers published in the July–December 1960 JOURNALS, is scheduled for publication in the June 1961 issue. Any discussion which did not reach the Editor in time for inclusion in the December 1960 Discussion Section will be included in the June 1961 issue.

Those who plan to contribute remarks for this Discussion Section should submit their comments or questions in triplicate to the Managing Editor of the JOURNAL, 1860 Broadway, New York 23, N. Y., *not later than March 1, 1960.* All discussion will be forwarded to the author(s) for reply before being printed in the JOURNAL.

Campbell, is concerned directly with the operation of the laboratory-scale processing equipment. The report, however, does contain data on rates of production, conversions to metal, and spectrographic and hardness studies of the niobium produced.

Scandinavian Countries Establish Joint Office in Washington, D. C., for Science Information

A Scandinavian Documentation Center, SCANDOC, was opened in Washington, D. C., on May 18, with the purpose of furthering the mutual exchange of science-tech information and documentation between the Scandinavian countries: Denmark, Finland, Norway and Sweden, and the U.S.A. and Canada. SCANDOC is a nonprofit organization rendering free service to all interested parties, and it is financed and directed by the Research Councils and Science Academies of the four Scandinavian countries through their common Scandinavian Council for Applied Research. SCANDOC will procure nonclassified and nonconfidential documents and information and channel this to the respective interested countries through information offices organized under the research councils and academies of the countries. It is the first time that an international office of this kind has been put up in Washington. SCANDOC is headed by Mr. Arne Sverdrup, a 39-year-old Norwegian scientist who is also accredited to the Norwegian Embassy as science attaché.

A principal task of SCANDOC will be the procurement, on request, of nonclassified and nonconfidential reports and documents not readily available through libraries, bookstores, and other regular channels. SCANDOC will also report to the Scandinavian Council for Applied Research on any such significant material published in the U.S.A. or Canada. The work of distributing this material in Scandinavia and of serving as contact organizations is delegated to four institutions: in Denmark, The Danish Technical Information Service (DTO); in Finland, Information Service of the State Institute for Technical Research (VTT); in Norway, The Committee for Technical Information Service of the Royal Norwegian Council for Scientific and Industrial Research (LU/NTNF); and in Sweden, Information Service of the Royal Swedish Academy of Engineering Sciences (UT/IVA).

The address of SCANDOC is: 2136 P St., N.W., Washington 7, D. C.

Two Strong New Piezoelectric Compounds Discovered

The discovery that zinc oxide and cadmium sulfide are strongly piezoelectric recently has been revealed by A. R. Hutson, of Bell Telephone Laboratories, in the current issue of *Physical Review Letters*. In order to demonstrate the piezoelectricity in zinc oxide, it first had to be "doped" with lithium to neutralize the excess conductivity which has masked the effect until now.

The degree of piezoelectricity exhibited by the doped zinc oxide is about four times as great as that of quartz, while the cadmium sulfide is twice as great. Confirming measurements were made on single crystals of zinc oxide grown both by vapor techniques and from a flux. The cadmium sulfide crystals were vapor-grown.

Both zinc oxide and cadmium sulfide long have been recognized as n-type semiconductors. Zinc oxide, in fact, usually shows a room temperature resistivity less than 10^3 ohm-cm. This relatively low resistivity effectively shorts out all experimental evidence of piezoelectricity.

Dr. Hutson decided to investigate the piezoelectric constants of these materials while studying some of their unusual conductivity properties, especially the large magnitude and temperature dependence of the phonon-drag effect observed in thermoelectric power measurements. A large piezoelectric constant seemed to explain these anomalies theoretically, but never had been observed experimentally.

The conductivity of the zinc oxide was "quenched" by diffusing lithium atoms into the material, to act as acceptors for the excess electrons which were contributing to the conductivity. When this was done, the resistivity of the material was raised from 10^3 to 10^{12} ohm-cm at room temperature.

Resonance-antiresonance measurements and direct squeeze measurements were made on vapor-phase grown needles and flux-grown platelets of zinc oxide, and on the vapor-phase grown cadmium sulfide. With dielectric constants of 8.2 and 9 for ZnO and CdS, respectively, electrochemical coupling coefficients were calculated to be approximately 0.4 for ZnO and 0.2 for CdS, compared with 0.095 for quartz.

Epitaxial Diffused Transistors

Major reductions in switching times and collector resistances of diffused base transistors have been realized at Bell Telephone Laboratories by the use of epitaxially grown films. These improvements have been achieved by combining diffused base technology with the epitaxial film technique. Films themselves also have been under investigation in a number of other laboratories.

Application of this technique has resulted in a reduction of the switching time of silicon devices by a factor of more than 10, and in a comparable reduction in the collector resistance. This major development is expected to have far-reaching implications in both the fabrication and application of semiconductor devices.

Diffused base transistors require a relatively high resistivity collector region in order to attain low capacitance and high voltage breakdown. Typically, to afford ease of mechanical handling, this region has been much thicker than required electrically. The excess thickness increases the collector resistance and the switching time.

Ideally, the thickness of the lightly doped collector region should be in the neighborhood of 0.1 mil, which is about a factor of 30 thinner than normally used. Semiconductor wafers prepared by conventional methods become extremely difficult, if not impossible, to handle as they approach this desired thinness. The problem can be solved by the use of expitaxial film techniques. Lightly doped expitaxial films are grown on and supported by a low-resistivity substrate giving the desired combination of electrical properties and mechanical strength.

Diffused base transistors made at Bell Telephone Labs. on expitaxial layers of both germanium and silicon have exhibited the theoretically predicted improvements.

New York Publisher Granted Rights to Soviet Journals

A contract covering the translation into English of 23 major Soviet scientific journals was renewed for 1960 and 1961 recently by representatives of Mezhdunarodnaya Kniga and Consultants Bureau Enterprises, Inc., a New York publishing house.

The agreement guarantees Consultants Bureau Enterprises, Inc., 227 W. 17 St., New York 11, N. Y., exclusive English-translation rights for these journals in the fields of chemistry, physics, biology, and medicine. The original arrangement was made between the two concerns in 1958 for one year only, and was the first such agreement ever reached between an American publisher and the Soviet

Union. The 1958 contract was renewed for one year in 1959.

Under the terms of the new two-year agreement, the Soviet agency facilitates advance receipt of Russian journals by the publisher here, and is pledged to use all means at its disposal to prevent infringement of the exclusive translation rights by any third party. Original art work and photographs appearing in the Russian periodicals also are rushed to the New York publisher by air mail. In return for these important advantages, Consultants Bureau is making what is described as a "reasonable royalty payment."

The journals covered in the agreement are: *Biochemistry; Bulletin of Experimental Biology and Medicine; Proceedings of the Academy of Sciences of the USSR (Doklady); Journal of General Chemistry; Journal of Analytical Chemistry; Journal of Applied Chemistry; Bulletin of the Academy of Sciences—Chemistry Section; Automation and Remote Control; Colloid Journal; Metallurgist; Microbiology; Plant Physiology; Soviet Physics—Technical Physics; Soviet Physics—Acoustics; Pharmacology and Toxicology; Soviet Physics—Crystallography; Soviet Astronomy; Antibiotics; Instruments and Experimental Techniques; Entomological Review; Industrial Laboratory; Solid State Physics; Glass and Ceramics.*

NBS Announces First Construction Phase for New Labs.

The National Bureau of Standards, U. S. Dept. of Commerce, has announced that work will begin during the next 12 months on site development and construction of the first three building units for the new Bureau laboratories to be located at Gaithersburg, Md.

Congress recently appropriated $23,500,000 to finance this initial phase in the relocation of the Bureau. In addition to the preparation of the site and installation of utilities, the first phase will include the construction of an Engineering Mechanics Lab., a Radiation Physics Lab., and the Power Plant. These two laboratory buildings were given priority among the 20 buildings to be constructed in the total relocation program because of their urgency in national science activities.

Relocation of the Bureau is necessary to provide modern laboratory facilities to meet the critical research responsibilities assigned to the Bureau, which has occupied its present Washington site since 1903. During that time, its responsibilities have greatly increased, largely as a result of the rapid expansion of technology and the growth of scientific research. Extensive programs of research and development now must be conducted in the physical sciences and engineering to meet the needs of science and industry for new and improved standards and measurement methods. The new site will enable the Bureau to plan and conduct a more up-to-date program consistent with its increasing responsibilities.

Many of the buildings on the present site are temporary, and even the permanent buildings are outmoded. Renovation and modernization would be costly, amounting to more than half the estimated cost of a complete new facility. Space for further expansion is also lacking on the present site.

The new laboratories will provide for a modern research operation. In addition, the new site will provide a rural location where scientific programs can be undertaken without interfering in community life and without urban interference to Bureau projects. The rural location will remove the Bureau's work from the variety of mechanical, electrical, and atmospheric disturbances present in a city, and will reduce the effect of these forces on precise scientific measurements.

A tract of approximately 550 acres of land near Gaithersburg, Md., was acquired four years ago for relocation of the Washington laboratories of the Bureau. The new site was selected after careful consideration as most suited to the special requirements of the Bureau's scientific and engineering programs. The choice was based upon a number of factors, including accessibility to roads and topography required for certain projects.

International Rectifier Corp. Acquires Dallons Labs., Inc.

Acquisition of Dallons Laboratories, Inc., of Los Angeles, was announced recently by International Rectifier Corp. of El Segundo, developers and manufacturers of semiconductor devices.

Dallons Labs. is a supplier of specialized medical electronic equipment and currently is producing aerospace medical instrumentation for the Project Mercury astronaut program.

The Los Angeles company has an extensive background in glass and quartz crystal technology. It also produces semiconductor devices, and specialized equipment for their production.

Dallons Labs. will operate as an autonomous, wholly owned subsidiary, with Dr. Oscar Dallons continuing as president, Franz Dallons as vice-president in charge of production, and Paul Dallons as vice-president in charge of glass and vacuum technology. The semiconductor equipment and activities will be consolidated in the International Rectifier facilities.

American Potash Plans Electrolytic Manganese Plant at Aberdeen, Miss.

Plans for the construction of a $5,000,000 electrolytic manganese metal manufacturing plant at Aberdeen, Miss., have been announced by American Potash & Chemical Corp. The plant will have an initial capacity of 10,000,000 pounds per year and will be laid out to provide for further expansions.

Final design and engineering is now in progress, and field construction is scheduled for fall at the company's 1600-acre site on the Tombigbee River seven miles outside of Aberdeen, with completion planned for late 1961.

Announcements from Publishers

"Purification of Americium Chloride Solutions by Mercury Cathode Electrolysis," March 1960. AEC Report REP-183,* 9 pages; 50 cents.

"A study of the Corrosive Effects of the Combustion Products of Boron Containing Fuels on Selected High Temperature Materials," F. J. Loprest and S. J. Tunkel, Thiokol Chemical Corp., for Wright Air Development Center, U. S. Air Force, Sept. 1959. Report PB 161421,* 331 pages; $5.00.

"The 'Improved' Free Volume Theory of Liquids, II," J. S. Dahler, Wright Air Development Center, and J. O. Hirschfelder, University of Wisconsin, for U. S. Air Force, Sept. 1959. Report PB 161407,* 197 pages; $3.00.

"Research in Physical Chemistry and Metallurgy of Semi-Conducting Materials," K. E. Bean and others, U. S. Army Signal Corps, Dec. 1957. Report PB 161353,* 40 pages; $1.00.

* Order from Office of Technical Services, U.S. Dept. of Commerce, Washington 25, D. C.

"Development of a Method to Accomplish Aluminum Deposition by Gas Plating," M. J. Hiler and W. C. Jenkin, Commonwealth Engineering Co. of Ohio, for Wright Air Development Center, U. S. Air Force, June 1959. Report PB 151923,* 64 pages; $1.75.

"Evaluation of Protective Coatings for Molybdenum Nozzle Guide Vanes," 1st Lt. J. R. Giancola, USAF, Materials Lab., Wright Air Development Center, June 1959. Report PB 151912,* 47 pages; $1.25.

"Tables of Thermodynamic Properties of Air Including Dissociation and Ionization from 1500°K to 15,000°K," K. J. Hilsenrath, M. Klein, and H. W. Wooley, National Bureau of Standards, Dec. 1959. Report PB 161311,* 147 pages; $2.75.

"Temperature Conversion Tables," W. A. Brodhecker, U. S. Naval Avionics Facility, Indianapolis, Ind., Nov. 1959. Report PB 161354,* 84 pages; $2.25.

"The Determination of Near Infrared Spectra," S. Anderson, R. Isaac, and M. Blankenship, Anderson Physical Lab., for Wright Air Development Center, U. S. Air Force, Sept. 1959. Report PB 161336,* 82 pages; $1.00.

* Order from Office of Technical Services, U. S. Dept. of Commerce, Washington 25, D. C.

New Products

Polyethylene Plugs. Polyethylene-coated plugs for use with saran-lined plug valves are being sold by the Saran Lined Pipe Co., Ferndale, Mich. According to the manufacturer, the Dow Chemical Co., the linear polyethylene plugs eliminate the "freezing" that sometimes occurs when saran plugs are used with saran-lined pipe. The plugs are available in eight sizes ranging from 1 to 6 in.

Military-Type Silicon Zener Voltage Reference Elements conforming to MIL-E-1/1060 (Navy) are now available from International Rectifier Corp., El Segundo, Calif. Units feature an extremely rugged assembly which can withstand the severe shock and vibration requirements of military semiconductor device specifications. They will provide a stability of ± 16 mv or better over a temperature range from −55°C to +100°C, with temperature coefficients of ± 0.002%/°C.

Carbon-14 Compounds. Three new radioactive carbon compounds, Cortisone-4-C^{14}, Cortisone-4-C^{14} Acetate, and 1,2,3,4-Dibenzanthracene-9-C^{14}, have been added to the list of carbon-14 compounds available from Nuclear-Chicago Corp. The new compounds, together with more than 200 other carbon-14, sulfur-35, phosphorus-32, and tritium compounds, are described and priced in the new Radiochemical Schedule F available from Nuclear-Chicago Corp., 359 E. Howard Ave., Des Plains, Ill.

Industrial Silicon Power Transistors. A comprehensive new group of 12 diffused-junction power transistors of the silicon n-p-n type has been announced by the RCA Semiconductor and Materials Div., Radio Corp. of America, Somerville, N. J. They feature high current and power dissipation ratings, high beta at high current, low saturation resistance, high power-handling capability, and top performance at high temperatures up to +175°C. **Intermediate-Power Germanium Transistors.** Six new intermediate-power germanium alloy-junction transistors of the p-n-p type for industrial and military applications also were announced. They feature low saturation resistance and low leakage currents, are hermetically sealed in metal cases, and have the dimensions which conform to the JEDEC TO-8 outline.

Literature from Industry

Preparation of Radioactive Samples is the topic of Nuclear-Chicago's seventh technical bulletin, which discusses radioactive sample preparation and counting difficulties and suggests appropriate laboratory techniques and equipment for obtaining the best possible results.

Technical Bulletin #7 will be sent on request from Nuclear-Chicago Corp., 359 E. Howard Ave., Des Plaines, Ill.

"Alcoa Bearings." This new booklet, Aluminum Co. of America's latest and most extensive collection of case histories, engineering and test data pertaining to sleeve bearings and bushings of the light metal, is being offered to industry.

The 90-page study can be obtained from Alcoa sales offices or by writing to Rm. 732, Alcoa Bldg., Pittsburgh 19, Pa.

"H-VW-M Plating and Polishing News." The latest edition of this quarterly is now available to all members of the metal finishing trade. The brochure features the latest equipment, supplies, and processes made possible through the research and development laboratories of H-VW-M.

To be placed on the mailing list to receive future copies, send your name, title, company's name, street address, zone number, and state to Hanson-Van Winkle-Munning Co., Church St., Matawan, N. J.

Brief Communications

The JOURNAL accepts short technical reports having unusual importance or timely interest, where speed of publication is a consideration. The communication may summarize results of important research justifying announcement before such time as a more detailed manuscript can be published. Consideration also will be given to reports of significant unfinished research which the author cannot pursue further, but the results of which are of potential use to others. Comments on papers already published in the JOURNAL should be reserved for the Discussion Section published biannually.

Submit communications in triplicate, typewritten double-spaced, to the Editor, Journal of The Electrochemical Society, 1860 Broadway, New York 23, N. Y.

"Properties and Uses of Commercially Available Cobalt Compounds." This two-page summary lists 46 organic and inorganic compounds, including the new potassium cobalticyanide, and provides information on uses, formula, per cent cobalt, molecular weight, specific gravity, crystalline form, melting point, and solubility.

The summary will be sent to persons addressing requests on company letterhead to the Cobalt Information Center, c/o Battelle Memorial Institute, 505 King Ave., Columbus 1, Ohio. Requesters abroad should write to Centre d'Information du Cobalt, 35 rue des Colonies, Brussels, Belgium.

Employment Situations

Positions Available

Research Chemist—Research Associate for American Electroplaters' Society Research Project No. 19, Galvanic Effects Associated with Coating Failure. To work at the National Bureau of Standards in Washington, D. C. Post-graduate work or research experience required. Reply to Fielding Ogburn, National Bureau of Standards, Washington 25, D. C.

Research Chemists—Research and development group seeks chemist or chemical physicist for solid-state work on cathodoluminescent and electroluminescent materials, photoconductors, and chemicals for electronic applications. Candidates should have Ph.D. or equivalent and be capable of independent work. Modern and well-equipped laboratories in Northeastern Pennsylvania. Publication of work encouraged.

Send résumé to: Dr. J. S. Smith, Manager of Chemical Research and Development, Chemical and Metallurgical Division, Sylvania Electric Products Inc., Towanda, Pa.

Advertiser's Index

The Electrochemical Society

INSTRUCTIONS TO AUTHORS OF PAPERS

Address all correspondence to the Editor, JOURNAL OF THE ELECTROCHEMICAL SOCIETY, 1860 BROADWAY, NEW YORK 23, N. Y.

FORM

Manuscripts submitted for publication should be in triplicate to expedite review. They should be typewritten, double-spaced, with 2½-4 cm (1-1½ in.) margins.

Title should be brief, followed by the author's name and his business or university connection.

Abstract of about 100 words should state the scope of the paper and give a brief summary of results.

ILLUSTRATIONS

Drawings will be reduced to column width, 8.3 cm (3¼ in.), after reduction should have lettering at least 0.15 cm (1/16 in.) high. Original drawings in India ink on tracing cloth or white paper are preferred. Curves may be drawn on coordinate paper only if the paper is ruled in blue. All lettering must be of lettering-guide quality. See sample drawing on reverse page.

Photographs must be glossy prints and mounted flat.

Captions for all figures must be included on a separate sheet. Captions and figure numbers should not appear in the body of the figure.

General—Figures should be used only when necessary. Omit drawings or photographs of familiar equipment. Figures from other publications are to be used only when the publication is not readily available, and should always be accompanied with written permission for reprinting.

SYMBOLS

If more than a few symbols are used, these should be defined in a list at the end of the paper, for example:

$a, b \ldots$ = empirical constants of Brown equation
f_i = fugacity of pure ith component, atm
D_e = bulk diffusion coefficient, cm²/sec

REFERENCES

Literature and patent references should be listed at the end of the paper on a separate sheet, in the order in which they are cited. They should be given in the style adopted by *Chemical Abstracts*. For example:

R. Freas, *Trans. Electrochem. Soc.*, **40**, 109 (1921).

H. T. S. Britton, "Hydrogen Ions," Vol **1**, p. 309, D. Van Nostrand Co., New York (1943).

H. F. Weiss (To Wood Conversion Co.), U. S. Pat. 1,695,445, Dec. 18, 1928.

UNITS OF MEASUREMENT

Metric units should be used throughout but, where desirable, English units may be given in parentheses.

Corrosion rates in the metric system should preferably be expressed as milligrams per square decimeter per day (mdd), and in the English system as inches penetration per year (ipy).

In reporting electrode potentials, the sign of the standard Zn/Zn^{++} electrode potential should be taken as negative; Cu/Cu^{++} as positive.

ABBREVIATIONS

Abbreviations should conform with the American Standards Association's list of "Abbreviations for Scientific and Engineering Terms."

GENERAL

Authors should be as brief as is consistent with clarity, and must omit all material which can be regarded as familiar to specialists in the particular field.

The use of proprietary names, trade-marks, and trade names should be avoided if possible. If used, these should be capitalized so that the owner's legal rights are not jeopardized.

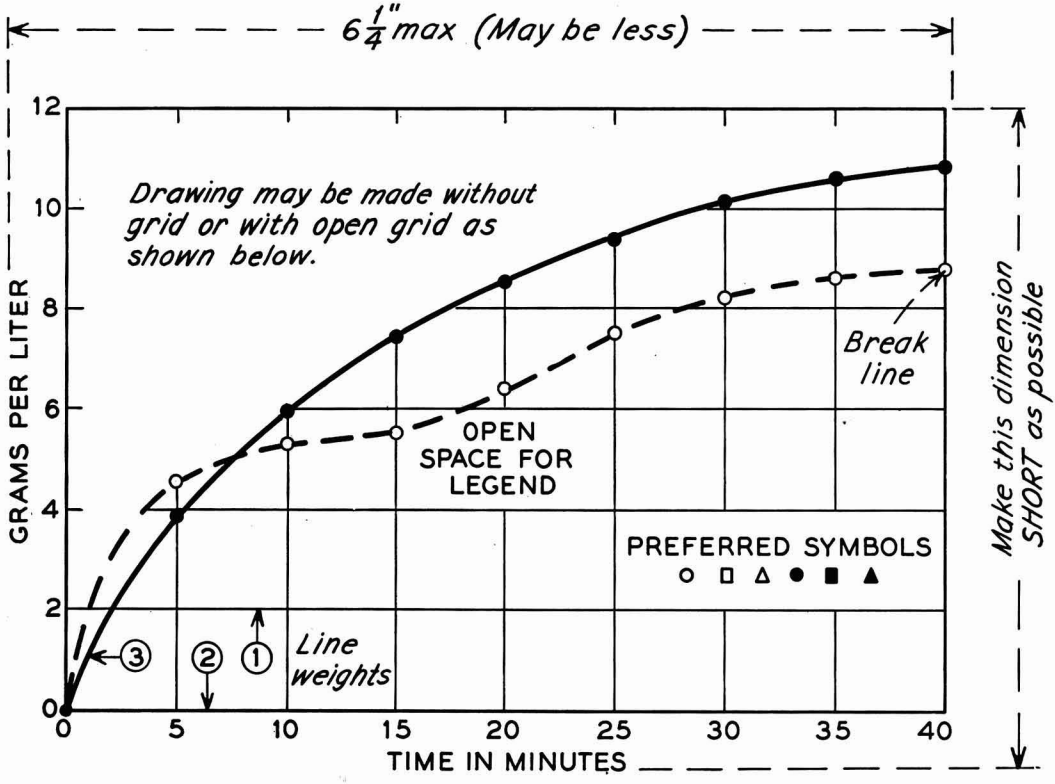

Remarks: Line weight 2 is used for borders and zero lines. When several curves are shown, each may be numbered and described in the caption. Lettering shown is approximately ⅛ in. In plotting current or potential as ordinate, increasing negative values should go down.

SAMPLE CURVE DRAWING FOR REDUCTION TO $\frac{1}{2}$ SIZE

The Electrochemical Society

Patron Members

Aluminum Co. of Canada, Ltd.,
Montreal, Que., Canada

International Nickel Co., Inc.,
New York, N. Y.

Olin Mathieson Chemical Corp.,
Niagara Falls, N. Y.
Industrial Chemicals Div., Research
and Development Dept.

Union Carbide Corp.
Divisions:
Union Carbide Metals Co.,
New York, N. Y.
National Carbon Co., New York, N. Y.

Westinghouse Electric Corp., Pittsburgh, Pa.

Sustaining Members

Air Reduction Co., Inc.,
New York, N. Y.

Ajax Electro Metallurgical Corp.,
Philadelphia, Pa.

Allen-Bradley Co., Milwaukee, Wis.

Allied Chemical & Dye Corp.
General Chemical Div., Morristown, N. J.
Solvay Process Div., Syracuse, N. Y.
(3 memberships)

Allied Research Products, Inc.,
Detroit, Mich.

Alloy Steel Products Co., Inc., Linden, N. J.

Aluminum Co. of America,
New Kensington, Pa.

American Metal Climax, Inc.,
New York, N. Y.

American Potash & Chemical Corp.,
Los Angeles, Calif. (2 memberships)

American Smelting and Refining Co.,
South Plainfield, N. J.

American Zinc Co. of Illinois,
East St. Louis, Ill.

American Zinc, Lead & Smelting Co.,
St. Louis, Mo.

American Zinc Oxide Co., Columbus, Ohio

M. Ames Chemical Works, Inc.,
Glens Falls, N. Y.

Auto City Plating Company Foundation,
Detroit, Mich.

Basic Inc., Maple Grove, Ohio

Bell Telephone Laboratories, Inc.,
New York, N. Y. (2 memberships)

Bethlehem Steel Co., Bethlehem, Pa.
(2 memberships)

Boeing Airplane Co., Seattle, Wash.

Burgess Battery Co., Freeport, Ill.
(4 memberships)

Canadian Industries Ltd., Montreal, Que.,
Canada

Carborundum Co., Niagara Falls, N. Y.

Catalyst Research Corp., Baltimore, Md.

Ciba Pharmaceutical Products, Inc., Summit,
N. J.

Columbian Carbon Co., New York, N. Y.

Columbia-Southern Chemical Corp.,
Pittsburgh, Pa.

Consolidated Mining & Smelting Co. of
Canada, Ltd., Trail, B. C., Canada
(2 memberships)

Continental Can Co., Inc., Chicago, Ill.

Cooper Metallurgical Associates, Cleveland,
Ohio

Corning Glass Works, Corning, N. Y.

Diamond Alkali Co., Painesville, Ohio
(2 memberships)

Dow Chemical Co., Midland, Mich.

Wilbur B. Driver Co., Newark, N. J.
(2 memberships)

E. I. du Pont de Nemours & Co., Inc.,
Wilmington, Del.

Eagle-Picher Co., Chemical Div., Joplin, Mo.

Eastman Kodak Co., Rochester, N. Y.

Thomas A. Edison Research Laboratory, Div.
of McGraw-Edison Co., West Orange, N. J.

Electric Auto-Lite Co., Toledo, Ohio
C & D Division, Conshohocken, Pa.

Electric Storage Battery Co., Yardley, Pa.

Englehard Industries, Inc., Newark, N. J.
(2 memberships)

The Eppley Laboratory, Inc., Newport, R. I.
(2 memberships)

Erie Resistor Corp., Erie, Pa.

Exmet Corp., Tuckahoe, N. Y.

Fairchild Semiconductor Corp., Palo Alto,
Calif.

Food Machinery & Chemical Corp.
Becco Chemical Div., Buffalo, N. Y.
Westvaco Chlor-Alkali Div., South
Charleston, W. Va.

Foote Mineral Co., Paoli, Pa.

Ford Motor Co., Dearborn, Mich.

General Electric Co., Schenectady, N. Y.
Chemistry & Chemical Engineering
Component, General Engineering
Laboratory
Chemistry Research Dept.
General Physics Research Dept.
Metallurgy & Ceramics Research Dept.
Aircraft Accessory Turbine Dept.,
West Lynn, Mass.

General Instrument Corp., Newark, N. J.

(Sustaining Members cont'd)

General Motors Corp.
Delco-Remy Div., Anderson, Ind.
Guide Lamp Div., Anderson, Ind.
Research Laboratories Div., Detroit, Mich.
General Transistor Corp., Jamaica, N. Y.
Gillette Safety Razor Co., Boston, Mass.
Globe-Union, Inc., Milwaukee, Wis.
Gould-National Batteries, Inc.,
Minneapolis, Minn.
Grace Electronic Chemicals, Inc.,
Baltimore, Md.
Great Lakes Carbon Corp., New York, N. Y.
Hanson-Van Winkle-Munning Co.,
Matawan, N. J. (2 memberships)
Harshaw Chemical Co., Cleveland, Ohio
(2 memberships)
Hercules Powder Co., Wilmington, Del.
Hill Cross Co., Inc., New York, N. Y.
Hoffman Electronics Corp., El Monte, Calif.
Hooker Chemical Corp., Niagara
Falls, N. Y. (3 memberships)
Hughes Aircraft Co., Culver City, Calif.
Industro Transistor Corp.,
Long Island City, N. Y.
International Business Machines Corp.,
Poughkeepsie, N. Y.
International Minerals & Chemical
Corp., Skokie, Ill.
ITT Laboratories, Nutley, N. J.
Jones & Laughlin Steel Corp.,
Pittsburgh, Pa.
K. W. Battery Co., Skokie, Ill.
Kaiser Aluminum & Chemical Corp.
Div. of Chemical Research,
Permanente, Calif.
Div. of Metallurgical Research,
Spokane, Wash.
Kennecott Copper Corp., New York, N. Y.
Keokuk Electro-Metals Co., Keokuk, Iowa
Libbey-Owens-Ford Glass Co., Toledo, Ohio
M. & C. Nuclear, Inc., Attleboro, Mass.
Mallinckrodt Chemical Works, St. Louis, Mo.
P. R. Mallory & Co., Indianapolis, Ind.
McGean Chemical Co., Cleveland, Ohio
Merck & Co., Inc., Rahway, N. J.
Metal & Thermit Corp., Detroit, Mich.
Minnesota Mining & Manufacturing Co.,
St. Paul, Minn.
Monsanto Chemical Co., St. Louis, Mo.
Motorola, Inc., Chicago, Ill.
National Cash Register Co., Dayton, Ohio
National Lead Co., New York, N. Y.
National Research Corp., Cambridge, Mass.
National Steel Corp., Weirton, W. Va.
New York Air Brake Co., Kinney Vacuum
Div., Boston, Mass.
Northern Electric Co., Montreal, Que.,
Canada
Norton Co., Worcester, Mass.
Olin Mathieson Chemical Corp.,
Research & Engineering Operations,
Energy Div., New Haven, Conn.
Ovitron Corp., Long Island City, N. Y.
Peerless Roll Leaf Co., Inc., Union City, N. J.
Pennsalt Chemicals Corp.,
Philadelphia, Pa.
Phelps Dodge Refining Corp., Maspeth, N. Y.
Philco Corp., Philadelphia, Pa.
Philips Laboratories, Inc., Irvington-on-
Hudson, N. Y.
Pittsburgh Metallurgical Co., Inc.,
Niagara Falls, N. Y.
Poor & Co., Promat Div., Waukegan, Ill.
Potash Co. of America,
Carlsbad, N. Mex.
Radio Corp. of America
Tube Div., Harrison, N. J.
RCA Victor Record Div., Indianapolis,
Ind.
Ray-O-Vac Co., Madison, Wis.
Raytheon Manufacturing Co.,
Waltham, Mass.
Reynolds Metals Co., Richmond, Va.
(2 memberships)
Rheem Semiconductor Corp.,
Mountain View, Calif.
Schering Corporation, Bloomfield, N. J.
Shawinigan Chemicals Ltd., Montreal, Que.,
Canada
Speer Carbon Co.
International Graphite & Electrode
Div., St. Marys, Pa. (2 memberships)
Sprague Electric Co., North Adams, Mass.
Stackpole Carbon Co., St. Marys, Pa.
Stauffer Chemical Co., New York, N. Y.
Sumner Chemical Co., Div. of
Miles Laboratories, Inc., Elkhart, Ind.
Sylvania Electric Products Inc., Bayside,
N. Y. (2 memberships)
Tennessee Products & Chemical Corp.,
Nashville, Tenn.
Texas Instruments, Inc., Dallas, Texas
Three Point Four Corp., Yonkers, N. Y.
Titanium Metals Corp. of America,
Henderson, Nev.
Tung-Sol Electric Inc.,
Newark, N. J.
Udylite Corp., Detroit, Mich.
(4 memberships)
Universal-Cyclops Steel Corp.,
Bridgeville, Pa.
Upjohn Co., Kalamazoo, Mich.
Victor Chemical Works, Chicago, Ill.
Western Electric Co., Inc., Chicago, Ill.
Wyandotte Chemicals Corp.,
Wyandotte, Mich.
Yardney Electric Corp., New York, N. Y.